Seismic Assessment, Repair and Retrofit of Existing Corroded Structures Using UHPC Jacketing

Nicolas Habib El-Joukhadar

A Dissertation Submitted to the Faculty of Graduate Studies in Partial Fulfillment of the Requirements for the Degree of Doctor of Philosophy

Graduate Program in Civil Engineering

York University

Toronto, Ontario

June 2022

Abstract

The bulk of our developed environment was constructed in the mid to late 20th century, when design codes did not address the importance of ductility and confinement, placing most of today's concrete infrastructure in danger in case of a seismic event. Current assessment guidelines such as Eurocode 8-III or ASCE 41-17 take the lack of detailing into consideration in the assessment procedure however, they do not address a major concern, reinforcement corrosion. In this dissertation, modifications to current assessment guidelines were proposed and validated in order to take corrosion damage into consideration. Expressions for residual material properties as well as residual mechanical properties of columns were proposed with reinforcement mass loss being the only variable. The viability of using UHPC as both a strengthening and protective material against corrosion was studied in this dissertation. It was found that UHPC fully mitigates corrosion in case no service cracks were present and significantly reduces the corrosion rate in case of cracks between 0.5mm and 2mm were present. The final portion of the dissertation deals with repair and strengthening of corroded lap-spliced columns. Six lap-spliced columns designed based on pre-1970s design standards were constructed and subjected to artificial corrosion. Some of the specimens were tested without any prior strengthening intervention to simulate an earthquake damaging an existing column. They were then repaired using UHPC jacketing and re-tested under cyclic displacement reversals while other columns were strengthened after corrosion and then tested. This was done in order to study the increase in strength and ductility in case the strengthening was done prior to or after seismic activity. The results show a significant increase in strength and ductility of the columns, imparted by thin UHPC jackets replacing the conventional concrete cover.

Dedication

I dedicate this dissertation to my late mother, Violette.

I still remember the day you were educating me on how important a college education was. I was maybe 8 years old, I asked you what was the highest degree attainable and you replied it was the Doctorate Degree.

Here I am mom, 19 years later, getting my Doctorate Degree.

Acknowledgements

The past four years have been very impactful on my life. I, for the first time, moved to another country to pursue my Doctorate. Moving from a small village in Lebanon to the Metropolitan city of Toronto was not easy, I faced several hurdles from the change in lifestyle to the change in the schooling system. Luckily, I had a great supervisor, a loving partner, and caring friends who helped me overcome these obstacles, and I am grateful for everyone who supported me during this time.

I would like to start off by thanking my supervisor Dr. Stavroula Pantazopoulou for granting me this opportunity to come and pursue my Doctorate at York University. In retrospect, my move to Canada in 2018 was probably my last chance of getting out of Lebanon. A year later the protests would begin, the economy would collapse, and everyone's money would disappear from the banks. If my offer from York had come a year later, I would not have been able to accept it, because I would not have been able to leave. Thus, I am eternally grateful and indebted to my supervisor, Dr. Pantazopoulou, for finding and believing in me at the right time. I also want to thank her for her continuous support during my degree, She has added a tremendous amount of value to my knowledge in Structural engineering.

I would also like to show my gratitude to Dr. Dan Palermo and Dr. Liam Butler for serving as examiners throughout my degree. They both offered me help whenever I asked and have given me valuable comments regarding my research.

I also want to thank everyone who has helped me during my experimental programs in the Highbay lab, starting with our lab technicians: Riad Rajab, Kunjan Rupakheti, Melissa Salem McLean, Adam McLean and David Marcinkiewicz. Thank you very much for your help. You always had my back when things got tough.

I also want to show my gratitude to my colleagues: Konstantinos Tsiotsias, Zoi Ralli and Rita Saikali who helped me adapt and settle in during my first year. I want to thank Mario Antoun, Austin Martins-Robalino, Ismail Mohammed, Arham malik, Daphne-Eleni Archonta and Adrien Sparling for helping me run my experiments.

I want to thank my family, especially my father, Habib, for supporting me emotionally during this time. He is one of the main reasons I chose the academic path as it has been the only

topic of our household growing up. I also want to show gratitude to my brother, Wissam, who was always in the shadows looking after me.

Last but not least, I want to show my gratitude to my emotional support and backbone, my love Elianne El-Amyouni, and my mentor George El-Amyouni. You both are the reason I decided to pursue my Doctorate degree. I hope to make you both proud.

Table of Contents

List of Figures

List of Tables

1. Introduction

1.1 Background

A large part of the existing reinforced concrete construction dates back to the 19th and 20th centuries, a time when the urban infrastructures were built in most cities around the world. Reinforced concrete is favored over other building materials because of the low cost of materials, the ease of application (could be shaped in any form), speed of construction, and what was originally through as a durable structural paradigm with low maintenance costs. However, it has been found that reinforced concrete structures are highly susceptible to many forms of deterioration, mainly the corrosion of embedded reinforcement (Mehta, 1991; Gjørv, 2014). It took a few decades after World War II before it became obvious that corrosion resulting from exposure to either marine environments or to urban CO2 pollution limits dramatically the service life of RC structures. Today, the extent of damage in the existing RC building stock and infrastructure is incalculable and extremely widespread, underscoring an urgent need for immediate development of methodologies for assessment, repair and rehabilitation of the affected built environment.

Portland cement which is used in conventional concrete is highly alkaline (pH around 12) if not exposed to CO_2 or chlorides. In reinforced concrete members, the cementitious gel creates a passive layer around the reinforcement bars that protects them from corrosion. Cracking (from mechanical loading or freezing and thawing), concrete carbonation, and chlorine ingress cause the destruction of that layer, allowing for the unrestricted flow of air and water to the reinforcement surface, causing corrosion. Concrete carbonation occurs naturally when carbon dioxide reacts with concrete and produces calcium carbonate. This process decreases the pH of concrete, and once it reaches a pH of 9, the functionality of the protective film is lost. The ferrous and ferric oxides produced from the corrosion process that follows gradually accumulate on the bar surface. Having a larger volume than the original steel, the corrosion products exert a bursting pressure on the concrete cover resulting in supplementary cracking and cover disintegration. This, in turn, accelerates further the corrosion process. Similar to carbonation, chloride ingress transforms the passive film and significantly accelerates the corrosion rate. Exposure to chlorides may occur due to several reasons, such as the use of deicing salts (sodium or magnesium chloride) on bridges to accelerate the melting of snow and ice, or in marine environments where concrete is constantly in contact with sea water and air (from tidal waves or windblown spray). Sourcing of sand,

aggregates, and mixing water from the sea or coastline deposits has been common in many parts of the world and may still occur in developing countries. In these circumstances the corrosive agents are embedded in corrosion rapidly reducing the time to depassivation of the protective film on the reinforcement (known as time to corrosion initiation, Tuutti, (1982)) making such structures even more susceptible to corrosion damage. Other causes of deterioration that lead to reinforcement corrosion are exposure to sulfates, alkali-silica reaction, and acid exposure.

Corrosion and its impacts also have huge economic repercussions both in North America and globally. In 2016, NACE International published the IMPACT study, where it estimates the cost of corrosion to be $2.5 trillion globally, accounting for 3.4% of the GDP. The two-year global study published at the CORROSION 2016 conference in Vancouver, B.C., assessed the economics of corrosion and the impact of managing corrosion in establishing industry best practices. It was found that applying corrosion deterrence best practices could result in savings of between 15-35 % of the cost of damage, or between $375-875 billion globally (NACE International, 2016). According to the ARTBA bridge report, the United States of America currently has over 45,000 deficient bridges (American Road & Transportation Builders Association, 2020). Thus, it is crucial to find an economic and durable solution to this problem.

Another problem that needs addressing is the lack of proper assessment guidelines for corroded structures. Current evaluation guidelines do not consider the state of reinforcement, which was proven to affect the member's residual mechanical characteristics, the failure mode and the consequences on seismic performance. In recent years, corrosion led to the collapse of a bridge in Genoa, Italy, resulting in the death of 43 people (Morandi Bridge, Genoa, Italy 2018). The prestressed bridge was only 51 years old, younger than a large portion of the existing built infrastructure. Therefore, it is very important to create assessment methods and tools that account explicitly for corrosion damage – i.e., condition assessment should be accounted for in all the structural evaluation criteria. In this dissertation, several modifications to current evaluation guidelines are proposed which result in specific details for quantifying the effect of corrosion damage in the modelling parameters and performance evaluation criteria of the established assessment frameworks (e.g. ASCE/SEI-41, 2017).

There are various treatments and protective measures against reinforcement corrosion such as cathodic protection, concrete replacement, epoxy coating etc., none of which can fully undo the

strength and deformability deprecation of the reinforcement, whereas with the exception of cathodic protection, most of these methods can't mitigate future corrosion development. There also are various strengthening methods for deficient structural members, such as the use of Fiber Reinforced Polymers (FRPs), steel jacketing, etc. all of which are addressed in the literature review. Nonetheless, none of the strengthening methods alleviate the future occurrence of reinforcement corrosion. This dissertation proposes a strengthening method that both significantly improves the performance of the structural member and mitigates future corrosion ingress.

1.2 Research Objectives and Significance

In a built environment where reinforced concrete is a predominant construction material, structural engineers are challenged with a tri-faceted problem with grave societal significance: Reinforced concrete structures, with poor detailing, exposed to corrosion for a long time, nearing the end of their design service life, and representing an irreplaceable investment on behalf of society that houses a significant fraction of the worlds' population, and serves the lifelines that enable the world economy.

This dissertation aims at tackling two practical components of the corrosion problem: First, an analytical study that addresses the needs of strength assessment of corroded members/structural systems, second, an experimental investigation that focuses on developing and proof-testing a retrofitting methodology that not only strengthens deficient structural members, but also eliminates the future progression of corrosion in the repaired member.

1.3 Thesis Organization

Chapter 2 provides a literature review of the behavior of reinforced concrete under various conditions and examine retrofitting strategies implemented by researches before us. Chapter 3 is the first portion of the analytical segment of the report, and presents the numerical modeling of corroded members. A thorough database on tested corroded reinforcement was assembled from the literature, wherefrom expressions for residual reinforcement material properties were formulated. These expressions allow the user to calculate residual reinforcement material properties using one variable: the reinforcement mass loss percentage. A detailed numerical procedure was also proposed using these and other expressions from the literature to facilitate finite element modeling of reinforced concrete members (taking corrosion damage into

consideration). The modeling procedure was validated and compared to other methodologies from the literature, and it was found that this work's proposed methodology yields more accurate results.

The second portion of the analytical segment of the report addresses modeling of corroded structural systems and is presented in Chapter 9. A database of tested corroded columns was assembled, from which reduction factors to columns mechanical properties (i.e stiffness, strength and ultimate deformation capacity) were formulated. These reduction factors are used to quickly estimate the residual resistance curves of corroded RC members. The importance of these factors lies in their serviceability. Assessment guidelines such as ASCE 41-17 and EC8-III only advise on calculating resistance curves of structural members without taking corrosion damage into consideration. Using the obtained reduction factors, engineers can estimate the residual resistance curve of corroded members and use the results in the form of plastic hinge properties in assessing a structural system on software such as SAP2000 or ETABS.

In the experimental segment of the report, the first step was studying the state-of-the-art of retrofitting corroded columns. It was found that none of the existing retrofitting strategies was able to both strengthen the member and suppress future development of corrosion.

Chapter 4 addresses the first experimental program's objective, which was to determine whether UHPC improves reinforcement durability and how effective the protection is in the presence of service cracks. The experimental program was able to prove that reinforcement embedded in un-cracked UHPC does not corrode at all, while in the presence of service cracks there was minimal corrosion development. UHPC, compared to normal concrete and other SHCC showed significant ability in suppressing corrosion development.

Chapter 5 addresses the second objective, which was studying the tension stiffening characteristics of UHPC engulfing corroded reinforcement. Tension stiffening properties of un-cracked and cracked UHPC was examined, along with several other parameters such as cover thickness, presence of corrosion and type of reinforcing fibers. Strain measurements were calculated using Digital Image Correlation (DIC) technology.

Finally, Chapters 6, 7, and 8 provide the main experimental program of the dissertation, which was studying the effectiveness of UHPC jacketing in both repair and strengthening of corroded lap-spliced columns. Six columns were designed based on pre 1970s design standards and were

subjected to artificial corrosion conditioning. Variables of the study were column height, number of reinforcement and bar diameter type. Some columns were tested pre-strengthening to simulate a repair job post-seismic event while others were strengthened before being tested. Results showed that UHPC was able to significantly improve the seismic behavior of strengthened and repaired columns. It was able to convert the failure mode of columns from a brittle shear failure or a bond/anchorage failure to a ductile seismic resistant column.

2. Literature Review

This chapter reviews past research conducted on corrosion science from a structural perspective. First, the mechanism of steel corrosion is reviewed, followed by an outline of the damaging effects of corrosion on mechanical strength of reinforcement and its effect on the overall structural behavior of reinforced concrete members. Furthermore, the final section of this chapter includes the state-of-the-art methods of retrofitting corrosion-affected, deficient structural members.

2.1. Steel Corrosion Mechanism

Corrosion of steel in concrete is an electrochemical process which requires the presence of an anode and a cathode. It is the same electrochemical process that occurs in a galvanic cell. However, in the case of reinforced concrete, the bar itself is the anode and the cathode. In order for corrosion to arise (without an impressed current), there should be two half-cell reactions: an anode which produces electrons and a cathode that receives the electrons. These two half-cells should be connected via a metallic conductor (reinforcement bar) to facilitate the transfer of electrons and there should be an electrolyte conductor (concrete pore solution) to act as a medium for the transfer of ions as presented in Figure 2-1.

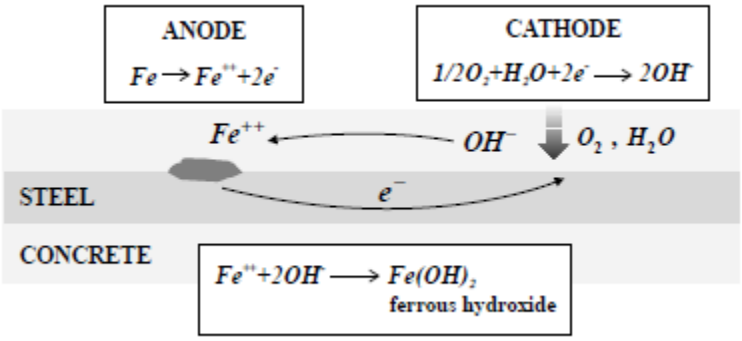

Figure 2-1. Corrosion Cell in Reinforced Concrete (Martín Pérez, 1999)

Corrosion begins when there is a difference in electrochemical potential because of any non-uniformity within the bar. Difference in potential occurs in many cases such as, having two different metals in concrete or if the pore solution along the steel-concrete interface has large differences in ion concentrations. At the anode, depending on the pH of the pore solution, existence of aggressive anions and the presence of an electrochemical potential at the steel surface, the probable anodic reactions are (ACI 222R-19, 2019):

$$Fe \rightarrow Fe^{2+} + 2e^- \quad (2\text{-}1)$$

$$2Fe^{2+} + 4OH^- \rightarrow 2Fe(OH)_2 \quad (2\text{-}2)$$

$$2Fe(OH)_2 + 0.5O_2 \rightarrow 2FeOOH + H_2O \quad (2\text{-}3)$$

$$Fe + OH^- + H_2O \rightarrow HFeO_2^- + H_2 \quad (2\text{-}4)$$

While at the cathode, depending on the pH of the pore solution and the availability of O_2 molecules, the probable cathodic half-cell reactions are:

$$2H_2O + O_2 + 4e^- \rightarrow 4OH^- \quad (2\text{-}5)$$

$$2H^+ + 2e^- \rightarrow H_2 \quad (2\text{-}6)$$

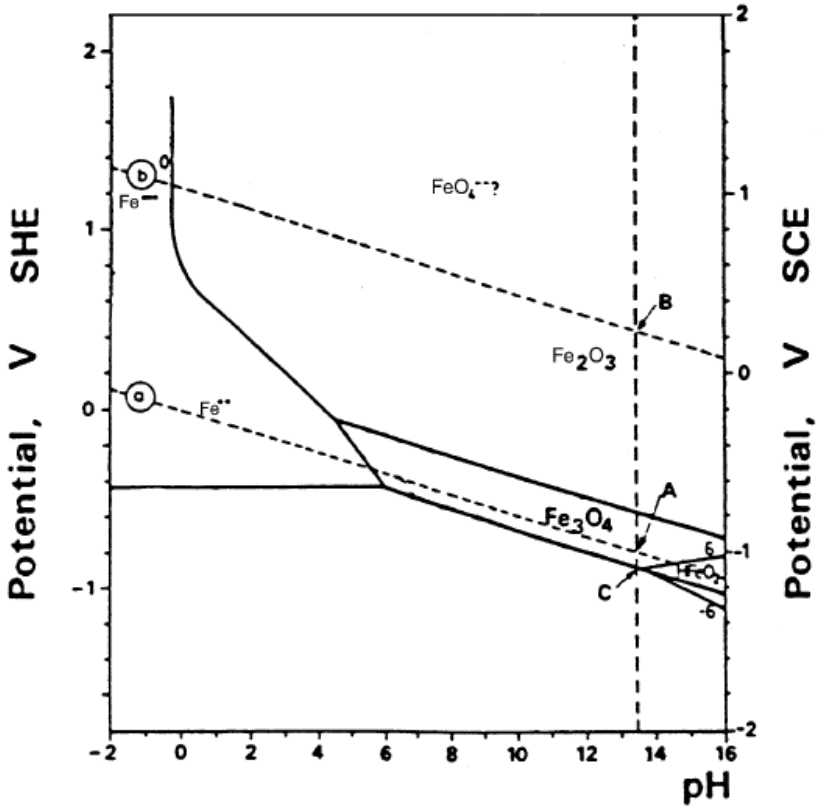

Figure 2-2. Potential pH Ranges of Stability of the Different Phases of Iron in Aqueous Solutions (Pourbaix, 1974).

The Pourbaix diagram in Figure 2-2 outlines the thermodynamic regions of stability for each element involved in the reactions mentioned above as a function of pH of the pore solution and

the potential. If concrete pore solution has a pH of 13-13.5, the most probable anodic half-cell reactions would be Equation (2-1) and Equation (2-2). If no other factors are introduced such as iron oxides (Fe_3O_4 and Fe_2O_3) and hydroxides, the compounds will form solids and might create a passive film around the bar. For Equation (2-3) to take place, pH of the concrete should be in its normal state (pH 13) but under high temperature (>60^oC) whereas pH should be raised for Equation (2-4) to take place (Townsend, 1972).

If the potential is lower than the upper dashed line, reaction given by Eq. (2-5) occurs, whereas if the potential is below the lower dashed line, Eq. (2-6) governs. Electrons released from iron atoms, are transferred from the anode to the cathode through the bar, while ferrous ions dissolve into the pore solution. If enough oxygen is present at the anode, ferrous hydroxide could oxidize into other corrosion products. As ferrous hydroxide transforms into higher oxides, the volume of the newly oxidized corrosion products increases as established in Figure 2-3. The increase in volume causes radial pressure around the bar in the concrete. The tensile stresses generated could cause cracking and spalling of the concrete cover if they exceed the tensile strength of concrete.

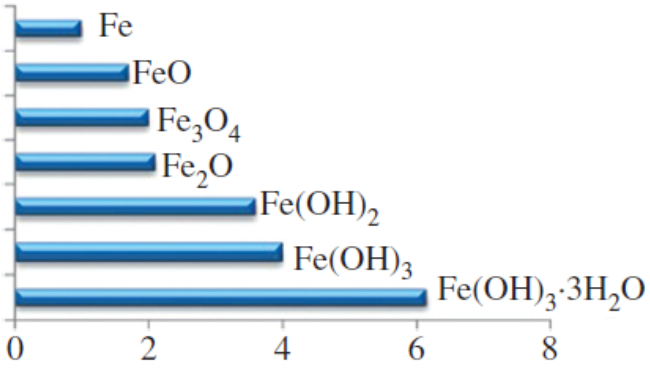

Figure 2-3. Relative Volume Ratio for Various Ferrous Oxides (Pantazopoulou et al., 2019).

2.1.1. Pitting & Uniform Corrosion

If the half-cell reactions along the bar are separated by small distances, they are called microcells and cause uniform general corrosion. This occurs when a uniform de-passivation of the protective film surrounding the reinforcing bar takes place, which is the case in which the concrete cover undergoes carbonation. If the half-cell reactions are located further apart, they are termed macro cell, and are known to cause pitting corrosion. This phenomenon occurs when a differential of

potential is established between a large cathodic area and a relatively small anodic site in the presence of high concentration of chloride ions.

Pitting corrosion is the occurrence of a significant localized loss in cross-sectional area, its dangers are that it is hard to detect, does not produce stains on the concrete surface, and is hard to predict and design against. The significant localized area loss dramatically decreases the flexural/tensile strength of a member and leads to brittle failure. This is mostly critical for pre-stressed members where tendons are under a constant stress which might lead to the sudden rupture of a wire (i.e. stress-corrosion, Morandi Bridge, Genoa, Italy 2018). General corrosion on the other hand, causes insignificant reduction in bar's cross-sectional area. However, it decreases the bars' bond strength radically changing (in some cases) the failure mode from flexural to anchorage failure.

2.2. Effect of Corrosion on the Mechanical Properties of Reinforcement Bars

Due to the negligible tensile strength of concrete, longitudinal reinforcement bars are used mainly in the tension zone of RC sections. The steel reinforcement adds to the ductile behavior of RC members and serves as an energy dissipating system in case of dynamic excitations. Thus, it is critical to understand the effect of corrosion on the reinforcement's mechanical properties. Allamt *et al.*, (1994) conducted an experiment on six reinforcement bar types: 3 hot-rolled and cold-straightened (8, 10 and 12 mm diameters) and 3 hot rolled only (12, 16 and 32 mm diameters). Bars were corroded under natural conditions for a duration of 16 months and then underwent a tensile test. It was concluded, due to the minimal weight loss experienced in 16 months of natural corrosion, that the tensile strength and ductility of reinforcement were not affected by corrosion However, Almusallam, (2001) investigated the residual mechanical properties of corroded reinforcement and found otherwise. The experiment consisted of testing steel bars with 6 mm and 12 mm diameters that were embedded in concrete specimens. The accelerated corrosion method incorporated was the impressed current method with a current density of 200 $\mu A/cm^2$. The concrete cover of specimens was immersed into a 5% sodium solution. After the end of the corrosion process, reinforcement was cleansed using Clarke's Solution and then subjected to a tensile test. A negligible increase in the true tensile strength of corroded bars was observed (using minimum bar area), while the nominal tensile strength (using the nominal bar area) radically decreased reaching 16% of residual strength at 80% corrosion. Palsson and Mirza, (2002) studied the mechanical response of corroded reinforcement bars of the abandoned Dickson Street Bridge

located in Montreal, Canada. A total of 103 specimens were gathered, each with a length of 250 mm. Specimens used in the tests were not mechanically damaged nor having any severe cross-sectional losses at the ends to ensure optimal gripping.

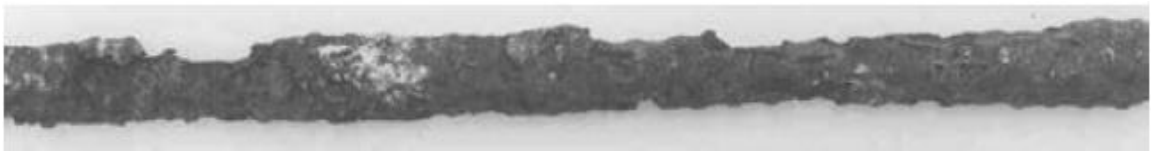

Figure 2-4. Sample Specimen from Abandoned Bridge in Montreal, Canada (Palsson and Mirza, 2002b).

Figure 2-4 shows a sample of a naturally corroded bar. A dramatic decrease in structural toughness was reported to be caused by the intense pitting corrosion. The loss in fracture energy was followed by a loss in tensile strength caused by the decrease in cross-sectional area. It was found that a 20% relative difference in area between the largest and smallest sections resulted in a 50% reduction in the strain at failure. Du et al., (2005) investigated the effect of reinforcement corrosion and compared results between two categories, i.e., bare bars and bars embedded in concrete. Each category contained plain and ribbed bars of various sizes which were corroded by impressed current using various current densities. It was found that the nominal yield and ultimate strength of corroded reinforcement reduced dramatically; this reduction was much faster when comparing pitting corrosion to uniform general corrosion. It was also found that for the same corrosion level, bare and embedded bars had similar behavior and that the type of bars (plain or ribbed) had an insignificant role on the behavior of corroded bars. Apostolopoulos, (2007) studied the mechanical properties of corroded S500s Tempcore steel using direct tension and low cycle fatigue tests. Seventy-five specimens were tested, of which 12 were direct tensile tests, and the rest were low cycle fatigue tests. Specimens were artificially corroded by exposure to salt spray for various periods of time (10 to 90 days). The results showed that with increasing corrosion, S500s Tempcore steel undergoes a drastic reduction in ductility and in the number of cycles to failure under low cycle fatigue. A significant drop in tensile strength was also observed. It was concluded that the service life of aged reinforced concrete structures in seismic areas is severely impacted by corrosion and that the degradation in material should be considered in future seismic evaluation guidelines. Experiments on BSt 420 steel, where bar specimens were corroded by salt spray

exposure for various periods showed direct correlation between exposure period, mass loss, and reduction in tensile strength and in ductility Apostolopoulos and Papadakis, (2008). Lee and Cho, (2009) investigated quantitatively and experimentally the relationship between the mechanical properties of reinforcement bars and the amount of corrosion. It was found that chlorine induced corrosion results in pitting, whereas the electrical corrosion method (Galvano static corrosion without the addition of chlorine) results in a uniform corrosion. The nominal yield, ultimate strength, yield strain, and ultimate strain decreased as corrosion increased; however, the effect of corrosion on the ductility was much higher than its effect on strength.

Experiments comparing the static tensile and high cycle fatigue behavior of artificially corroded and naturally corroded bars showed significant reduction in ductility and strength of reinforcement, with the reduction in ultimate strength being higher than that of the yielding strength (Zhang *et al.*, 2012). It was also reported that the fatigue life was affected by corrosion more than the tensile strength and that it decreased radically as corrosion increased. Results from artificially corroded bars were more conservative than those of naturally corroded bars and the cause was attributed to the difference in corrosion distribution along the bar. A concept called equivalent cross-sectional area was introduced to quantify the influence of corrosion on the tensile and fatigue life of corroded bars. A model for calculating the fatigue life of corroded bars considering joint effects of degree of corrosion and the stress range of fatigue loading was also proposed.

A long-term project that began in 1984 at Laboratoire Matériaux et Durabilité des Constructions at INSA-Toulouse in France examined the effect of simulated natural corrosion environment (salt fog) using reinforced concrete beam specimens. Corrosion appeared randomly along the length and perimeter of the embedded beam bars. Two methods of determining the residual bar diameter were used, the first using a Vernier Caliper and the second from the mass loss using Eq. 2-1.

$$\%d = 100\left[1 - \sqrt{1 - \frac{\Delta M}{M_0}}\right] \tag{2-1}$$

Where, %d is the percentage of diameter loss, ΔM is the mass loss and M_0 is the original mass of steel. The residual cross-sectional area was best approximated when using the residual diameter calculated from the mass loss. Surprisingly it was concluded that the true yield stress (calculated from the tensile force and the true reduced cross-sectional area) was constant with the increase in corrosion level, however the true ultimate stress appeared to increase with the level of corrosion.

It was also reported that the maximum elongation decreased drastically with the increase of corrosion level which led to a significant effect on the structural reliability (François, Khan and Dang, 2013). Simulated corroded bars were used to model the area reduction of actual corroded bars. Simulation of bar area loss was affected by sawing off parts of the cross-section. Three forms of simulated corrosion were adopted and are shown in Figure 2-5 below.

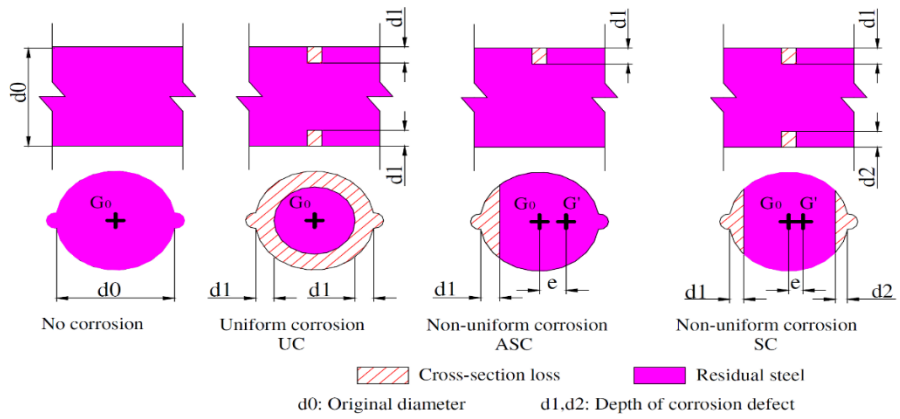

Figure 2-5. Different Forms of Simulated Corrosion (Zhu and François, 2014)

Results from static tensile tests showed that both naturally corroded and simulated corroded bars maintained their true natural yield strength which brought the authors to the conclusion that using the mass loss to determine the area loss on small pieces of bars is a relevant method to calculate the effective residual cross-section (Zhu and François, 2014). The true ultimate strength measured of naturally corroded bars was higher than that of the simulated corroded bars, while the simulated corroded bars maintained their original true ultimate strength. The discrepancy was attributed to the heterogeneous shape of the naturally corroded steel's cross-section along the bar's length which creates eccentricities. Ductility was also found to be mostly affected by corrosion and mainly by the geometry of the pit; concentric cross-section loss simulating a uniformly corroded bar showed higher ductility than the non-uniform area-loss arrangement. Some of the corroded bars' ultimate strain fell below Eurocode 2 requirements and should be avoided as it might result in pre-mature brittle failure, or it would fail in forming a plastic hinge and not absorb the required deformation energy in case of earthquakes.

A large test program on 40 corroded bars under monotonic loading and 140 corroded bars under fatigue tests showed that the nominal yield and ultimate stresses measured under monotonic loading were highly dependent on the corrosion degree (Fernandez, Bairán and Marí, 2015). The

modulus of elasticity and ductility showed a higher dispersion in results in comparison with yield and ultimate strengths. Premature failure in specimens occurred due to the high decrease in ductility. The mechanical properties were found not to be only related to the corrosion degree. There was a high influence from different parameters, such as stress concentration, non-homogeneity of steel bar's properties, and shifting of the center of gravity of the cross-section due to the non-uniformity of mass loss along the bar. Pit depth showed a greater effect on fatigue life than the pit length, the pit length having an effect for fatigue life only when the length/diameter ratio was smaller than 2. It was also found that the fatigue life of highly corroded bars was severely reduced regardless of the stress range applied.

The effect of corrosion on rebars embedded in concrete beams that were pre-cracked with several different crack widths was studied using a two phase corrosion process: a three-year period of wetting and drying in a 5% NaCl solution followed by a one-year long phase of natural corrosion by watering (Lu *et al.*, 2016). From visual inspection, it was reported that the concrete cover and crack width highly affected the diameter loss along the bar especially since localized corrosion was found at the location of cracks. Nominal yield and ultimate strengths decreased linearly with corrosion intensity, with natural pitting corrosion having a more dramatic effect on tensile strength than that of corrosion caused by impressed current. The reduction of maximum elongation and total energy was even greater and residual properties did not meet the code requirements.

2.3. Effect of Corrosion on Bond Strength

Bond between reinforcement bars and surrounding concrete is essential for composite action of reinforced concrete and bar development. Bond stresses effect the force transfer from the reinforcing bar to concrete through the following three mechanisms of resistance: chemical adhesion, friction, and mechanical interlock. Of those, chemical adhesion is usually neglected due to its small contribution to the bond strength of reinforcement bars, particularly in the case of corrosion as it breaks down at infinitesimal slip magnitudes.

Investigations on the effect of corrosion on bond strength of bars was initiated a couple of decades ago. From the first published research on the topic it was observed that slight amounts of corrosion may increase the bond strength but for higher corrosion intensities bond strength deteriorates rapidly with increasing corrosion (Al-Sulaimani *et al.*, 1990); these results were confirmed by several follow-up investigations (Almusallam *et al.*, 1996; P. S. Mangat and Elgarf, 1999; Stanish

et al., 1999; Zhao *et al.*, 2013). It was postulated that corrosion has no negative effect on bond strength as long as there are no visible longitudinal cracks in the cover initiated by corrosion (fib bulletin #10, 2000). At low levels of corrosion, rust increases the roughness of the bar. The corrosion products, having a larger volume than steel, exhibit an expansive pressure on the bar-concrete interface; these two effects cause an increase in the frictional mechanism of the bond strength. However, when the expansive pressure resulting from the corrosion products exceeds the tensile strength of concrete, cracking occurs, and the bond strength is decreased significantly (Tastani and Pantazopoulou, 2007).

Figure 2-6 shows the variation of relative bond strengths as a function of the degree of corrosion quantified by the percentage of bar mass loss (η) (Lin *et al.*, 2019). All filled dots in the Figure refer to confined specimens using stirrups while the rest were unconfined. A general trend could be easily identified for the unconfined specimens, where bond strength increases initially and then decreases dramatically. But a discrepancy is identified in terms of the critical corrosion level (when the relative bond strength drops below 1), ranging between 0.3% and 4.8%. The scatter could be attributed to the different materials used, specimen dimension, corrosion method, current densities, test setup, and loading procedures used (Lin *et al.*, 2019).

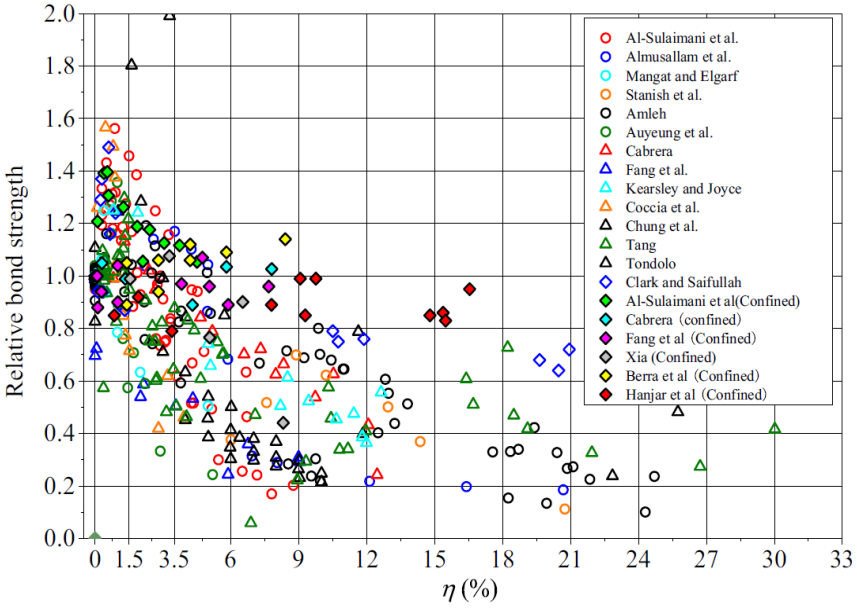

Figure 2-6. Relative Bond Strength with Increasing Degrees of Corrosion (Lin *et al.*, 2019)

2.3.1. Bond and Lateral Confinement

Lateral confinement greatly influences the bond strength of both corroded and non-corroded bars. Confinement could be contributed by concrete cover, stirrups, or externally applied confining pressures (FRP or steel jacketing) (Tepfers, 1979; Harajli, 2004; Li *et al.*, 2016).

2.3.1.1. Concrete Cover

Concrete cover thickness has a strong influence on bond strength of non-corroded bars since cover splitting failure limits the development capacity. It has been observed that concrete cover thickness also influences the bond strength of corroded bars prior to cracking (Li *et al.*, 2016). For large concrete covers, an influence of the cover on the bond strength is also observed after crack initiation. Experimental evidence shows that even at high degrees of corrosion, specimens with large covers had a higher bond strength than specimens with smaller covers (Al-Sulaimani *et al.*, 1990; Amleh, Mirza and Ahwazi, 2000); even after cracking, some cover confinement still exists because concrete does not lose instantaneously all of its tensile strength as shown in Figure 2-7.

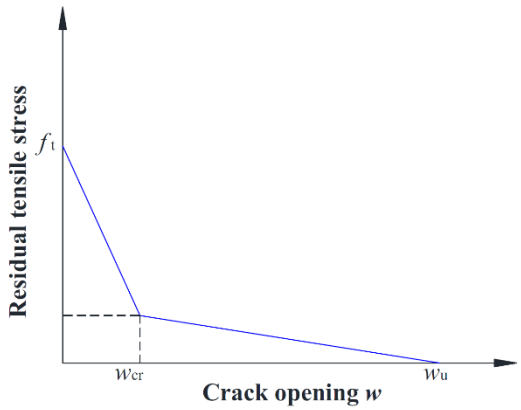

Figure 2-7. Stress-Crack Opening Relationship for Uniaxial Tension of Concrete (fib Model Code, 2010)

2.3.1.2. Un-corroded Stirrups

Most bond tests in the literature involve unconfined specimens which is not the case in the majority real life structural members. It has been shown that confinement greatly influences the bond strength and bond stress-slip relationship especially in the presence of corrosion. Corrosion does not affect much the bond strength in the presence of un-corroded stirrups (Fang *et al.*, 2004; Fischer, Ozbolt and Gehlen, 2010), but rather, bond strength may even increase in the presence of

such stirrups as opposed to unconfined specimens (Rodriguez and Ortega, 1994; Hanjari, Coronelli and Lundgren, 2011, Berra, Castellani and Coronelli, 1997).

2.3.1.3. Corroded Stirrups

The above observations apply to lab experiments or cases where stirrup replacement has been implemented for retrofits. In actual structures, however, stirrups tend to corrode prior to the longitudinal bars due to their proximity to the concrete surface and are usually more heavily damaged than longitudinal bars because of their smaller diameter size (Tastani and Pantazopoulou, 2007; Fu *et al.*, 2017). The chemical composition of stirrups also affects the corrosion process. Since stirrups are made of mild steel and longitudinal bars are made of low alloy steel that allows the occurrence of a macro cell formation, stirrups act as anodes and the main bars act as cathodes. Flexural cracks also increase the corrosion process of stirrups where corrosion byproducts having a larger volume than steel increase the crack widths also quickening the corrosion rate. Pull out tests on confined specimens having corroded stirrups and longitudinal bars have shown that even corroded stirrup confinement may engage a greater bond resistance in the encased longitudinal bars as compared to unconfined specimens (Tondolo, 2015); but in fact, a reduction in bond strength in specimens with corroded stirrups as compared to uncorroded stirrups has been observed, especially at high degrees of corrosion (Hanjari, Coronelli and Lundgren, 2011; Coronelli, Hanjari and Lundgren, 2013).

2.3.1.4. Effect of fiber reinforced polymers (FRPs) on bond of corroded reinforcement

FRP wraps have been increasingly used for structural purposes due to their high strength and the ease of application. With regards to corrosion, FRP wraps have been claimed to act as a barrier that obstruct the ingress of corrosive agents decreasing the corrosion rate, providing passive confinement and impeding any crack propagation of concrete cover. Experiments have shown that confinement effected by CFRP wrapping increased the bond strength of bar anchorages, delayed the onset of bar slip, and changed the failure mode from splitting to a ductile pullout mode (Soudki and Sherwood, 2003). Pull out-out tests conducted on pre-repaired and post-repaired CFRP strengthened specimens showed an increase in bond strength at medium and high degrees of corrosion. It was also noticed that strengthening prior to the initiation of corrosion and having large

diameter bars allow the CFRP wrapping to have a greater impact on bond strength as can be seen in Figure 2-8 (Papakonstantinou, Balaguru and Auyeung, 2011).

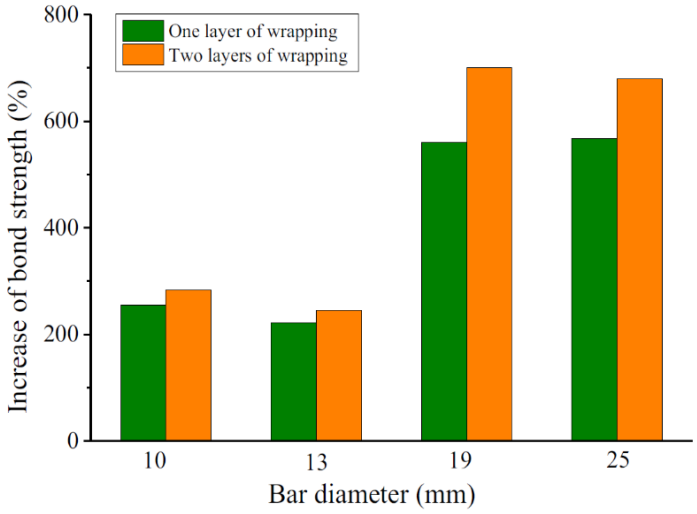

Figure 2-8. Increase of Bond Strength due to CFRP Strengthening (Papakonstantinou, Balaguru and Auyeung, 2011).

2.3.1.5. Fiber Reinforced Concrete

Fiber reinforced concrete (FRC) outperforms normal concrete especially when it comes to the intrinsic ductility of the material in tension, suppression of cracking, and maintaining bond strength. Bond strength of corroded bars embedded in concrete containing synthetic fibers perform better than plain concrete specimens at different corrosion degrees (Al-Sulaimani *et al.*, 1990); corrosion induced cracking was delayed, and bond strength was increased at late stages by about 85% (Haddad and Ashteyate, 2001). Relevant studies using steel fibers, polyvinyl alcohol fibers, nylon fibers, and polypropylene fibers reported concurring findings for all fiber types (Xu and Cai, 2010; Berrocal *et al.*, 2017; Farhan, Sheikh and Hadi, 2018). Corrosion of bars embedded in FRC does not affect the bond strength prior to 10%-15% mass loss, but the benefits of fiber reinforcement aren't apparent in specimens having large cover to diameter ratios (Hou *et al.*, 2017).

2.4. Effect of Corrosion on Flexural and Shear Response of RC Beams

2.4.1. Flexural Behavior of Corroded Beams

The effect of corrosion rate on the flexural behavior of RC beams in terms of strength and ductility has been studied experimentally. It was observed that a 10% mass loss of main reinforcement bars using a current density of 2000 $\mu A/cm^2$ results in a 60% reduction in flexural strength and a 77% reduction in deformation capacity. However, a 10% mass loss of main reinforcement bars attained by a current density of 4000 $\mu A/cm^2$ led to a 70% reduction in flexural strength and a 77% reduction in deformation capacity. This could be attributed to the larger cracks in concrete cover resulting from higher corrosion rates which reduce the concrete's compressive strength (Mangat and Elgarf, 1999).

Beams that were conditioned in an artificial climate to induce corrosion for 14 years under flexural loading demonstrated 35% reduction in flexural strength and around 70% reduction in deformation capacity after reaching a 20% mass loss. It was concluded that for adequately anchored longitudinal bars, the flexural strength of corroded beams is controlled by the reduction in diameter of the bars and not by the loss of bond strength (Castel, François and Arliguie, 2000).

Cyclic load tests on cantilever beams having undergone various degrees of transverse reinforcement mass loss percentages (1.7%, 3.08%, 4.08%, and 8.03%) led to flexural failure except for the 8.03% mass loss case (Ou and Chen, 2014). Flexural cracks progressed through the section with increasing drift ratio. Cover spalling occurred at 3% drift and buckling of main reinforcement occurred at 5% drift which also lead to crushing of core concrete. For lightly corroded beams (<5% mass loss) reduction in load carrying capacity began after reaching 4% drift and no bar fracture was observed throughout the tests. However, the mode of failure of the beam having 8.03% mass loss switched to flexural-shear failure, and the maximum strength was reached at only 0.8%.

Studies on the effect of sustained loading on corrosion rate in beams showed that the rate of cover cracking caused by corrosion increased by around 22% in the loaded beams as opposed to the unloaded ones. A linear relationship was found between area loss caused by corrosion of the longitudinal reinforcement and the residual flexural capacity of the beams. The largest implication of corrosion found was its effect on the drift ratio ductility of the beams, especially when the mass

loss was greater than 15%, where severe pitting corrosion was recorded. There is evidence that the most severe impact on the load carrying capacity of corroded RC beams is the maximum pitting depth rather than average corrosion penetration (Torres-Acosta, Navarro-Gutierrez and Terán-Guillén, 2007). Concrete cover cracking caused by corrosion was more intense in dry environments as opposed to wet environments despite that a wet setting accelerates pitting corrosion. The experimental results indicated that a 10% mass loss of longitudinal reinforcement resulted in 60% reduction of a beam's flexural capacity.

The effect of corrosion of high-ductility smooth reinforcement on the flexural behavior of beams was studied for mass loss fractions in the range of (4%-10%) (Cairns, Du and Law, 2008). It was found that the failure modes of the beams weren't very much affected and that corroded specimens had a higher flexural strength than the non-corroded specimens. This is due to the increase of bond strength between the plain round bars and the concrete caused by the pressure created by corrosion products along the bar and especially in the anchorage region. Corroded 26-year-old short beams conditioned under simulated corrosion climate that simulated the effects of service life exposure was studied under three-point bending (Zhu *et al.*, 2013). It was found that the corroded beams' failure mode shifted from brittle shear to a ductile flexural mode of failure. Corrosion was not constant over the length of the beam, even though there were corrosion induced cracks and concrete spalling near the supports. (Note that in the study considered sufficient bar anchorage was provided to support the flexural failure.)

Four groups of two-span beams (indeterminate members) under different levels of corrosion were also considered (Fernandez *et al.*, 2018). Group 1 had 10% mass loss, Group 2 had 15% mass loss, Group 3 had 20% mass loss, and Group 4 comprised un-corroded beams. Each group had three replicas corroded while subjected to service load. It was found that simultaneous presence of loading increased the corrosion rate and developed premature brittle failures by longitudinal splitting. Tests on several specimens conditioned in a chloride environment for years showed that about 1% of cross-sectional loss of main reinforcement led to about 1% decrease in yield strength and around 0.85% decrease in ultimate strength, whereas the maximum area loss of main bars was around 1.85% on average, per year (Zhu and François, 2014).

In the absence of any shear reinforcement, RC beams developed shear strength that was reduced by 60% relative to the uncorroded condition (Al-Saidy *et al.*, 2016). Corroded beams containing

transverse reinforcement lost strength but still had a ductile failure, the reduction in ultimate deflection reaching 25% for beams having 7.5% mass loss of the main bars. Similar strength losses were reported by other experimentalists (Fernandez *et al.*, 2018); so reductions in the order of 55% of load baring capacity of unconfined beams and 26-39% for confined beams were observed for corrosion levels between 15-39%. Tied beams that did not fail prematurely exhibited up to 30% higher redistribution of internal moments than un-corroded beams; it was determined that structural redundancy (indeterminacy) has an indirect beneficial structural outcome opposing the destructive effect of corrosion; however, in the case of pitting corrosion a 56% reduction in load bearing capacity was seen. The governing aspect of load bearing capacity was the deprecation of reinforcement to concrete bond: all levels of corrosion led to a commensurate decay in bond strength which controlled the failure mode.

The effect of corrosion on different forms of detailing which included over-reinforced, balanced reinforced, under-reinforced, and severely under-reinforced beams was also explored (Du, Clark and Chan, 2007). They observed that corrosion alters the failure modes of beams, where the over-reinforced corroded beams' failure mode changed from brittle to a less brittle or ductile manner, whereas in the case of under-reinforced beams, the failure mode became less ductile or brittle, owing to the reduction in elongation capacity of corroded reinforcement. Pre-mature rupture of reinforcement was reported for mass losses over 10% in severely under-reinforced beams.

A collection of corroded and un-corroded beams with different cross-sectional dimensions and rebar diameter size were tested under four point loading (Azad, Ahmad and Al-Gohi, 2010): it was observed that for slightly corroded beams (< 10% mass loss) the beam strength was governed by the residual cross-sectional area of reinforcement bars, whereas for higher mass loss fractions, residual flexural strength was affected by many factors including bar pitting, reduced bond strength and concrete damage. It was also found that corroded beams undergo larger deflections as opposed to beams in pristine condition which could be attributed to the degradation of flexural stiffness. It was seen that the mass loss of small and large bars isn't equal, with larger diameter bars undergoing a smaller mass loss.

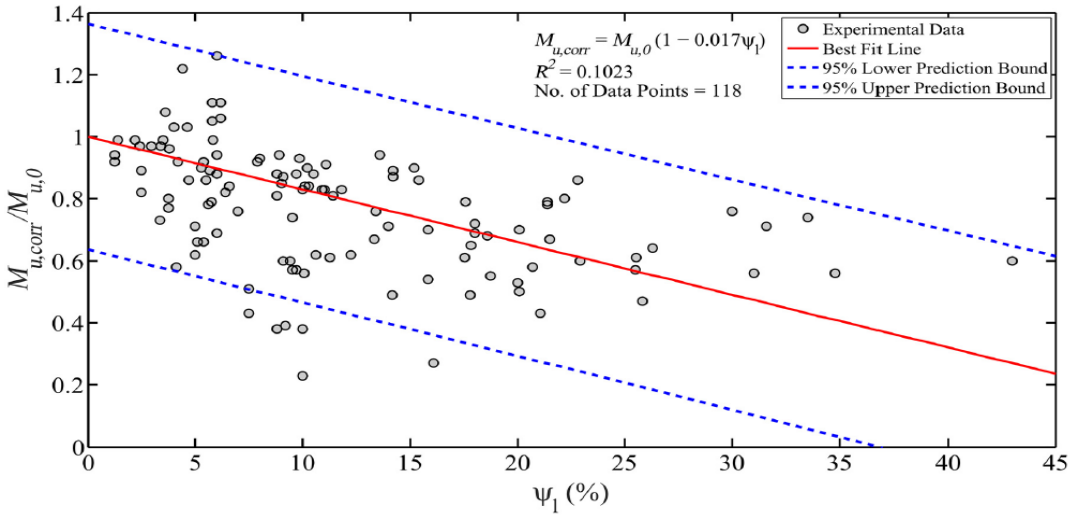

Figure 2-9. Impact of Longitudinal Reinforcement Corrosion on Residual Moment Capacity (Kashani, Maddocks and Dizaj, 2019)

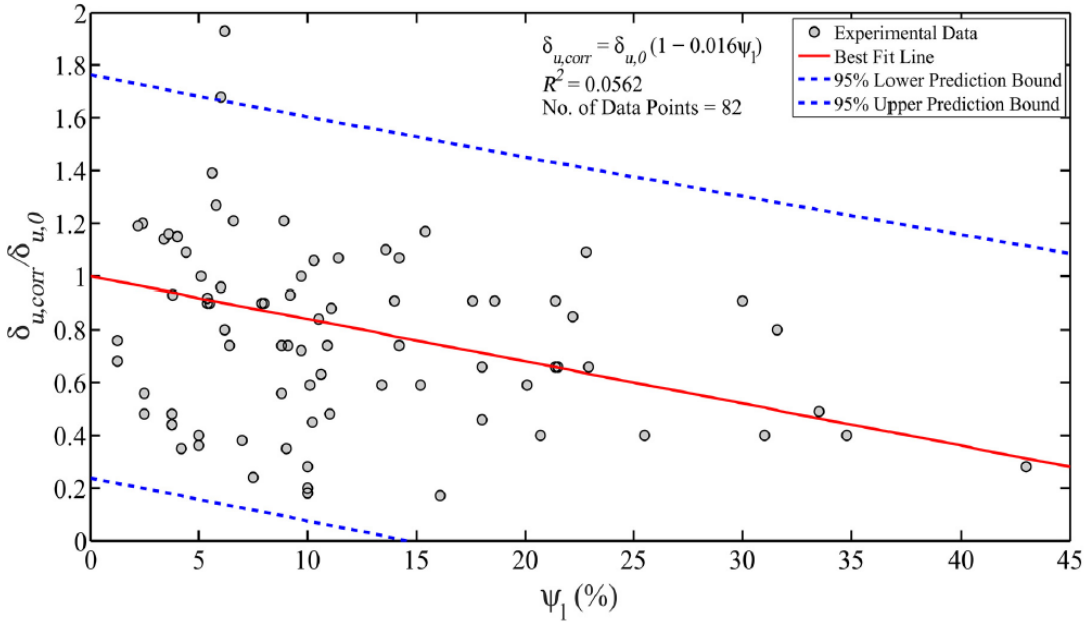

Figure 2-10. Impact of Longitudinal Reinforcement Corrosion on Residual Maximum Deflection Capacity (Kashani, Maddocks and Dizaj, 2019)

Figures 2-9 and 2-10 show the effect of corrosion on RC beam's residual moment capacity and maximum deflection capacity. Where $M_{u,0}$ and $\delta_{u,0}$ are the ultimate moment capacity and maximum deflection capacity (respectively) of an RC beam in pristine condition, $M_{u,corr}$ and $\delta_{u,corr}$ are the ultimate moment capacity and maximum deflection capacity (respectively) of a corroded RC beam and $\Psi_1(\%)$ is the mass loss in percent. Both figures clearly illustrate the decline in residual moment

and deflection capacity as corrosion increases. The scatter of results is due to the different corrosion conditions and test setups followed in each experiment.

2.4.2. Shear Behavior of Corroded Beams

In structural members, stirrups are the first to face corrosion because of their proximity to the exposed free face as opposed to the main reinforcement bars, whereas it was stated earlier that smaller sized bars corrode faster than larger bars. It is therefore expected that corrosion might have a greater impact on the shear strength rather than the flexural behavior of beams. An experimental investigation was conducted on three different types of corroded RC beams (Rectangular, T-Sections and inverted T-Sections) where only the transverse reinforcements had been corroded by accelerated conditioning while the main reinforcements was epoxy coated (Higgins and Farrow, 2006); benchmark mass loss factions were: 12% mass loss for light damage, 20% mass loss for moderate damage, and 40% mass loss for severe damage. It was reported that diagonal shear cracking occurred at lower levels of load than in the case of un-corroded identical elements, whereas corroded stirrups were not able to restrain the cracks. Beams with high degrees of corrosion formed severe pits and developed a brittle failure after the onset of diagonal shear cracks.

A similar experimental investigation on 17 reinforced concrete beams with different variables including type of transverse reinforcement, corrosion degrees, and repair availability was conducted whereby only the transverse reinforcement was corroded and the main reinforcement was epoxy coated for protection (Alaskar, 2013). It was observed that 8% mass loss results in an increase in shear strength; this could be attributed to the increase of bond strength caused by corrosion products. For higher corrosion rates, a linear reduction in shear strength was seen, where 15.6% mass loss resulted in 14.4% decrease in shear capacity. In the case of deep beams with corroded shear reinforcement, it was found that a 20% mass loss in shear reinforcement led to a 53% reduction in ultimate shear capacity of the beams, while decreasing the shear span-to-depth ratio of beams intensified the shear strength loss (Suffern, El-Sayed and Soudki, 2010). The shear behavior of beams having a shear span to effective depth ratio of 1.75 and corroded stirrup and inclined bars was also considered (Wang *et al.*, 2015): It was found that a mass loss less than 10% had minimal influence on the shear strength but a profound influence on stiffness due to corrosion cracking; for higher mass loss ratios, there was a clear decrease in shear capacity. Failure modes were not affected, but ductility was reduced by premature rupture of bars.

Another study illustrated that the mechanism of shear failure is also affected by corrosion (Xia, Jin and Li, 2011). Un-corroded beams failed in shear by concrete crushing in compression while corroded beams fail in shear by the rupture of shear reinforcement. Mass loss in shear reinforcement more than 10% resulted in a substantial reduction in shear strength. Beams designed to fail in shear prior to reaching their flexural strength were also examined under three-point loading, where one shear span was heavily shear-reinforced to ensure failure in the other shear-span (El-Sayed et al., 2016). Variables were spacing of shear reinforcement (three different spacings) and the corrosion degree (two degrees). It was found that up until 7.2% mass loss, no shear strength reduction was recorded. The residual relative shear strength was estimated based on crack width instead of mass loss to enable non-destructive evaluation; the procedure could be incorporated into the current shear design procedures such as the conventional sectional method for slender beams and the direct strut and tie model for deep beams. The method was validated with experimental results by (Suffern et al., 2010; Khan et al., 2014; El-Sayed et al., 2016).

Other highly corroded deep beams tested under three-point bending after simulated 26-year long corrosion exposure also illustrated that the failure mode was not affected by the corrosion of reinforcement; but corroded transverse reinforcement which was activated when the compressive strut failed, led to a loss in ductility of the beams (Khan et al., 2014).

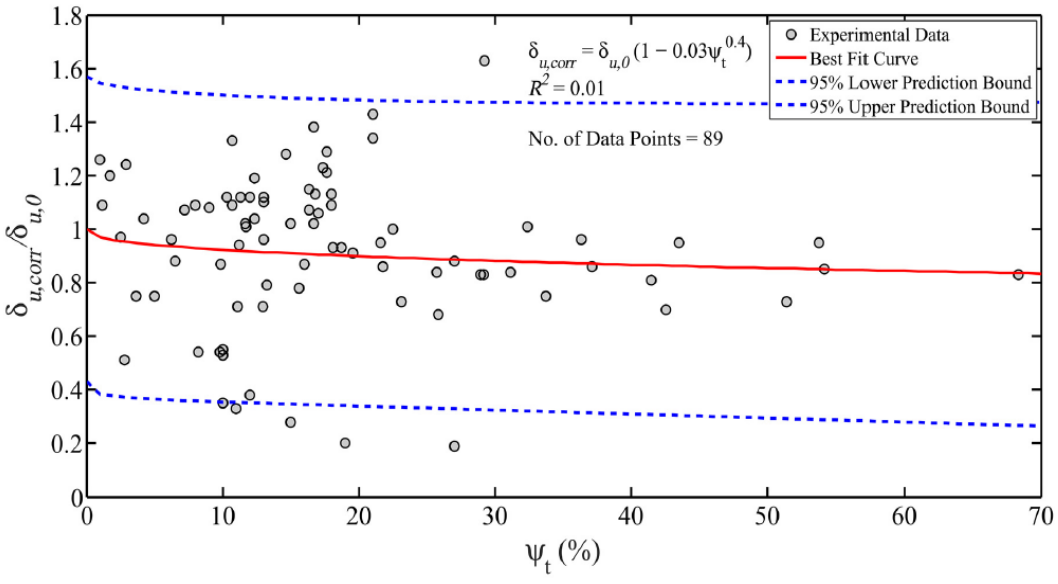

Figure 2-11. Impact of Shear Reinforcement Corrosion on Residual Maximum Shear Capacity (Kashani et al., 2019)

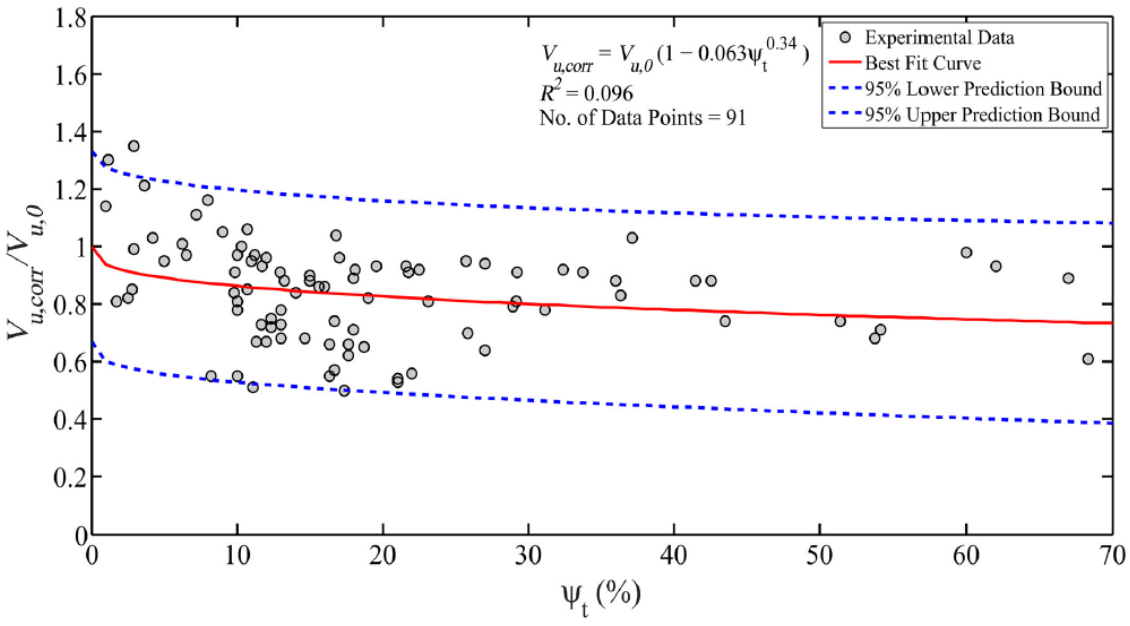

Figure 2-12. Impact of Shear Reinforcement Corrosion on Residual Maximum Deflection Capacity (Kashani et al., 2019)

Figures 2-11 and 2-12 show the degrading effect of shear reinforcement corrosion on a RC beam's residual shear strength and deformation capacity ($V_{u,0}$ and $\delta_{u,0}$ are the ultimate shear strength and maximum deflection respectively, of an RC beam in pristine condition, $V_{u,corr}$ and $\delta_{u,corr}$ are the corresponding values of a corroded RC beam; parameter $\Psi_1(\%)$ is the mass loss ratio.)

2.5. Effect of Reinforcement Corrosion on Columns

Failure mechanisms observed in reinforced concrete bridge piers in previous earthquakes (San Fernando, 1971; Loma Prieta, 1989; Northridge, 1994; Kobe, 1995) have been identified as buckling of longitudinal reinforcement with crushing of core concrete, fracture of main reinforcement under tensile stresses, shear failure as well as bond failure. These mechanisms are owing to lack of confining reinforcement, especially in old construction. The problem is especially critical in the presence of corrosion due its multifaceted effects on the stress-strain behavior of RC members as discussed in the preceding. In order to find adequate solutions to retrofitting corroded bridge piers for earthquake resistance, the various effects of corrosion on the behavior of columns under cyclic loading need to be understood. The following sections will discuss the effects of corrosion on the axial and flexural strengths of rectangular and circular RC columns.

2.5.1. Effect of Corrosion on Axial Compression Strength of RC Columns

Several experimental investigations were carried out in the early 2000s on the effect of corrosion on short RC columns and investigated the effectiveness of different forms of retrofitting (Lee et al., 2000; Pantazopoulou et al., 2001; Bae et al., 2005). It was found that longitudinal and transverse bar corrosion greatly impacted the resistance curve of the columns under axial loading, causing a dramatic reduction in available ductility and crushing strain while the compressive strength was also affected, but to a lesser degree (Vu et al., 2017). Several column cross-sectional shapes, reinforcement ratios, and corrosion degrees (mass loss) have been considered. The post-peak softening branch became much steeper than that of un-corroded columns with increasing mass loss; failure shifted from ductile to an increasingly brittle mode. As in other experiments, mass loss less than 10% did not significantly affect the behavior of columns.

Lee et al. (2009) reported that the ductility of corroded columns under compressive stress was reduced by about 70%. In order to explore the internal damage in the unrepaired corroded RC columns, slices were cut through the cross-section. The slices showed radial cracks in the concrete cover along the length of the corroded bars; furthermore, a single crack was identified that had been molded by a hoop around the spiral reinforcement which lead to the delamination of the cover. This was an interesting finding that clarified the influence of corrosion on the axial strength of corroded columns.

2.5.2. Effect of Corrosion on the Flexural Behavior of Columns

The effect of corrosion on the seismic behavior of corrosion damaged rectangular columns was investigated by Meda et al, (2014). Prior to corroding columns, tests were conducted on bare bars and on identical bars embedded in concrete in order to calibrate Faraday's law so as to accurately calculate the corrosion degree in columns. It was found that a correction factor of 1.3 was required, whereas a difference in morphology of corrosion product development and distribution was noted between corroded bare and embedded bars: bare bars formed pits and embedded bars had a uniformly distributed corrosion along their length. It was also reported that corrosion significantly affected the cyclic behavior of columns, where for a 20% mass loss in longitudinal reinforcement, a 30% reduction in ultimate strength and 50% reduction in ultimate drift capacity occurred.

An experimental investigation was conducted on 13 circular columns tested under cyclic displacement reversals and a constant axial load ratio ranging between 0.15 and 0.9 (Ma et al., 2015); corrosion levels reached or exceeded 15%. The failure mode shifted from ductile to brittle failure in highly corroded columns carrying high axial loads. Such heavily loaded columns having a mass loss between 10%-20%, had a very poor seismic performance in terms of hysteretic response, stiffness, ductility, and energy dissipation.

Four rectangular columns three of which were corroded to several degrees under cyclic reversals in their weak axis were also tested (Guo et al., 2015). It was observed that ties underwent higher mass loss than longitudinal reinforcement which lead to the fracture of some of them while testing. Degradation of the seismic response in terms of stiffness, strength, and ductility as well as the mean curvature of the plastic hinge region increased with the increase of corrosion degree. In a similar test series on four corroded RC columns under cyclic loading it was demonstrated that the seismic response is impacted by mass loss, marked by a severe reduction in ultimate drift capacity, ductility, energy absorption and ultimate strength (Yang & Cai, 2016). The following equations were drawn from the experimental investigation for predicting the residual ductility and energy absorption of corroded columns as a function of the mass loss fraction, x:

$$\mu_{cor}/\mu_0 = 1-0.019x \quad (2\text{-}2)$$

$$E_{cor}/E_0 = 1-0.027x \quad (2\text{-}3)$$

Where μ_0 and E_0 are the ductility and energy absorption capacity respectively for the non-corroded column and μ_{cor} and E_{cor} are the respective variables for corroded columns. Tests on six full scaled column specimens confirmed the deprecating effect on strength, stiffness, and drift capacity (Rajput & Sharma, 2019). The effect on deteriorated stirrups can be severe enough to eliminate any confinement originally designed for. Peripheral ties were much more affected by corrosion than cross/diamond ties due to their high exposure to chlorides. Lateral load capacity decreased by 27% and 55% for specimens having 10% and 15% mass loss respectively, whereas corrosion also affected the axial load carrying capacity of the columns.

An interesting study which is used for benchmarking finite element modelling of corroded columns in the remainder of this thesis was conducted by Goksu and Ilki (2016). Six columns compliant with modern seismic provisions were corroded by applying a constant voltage (6V). While the

reference uncorroded column was able to withstand cycles reaching to 8% drift and maintaining the lateral strength, the corroded columns failed at earlier stages by rupture of the longitudinal bars. Hysteretic loops of corroded columns were marked by severe pinching which was not apparent in the control specimen; this was attributed to the loss of ductility and effective area of reinforcement bars underlining the importance of consideration of the state of reinforcement in seismic evaluation procedures, as unexpected premature failures are possible due to corrosion (Goksu & Ilki, 2016).

Subsequent to these tests, eight full-scale specimens were also reported (Vu and Li, 2018), six of which were corroded to various degrees. Specimens were separated into two groups having two different axial load ratios (0.15 and 0.35) and were subjected to cyclic lateral displacement reversals. The detrimental effect of corrosion on the hysteretic response of columns in terms of ductility, lateral capacity, and drift as well as the energy absorption capacity were re-affirmed in this study. Three different failure modes were reported: flexural, shear and axial crushing. Un-corroded specimens and lightly corroded specimens failed in flexure, whereas highly corroded specimens and/or highly axially loaded specimens failed in a flexure-shear manner. An empirical model to estimate the residual flexural and shear strengths of corroded columns was proposed and calibrated with the test results. Earlier experiments conducted on four 20-year-old, naturally corroded short columns had been used to study the effect of corrosion on the shear strength of columns (Ma et al., 2000). Mass losses recorded in the 20-year-old columns varied between 2.2% and 4.9%. Axial force had a determining role on the mode of failure exhibited: for an axial ratio = 0.19, the columns failed in shear-bond failure and developed a displacement ductility of 3.6. But when the axial ratio was increased to 0.38, the columns developed a shear-compression failure and the ductility decreased to 1.7; it was concluded that such low degrees of mass loss could not significantly alter the shear and flexural strengths of the columns.

Four rectangular reinforced concrete columns with a rectangular section and different axial loads and corrosion degrees were considered along with two control specimens. The extent of corrosion affected the cracking load and the post-peak behavior; as bond failure controlled the response, it was found that corrosion improved the ductility ratio, but decreased the amount of energy dissipated on account of excessive pinching (Li et al., 2018). Similar results were obtained by other researchers (Apostolopoulos et al., 2019).

Tests on the effect of corrosion in the splash and tidal zone of six column specimens (rather than at the end regions) with a circular cross section and various degrees of corrosion showed that for a mass loss less than 8.7% the hysteretic behavior of the corroded column was similar to that of an un-corroded column; however, for a mass loss of 17.6% and higher, the hysteretic response was significantly degraded in terms of strength, deformation, and energy dissipation. The position of plastic-hinge formation was highly dependent on the corrosion degree in the splash and tidal zone. For no or low corrosion, the plastic hinge occurred at the column's end. For a moderate amount of corrosion, two plastic hinges formed, one at the column's end and one in the splash and tidal zone. When the corrosion degree became severe, only one plastic hinge formed at the splash and tidal zone (Yuan et al., 2017).

2.6. Corroded Column Repair and Retrofitting Methods

Seismic repair and retrofitting of reinforced concrete columns has been a priority topic for the earthquake engineering community for at least three decades. During an earthquake, the imposed displacement demands are carried by the columns (or piers) of a structure while at the same time they support the overburden gravity loads of the superstructure. Therefore, safety of people and property rely on the ability of the columns to sway laterally in response to the imposed lateral drift demands in the presence of significant axial compression. Reinforced concrete structures built prior to the incorporation of seismic detailing in the 1970s do not contain ductile columns which makes them vulnerable to earthquakes. Ageing such as reinforcement corrosion further increases the vulnerability of older construction. In response to this state of affairs the engineering community has invested much research effort and innovation into the development of retrofitting methods that could upgrade substandard columns so as to meet contemporary expectations for ductile response. These efforts are outlined in the following section with reference to the retrofitting technique used.

2.6.1. Reinforced Concrete and Mortar Jacketing

The earliest form of retrofitting and repairing damaged RC columns was by reinforced concrete jacketing. In this method, the column's section is increased by casting a perimeter layer over a critical segment or the entire length of the column; roughening of the surface of the existing section, and use of anchors or bolts were relied upon to engage interaction between the jacket and the encased column. Although this technique improves the column's axial load capacity, flexural

resistance, and drift capacity, it is costly, time consuming, and aesthetically inconvenient as it increases the column's geometry and size. It is considered a global intervention because it effects a stiffness increase for the building, which means that to avoid local damage it is necessary to extend to subsequent floors by continuing the added longitudinal reinforcement through the floor slabs, thereby leading to excessive disruption of the building. In recent years this form of jacketing has been replaced with the use of thin layers of high-performance cementitious materials without longitudinal bars, thereby moderating the global consequences on the structural period and the magnitude of seismic demands.

Efficiency of column strengthening using RC jacketing is evaluated by the improvement of the mode of failure (Chang et al., 2014). For pre-damaged columns, jacketing may recover the strength and ductility, however if yield penetration has occurred along the longitudinal reinforcement during the initial stage of damage, then the member stiffness cannot be fully recovered, particularly in highly damaged columns (Lehman et al., 2001). Delamination of the jacket has also been reported on account of limited bond strength between the jacket and the encased original column (Vandoros and Dritsos, 2008).

2.6.2. Steel Jacketing

Steel Jacketing is a retrofitting strategy widely used in the industry. This method involves mounting a structural steel sheet around the deficient member and welded at the joint. Mortar and grout are then used to fill the void between the RC section and the steel (Liu, et al., 2019). This strategy is considered costly, labor intensive, and requires regular maintenance. However, it is very effective in enhancing the seismic performance of deficient structural members. The change in cross-sectional dimension affects the structure's stiffness so it qualifies as a global intervention technique. Tests with steel jackets of various shapes (circular and rectangular) showed a stable cyclic response to ductility ratios of 6 or more (Daudey & Filiatrault, 2000). Bolting a steel plate to the flexural face of columns was found to significantly delay the concrete crushing of concrete in the plastic hinge region (Wu, et al., 2003). Prestressed light steel jackets (Fakharifarh, et al., 2016) led to an increase in ductility and ultimate strength of the columns by 140% and 115% respectively, while stiffness was restored to 80% of the as-built stiffness. Similar findings were reported when applying steel jackets to rectangular section columns, (Zhou & Liu, 2010), whereas

a variety of modifications and practical improvements have been also considered (Choi, et al., 2013), (Pudjisuryadi, et al., 2015), (Wang, et al., 2017).

2.6.3. Externally Bonded Fiber-Reinforced Polymer Jacketing

FRP jacketing is probably the most popular seismic retrofitting method on account of its versatility, fast application, but also because it is only a local intervention (i.e., it does not affect the global stiffness of the structure, while at the same time effectively suppresses premature modes of failure in poorly detailed members). FRPs have been linked to several limitations – i.e., the effectiveness in the material usage is in the range of 30% and 35%, it also is susceptible to fire (Kotynia, et al., 2008). Early studies (Lee, et al., 2003) have shown that after hardening of the infused epoxy, FRP jackets form an impermeable barrier that is effective in delaying the rate of corrosion in the encased members by depriving the system from the free ingress of the corrosive agents (flow of Oxygen, water and chlorides). Nevertheless, some objections exist to this – the argument has been that when trapped inside, chlorides will continue to dissipate the reinforcement by engaging forms of corrosion that produce non-expansive products, the result being that eventually greater damage may be caused silently (i.e. without the visible signs that warn of corrosion).

2.6.4. Near-surface mounted fiber-reinforced polymer jacketing

Near-surface mounted jacketing method consists of creating grooves in the concrete cover in which FRP bars are attached using bonding materials, such as grout. Frequently, the NSM system is used along with externally bonded FRP jacketing. With the intention of increasing the flexural strength of the column, NSM FRP bars are customarily used in the longitudinal direction. For instance, Hasan et al. studied the repair efficiency of 3 partly fractured RC columns with CFRP laminate strengthening & NSM rebar repair. The studies have shown that the specimens with CFRP wrapping established enhanced the crack formation and propagation whereas the NSM-FRP jacketing enhanced the energy dissipation, load capacity, and ductility of the tested columns (Hasan, et al., 2016).

2.6.5. Shape memory alloy wire jacketing

Shape memory alloys (SMAs) have been considered as a strengthening material by several researchers due to its super elasticity, durability and shape memory effect. Cho et al. (2013) studied the efficiency of seismic retrofit using two types of SMA alloys, nickel-titanium alloys, and nickel-

titanium-niobium. The SMA jackets were anchored into the concrete section. It was found that using SMA as a retrofitting material leads to an increase in ductility of lap-spliced columns. Furthermore, it was found that SMA-strengthened lap-spliced columns had an enhanced behavior relative to un-strengthened non-lap-spliced columns (Choi, et al., 2013).

2.6.4 UHPC Jacketing

UHPC is considered one of the most recent repair material in the industry. Its use has been somewhat limited in the built environment, however it is becoming more and more common as more research is being conducted on its performance and reliability. Doiron (2016) reports several projects conducted by Lafarge North America Inc. in Canada where they had used UHPC as a repair material in infrastructure restoration projects. These projects include the rehabilitation of CN rail in Montreal, QC where they used UHPC jacketing, this project was conducted in 2013. Mission bridge seismic retrofit at Abbotsford, BC. It was reported that the use of UHPC jacketing instead of traditional pile compaction techniques provided $1.5 Million (CAD) in savings to the project. This retrofit project receive the 2015 ACI excellence in concrete award in the repair and restoration category. The third reported project is the Hooper Rd, Town of Union in New York. The report shows how the contractor was able to leverage the characteristics of UHPC in order to save time in completing the project. The replacement project was completed in 21 days in 2014. Finally, we have the Hagwilget bridge in New Hazelton, BC. The bridge was experiencing corrosion and the base of bent legs. Due to the congestion and minimal space available to transfer concentrated loads from the bent leg into its pedestal, it was proposed to use a high strength concrete that has high tensile strength, optimum flow-ability, no shrinkage and no permeability. The only option was the usage of UHPC as a repair material to solve this problem. The project was completed in 2015 by rehabilitating in 32 bent legs in total.

Meda et al. (2016) investigated the effectiveness of HPFRC jacket as a repair and strengthening material for corroded RC columns. They had tested three columns representing three configurations. They had a control uncorroded specimen and two corroded specimens. One of the corroded specimens was tested and then repaired only to be retested again, this simulated the repair a column that was damaged by an earthquake event. The third column was corroded and then strengthened before being tested to simulate strengthening before an earthquake event. The repair/retrofit method adopted consisted of removing the concrete cover only around the

longitudinal reinforcement, and then sandblasting the surface. HPFRC jacket was added in a manner that increased the whole sectional area by 60%. The study's findings were relatively limited, the authors recommended the use of HPFRC for rehabilitation of columns with low concrete strength, low reinforcement ratio, concrete damage and reinforcement corrosion.

Dagenais et al. (2018) conducted a thorough investigation into the effectiveness of UHPC in seismically retrofitting rectangular bridge piers with deficient lap splices. The program consisted of testing five rehabilitated columns and one control column. The retrofitting strategy used was to replace the perimeter concrete with UHPC. The problem with this methodology was that they did not extend the repair into the footing, thus the failure of the retrofitted columns was always at the base at the UHPC-NC interface. The study showed that UHPC was able to mitigate lap-splice failure in the columns.

Farzad et al. (2019) proposed a retrofitting method of bridge piers using UHPC. A main test variable was to simulate damage caused by corrosion without corroding the specimens. The damage was represented in alteration of the sectional geometry and removal of concrete in certain locations at the base of the column. The problem with this approach is that reinforcement is not damaged nor the bond strength of reinforcement is altered. Thus the results are not very reliable. Nonetheless, it was observed that UHPC significantly improves the seismic behavior of columns. It was also reported that UHPC with 2% and 4% volumetric fiber ratio resulted in similar behavior. The cover thickness however plays a role in shifting the failure location either above or below the repaired section which should be taken into account as a design consideration.

2.1. References

Abdel-Mooty, M., Issa, M., Farag, H. & Bitar, M., 2006. Seismic Upgrading of Square and Rectangular RC Columns using FRP Wrapping. *Wessex Institute of Technology.*

Abdullah, T., 2003. An investigation into the behavior and strength of reinforced concrete columns strengthened with ferrocement jackets. *Cem. Concr. Compos.*, Volume 25, pp. 233-242.

ACI 222R-19, 2019. Guide to Protection of Reinforcing Steel in Concrete Against Corrosion. *American Concrete Institute,* pp. 1-65.

Afshin, H., Shirazi, M. & Abedi, K., 2015. Experimental and numerical study about seismic retrofitting of corrosion-damaged reinforced concrete column. *Transp. Res. Rec,* Volume 2522, pp. 70-78.

Alaskar, A., 2013. *Shear Behaviour of Slender RC Beams with Corroded Web Reinforcement. UWSpace. http://hdl.handle.net/10012/7472*

Allamt, I.M.;, 1994. Influence of atmospheric corrosion on the mechanical properties of reinforcing steel. *Construction and Building Materials.*

Almusallam, A.A.;, 1996. Effect of reinforcement corrosion on bond strength. *Construction and Building Materials,* Volume 10, pp. 123-129.

Almusallam, A.A.;, 2001. Effect of degree of corrosion on the properties of reinforcing steel bars. *Construction and Building Materials,* pp. 361-368.

Al-Saidy, A.H.;, 2016. Structural behavior of corroded RC beams with/without stirrups repaired with CFRP sheets. *Materials and Structures,* Volume 49, pp. 3733-3747.

Al-Sulaimani, G.J.;, 1990. Influence of Corrosion and Cracking on Bond Behavior and Strength of Reinforced Concrete Members. *ACI Structural Journal,* Volume 87, pp. 220-231.

Amleh, L., Mirza, M. & Ahwazi, B., 2000. *Bond deterioration of reinforcing steel in concrete due to corrosion. McGill University, Department of Civil Engineering.*

Apostolopoulos, C., 2007. Mechanical behavior of corroded reinforcing steel bars S500s tempcore under low cycle fatigue. *Construction and Building Materials,* pp. 1447-1456.

Apostolopoulos, C., Drakakaki, A. & Basdeki, M., 2019. Seismic assesment of RC column under seismic loads. *International Journal of Structural Integrity,* Volume 10, pp. 41-54.

Apostolopoulos, C. & Papadakis, V., 2008. Consequences of steel corrosion on the ductility properties of reinforcement bar. *Construction and Building Materials,* pp. 2316-2324.

Aquino, W. & Hawkins, N., 2007. Seismic retrofitting of corroded reinforced concrete columns using carbon composites. *ACI Struct. J,* Volume 104, pp. 348-356.

Association, A. R. &. T. B., 2020. *ARTBA Bridge Report. https://artbabridgereport.org/*

Azad, A., Ahmad, S. & Al-Gohi, B., 2010. Flexural strength of corroded reinforced concrete beams. *Magazine of Concrete Research,* Volume 62, pp. 405-414.

Bae, S., Belarbi, A. & Myers, J., 2005. Performance of Corrosion-Damaged RC Columns Repaired by CFRP Sheets. *Special Publications,* Volume 230, pp. 1447-1464.

Berra, M., Castellani, A. & Coronelli, D., 1997. Bond in reinforced concrete and corrosion of bars. *Structural Faults and Repair,* Volume 113, pp. 349-357.

Berrocal, C.G.;, 2017. Corrosion-induced cracking and bond behaviour of corroded reinforcement bars in SFRC. *Composites Part B: Engineering,* Volume 113, pp. 123-137.

Bournas, D., Lontou, P., Papanicolaou, C. & Triantafillou, T., 2007. Textile-reinforced mortar versus fibre-reinforced polymer confinement in reinforced concrete columns. *ACI. Struct. J,* Volume 104, pp. 740-748.

Bournas, D. & Triantafillou, T., 2009. Flexural strengthening of reinforced concrete columns with near-surface-mounted FRP or stainless teel. *ACI Struct J,* Volume 106, pp. 495-505.

Bousias, S., Spathis, A. & Fardis, M., 2007. Seismic retrofitting of columns with lap spliced smooth bars through FRP or concrete jackets. *J. Earthq. Eng,* Volume 11, pp. 653-674.

Bousias, S. et al., 2004. Fibre-reinforced polymer retroftitting of rectangular reinforced concrete columns with or without corrosion. *ACI Struct. J,* Volume 101, pp. 512-520.

Cairns, J., Du, Y. & Law, D., 2008. Structural performance of corrosion-damaged concrete beams. *Magazine of Concrete Research,* Volume 60, pp. 359-370.

Castel, A., François, R. & Arliguire, G., 2000. Mechanical behaviour of corroded reinforced concrete beams-Part 1: Experimental study of corroded beams. *Materials and Structures,* Volume 33, pp. 539-544.

Castillo, E., Griffith, M. & Ingham, J., 2018. Seismic behavior of RC columns flexurally strengthened with FRP sheets and FRP anchors. *Compos. Struct,* Volume 203, pp. 382-395.

Chang, C., Kim, S., Park, D. & Choi, S., 2014. Experimental investigation of reinforced concrete columns retrofitted with polyester sheet. *Earthq. Struct,* Volume 6, pp. 237-250.

Chang, S., Chen, T., Tran, N. & Liao, W., 2014. Seismic retrofitting of RC columns with RC jackets and wing walls with different structural details. *Earthq. Eng. Vib,* Volume 13, pp. 279-292.

Cho, C. et al., 2018. Strengthening of reinforced conrete columns by High-Peroformance FIbre-Reinforced Cementitious Composite (HPFRC) sprayed mortar with strengthening bars. *Compos. Struct,* Volume 2018, pp. 1078-1086.

Cho, C., Kim, Y., Feo, L. & Hui, D., 2012. Cyclic responses of reinforced concrete composite columns strengthened in the plastic hinge region by HPFRC mortar. *Compos. Struct.,* Volume 94, pp. 2246-2253.

Choi, E., Cho, B. & Lee, S., 2015. Seismic retrofit of circular RC columns through using tensioned GFRP wires winding. *Compos. Part B Eng,* Volume 83, pp. 216-225.

Choi, E., Chung, Y., Park, C. & Kim, D., 2013. Seismic performance of circular RC columns retrofitted with prefabricated steel wrapping jackets. *Mag. Concr. Res.,* Volume 65, pp. 1429-1440.

Chou, C., Lee , C., Wu, K. & Chin, V., 2018. Development and validation of a FRP-wrapped spiral corrugated tube for seismic performance of circular concrete columns. *Constr. Build. Mater,* Volume 170, pp. 498-511.

Colomb, F., Tobbi, H., Ferrier, E. & Hamelin, P., 2008. Seismic retrofit of reinforced concrete short columns by FRP materials. *Compos. Struct,* Volume 82, pp. 475-487.

Coronelli, D., Hanjari, K. & Lundgren, K., 2013. Severly Corroded RC with Cover Cracking. *Journal of Structural Engineering,* Volume 139, pp. 221-232.

Dagenais, M., Massicotte, B. & Boucher-Proulx, G., 2018. Seismic Retrofitting of Rectangular Bridge Piers with Deficient Lap Splices Using Ultrahigh-Performance Fibre-Reinforced Concrete. *J. Bridge Eng,* Volume 23.

Dai, J., Lam , L. & Ueda, T., 2012. Seismic retrofit of square RC columns with polyethylene terephthalate (PET) fibre reinforced polymer composites. *Constr. Build. Mater.,* Volume 27, pp. 206-217.

Daudey, X. & Filiafrault, A., 2000. Seismic evaluation and retrofit with steel jackets of reinforced concrete bridge piers detailed with lap-splices. *Can. J. Civil Eng.,* Volume 27, pp. 1-16.

Del Zoppo, M. et al., 2017. FRP for seismic strengthening of shear controlled RC columns: Experience from earthquakes and experimental analysis. *Compos. Part B Eng,* Volume 129, pp. 47-57.

Deng, M., Zhang, Y. & Li, Q., 2018. Shear strengthening of RC short columns with ECC jacket: Cyclic behavior tests. *Eng. Struct,* Volume 160, pp. 535-545.

Doiron, G. (2016) 'Pier Repair/Retrofit Using UHPC Examples of Completed Projects in North America', in First International Interactive Symposium on UHPC.

Du, Y., Clark, L. & Chan, A., 2005. Residual capacity of corroded reinforcing bars. *Magazine of Concrete Research,* pp. 135-147.

Du, Y., Clark, L. & Chan, A., 2007. Impact of Reinforcement and Corrosion on Ductile Behavior of Reinforced Concrete Beams. *ACI Structural Journal,* Volume 104, pp. 285-293.

ElGawady, M., Endeshaw, M., McLean, D. & Sack, R., 2010. Retrofitting of rectangular columns with deficient lap splices. *J. Compos. Constr,* Volume 14, pp. 22-35.

El-Sayed, A., Hussain, R. & Shuraim, A., 2016. influence of Stirrup Corrosion on SHear Strength of Reinforced Concrete Slender Beams. *ACI Structural Journal,* Volume 113, pp. 1223-1232.

ElSouri, A. & Harajli, M., 2011. Seismic repair and strengthening of lap splices in RC columns: Carbon fibre-reinforced polymer versus steel confinement. *J. Compos. Constr,* Volume 15, pp. 721-731.

Eshghi, S. & Zanjanizadeh, V., 2008. Retrofit of slender square reinforced concrete columns with glass fibre-reinforced polymer for seismic resistance. *Iran. J. Sci. Technol. B,* Volume 32, pp. 437-450.

Fahmy, M. & Wu, Z., 2016. Exploratory study of seismic response of deficient lap-splice columns retrofitted with near surface-mounted basalt FRP bars. *J. Struct. Eng,* Volume 142.

Fakharifarh, M. et al., 2016. Rapid repair of earthquake-damaged RC columns with prestressed steel jackets. *J. Bridge Eng,* Volume 21.

Fakharifar, M., Chen, G., Arezoumandi, M. & Eigawady, M., 2015. Hybrid jackting for rapid repair of seismically damaged reinforced concrete column. *TRansp. Rs. Rec,* Volume 2522, pp. 70-78.

Fang, C.;, 2004. Corrosion influence on bond in reinforced concrete. *Cement and Concrete Research,* Volume 34, pp. 2159-2167.

Farhan, N., Sheikh, M. & Hadi, M., 2018. Experimental Investigation on the Effect of Corrosion on the Bond Between Reinforcing Steel Bars and Fibre Reinforced Geopolymer Concrete. *Structures,* Volume 14, pp. 251-261.

Farzad, M., Shafieifar, M. and Azizinamini, A. (2019) 'Retrofitting of Bridge Columns Using UHPC', Journal of Bridge Engineering. American Society of Civil Engineers, 24(12), p. 04019121. doi: 10.1061/(ASCE)BE.1943-5592.0001497.

Faustino, P. & Chastre, C., 2016. Damage effect on concrete columns confined with carbon composites. *ACI Struct. J.,* Volume 113, pp. 951-962.

Fernandez, I.;, 2018. Ultimate Capacity of Corroded Statically Indeterminate Reinforced Concrete Members. *International Journal of Concrete Structures and Materials,* Volume 12, p. 75.

Fernandez, I., Bairán, J. & Marí, A., 2015. Corrosion effects on the mechanical properties of reinforcing steel bars. Fatigue and σ–ε behavior. *Construction and Building Materials,* Volume 101, pp. 772-783.

fib Model Code (2010) *Fib model code for concrete structures 2010*. Bulletin 65.

Fishcer, C., Ozbolt, J. & Gehlen, C., 2010. Experimental investigation on the effect of corrosion on bond of deformed bars. *8th fib PhD Symposium,* pp. 1-6.

François, R., Khan, I. & Dang, V., 2013. Impact of corrosion on mechanical properties of steel embedded in 27-year-old corroded reinforced concrete beams. *Materials and Structures,* Volume 46, pp. 899-910.

Fu, C.;, 2017. Corrosion characteristics of a 4-year naturally corroded reinforced concrete beam with load-induced transverse cracks. *Corrosion Science,* pp. 11-23.

Galal, K., Arafa, A. & Ghobarah, A., 2005. Retrofit of RC square short columns. *Eng. Struct,* pp. 801-813.

Ghatte, H. et al., 2019. Seismic retrofit of full-scale substandard extended rectangular RC columns through CFRP jacketing. Test results and design recommendation. *J. Compos. Constr,* Volume 23.

Ghobarah, A. & Galal, K., 2004. Seismic rehabilitation of short rectangular RC columns. *J. Earthq. Eng,* Volume 8, pp. 45-68.

Ghosh, K. & Sheikh, S., 2007. Seismic upgrade with carbon fibre-reinforced polymer of columns containing lap-spliced reinforcing bars. *ACI Struct. J,* Volume 104, pp. 227-236.

Gjørv, O., 2014. Durability Design of Concrete Structures in Severe Environments. *CRC Press.*

Goksu, C. & Ilki, A., 2016. Seismic Behavior of Reinforced Concrete Columns with Corroded Deformed Reinforcing Bars. *ACI Structural Journal,* Volume 113, pp. 1053-1064.

Guo, A.;, 2015. Experimental investigation on the cyclic performance of reinforced concrete piers with chloride-induced corrosion in marine environment. *Engineering Structures,* Volume 105, pp. 1-11.

Haddad, R. & Ashteyate, A., 2001. Role of synthetic fibers in delaying steel corrosion cracks and improving bond with concrete. *Canadian Journal of Civil Engineering,* Volume 28, pp. 787-793.

Hanjari, K., Coronelli, D. & Lundgren, K., 2011. Bond capacity of severly corroded bars with corroded stirrups. *Magazine of Concrete Research,* Volume 63, pp. 953-968.

Harajli, M., 2006. Seismic behavior of RC columns with bond-critical regions in rectangular reinforced concrete columns using fibre-reinforced polymer wraps. *ACI Struct. J,* Volume 103, pp. 874-884.

Harajli, M. & Dagher, F., 2008. Seismic strengthening of bond-critical regions in a rectangular reinforced concrete columns using fibre-reinforced polymer wraps. *ACI Struct. J,* Volume 105, pp. 68-77.

Harajli, M. & Khalil, Z., 2008. Seismic FRP retrofit of bond-Critical regions in circular RC columns: Validation of proposed design methods. *ACI Struct J,* Volume 105, pp. 760-769.

Harajli, M. & Rteil, A., 2004. Effect of confinement using fibre-reinforced polymer or fibre-reinforced concrete on seismic performance of gravity load-designed columns. *ACI Struct. J,* Volume 101, pp. 47-56.

Harajli, M. & Rteil, A., 2004. Effect of confinement using fibre-reinforced polymer or fibre-reinforced concrete on seismic performance of gravity load-designed columns. *ACI Struct. J,* Volume 101, pp. 47-56.

Haroun, M. & Elsanadedy, H., 2005. Behavior of Cyclically Loaded Squat Reinforced Concrete Bridge Columns Upgraded with Advanced Composite-Material Jackets. *J. Bridge Eng,* Volume 10, pp. 749-757.

Harries, K., Ricles, J., Pessiki, S. & Sause, R., 2006. Seismic retrofit of lap splices in nonductile square columns using carbon fibre-reinforced jackets. *ACI Struct. J,* Volume 105, pp. 874-884.

Hasan, Q., Tekeli, H. & Demir, F., 2016. NSM Rebar and CFRP laminate strengthening for RC columns subjected to cyclic loading. *Constr. Build. Mater,* Volume 119, pp. 21-30.

Hashemi, M. et al., 2017. Application of hybrid simulation for collapse assesment of post-earthquake CFRP-repaired RC columns. *J. Struct. Eng.,* Volume 143.

Higgins, C. & Farrow, W., 2006. Tests of Reinforced Concrete Beams with Corrosion Damaged Stirrups. *ACI Structural Journal,* Volume 103, pp. 133-141.

Hou, L.;, 2017. Effect of corrosion on bond behaviors of rebar embedded in ultra-high toughness cementitious composite. *Construction and Building Materials,* Volume 138, pp. 141-150.

International, N., 2016. *International Measures of Prevention, Application, and Economics of Corrosion Technologies Study. http://impact.nace.org/*

Jiang, S., Zeng, X., Shen, S. & Xu, X., 2016. Experimental studies on the seismic behavior of earthquake-damaged circular bridge columns repaired by using combination of near-surface-mounted BFRP bars with external BFRP sheets jacketing. *Eng. Struct,* Volume 106, pp. 317-331.

Juntanalikt, P., Jirawattanasomkul, T. & Pimanmas, A., 2016. Experimental and numerical study of strengthening non-ductile RC columns with and without lap splice by Carbon Fibre Reinforced Polymer (CFRP) jacketing. *Eng. Struct,* Volume 125, pp. 400-418.

Kalyoncuoglu, A., Ghaffari, P., Goksu, C. & Ilki, A., 2013. Rehabilitation of corrosion-damaged substandard RC columns using FPR sheets.. *Adv. Mater Res.,* pp. 639-640.

Kashami, M., Maddocks, J. & Dizaj, E., 2019. Residual Capacity of Corroded Reinforced Concrete Bridge Components: State-of-the-Art Review. *Journal of Bridge Engineering,* Volume 24.

Khan, I., François, R. & Castel, A., 2014. Experimental and analytical study of corroded shear-critical reinforced concrete beams. *Materials and Structures,* Volume 47, pp. 1467-1481.

Kotynia, R., Baky, H., K.W., N. & U.A, E., 2008. Flexural strengthening of RC beams with externally bonded CFRP systems: Test results and 3D nonlinear FE analysis. *J. Compos. Constr.,* Volume 12, pp. 190-201.

Law, D. & Molyneaux, T., 2017. Impact of corrosion on bond in uncracked concrete with confined and unconfined rebar. *Construction and Building Practices,* Volume 155, pp. 550-559.

Lee, H.S.;, 2009. Evaluation of the mechanical properties of steel reinforcement embedded in concrete specimen as a function of the degree of reinforcement corrosion. Volume 157, pp. 81-88.

Lee, C., Bonacci, J. F., Thomas, M. D., Maalej, M., Khajehpour, S., Hearn, N., Pantazopoulou, S., & Sheikh, S., 2000. Accelerated corrosion and repair of reinforced concrete columns using carbon fibre reinforced polymer sheets. Canadian Journal of Civil Engineering, 27(5), 941–948. https://doi.org/10.1139/l00-030

Lee, H., Kage, T., Noguchi, T. & Tomosawa, F., 2003. An experimental study on the retrofitting effects of reinforced concrete columns damaged by rebar corrosion strengthened with carbon fibre sheets. *Cem. Concr. Res.,* Volume 33, pp. 563-570.

Lee, K., Lee, B. & Seo, S., 2016. A seismic strengthening technique for reinforced concrete columns using sprayed FRP. *Polymers (Basel),* Volume 8, p. 107.

Lehman, D.E.;, 2001. Repair of Earthquake-Damaged Bridge Columns. *ACI Structural Journal,* Volume 98, pp. 233-242.

Lehman, D., Gookin, S., Nacamuli, A. & Moehle, J., 2001. Repair of earthquale-damaged bridge columns. *ACI Struct. J,* Volume 98, pp. 233-242.

Li, D.;, 2018. Influence of Non-uniform corrosion of steel bars on the seismic behavior of reinforced concrete columns. *Construction and Building Materials,* Volume 167, pp. 20-32.

Li, J., Gong, J. & Wang, L., 2009. Seismic behavior of corrosion-damaged reinforced concrete columns strengthened using combined carbon fibre-reinforced polymer and steel jacket. *Constr. Build. Mater,* Volume 23, pp. 2653-2663.

Li, J. & Li, Y., 2014. Experimental and theoratical study on the seismic performance of corroded RC circular columns strengthened with hybrid fibre reinforced polymers. *Polym. Polym. Compos,* pp. 1592-1599.

Lin, H., 2019. State-of-the-art review on the bond properties of corroded reinforcing steel bar. *Construction and Building Materials,* Volume 213, pp. 216-233.

Liu, C. et al., 2017. Experimental study on seismic performance of reinforced concrete column retrofitted by assymetric increased single lateral section. *Adv. Struct. Eng,* Volume 20, pp. 1325-1339.

Liu, J. & Sheikh, S., 2013. Fibre-reinforced polymer-confined circular columns under simulated seismic loads. *ACI Struct J,* Volume 110, pp. 941-951.

Liu, X. & Li, Y., 2018. Experimental study of seismic behavior of partially corrosion-damaged reinforced concrete columns strengthened with FRP composites with large deformability. *Constr. Build. Mater,* Volume 191, pp. 1071-1081.

Liu, X., Lu, Z.-D. & Li, L.-Z., 2019. The use of bolted side plates for shear strengthening of RC beams: A review. *Sustainability* , Volume 10, p. 4658.

Li, X. et al., 2013. Seismic retrofitting of rectangular reinforced concrete columns using fibre composites for enhanced flexrual strength. *J. Reinf. Plast. Comp,* Volume 32, pp. 619-630.

Lu, C.;, 2016. Mechanical properties of corroded steel bears in pre-cracked concrete suffering from chloride attack. *Construction and Buildign Materials, Volume* 123, pp. 649-660. 10.1016/J.CONBUILDMAT.2016.07.032

Lu, Y. et al., 2019. Seismic behavior of RC square columns strengthened with self-compacting concrete-filled CFRP-steel tubes. *J. Bridge Eng,* Volume 24.

Ma, G. & Li, H., 2015. Experimental study of the seismic behavior of pre-damaged reinforced-concrete columns retrofitted with basalt fibre-reinforced polymer. *J. Compos Constr,* Volume 19.

Mander, J., Priestley, M. & Park, R., 1988. Theoratical Stress-Strain Model for Confined Concrete. *Journal of Structural Engineering,* Volume 114, pp. 1804-1826.

Mangat, P. & Elgarf, M., 1999. Flexural Strength of Concrete Beams with Corroding Reinforcement. *ACI Structural Journal,* Volume 96, pp. 194-158.

Ma, R., Xiao, Y. & Li, K., 2000. Full-scale testing of a parking structure column retrofitted with carbon fibre reinforced composites. *Constr. Build Mater.,* Volume 14, pp. 63-71.

Meda, A.;, 2014. Experimental evaluation of the corrosion influence on the cyclic behavior of RC columns. *Engineering Structures,* Volume 76, pp. 112-123.

Meda, A., Mostosi, S., Rinaldi, Z. & Riva, P., 2016. Corroded RC columns repair and strengthening with high performance fibre reinforced concrete jacket. *Mater. Struct,* Volume 49, pp. 1967-1978.

Mehta, P., 1991. Durability of Concrete-Fifty Years of Progress. Proceedings of *Durability of Concrete. Second International Conference.* Montreal, Canada. August 4-9 Volume 1.

Memon, M. & Sheikh, S., 2005. Seismic resistance of square concrete columns retrofitted with glass fibre-reinforced polymer. *ACI Struct. J,* Volume 102, pp. 774-783.

Napoli, A. & Realfonzo, R., 2015. RC columns strengthened with novel CFRP systems: An experimental study. *Polymers (Basel),* Volume 7, pp. 2044-2060.

Ouyang, L. J., Gao, W., Zhen, B. & Lu , Z., 2017. Seismic retrofit of square reinforced concrete columns using basalt and carbon fibre-reinforced polymer sheets: A comparative sudy. *Compos. Struct,* Volume 162, pp. 294-307.

Ou, Y. & Chen, H., 2014. Cyclic Behavior of Reinforced Concrete Beams with Corroded Transverse Steel Reinforcement. *Journal of Structural Engineering,* Volume 140.

Ou, Y. & Truong, A., 2018. Cyclic behavior of reinforced concrete L-and T-columns retrofitted from rectangular columns. *Eng. Struct,* Volume 177, pp. 147-159.

Ozcan, O., Binici, B. & Ozcebe, G., 2008. Improving seismic performance of deficient reinforced concrete columns using carbon fibre-reinforced polymers. *Eng. Struct,* Volume 30, pp. 1632-1646.

Palsson, R. & Mirza, M., 2002. Mechanical Response of Corroded Steel Reinforcement of Abandoned Concrete Bridge. *ACI Structural Journal,* pp. 157-162.

Pantazopoulou, S.J.;, 2019. The performance of corroded lap splices in reinforced concrete beams. *Corrosion Reviews,* pp. 31-44.

Papakonstantinou, C., Balaguru, P. & Auyeung, Y., 2011. Influence of FRP confinement on bond behavior of corroded steel reinforcement. *Cement and Concrete Composites,* Volume 33, pp. 611-621.

Parks, J., Brown, D., Ameli, M. & Pantelides, C., 2016. Seismic repair of severly damaged precase reinforced concrete bridge columns connected with grouted splice sleeves. *ACI Struct. J,* Volume 113, pp. 615-626.

Paultre, P., Boucher-Trudeau, M., Eid, R. & Roy, N., 2016. Behavior of circular reinforced-concrete columns confined with carbon fibre-reinforced polymers under cyclic flexure and constant axial load. *J. Compos. Constr,* Volume 20.

Peng, Y., Gu, Q., Gao, R. & Bitewlgn, G., 2014. Experimental research on seismic behavior of seismically damaged RC frame column strengthened with sprayed hybrid BF/CFRP. *Appl. Mech. Mater,* pp. 501-504.

Martın-Pérez, B., 1999. Service life modelling of RC higway structures exposed to chlorides (Doctoral dissertation, University of Toronto).

Pourbaix, M. (1974) Atlas of electrochemical equilibria in aqueous solutions / by Marcel Pourbaix ; translated from the French by James A. Franklin (except sections I, III 5, and III 6, which were originally written in English). 2d English ed. Houston, Tex: National Association of Corrosion Engineers..

Pudjisuryadi, P., Tavio & Suprobo, P., 2015. Performance of square reinforced concrete columns externally confined by steel angle collars under combined axial and lateral Load. *Procedia Eng,* Volume 125, pp. 1043-1049.

Rajput, A., Sharma, U. & Engineer, K., 2019. Seismic retrofitting of corroded RC columns using advanced composite materials. *Eng. Struct,* Volume 181, pp. 35-46.

Raza, S. et al., 2019. Strengthening and Repair of Reinforced Concrete Columns by Jacketing: State-of-the-Art Review. *MDPI,* pp. 1-26.

Realfonzo, R. & Napoli, A., 2009. Cyclic behavior of RC columns strengthened by FRP and steel devices. *J. Struct. Eng,* Volume 135, pp. 1164-1176.

Rodrigues, H., Furtado, A. & Arede, A., 2017. Experimental evaluation of energy dissipation and viscous damping of repaired and strengthened RC columns with CFRP jacketing under biaxial load. *Eng. Struct.,* Volume 145, pp. 162-175.

Rodrigues, H. et al., 2018. Experimental study of repaired RC columns subjected to unaxial and biaxial horizontal loading and variable axial load with longitudinal reinforcement welded steel bars solutions. *Eng. Struct,* Volume 155, pp. 371-386.

Rodriguez, J. & Ortega, J., 1994. Corrosion of reinforcing bars and service life of reinforced concrete structures: corrosion and bond deterioration. *International Conference on Concrete across Borders,* pp. 315-326.

Sarafraz, M. & Danesh, F., 2012. New technique for flexural strengthening of RC columns with NSM FRP bars. *Mag. Concr. Res,* Volume 64, pp. 151-161.

Sausse, R. et al., 2004. Flexural behavior of concrete columns retrofitted with carbon fibre-reinforced polymer jackets. *ACI Struct. J,* Volume 101, pp. 708-716.

Seifi, A., Hosseini, A., Marefat, M. & Khanmohammadi, M., 2018. Seismic retrofitting of old-type RC columns with different lap splices by NSM GFRP and steel bars. *Struct. Des. Tall. Spec,* Volume 27.

Seo, H., Kim, J. & Kwon, M., 2016. Evaluation of damaged RC columns with GFRP-strip device. *J. Compos. Constr,* Volume 20.

Seyhan, E., Goksu, C. & Uzunhasanoglu, A., 2015. Seismic behavior of substandard RC columns retrofitted with embedded aramid fibre reinforced polymer (AFRP) reinforcement. *Polymers (Basel),* Volume 7, pp. 2535-2557.

Sheikh, S. & Yau, G., 2002. Seismic behavior of concrete columns confined with steel and fibre-reinforced polymers. *ACI Struct. J,* Volume 99, pp. 72-80.

Soudki, K. & Sherwood, T., 2003. Bond Behavior of Corroded Steel Reinforcement in Concrete Wrapped with Carbon FIber Reinforced Polymer Sheets. *Journal of Materials in Civil Engineering,* Volume 15, pp. 358-370.

Stanish, K., Hooton, R. & Pantazopoulou, S., 1999. Corrosion Effects on Bond Strength in Reinforced Concrete. *ACI Structrual Journal,* Volume 96, pp. 915-921.

Suffern, C., El-Sayed, A. & Soudki, K., 2010. Shear strength of disturbed regions with corroded stirrups in reinforced concrete beams. *Canadian Journal of Civil Engineering,* Volume 37, pp. 1045-1056.

Tastani, S. & Pantazopoulous, S., 2007. Behavior of Corroded Bar Anchorages. *ACI Structural Journal*, Volume 104, pp. 756-766.

Tepfers, R., 1979. Cracking of concrete cover along anchored deformed reinforcing bars. *Magazine of Concrete Research,* Volume 31, pp. 3-12.

Thermou, G. & Pantazopoulou, S., 2009. Fibre-reinforced polymer retrofitting of pre-damaged substandard RC prismatic members. *J. Compos. Constr,* Volume 13, pp. 535-546.

Tondolo, F., 926-932. Bond behaviour with reinforcement corrosion. *Construction and Building Materials,* p. 2015.

Torres-Acosta, A., Navarro-Guiterrez, S. & Terán-Guillén, J., 2007. Residual flexure capacity of corroded reinforced concrete beams. *Engineering Structures,* Volume 29, pp. 1145-1152.

Townsend, H., 1972. *Potential-pH Diagrams at Elevated Temperature for the System Fe-H20.*

Vandoros, K. & Dritsos, S., 2008. Concrete jacket construction detail effectiveness when strengthening RC columns. *Constr. Build. Mater.,* Volume 22, pp. 264-276.

Vandoros, K. & Dritsos, S., 2008. Concrete jacket construction detail effectiveness when strengthening RC columns. *Construction and Building Materials,* Volume 22, pp. 264-276.

Vrettos, I., Kefala, E. & Triantafillou, T., 2013. Innovative flexural strengthening of reinforced concrete columns using carbon-fibre anchors. *ACI Struct. J,* Volume 110, pp. 63-70.

Vu, N. & Li, B., 2018. Seismic Performance of Flexural Reinforced Concrete Columns with Corroded Reinforcement. *ACI Structural Journal,* Volume 115, pp. 1253-1266.

Vu, N., Yu, B. & Li, B., 2017. Stress-strain model for confined concrete with corroded transverse reinforcement. *Engineering Structures,* Volume 151, pp. 472-487.

Wang, L.;, 2015. Effects of stirrup and inclined bar corrosion on shear behavior of RC beams. *Construction and Building Materials,* Volume 151, pp. 537-546.

Wang, X.;, 2011. Bond strength of corroded steel bars in reinforced concrete structural elements strengthened with CFRP sheets. *Cement and Concrete Composites,* Volume 33, pp. 513-519.

Wang, D., Huang, L., Yu, T. & Wang, Z., 2017. Seismic performance of CFRP-retrofitted large-scale square RC columns with high axial compression ratios. *J. Compos. Constr,* Volume 21.

Wang, D., Wang, Z., Yu, T. & Li, H., 2018. Seismic performance of CFRP-retrofitted large-scale rectangular RC columns under lateral loading in different locations. *Compos. Struct.,* Volume 192, pp. 475-488.

Wang, J., Yang, J. & Cheng , L., 2019. Experimental study of seismic behavior of high-strength RC columns strengthened with CFRP subjected to cyclic loading. *J. Struct. Eng,* Volume 145.

Wang, L. et al., 2017. Seismic behavior of preloaded rectangular RC columns strengthened with precambered steel plates under high axial load ratios. *Eng. Struct,* Volume 152, pp. 683-697.

Wu, Y., Griffith, M. & Oehlers, D., 2003. Improving the strength and ductility of rectangular reinforced concrete columns through composite partial interaction: Tests. *J. Struct. Eng.,* Volume 129, pp. 1183-1190.

Wu, Y., Liu, T. & Wang, L., 2008. Experimental investigation on seismic retrofitting of square RC columns by carbon FRP sheet confinement combined with transverse short glass FRP bars in bored holes. *J. Compos. Constr,* Volume 12, pp. 53-60.

Xia, J., Jin, W. & Li, L., 2011. Shear performance of reinforced concrete beams with corroded stirrups in chloride environment. *Corrosion Science,* Volume 53, pp. 1794-1806.

Xue, J. et al., 2018. Severly damaged reinforced concrete circular columns repaired by turned steel rebar and high-performance concrete jacketing with steel or polymer fibres. *Appl. Sci,* Volume 8, p. 1671.

Xu, S. & Cai, X., 2010. *Bond behavior of corroded reinforcing bar and ultra high toughness cementitious composites (UHTCC).* Assessment, Durability, Monitoring and Retrofitting of Concrete Structures/eds. B. H. Oh,Seoul, 794-800 (2010).

Yalcin, C., Kaya, O. & Sinangil, M., 2008. Seismic retrofitting of R/C columns having plain rebars using CFRP sheets for improved strength and ductility. *Constr. Build Mater.,* Volume 22, pp. 295-307.

Yang, J. & Wang, J., 2018. Seismic performance of shear-controlled CFRP-strengthened high-strength concrete square columns under simulated seismic load. *J. Compos. Constr,* Volume 22.

Ye, L., Yue, Q., Zhao, S. & Li, Q., 2002. Shear strength of reinforced concrete columns strengthened with carbon-fibre-reinforced plastic cheet. *J. Struct. Eng.,* Volume 128, pp. 1527-1534.

Youm, K. et al., 2007. Seismic performance of lap-spliced columns with glass FRP. *Mag. Concr. Res,* Volume 59, pp. 189-198.

Yuan, W., Guo, A. & Li, H., 2017. Experimental investigation on the cyclic behaviors of corroded coastal bridge piers with transfer of plastic hinge due to non-uniform corrosion. *Soil Dynamic and Earthquake Engineering,* Volume 102, pp. 112-123.

Zhang, W.;, 2012. Bond behaviour of normal/recycled concrete and corroded steel bars. *Construction and Building Materials,* Volume 48, pp. 348-359.

Zhao, Y.;, 2013. Bond behaviour of normal/recycled concrete and corroded steel bars. *Construction and Building Materials,* Volume 48, pp. 348-359.

Zhou, C., Lu, X., Hi, H. & Tian, T., 2016. Experimental study on seismic behavior of circular RC columns strengthened with pre-stressed FRP strips. *Earthq. Eng. Eng. Vib,* Volume 12, pp. 625-642.

Zhou, X. & Liu, J., 2010. Seismic behavior and shear strength of tubed RC short columns. *J. Constr. Steel. Res.,* Volume 66, pp. 385-397.

Zhu, W.;, 2013. Effect of corrosion of reinforcement on the mechanical behaviour of highly corroded RC beams. *Engineering Structures,* Volume 56, pp. 544-554.

Zhu, W. & François, R., 2014b. Experimental investigation of the relationships between residual cross-section shapes and the ductility of corroded bars. *Cornstruction and Building Materials,* Volume 69, pp. 335-345.

3. Modeling the Behavior of Corroded RC Members

3.1. Introduction

As was mentioned in the introduction, the extent of damage in the existing RC building stock and infrastructure is incalculable and extremely widespread, underscoring an urgent need for immediate development of methodologies for assessment, repair and rehabilitation of the affected built environment (American Road & Transportation Builders Association, 2020).

Corrosion damaged structures are frequently found in regions of moderate or high seismicity. Having been constructed at the height of industrial urbanization, these structures may have been under-designed for earthquake resistance at the outset, as it was not till the 1980's when a major shift occurred in earthquake design practice incorporating advanced detailing to secure some degree of seismic resilience.

From a seismic assessment perspective, it is noted that corrosion can reduce a well-designed structure into as critical a condition as a poorly detailed one. Corrosion affects first the bar diameter of stirrups due to their proximity to the member surface (Fernandez and Berrocal, 2019); thinner and embrittled stirrups result in ineffective confinement and poor lateral support of the longitudinal reinforcement (Tastani and Pantazopoulou, 2005). Accumulation of rust along the bar surface, cracked covers owing to the dilative pressures of the iron oxides, and reduction of the height of bar ribs, all contribute to the effective reduction of bond strength and development capacity of lap splices and anchorages (Tastani and Pantazopoulou, 2007). Reduced bar area of longitudinal reinforcement also affects the primary member strength (Vu and Li, 2018).

Accurate modelling of the affected structural members is therefore essential for the relevance of the assessment exercise. This refers to the need for a faithful representation of the corrosion impacted, reduced reinforcement areas and mechanical characteristics of the embrittled materials and of the functional implications of cracking, such as the uninhibited tension reinforcement sliding and the increased tendency for compression buckling of reinforcement restrained by reduced stirrup sections. A high level of modelling complexity needs to be employed in this regard. There are several studies on numerical modelling of corroded reinforced concrete structures, and a few methodologies have been proposed, marked by an essential tradeoff between the degree of complexity and accuracy (Vu, Yu and Li, 2016; Di Carlo, Meda and Rinaldi, 2017;

El-Joukhadar, Tsiotsias and Pantazopoulou, 2019; Parulekar *et al.*, 2020; Molaioni, Carlo and Rinaldi, 2021). Aiming to address the need for a systematic procedure for seismic assessment of corrosion-affected columns, a nonlinear computational modelling strategy for pier columns is assembled and calibrated against experimental evidence; the approach takes into consideration the effects of corrosion on bar properties and the condition of cover and bond degradation so as to test that the model can actually reproduce the observed behavior of corroded members. This is subsequently used to study the sensitivity of the primary seismic response indices to the degree of corrosion.

3.2. Corrosion Mechanisms Affecting Column Resistance

Verification of seismic evaluation of RC columns and piers follows the performance criteria provided in ASCE 41 (2017) and ACI-374 (2016). Such procedures may be calculation-intensive, and they demand extensive information with regards to reinforcement ratios and detailing. The purpose of such assessment methods is to compare the demands that a credible future seismic hazard will impose on a column with a dependable estimate of the component's deformation capacity, in order to foresee future seismic performance and expected damage. Corrosion is not addressed explicitly in this process although it is implicitly understood that a structure which has been exposed to the elements for several decades definitely carries a high risk of reinforcement corrosion and cover concrete degradation as a result of carbonation – a process exacerbated by the use of de-icing salts in infrastructure.

Corrosion affects the response of a RC component through many different ways, a most obvious being its impact on structural material properties. During the early service life of a concrete structure, reinforcement is protected from corrosive activity by the high alkalinity of concrete. The "initiation period" (Tuutti, 1982), is the time required to reduce the pH around the bar so as to make the reaction between oxygen and the iron compounds of the bar material, possible. This occurs either through carbonation or due to gradual concentration of chloride ions on the bar surface, transported by moisture through concrete's capillary pores. The corrosion propagation period is the ensuing phase of oxidation of iron (producing ferrous and ferric oxides), which results in rust accumulation over the bar – concrete interface. Corrosion by-products (various oxides) differ in volume, occupying two to ten times the volume of steel (the volume is higher when the iron oxides are fully hydrated, into chemically stable forms of rust).

Apart from the bar area reduction and the embrittlement of the material which occurs due to the gradual breakdown of the iron compounds in the material microstructure, the increased volume occupied by the bar and newly formed rust, exerts a radial bursting pressure around the reinforcement, leading to radial cracking of the concrete cover along the bar length. Cracks in the concrete cover lead to a reduction in the section's strength and stiffness; the loss of reinforcement section also contributes to strength and stiffness deprecation, which will be explored in the present work. Cracks also facilitate the future ingress of corrosive agents to the reinforcement which further increases the rate of corrosion. The mechanistic implications of these processes are modelled in the present study, using finite element modelling of the affected materials since component modeling highly depends on material properties.

3.3. Models of Corroded Material Properties

The following sections build on the available experimental evidence in order to develop quantitative models that may be used for simulation of the mechanical behavior of corroded columns – a step that is essential for detailed seismic evaluation of corroded structural components. The work comprises three attributes:

(a) an updated database of material tests on corroded bar samples is used to derive attenuated properties for yield strength and deformation capacity of rebars.

(b) quantitative models accounting for the loss of bond-slip resistance of corroded bars embedded in concrete are reviewed and formulated with reference to bar mass loss (%).

(c) modeling the effects of rust expansion in propagating cracks and reducing the strength of the concrete cover.

Detailed finite element models are developed for columns considering the results of (a), (b) and (c). Calibration against well-known experiments conducted on columns subjected to corrosion follows, as a means of model validation.

Next, a parametric evaluation of the validated column models is used in order to reproduce and correlate the experimental trends of relevant component tests assembled in a database. The combined results of the parametric study and the experimental database are used to support the derivation of attenuation expressions for modifying the established performance criteria for

columns and piers. The attenuated resistance curves are proposed for seismic evaluation of corrosion damaged components within the framework of the existing seismic assessment guidelines.

3.3.1. Modeling of the Stress-Strain Response of Corroded Reinforcement

There have been many attempts at quantifying the degradation in mechanical properties of reinforcement due to corrosion (Almusallam, 2001b; Palsson and Mirza, 2002a; Du, Clark and Chan, 2005; Apostolopoulos, 2007; Apostolopoulos and Papadakis, 2008; Lee and Cho, 2009; Dang and François, 2013; Fernandez, Bairán and Marí, 2015; Lu *et al.*, 2016; Fernandez and Berrocal, 2019). It has been found that corrosion causes a significant reduction in ductility, yielding and ultimate tensile strength of reinforcing bars. More susceptible are inclusions in the metal alloy which appeared more frequently in reinforcing steel produced in the latter half of the 20th century (Takuya, Ryuta and Masayuki, 2020). A database of experimentally tested corroded reinforcement was primarily assembled for the needs of the present study (El-Joukhadar, Tsiotsias and Pantazopoulou, 2019). This database has been continuously updated and it now comprises more than 300 coupon test results. The gathered data are plotted in three different graphs as shown in Figures. (3-1, 3-2 and 3-3) for the residual yield strength, residual ultimate strength and residual ultimate elongation capacity (at fracture) of corroded bars with respect to increasing reinforcement mass loss, x. It is noted that mass loss of reinforcement bars is used commonly in the literature to quantify the extent of corrosion, but it may be a relatively insensitive index when it comes to quantifying the very critical implications of pitting. In cases of pitting corrosion, the mass loss is concentrated locally, and thus the bar section undergoes a dramatic reduction with ensuing implications of bar load carrying capacity. In the absence of local pitting, corrosion may be assumed as being distributed uniformly over the bar – this type of damage occurs in mild steel in the presence of carbonation. For this process, the geometric relationship given by Equation (3-1) may be used to calculate the reduced bar diameter, D_{cor} , after corrosion, given the value of x (in percent). In Equation (3-1), M_0 and D_0 are the mass per unit length and diameter of the uncorroded bar(s), and M_{cor} is the residual mass per unit length of the corroded bar(s).

$$x = \frac{M_0 - M_{cor}}{M_0} \cdot 100 = \left(1 - \left(\frac{D_{Cor}}{D_0}\right)^2\right) \cdot 100 \rightarrow D_{cor} = D_o \cdot \sqrt{1 - \frac{x}{100}} \quad (3\text{-}1)$$

The experimental data points plotted in Figures (3-1, 3-2 and 3-3) were divided into two categories depending on the corrosion conditioning process. The first category (marked with triangles)

corresponds to tests conducted on naturally corroded bar samples (or corroded in a simulated natural climate environment). The second category, represented by circles, corresponds to galvanostatic or potentiostatic corrosion (by using impressed current or voltage). It is noted that both types of corrosion process affect in the same way the material strength (Figure 3-1 and 3-2), however the reduction in material strain capacity is much more dramatic in the case of natural corrosion (Figure 3-3).

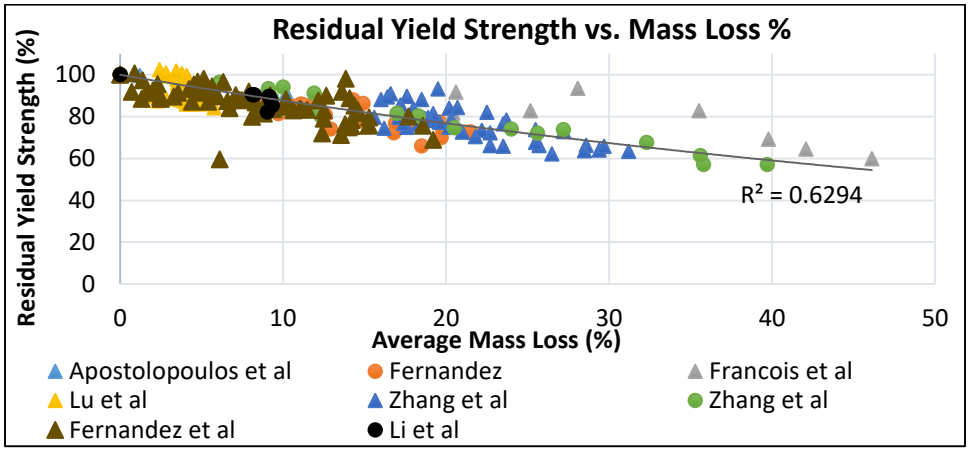

Figure 3-1. Residual yield strength of corroded reinforcement with increasing mass loss.

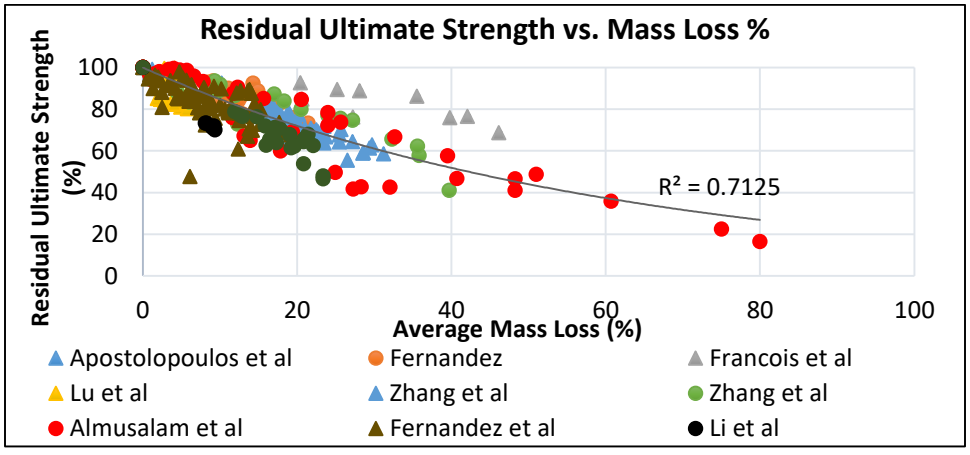

Figure 3-2. Residual ultimate strength capacity of corroded reinforcement with increasing mass loss.

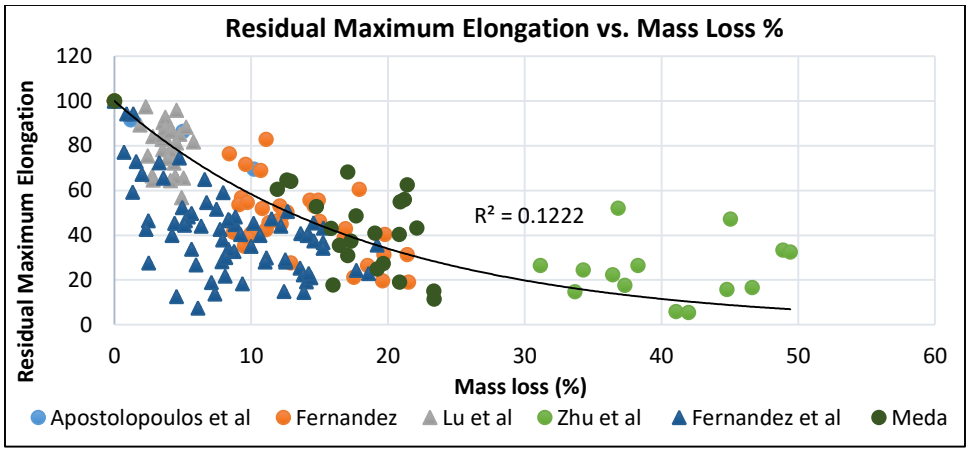

Figure 3-3. Residual maximum elongation capacity of corroded reinforcement with increasing mass loss.

Expressions for residual material properties were formulated through exponential regression. Equations (3-2, 3-3 and 3-4) represent the residual yield strength, $f_{y,res}$, ultimate strength, $f_{u,res}$ and ultimate elongation, $\varepsilon_{u,res}$, of corroded bars with increasing amount of average steel mass loss ratio, x.

$$f_{y,res} = f_y \cdot e^{-0.013x} \tag{3-2}$$

$$f_{u,res} = f_u \cdot \mathrm{e}^{-0.016x} \tag{3-3}$$

$$\varepsilon_{u,res} = \varepsilon_u \cdot e^{-0.054x} \tag{3-4}$$

In Equations. (3-2, 3-3 and 3-4), parameters f_y, f_u and ε_u represent the reference uncorroded values for yield, ultimate strength and ultimate strain capacity, respectively. For example, based on the experimental evidence summarized by the above equations, for a mass loss ratio of $x=10\%$, Eqns. (3-2 to 3-4) lead to, $f_{y,res}=0.88 \cdot f_y$, $f_{u,res}=0.85 \cdot f_u$, and $\varepsilon_{u,res}=0.58 \cdot \varepsilon_u$ and a residual bar diameter $D_{cor} = 0.94D_o$.

Figure 3-3 shows a large scatter in data, especially between naturally corroded and artificially corroded reinforcement bars. This is attributed to the random presence of pits in the tested bars, thus a more accurate representation of the results would be in terms of pit depth as opposed to reinforcement mass loss.

3.3.2. Bond Modeling of Corroded Reinforcement

Ribbed reinforcement is bonded to the surrounding concrete through cohesion and mechanical interlock. It was stated in Chapter 2 that the cohesion component is lost at infinitesimal levels of relative translation of the bar from concrete (slip). The main mechanism of stress-transfer between the two materials is mechanical interlock where the ribs bear on the surrounding concrete. The bearing stresses are resolved to a radial and a longitudinal component as depicted in Figure 3-4. It is noted that both stress terms are needed to support bar development. The component parallel to the bar axis represents the bond stress which is essential for stress transfer. The radial pressures can lead to splitting failure in the cover. Bond failure could either be dominated by the longitudinal forces acting at the tips of the ribs that define the bar interface - which lead to a pullout failure, or by the radial pressures which require tensile hoop stresses in the cover, and may result in splitting failure. This is the most common mode of failure unless high confinement and/or a thick concrete cover is present – both of those being relatively unlikely in older piers and columns.

In the presence of corrosion, rust accumulation on the steel-concrete interface severely affects the bond strength of reinforcement, through three mechanisms: first the bursting pressures imparted by the expanding rust on the cover, compete with radial pressures required to support bond strength, for the same resource, namely the hoop tensile strength of the cover. The second mechanism is through reduction of the rib height and therefore the mechanical interlock; last, the rust accumulation that interpolates between cover and the bar creates a slippery interface that reduces interface friction. All of the above lead to eventual loss of mechanical interlock and therefore bar development capacity(Almusallam *et al.*, 1996; P. S. Mangat and Elgarf, 1999; Tastani and Pantazopoulou, 2007; Prieto, Tanner and Andrade, 2011; Zhao *et al.*, 2013; Berrocal *et al.*, 2017; Lin *et al.*, 2019; Koulouris and Apostolopoulos, 2020; Robuschi *et al.*, 2020).

Table 3-1 outlines the estimated magnitude of reduction in residual bond strength of corroded reinforcement as recommended by fib Model Code, (2010) based on extensive evaluation of published experimental evidence. This approach is maintained in the draft new fib-Model Code, (2020).

Table 3-1. Magnitude of the Reduction in Residual Bond Strength of Corroded Reinforcement fib Model Code (2010)

Corrosion Penetration mm.	Equivalent Surface Crack mm.	Confinement	Residual Capacity (% of f_b). Bar Type:	
			Ribbed	Plain
0.05	0.2-0.4		50-70	70-90
0.1	0.4-0.8	No stirrups	40-50	50-60
0.25	1.0-2.0		25-40	30-40
0.05	0.2-0.4		95-100	95-100
0.1	0.4-0.8	with Stirrups	70-80	95-100
0.25	1.0-2.0		60-75	90-100

The percent reduction of the available bond strength is estimated from Table 3-1, considering the presence (or lack of), of stirrup confinement, using the depth of corrosion penetration, C_p. This is approximated from the residual bar diameter D_{cor} in Equation (3-1) (measured from invasive investigations on site, or back-calculated from the mass loss ratio x), using Equation (3-5):

$$C_p = (D_0 - D_{cor})/2 = 0.5 \cdot D_0 \left(1 - \sqrt{1 - \frac{x}{100}}\right) \quad (3\text{-}5)$$

For example, a 10% (in mass loss) corroded 15M bar having an original diameter of D_0 = 16mm (0.63in) results in a residual diameter of D_{cor} = 15.17mm (0.6 in). In this case, the corrosion penetration would be C_p = 0.41mm (0.016 in). With this information, the residual bond strength may be obtained from Table 3-1 using either interpolation or extrapolation.

3.3.3. Modeling of the Cracked Concrete Cover

As mentioned in the preceding, the accumulation of corrosion by-products results in cracking of the concrete cover. For a more accurate assessment, the reduction of concrete cover strength must be taken into consideration as it affects both the strength and stiffness of structural components. Coronelli and Gambarova (2004) accounted for the softening effect on the compressive strength resulting from the transverse splitting strain in the cover, ε_1, and the commensurate reduction in the elastic modulus using the corresponding compression softening factor from the modified diagonal compression field theory (Vecchio and Collins, 1986). The source of cracking and the effect on strength reduction is depicted in Figure 3-4.

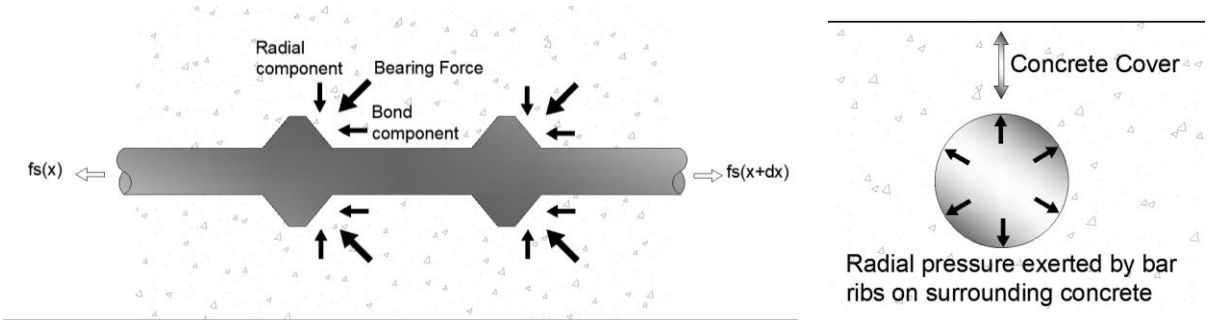

Figure 3-4. Development of stresses along the steel-concrete interface. (Ribs are exaggerated for illustration purposes)

Thus, the residual compressive strength of the concrete cover is calculated using Equation (3-6).

$$f_{c\,res} = \frac{f_c'}{1+0.1\frac{\varepsilon_1}{\varepsilon_{co}}}\ ; \quad \text{and,}\ \ E_{c,res} = E_c \cdot \left(f_{c,res}/f_c'\right) \tag{3-6}$$

In Equation (3-6), ε_{co} is the strain at peak compressive strength (=0.002), and ε_1 is the average tensile strain that is caused by lateral expansion of the products of longitudinal bar corrosion. It represents a smeared measure of splitting crack widths of the cover. Therefore, ε_1 is obtained from Equation (3-7):

$$\varepsilon_1 = N_{cb} \cdot \left[\pi \cdot (\alpha_{rs} - 1) \cdot 2C_p\right]/b \tag{3-7}$$

Parameter N_{cb} represents the number of bars present in the cross-section's compression zone, D_b is the bar diameter, b is the width of the cross-section and α_{rs} is the volume ratio of the oxides with respect to the parent metal.

To illustrate the magnitude of this effect, the case of two column cross sections is considered for comparison: both have 3 bars in the compression zone, the first with bar size of 20M and the second with bar size of 15M. All other column parameters are identical, including α_{rs}=6. Assuming a 10% mass loss for both sections due to corrosion, the calculated C_p values are 0.5 and 0.41 for both sections respectively. According to Equation (3-7) the average tensile strain that is caused by lateral expansion of the products of longitudinal bar (ε_1) is reduced from 0.094 to 0.077 when reducing the bar size from 20M to 15M, and the corresponding effect of concrete residual compressive strength is 17% and 20% of f_c. Therefore, the compressive strength of the corrosion cracked cover is reduced to about 1/5th of the normal concrete strength.

3.4. Validation of the Proposed Modeling Approach

The relevance and accuracy of the methodology recommended for simulation of the mechanical behaviour of corroded elements is validated in this section through correlation with the experimental response of tested corroded components. The published experimental investigation by Goksu and Ilki (2016) on the performance of corroded lap-spliced columns under reversed cyclic loading was selected from the literature because of the breadth of scope of the test program and the availability of the required data. Modelling was implemented in the nonlinear finite element analysis (FEA) platform ATENA Science-GID (Cervenka Consulting, 2007), however the same concepts may as well be applied to any other pertinent software for reinforced concrete.

3.4.1. Column Detailing

Specimens tested by Goksu and Ilki (2016), were scaled models of structural columns (at a scale of 1:2). They were detailed as shown in Figure 3-5. The typical column had an effective shear span of L_s = 1.2 m and a cross-section of 200 mm width by 300 mm total depth; with an aspect ratio of 1:4 the columns were designed to develop response dominated by flexural curvature. The column was reinforced with *4Φ14* reinforcement bars lapped at the base over a lap length of *40Φ* = 560mm. Total longitudinal reinforcement ratio calculated over the column core was 1.6%. Shear reinforcement consisted of Φ8 bars spaced at 100mm, with an unsupported bar aspect ratio equal to *s/Φ=100/14=7*. The applied axial load was 282 KN, equivalent to about 20% of the column's axial load capacity (this was calculated as $0.2f_c'A_g$). For validation purposes, columns NS-X00, NS-X09, NS-X16 and NS-X22 were modelled. (Specimen identification codes are maintained as per the reference study. The numeral following X represents the fraction of mass loss of reinforcement after corrosion - for example X09 means that the specimen has undergone 9% reinforcement mass loss, while the term NS represents the strength characteristic of concrete, N is for Normal, and S is for strength).

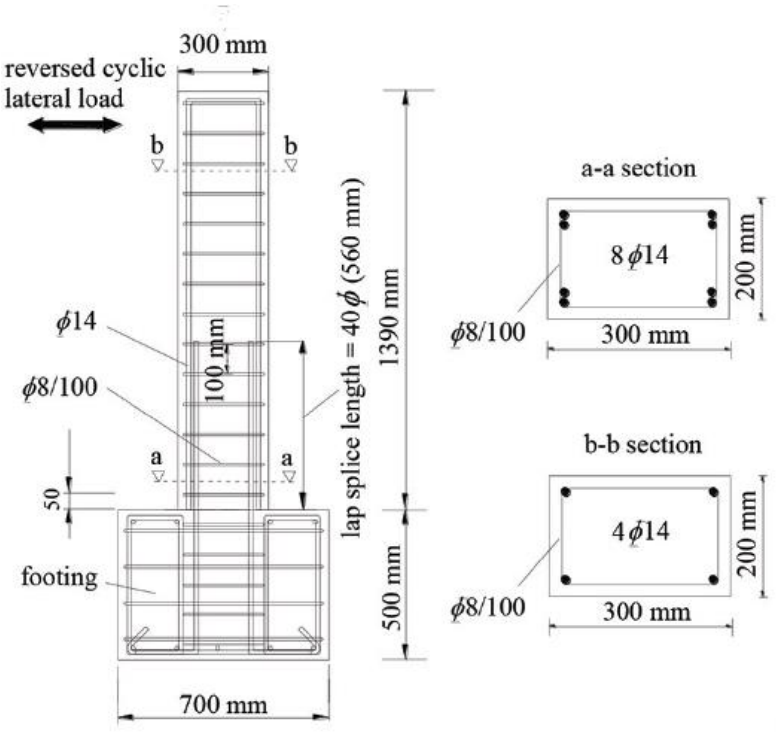

Figure 3-5. Column detailing reported by Goksu and Ilki (2016) (figure from the reference study)

3.4.2. Modeling and Discretization

Figure 3-6 depicts the testing arrangement and the model discretization. Considering fixity at top and bottom of the actual column when undergoing relative lateral displacement, only half of the column was modeled in the tests, being represented as a laterally swaying cantilever. The lateral displacement at the tip of the cantilever divided by the shear span of the element is the drift ratio: equal drift and the same constant shear are the two variables that relate the cantilever model with the actual full length prototype column. Taking advantage of the symmetry of the cross section in the transverse direction (i.e. *x-z* is the plane of symmetry, at $y=0$) only half of the cantilever cross section was modeled, with the condition that $u_y(x,0,z)=0$.

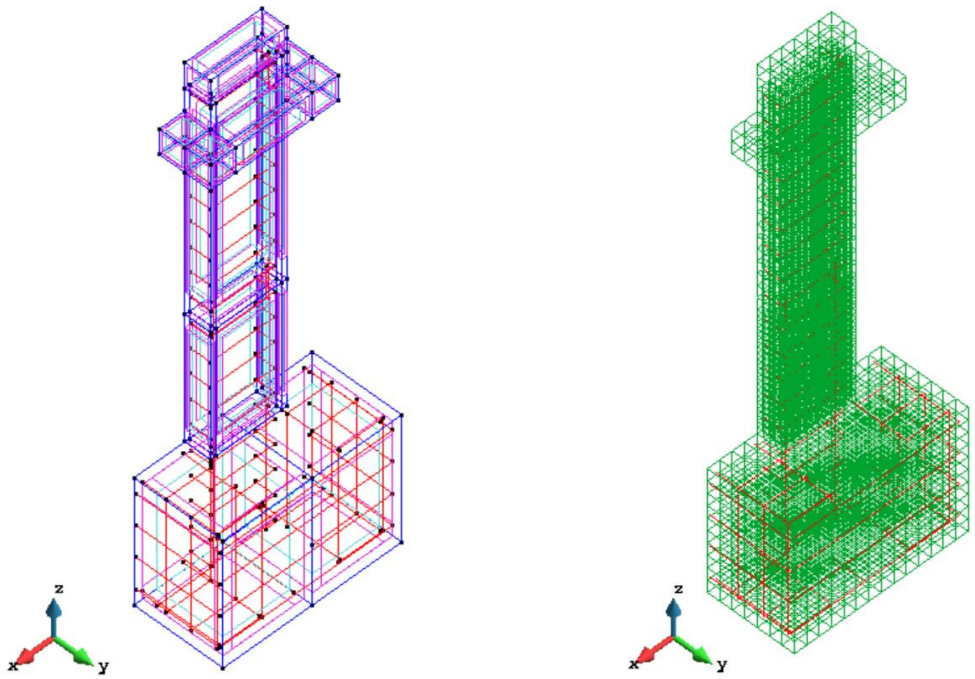

Figure 3-6. Finite element model as shown in the ATENA Science-GiD interface.

All nodes on the bottom surface of the foundation were restrained from vertical movement ($u_z(x,y,0)=0$). A *100 mm* (4 in) thick plate was used at the top of the cantilever cross section to apply the axial force in the form of distributed constant vertical pressure (p = *-5.0 MPa*). Two additional *100 mm* thick plates were used at the front and back sides of the column at 1.2 m from the critical section to apply the lateral displacement at the centroid (*-0.1m, 0.0 m, 1.2m*) These auxiliary elements were assigned "3D Elastic Isotropic" steel material, fully bonded on the column at the loading point, in order to enable more uniform spreading of the load in the contact surfaces and to avoid local convergence problems.

The concrete material model implemented in the simulation was "3D Nonlinear Cementitious2", where the biaxial strength failure envelope under plane stress is specified in the input. The nonlinearity of the concrete is dependent on the equivalent uniaxial strain ε^{eq}. The equivalent uniaxial strain is defined as the strain that is produced by the stress σ_{ci} in a uniaxial test with the modulus E_{ci} in the direction i ($\varepsilon^{eq} = \sigma_{ci}/E_{ci}$). The complete equivalent uniaxial stress-strain diagram for concrete is shown in Figure 3-7. Concrete compressive strength f_c' was 25 MPa, tensile strength f_t was taken equal to 2.5 MPa. A modulus of elasticity E_c=22,500 MPa was assigned to the material. The concrete fracture energy, *GF*, was set equal to *130 N/m*, determined based on the Model Code 2010 expression: $GF = 73 \cdot (f'_c)^{0.18}$. A fully rotated crack model was used, where the axis of the

principal stress and principal strain coincide throughout loading and crack formation in the model, which leads to eliminating the development of shear strains along the crack plane. The degradation from the elastic slope in the unloading branch from the compression stress-strain envelope is controlled by the unloading factor f_U which in the model was taken equal to *0.1*. This factor ranges between 0-0.99, where 0 corresponds to unloading to the origin (as shown in Figure 3-7) while 0.99 corresponds to concrete unloading parallel to the initial stiffness.

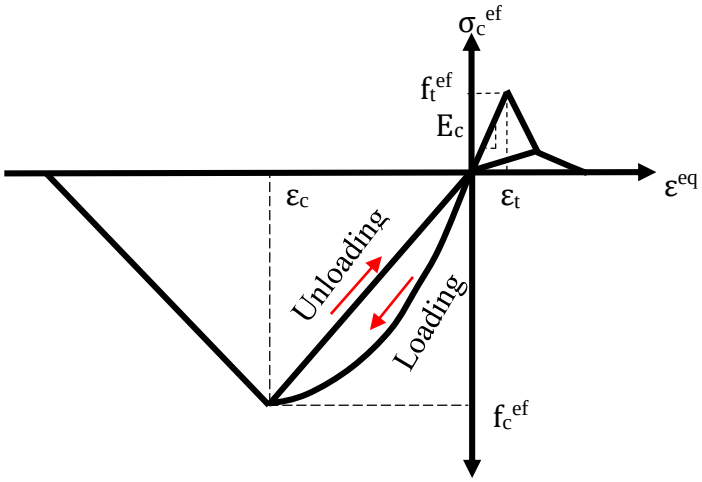

Figure 3-7. Equivalent stress-strain law for concrete in the FEA.

Reinforcing bars were modelled as truss elements using the "Reinforcement" option, with a *bilinear with hardening* type of uniaxial stress-strain behavior with a steel modulus E_s equal to 200,000 MPa. Other input properties are listed in Table 3-2. In order to account for the effects of corrosion, several interventions were made in the nonlinear model of the column. Therefore, the reinforcement material properties of the models representing the corroded columns were modified from the reference case NS-X00, according to Equations (3-2, 3-3 and 3-4). Note that bar diameters for both ties and longitudinal reinforcement were not reduced in the model because the effective reduction in bar strength due to corrosion was already accounted for in deriving Equations (3-2, 3-3 and 3-4). The hysteretic response of the reinforcement was modelled using Equations (3-8 to 3-11, which represent the model by Menengotto and Pinto, (1973), with a Bauschinger R value = 7, C_1 value = 5000 and C_2 value = 20.

$$\sigma = (\sigma_o - \sigma_r)\sigma^* + \sigma_r \qquad (3\text{-}8)$$

$$\sigma^* = b\varepsilon^* + \frac{(1-b)\varepsilon^*}{(1+\varepsilon^{*R})^{\frac{1}{R}}} \quad (3\text{-}9)$$

$$\varepsilon^* = \frac{\varepsilon-\varepsilon_r}{\varepsilon_o-\varepsilon_r} \quad (3\text{-}10)$$

$$R = R_o - \frac{C_1\xi}{C_2+\xi} \quad (3\text{-}11)$$

Where, C_1 , C_2 and R are defined by the user. The subscript ($_o$) of strain (ε_o) and stress (σ_o) presents the start point of the hysteretic branch while ($_r$) of strain (ε_r) and stress (σ_r) represents the end point of the branch. Parameter ε is the strain corresponding to the stress σ. Figure 3-8 illustrates the calculated cyclic stress strain response of the reinforcement with these variables, for the onset of unloading occurring at a strain of 0.005.

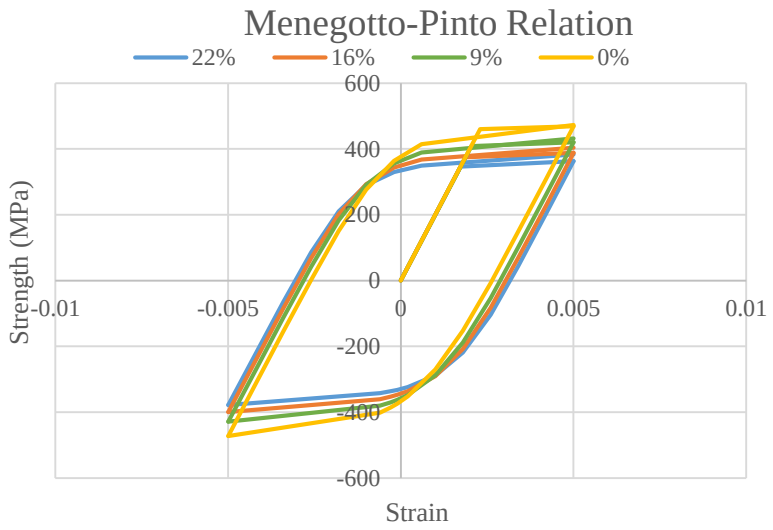

Figure 3-8. Menegotto-Pinto relationship for steel used for modelling Goksu and Ilki's columns

Bond material connecting the steel nodes with spatially coincident nodes in the concrete was assigned to the main reinforcement using the "Bond for Reinforcement" model. Here, the part of reinforcement anchored inside the support footing was considered in perfect contact with the concrete and in pristine condition. For the reinforcement in the deformable part of the member, the bond stress-slip law was modelled according to the Model Code 2010, where bond strength of the longitudinal bars was governed by splitting failure $f_{bd} = 8\cdot(f'_c/25)^{0.25} = 8$ *MPa* rather than pullout failure $f_{bd} = 2.5\sqrt{f'_c} = 12.5$ *MPa*. Thus, it was assumed that the corroded columns' bond strength was governed by splitting failure due to pre-existing cover cracking resulting from

corrosion accumulation. Bond strength reduction of corroded reinforcement was applied in accordance with Table 3-1 with reference to the analytical Bond-Slip relationship of the Model Code 2010.

Table 3-2. Calculated residual material properties of corroded columns using proposed expressions

Column ID		NS-X0	NS-X9	NS-X16	NS-X22
Mass loss (%)		0	9	16	22
Yield Strength f_y MPa	Main	460	409	374	346
	Ties	486	432	395	365
Ultimate Strength f_u MPa	Main	652	565	505	459
	Ties	681	590	527	479
Maximum Elongation Capacity ε_u	Main	0.116	0.071	0.049	0.035
	Ties	0.134	0.083	0.057	0.041
Concrete Cover compressive strength f_c		25	6.73	4.22	3.17

Figure 3-9 depicts the assumed bond-slip envelopes for longitudinal reinforcement, where it is illustrated that the peak and degraded values depend on the degree of corrosion. For the corresponding slip values of the corroded bond models, slip value S_3, corresponding to the onset of the post-peak residual bond with unrestrained slip beyond, was taken equal to half the distance between successive ribs, i.e., it was assigned the same values for both corroded and uncorroded bars. No plateau was considered at peak strength in the bond-slip envelope, which would correspond to a pullout response mechanism; thus, the slip value at attainment of bond strength, S_1, coincided with the slip S_2 that corresponds to the onset of post-peak degradation of bond (S_1= S_2). The S_1 value was interpolated based on the values of the uncorroded splitting bond-slip model (Model Code 2010) given the reduced peak bond strength; therefore, all the degraded bond-slip relationships were assumed to have the same initial slope.

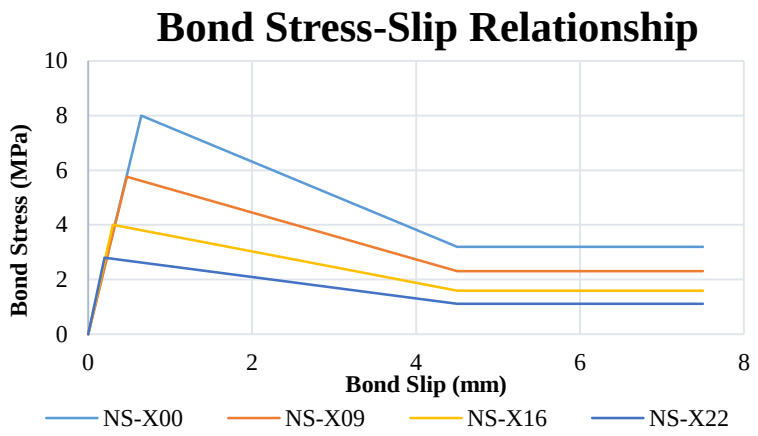

Figure 3-9. Bond Stress-Slip relationship for modeling Goksu and Ilki's columns

Figure 3-10 depicts the unloading/reloading rules used to model the hysteretic behavior of bond-slip using the software module "bar w/ memory bond material". In this model, reversal of load corresponds to reversing the direction of bond stress; once the peak is exceeded in the bond slip envelope pointwise along the bar, then, upon reversal of the loading direction, the bond stress value is set equal to the residual value and opposite in direction to what it had during loading along the envelope. Reversal occurs with no change in the magnitude of slip (i.e., the unloading branch is perpendicular to the slip axis in the diagram). The residual value is equal to the magnitude defined in the horizontal branch of the bond slip law of Figure 3-9 and is therefore different for each level of corrosion; in this study the residual bond strength was taken equal to 0.4 times the respective bond strength. Figure 3-10 displays the behavior of the cyclic loading and unloading rules of the hysteretic model.

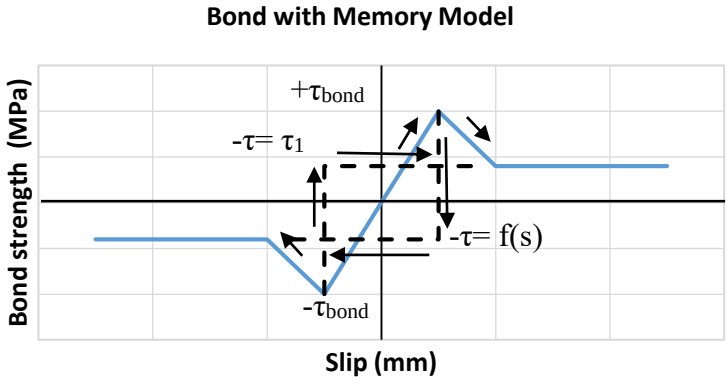

Figure 3-10. Bond with Memory Model for cyclic columns

Concrete cover cracking was accounted for by reducing the compressive and tensile strengths of the concrete cover material; the compressive strength was reduced according to Equation (3-6) and the tensile strength was assumed to be entirely lost (i.e., neglected).

The column was meshed using 2.5 cm hexahedral elements for the first 0.5 m of the shear span length, while the rest of the shear span was discretized into 5 cm elements. This mesh arrangement was found to be the most efficient discretization in terms of result accuracy and computational time.

3.4.3. Finite Element Analysis Results.

Resistance curves obtained from the finite element analysis to a displacement history are plotted in Figure 3-12 and compared with the experimental results of Goksu and Ilki (2016).

Figure 3-12 displays the hysteretic response plots of the lateral resistance of the cantilever column against the lateral displacement at the top of the cantilever column. Note here that lateral resistance force was corrected to account for the P-Delta effect contributed by the applied axial load, to eliminate the lateral degradation due to second order effects. This correction is necessary in order for the FE results to be comparable with the experimental values. This is because in the experiment the axial load was applied with the help of tensioned rods that followed the column chord going through the centroidal axis (i.e., at *x=0*) of the column cross section at the base of the column, whereas in the F.E. study the axial load was applied as a normal force acting in the *z* axis and following the cantilever top as it displaced in the *x*-axis. Therefore, the corrected lateral resistance force for the finite element model was calculated based on Equation 3-12.

$$V_{res} = \frac{M}{L_s} + P\theta \tag{3-12}$$

Where the term $P\theta$ is added to all lateral resistance values obtained from the finite element analysis.

Due to the test setup of experimental columns of Goksu and Ilki (2016), it is predicted that the lateral resistance has an additional component due the inclined axial load that was applied by the rods as shown in Figure 3-11. Therefore, the lateral resistance values of the Gosku and Ilki (2016) experiment was also corrected according to Equation 3-13.

$$V_{res} = V_{exp} + P \cdot \theta \cdot cos\theta_{tip} - P \cdot sin\theta_{tip} \tag{3-13}$$

Where θ_{tip} = 1.2θ

The models were able to replicate with consistency the behavior of the experimentally tested columns. Some minor discrepancies were observed in the comparisons: for example, in specimen NS-X00, it is noted that the model showed a symmetric response having a maximum load of about 50kN in both directions, while the tested column did not. This behavior is common in testing columns; although not significant in magnitude when seen in the context of the entire scope of the calibration study, the asymmetry seen in the experiment is attributed to several factors such as tolerances in the column fabrication, testing setup and hardware compliances, etc. The models also successfully replicated the hysteretic behavior of the tested column, which is a critical attribute for the relevance and validity of the correlation**.** In addition, the model successfully replicated the bond-failure in column NS-22 at a displacement level of 50mm. Crack patterns with minimum crack width of 1 mm and concrete stresses at ultimate displacements for columns NS-X00, NS-X09, NS-X16 and NS-X22 are illustrated in Figure 3-12. The consistency between experimental observation and F.E. simulation results are considered adequate evidence for validation of the model. The modeling procedure is used next, in order to explore the parametric sensitivity of the problem.

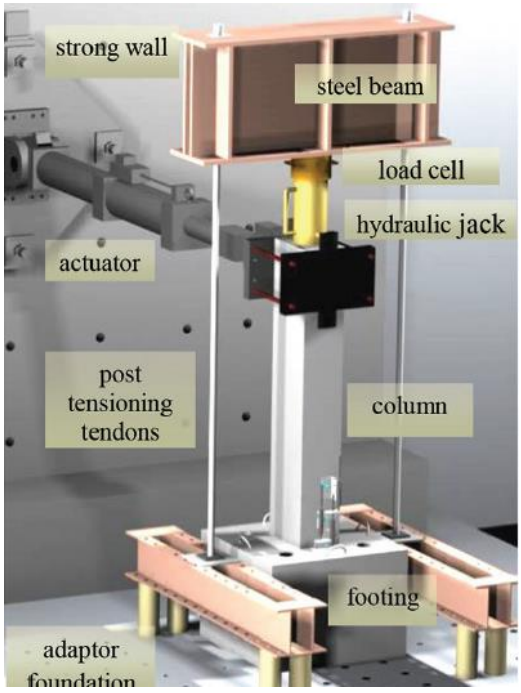

Figure 3-11. Goksu and Ilki's test setup

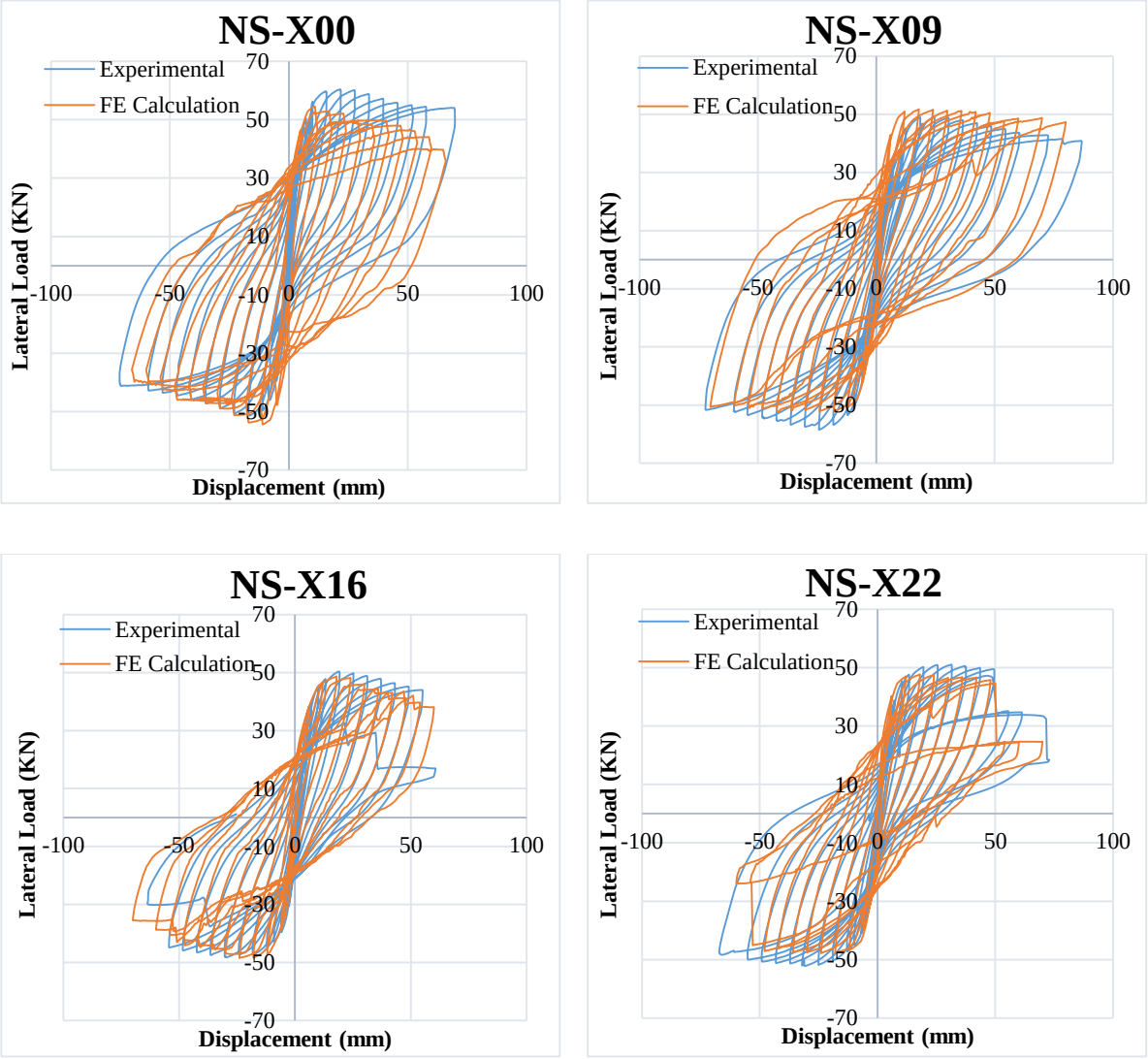

Figure 3-12. Hysteretic responses of the finite element analysis plotted over the hysteretic response of experimentally tested columns reported by Goksu and Ilki (2016).

3.5. Numerical Investigation

Using the proposed modeling procedure, the effect of corrosion on anchored (continuous reinforcement) and lap-spliced columns was investigated numerically. The objective here was intended to identify the effect of corrosion on the response envelope, so as to link the corrosion mass loss with the magnitude of the principal indices of lateral resistance (i.e. effect on stiffness, strength, and deformation capacity). The columns studied represent pre-1970's design standards having short lap splices located in the critical regions, poor concrete strength and sparse transverse

reinforcement. The main variables of the study were, the degree of corrosion as measured by steel mass loss (0%, 10% and 20%) and the presence or absence of lap-splices; the specimen identification code begins with A or L (for anchored or lap spliced longitudinal reinforcement), followed with the mass loss percentage.

Details regarding column characteristics, study variables and material properties are presented in Table 3-3. Column detailing is shown in Figure 3-13; columns had a 300mm square cross section; a shear span of 1.65m (5.41 ft) reinforced with 4-15M bars and 8mm diameter stirrups spaced at $s=d$ = 250mm (9.84 in). Lap-spliced columns had a lap length $l_p = 24\ D_b$ = 384mm (15.12 in) which represents older design practice. Concrete compressive strength was taken as f'_c=25 MPa (3.63 Ksi).

Table 3-3. IDs of columns from numerical investigation with calculated residual material properties.

		Anchored Columns			*Lap-Spliced Columns*		
Corrosion Level:		0%	10%	20%	0%	10%	20%
Case ID		A-0	A-10	A-20	L-0	L-10	L-20
Yield Strength f_y	Main	420	369(53)	324(47)	420(61)	369(53)	324(47)
MPa (Ksi)	Ties	300	263(38)	231(34)	300(44)	263(38)	231(34)
Ultimate Strength	Main	550(80)	469(68)	399(58)	550(80)	469(68)	399(58)
f_u	Ties	380(55)	324	276	380	324	276
Maximum	Main	0.2	0.117	0.068	0.2	0.117	0.068
Elongation Capacity ε_u	Ties	0.2	0.117	0.068	0.2	0.117	0.068
Concrete Cover compressive strength f_c		25	6.21	3.46	25	6.21	3.46

Columns were modeled using ATENA-GiD (Cervenka Consulting, 2007) following the proposed methodology. Columns were analyzed using the reversed cyclic displacement history shown in Figure 3-14, while maintaining an overbearing axial load ratio of $\nu = 0.2$.

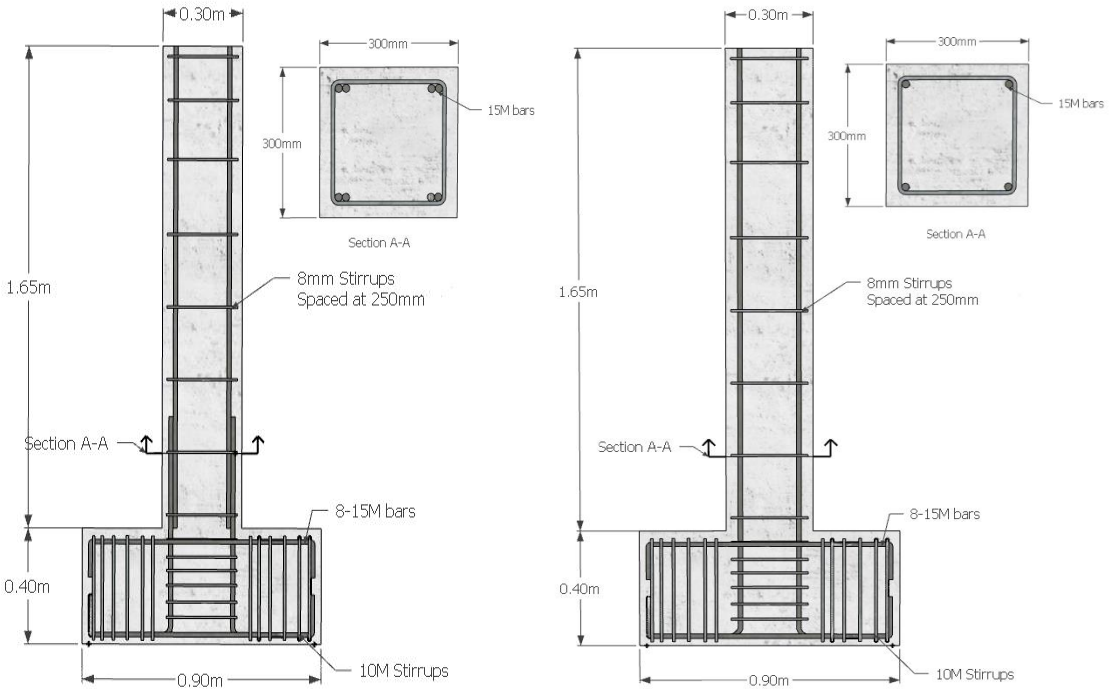

Figure 3-13. Detailing of standard columns for numerical investigation. Lap-spliced column (left), Anchored column (right)

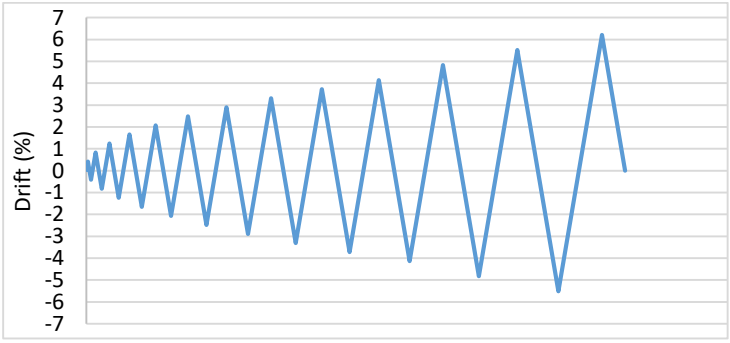

Figure 3-14. Loading protocol of columns in the numerical investigation.

3.5.1. Finite Element Analysis Results

Figure 3-15 displays the hysteretic responses and the respective backbone curves for uncorroded columns and corroded columns (with 10% and 20% mass loss) with and without lap splices at the critical region. Note that in each case, the load values in the response curves (i.e., the values on the vertical axis of the plots) have been normalized with respect to the corresponding peak value calculated for the corresponding uncorroded column with continuously anchored reinforcement, equal to V = 61 KN. This was done in order to facilitate the comparative degradation process with increasing mass loss for the entire group of models.

From Figs. 3-15 (A-0) and (L-0), it is observed that the uncorroded anchored column showed a 10% higher maximum strength than its twin lap-spliced column; however, the strength was not maintained at larger lateral displacements. The anchored column showed a quicker strength degradation relative to the lap-spliced column in the post-peak region. At 3.5% drift, the lap-spliced column had a 25% higher strength than the anchored column. This was attributed to the fact that lap-splice failure is energy dissipating and leads to a gradual strength reduction as opposed to the anchored columns. The latter, due to the continuity of the reinforcement, builds up more energy, and then would results in a sudden decrease in load carrying capacity once failure is initiated.

From Figure 3-15 (A-10) and (L-10) it was observed that the presence of corrosion led to a reduction in strength by 10% and 25% for the anchored and lap-spliced cases, respectively. The anchored corroded column maintained a higher strength with increasing drift magnitude, relative to its twin lap-spliced column, unlike the case in the uncorroded examples. The ultimate deformation of corroded columns with a 10% mass loss was reduced by 30%.

Columns with 20% mass loss experienced the most severe damage as may be seen in Figure 3-15 (C) and (C'). The columns experienced a strength reduction by 20% and 40% for the anchored and lap-spliced columns respectively, while the ultimate deformation capacity shrunk by 45%.

Figures 3-16 (A) and (B) show the backbone curves of the collection of anchored and lap-spliced columns respectively. The y-axis represents the lateral strength relative to the uncorroded model of each group (anchored or lap-spliced) as opposed to Figure 3-15 where strengths were normalized to the anchored uncorroded column.

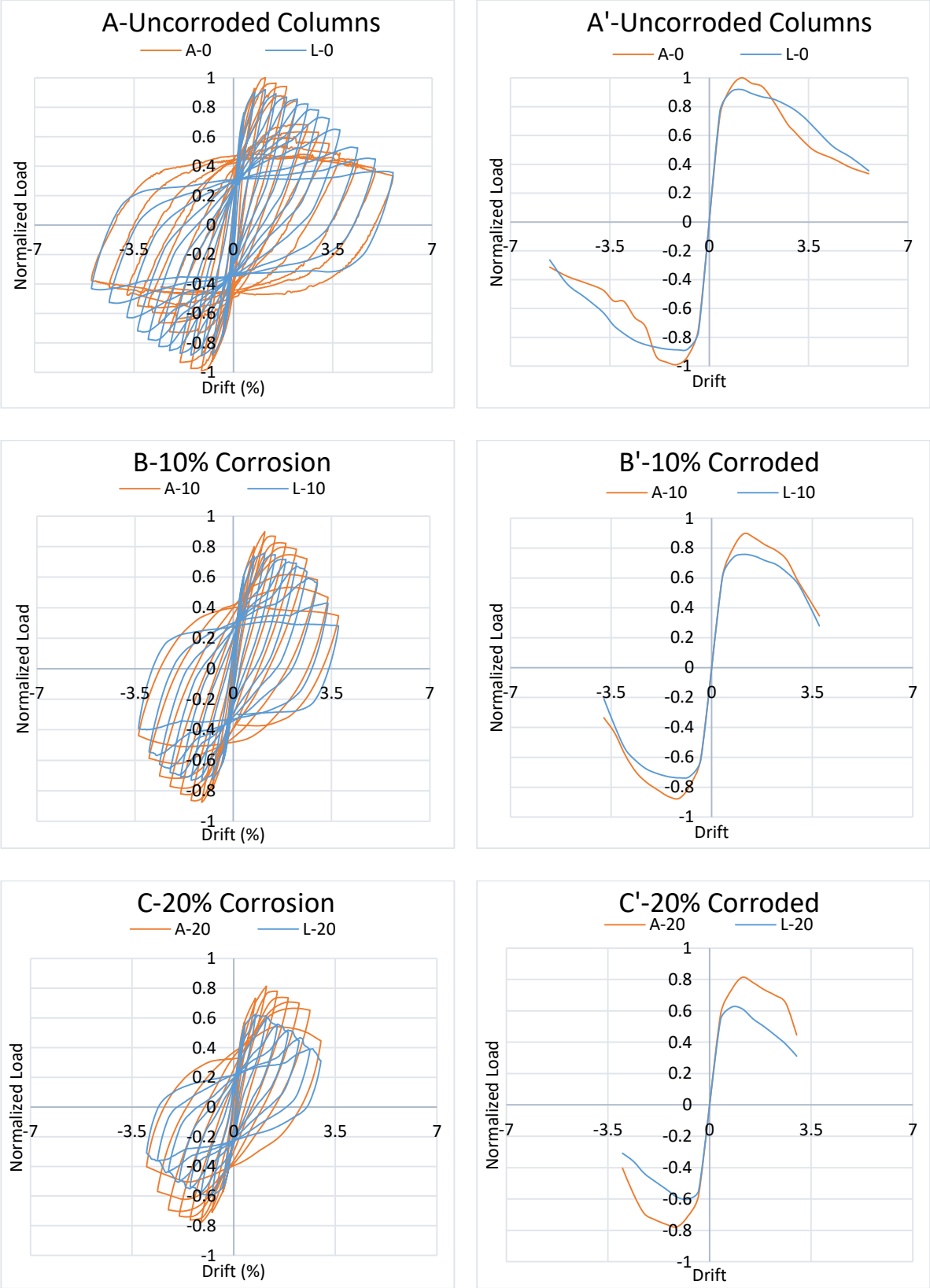

Figure 3-15. Hysteretic response and backbone curves of columns from the numerical study

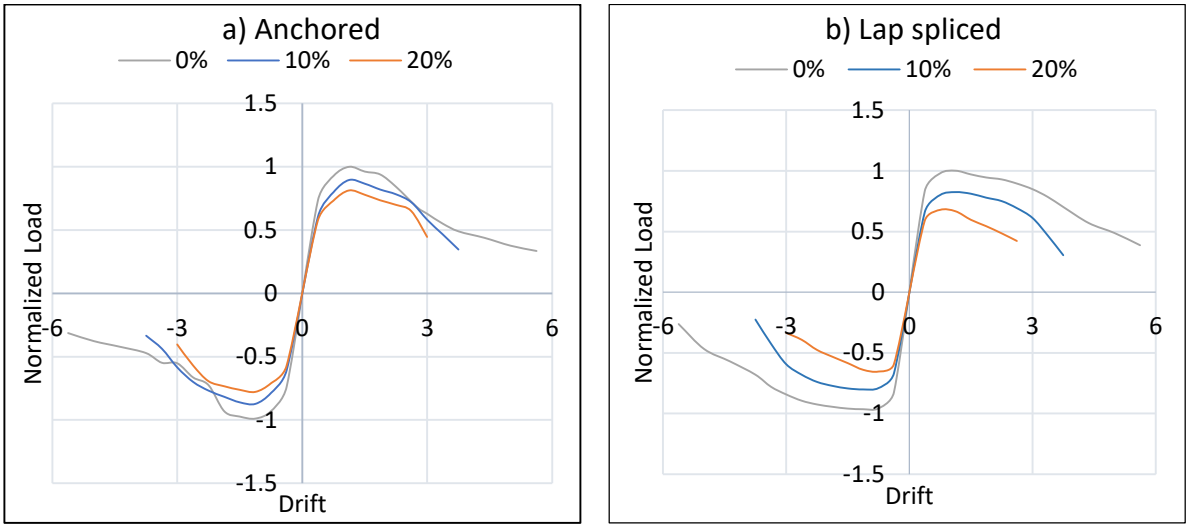

Figure 3-16. Backbone Curves of anchored and lap-spliced columns

3.5.2. Model Validation

Data regarding the backbone attenuation with increasing corrosion obtained from the current numerical investigation are compared with the respective trends obtained from a database of experimentally tested corroded columns assembled from literature reported by El-Joukhadar et al. (2019); the database contains 20+ column specimens comprising either continuously anchored, or lap-spliced reinforcement and having been subjected to accelerated corrosion conditioning prior to lateral load testing. Figure 3-17 plots the residual strength capacity of the corroded columns relative to the undamaged version of otherwise identical specimens from each reference study included in the database. The degree of corrosion of each specimen is given in the horizontal axis; strength values are given at relative drift ratios of 0.5%, 1% and 2% (each experiment is represented by a single black circle). Also plotted in the figures are the results of the parametric study conducted in the preceding, where red circles represent the A group of cases, and yellow represent the L group. It is noted that the residual lateral load strength estimates, given as a fraction of the corresponding uncorroded values of the modeled columns, fall within the cloud of experimental data. Furthermore, the residual capacity of lap-spliced columns showed a higher degradation of peak strength with increased corrosion levels compared to the rest of the data set.

The experimental and analytical trends depicted in Figure 3-17 provide evidence of further validation of the results obtained from the proposed modeling procedure. They also provide a

basis for quantifying the required modification (in order to account for corrosion) of the backbone curves specified by ASCE/SEI 41 (2017) for column seismic assessment.

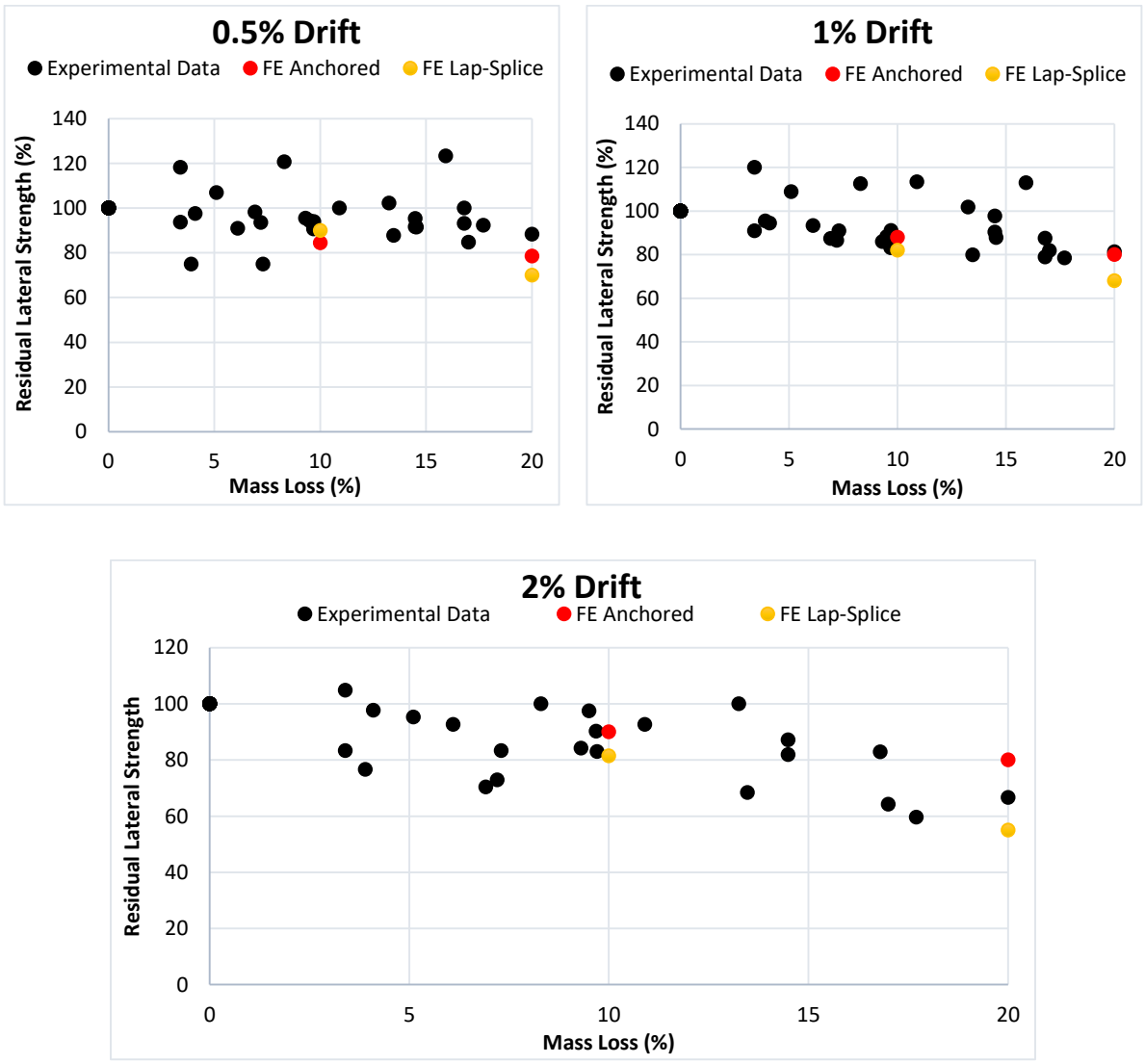

Figure 3-17. Model validation through comparison of residual lateral strength at 0.5%, 1% and 2% drift of calculated results vs experimentally tested columns from the literature.

3.6. Conclusions

This study focuses on developing a clear and easy-to-use methodology for taking corrosion damage into consideration while using existing modeling techniques for practicing engineers. The proposed model was validated by successfully replicating the behavior of experimentally tested corroded columns. After validating the model, a numerical investigation was carried out to study the effect of corrosion on twin lap-spliced and anchored columns. The following are the main conclusions from the study:

- New expressions for residual corroded reinforcement material properties are proposed. These expressions were obtained through regression analysis after assembling a database of different experimentally tested corroded reinforcement samples.
- A straightforward finite element modeling procedure was proposed accounting for corrosion damage in modelling structural components. The model was then validated against experimentally tested corroded columns.
- The numerical study showed that corrosion damage is more severe in the case of lap-spliced columns, showing a 40% strength reduction at 20% reinforcement mass loss due to corrosion, relative to anchored columns that lost 20% in strength at the same level of corrosion.
- The most affected mechanical property in corroded columns was the ultimate deformation capacity, where recorded degradation reached 45%.

3.7. References

ACI-374 (2016) *ACI 374 - Guide to Nonlinear Modeling Parameters for Earthquake-Resistant Structures*. Available at: www.concrete.org (Accessed: 27 March 2022).

ACI 222R-19 (2019) 'Guide to Protection of Reinforcing Steel in Concrete Against Corrosion', *American Concrete Institute*, pp. 1–65.

Al-Saidy, A. H. *et al.* (2016) 'Structural behavior of corroded RC beams with/without stirrups repaired with CFRP sheets', *Materials and Structures*. Springer Netherlands, 49(9), pp. 3733–3747. doi: 10.1617/s11527-015-0751-y.

Al-Sulaimani, G. J. *et al.* (1990) 'Influence of corrosion and cracking on bond behavior and strength of reinforced concrete members', *ACI Structural Journal*, 87(2), pp. 220–231. doi: 10.14359/2732.

Alaskar, A. (2013) 'Shear Behaviour of Slender RC Beams with Corroded Web Reinforcement'. University of Waterloo. Available at: https://uwspace.uwaterloo.ca/handle/10012/7472 (Accessed: 15 July 2019).

Allamt, I. M. *et al.* (1994) *Influence of atmospheric corrosion on the mechanical properties of reinforcing steel, Construction and Building Materials*.

Almusallam, A. A. *et al.* (1996) 'Effect of reinforcement corrosion on bond strength', *Construction and Building Materials*. Elsevier, 10(2), pp. 123–129. doi: 10.1016/0950-0618(95)00077-1.

Almusallam, A. A. (2001a) 'Effect of degree of corrosion on the properties of reinforcing steel bars', *Construction and Building Materials*. Elsevier, 15(8), pp. 361–368. doi: 10.1016/S0950-0618(01)00009-5.

Almusallam, A. A. (2001b) 'Effect of degree of corrosion on the properties of reinforcing steel bars', *Construction and Building Materials*. Elsevier, 15(8), pp. 361–368. doi: 10.1016/S0950-0618(01)00009-5.

Alonso, C. *et al.* (1998) 'Factors controlling cracking of concrete affected by reinforcement corrosion', *Materials and Structures*. Kluwer Academic Publishers, 31(7), pp. 435–441. doi: 10.1007/BF02480466.

American Road & Transportation Builders Association (2020) *ARTBA Bridge Report*. Available at: https://artbabridgereport.org/ (Accessed: 6 July 2020).

Amleh, L., Mirza, M. and Ahwazi, B. (2000) 'Bond deterioration of reinforcing steel in concrete due to corrosion'. Available at: https://books.google.com/books?hl=en&lr=&id=F8HosZdH8BUC&oi=fnd&pg=PA247&ots=Iq_HHO_T-s&sig=3ytv3HtTEhxTvU9yTJRyH6PPLrk (Accessed: 5 July 2019).

Andrade, C., Alonso, M. C. and Gonzalez, J. A. (1990) 'Initial effort to use the corrosion rate measurements for estimating rebar durability', *ASTM Special Technical Publication*. ASTM

International, (1065), pp. 29–37. doi: 10.1520/stp25013s.

Andrade, C. and González, J. A. (1978) 'Quantitative measurements of corrosion rate of reinforcing steels embedded in concrete using polarization resistance measurements', *Materials and Corrosion*, 29(8), pp. 515–519. doi: 10.1002/maco.19780290804.

Apostolopoulos, C. A. (2007) 'Mechanical behavior of corroded reinforcing steel bars S500s tempcore under low cycle fatigue', *Construction and Building Materials*. Elsevier, 21(7), pp. 1447–1456. doi: 10.1016/J.CONBUILDMAT.2006.07.008.

Apostolopoulos, C. A. and Papadakis, V. G. (2008) 'Consequences of steel corrosion on the ductility properties of reinforcement bar', *Construction and Building Materials*. Elsevier, 22(12), pp. 2316–2324. doi: 10.1016/J.CONBUILDMAT.2007.10.006.

Apostolopoulos, C., Drakakaki, A. and Basdeki, M. (2019) 'Seismic assessment of RC column under seismic loads', *International Journal of Structural Integrity*. Emerald Publishing Limited , 10(1), pp. 41–54. doi: 10.1108/IJSI-02-2018-0013.

ASCE 41 (2017) *Seismic Evaluation and Retrofit of Existing Buildings, Seismic Evaluation and Retrofit of Existing Buildings*. American Society of Civil Engineers. doi: 10.1061/9780784414859.

Azad, A. K., Ahmad, S. and Al-Gohi, B. H. A. (2010) 'Flexural strength of corroded reinforced concrete beams', *Magazine of Concrete Research*. Thomas Telford Ltd , 62(6), pp. 405–414. doi: 10.1680/macr.2010.62.6.405.

Berra, M., Castellani, A. and Coronelli, D. (1997) 'Bond in reinforced concrete and corrosion of bars', in *Structural Faults and Repair*. Edinburgh, UK, pp. 349–357.

Berrocal, C. G. *et al.* (2017) 'Corrosion-induced cracking and bond behaviour of corroded reinforcement bars in SFRC', *Composites Part B: Engineering*. Elsevier, 113, pp. 123–137. doi: 10.1016/J.COMPOSITESB.2017.01.020.

Blaber, J., Adair, & B. and Antoniou, & A. (no date) 'Ncorr: Open-Source 2D Digital Image Correlation Matlab Software'. doi: 10.1007/s11340-015-0009-1.

Cairns, J., Du, Y. and Law, D. (2008) 'Structural performance of corrosion-damaged concrete

beams', *Magazine of Concrete Research*. Thomas Telford Ltd , 60(5), pp. 359–370. doi: 10.1680/macr.2007.00102.

Di Carlo, F., Meda, A. and Rinaldi, Z. (2017) 'Numerical cyclic behaviour of un-corroded and corroded RC columns reinforced with HPFRC jacket', *Composite Structures*. Elsevier, 163, pp. 432–443. doi: 10.1016/J.COMPSTRUCT.2016.12.038.

Castel, A., François, R. and Arliguie, G. (2000) 'Mechanical behaviour of corroded reinforced concrete beams—Part 1: Experimental study of corroded beams', *Materials and Structures*. Kluwer Academic Publishers, 33(9), pp. 539–544. doi: 10.1007/BF02480533.

CEN (2005) *EN 1998 - 3 Eurocode 8-Design of structures for earthquake resistance-Part 3: Assessment and retrofitting of buildings*.

Cervenka Consulting (2007) 'ATENA Program Documentation'. Prague, Czech Republic.

Civjan, S. A. *et al.* (2005) 'Effectiveness of corrosion inhibiting admixture combinations in structural concrete', *Cement and Concrete Composites*. Elsevier, 27(6), pp. 688–703. doi: 10.1016/J.CEMCONCOMP.2004.07.007.

Coronelli, D. and Gambarova, P. (2004) 'Structural Assessment of Corroded Reinforced Concrete Beams: Modeling Guidelines', *Journal of Structural Engineering*. American Society of Civil Engineers, 130(8), pp. 1214–1224. doi: 10.1061/(ASCE)0733-9445(2004)130:8(1214).

Coronelli, D., Hanjari, K. Z. and Lundgren, K. (2013) 'Severely Corroded RC with Cover Cracking', *Journal of Structural Engineering*, 139(2), pp. 221–232. doi: 10.1061/(ASCE)ST.1943-541X.0000633.

Dang, V. H. and François, R. (2013) 'Influence of long-term corrosion in chloride environment on mechanical behaviour of RC beam', *Engineering Structures*. Elsevier, 48, pp. 558–568. doi: 10.1016/j.engstruct.2012.09.021.

Darwin, D. and Pecknold, D. (1974) *INELASTIC MODEL FOR CYCLIC BIAXIAL LOADING OF REINFORCED CONCRETE*. Illinois, Urbana. Available at: https://www.semanticscholar.org/paper/INELASTIC-MODEL-FOR-CYCLIC-BIAXIAL-LOADING-OF-Darwin-Pecknold/5d1fb39809798f4c65b2dfa0fad5c06dd82e2a6f (Accessed: 20 July 2022).

Du, Y., Clark, L. A. and Chan, A. H. C. (2007) 'Impact of Reinforcement Corrosion on Ductile Behavior of Reinforced Concrete Beams', *ACI Structural Journal*, 104(3), pp. 285–293. doi: 10.14359/18618.

Du, Y. G., Clark, L. A. and Chan, A. H. C. (2005) 'Residual capacity of corroded reinforcing bars', *Magazine of Concrete Research*. Thomas Telford Ltd , 57(3), pp. 135–147. doi: 10.1680/macr.2005.57.3.135.

El-Joukhadar, N., Tsiotsias, K. and Pantazopoulou, S. (2019) 'Consideration of the state of corrosion in seismic assessment of columns', *International Journal of Structural Integrity*. Emerald Group Publishing Ltd. doi: 10.1108/IJSI-07-2019-0065.

Fakhri, H., Ragalwar, K. A. and Ranade, R. (2019) 'On the use of Strain-Hardening Cementitious Composite covers to mitigate corrosion in reinforced concrete structures', *Construction and Building Materials*. Elsevier Ltd, 224, pp. 850–862. doi: 10.1016/j.conbuildmat.2019.07.052.

Fang, C. *et al.* (2004) 'Corrosion influence on bond in reinforced concrete', *Cement and Concrete Research*. Pergamon, 34(11), pp. 2159–2167. doi: 10.1016/J.CEMCONRES.2004.04.006.

Farhan, N. A., Sheikh, M. N. and Hadi, M. N. S. (2018) 'Experimental Investigation on the Effect of Corrosion on the Bond Between Reinforcing Steel Bars and Fibre Reinforced Geopolymer Concrete', *Structures*. Elsevier, 14, pp. 251–261. doi: 10.1016/J.ISTRUC.2018.03.013.

Fernandez, I. *et al.* (2018) 'Ultimate Capacity of Corroded Statically Indeterminate Reinforced Concrete Members', *International Journal of Concrete Structures and Materials*. Springer Singapore, 12(1), p. 75. doi: 10.1186/s40069-018-0297-9.

Fernandez, I., Bairán, J. M. and Marí, A. R. (2015) 'Corrosion effects on the mechanical properties of reinforcing steel bars. Fatigue and σ–ε behavior', *Construction and Building Materials*. Elsevier, 101, pp. 772–783. doi: 10.1016/J.CONBUILDMAT.2015.10.139.

Fernandez, I. and Berrocal, C. G. (2019) 'Mechanical Properties of 30 Year-Old Naturally Corroded Steel Reinforcing Bars', *International Journal of Concrete Structures and Materials*.

Korea Concrete Institute, 13(1), p. 9. doi: 10.1186/s40069-018-0308-x.

Fernandez, I., Lundgren, K. and Zandi, K. (2018) 'Evaluation of corrosion level of naturally corroded bars using different cleaning methods, computed tomography, and 3D optical scanning', *Materials and Structures/Materiaux et Constructions*. Springer Netherlands, 51(3), pp. 1–13. doi: 10.1617/s11527-018-1206-z.

fib-Model Code (2020) 'Model Code 2020, Draft version MC2020', in. fib.

fib bulletin #10 (2000) *Bond of reinforcement in concrete : state-of-art report*. International Federation for Structural Concrete. Available at: https://www.fib-international.org/publications/fib-bulletins/bond-of-reinforcement-in-concrete-pdf-detail.html (Accessed: 3 July 2019).

fib Model Code (2010) *Fib model code for concrete structures 2010*.

Fischer, C., Ozbolt, J. and Gehlen, C. (2010) 'Numerical investigation on bond behavior of corroded reinforcement', in *7th International Conference on Fracture Mechanics of Concrete and Concrete Structures*. Jeju, Korea, pp. 779–785.

François, R. and Arliguie, G. (1998) 'Influence of Service Cracking on Reinforcement Steel Corrosion', *Journal of Materials in Civil Engineering*, 10(1), pp. 14–20. doi: 10.1061/(ASCE)0899-1561(1998)10:1(14).

François, R., Khan, I. and Dang, V. H. (2013) 'Impact of corrosion on mechanical properties of steel embedded in 27-year-old corroded reinforced concrete beams', *Materials and Structures*. Springer Netherlands, 46(6), pp. 899–910. doi: 10.1617/s11527-012-9941-z.

Fu, C. *et al.* (2017) 'Corrosion characteristics of a 4-year naturally corroded reinforced concrete beam with load-induced transverse cracks', *Corrosion Science*. Pergamon, 117, pp. 11–23. doi: 10.1016/J.CORSCI.2017.01.002.

Ganesh, P. and Ramachandra Murthy, A. (2020) 'Simulation of surface preparations to predict the bond behaviour between normal strength concrete and ultra-high performance concrete', *Construction and Building Materials*. Elsevier, 250, p. 118871. doi: 10.1016/J.CONBUILDMAT.2020.118871.

Gjørv, O. E. (2014) *Durability Design of Concrete Structures in Severe Environments*. CRC Press. doi: 10.1201/b16469.

Goksu, C. and Ilki, A. (2016) 'Seismic Behavior of Reinforced Concrete Columns with Corroded Deformed Reinforcing Bars', *ACI Structural Journal*, 113(5), pp. 1053–1064. doi: 10.14359/51689030.

Haddad, R. H. and Ashteyate, A. M. (2001) 'Role of synthetic fibers in delaying steel corrosion cracks and improving bond with concrete', *Canadian Journal of Civil Engineering*. NRC Research Press Ottawa, Canada , 28(5), pp. 787–793. doi: 10.1139/l01-037.

Hanjari, K. Z., Coronelli, D. and Lundgren, K. (2011) 'Bond capacity of severely corroded bars with corroded stirrups', *Magazine of Concrete Research*. Thomas Telford Ltd , 63(12), pp. 953–968. doi: 10.1680/macr.10.00200.

Harajli, M. H. (2004) 'Comparison of Bond Strength of Steel Bars in Normal- and High-Strength Concrete', *Journal of Materials in Civil Engineering*, 16(4), pp. 365–374. doi: 10.1061/(ASCE)0899-1561(2004)16:4(365).

Higgins, C. and Farrow, W. C. (2006) 'Tests of Reinforced Concrete Beams with Corrosion-Damaged Stirrups', *ACI Structural Journal*, 103(1), pp. 133–141. doi: 10.14359/15094.

Hou, L. *et al.* (2017) 'Effect of corrosion on bond behaviors of rebar embedded in ultra-high toughness cementitious composite', *Construction and Building Materials*. Elsevier, 138, pp. 141–150. doi: 10.1016/J.CONBUILDMAT.2017.02.008.

Hung, C. C., Lee, H. S. and Chan, S. N. (2019) 'Tension-stiffening effect in steel-reinforced UHPC composites: Constitutive model and effects of steel fibers, loading patterns, and rebar sizes', *Composites Part B: Engineering*. Elsevier Ltd, 158, pp. 269–278. doi: 10.1016/j.compositesb.2018.09.091.

Ioannou, A. *et al.* (2022) 'Experimental Testing of ECC Jackets for Repair of Pre-Damaged R . C . Members Experimental Testing of ECC Jackets for Repair of Pre-Damaged R . C . Members under Cyclic Loading', in *12th National Conference on Earthquake Engineering*. Salt Lake City, Utah: Earthquake Engineering Research Institute, pp. 1–5.

Kashani, M. M., Maddocks, J. and Dizaj, E. A. (2019) 'Residual Capacity of Corroded

Reinforced Concrete Bridge Components: State-of-the-Art Review', *Journal of Bridge Engineering*, 24(7), p. 03119001. doi: 10.1061/(ASCE)BE.1943-5592.0001429.

Kondratova, I. L., Montes, P. and Bremner, T. W. (2000) 'Accelerated Corrosion Testing Results for Specimens Containing Uncoated Reinforcing Steel and Corrosion Inhibitors', *Special Publication*, 192, pp. 789–806. doi: 10.14359/5785.

Koulouris, K. and Apostolopoulos, C. (2020) 'An Experimental Study on Effects of Corrosion and Stirrups Spacing on Bond Behavior of Reinforced Concrete', *Metals*. MDPI AG, 10(10), p. 1327. doi: 10.3390/met10101327.

Lee, H. S. and Cho, Y. S. (2009) 'Evaluation of the mechanical properties of steel reinforcement embedded in concrete specimen as a function of the degree of reinforcement corrosion', in *International Journal of Fracture*. Springer, pp. 81–88. doi: 10.1007/s10704-009-9334-7.

Li, D. *et al.* (2018) 'Influence of Non-uniform corrosion of steel bars on the seismic behavior of reinforced concrete columns', *Construction and Building Materials*. Elsevier, 167, pp. 20–32. doi: 10.1016/J.CONBUILDMAT.2018.01.149.

Li, J., Gong, J. and Wang, L. (2009) 'Seismic behavior of corrosion-damaged reinforced concrete columns strengthened using combined carbon fiber-reinforced polymer and steel jacket', *Construction and Building Materials*. Elsevier, 23(7), pp. 2653–2663. doi: 10.1016/J.CONBUILDMAT.2009.01.003.

Li, X. *et al.* (2016) 'Effect of loading rate on the bond behaviour of deformed steel bars in concrete subjected to lateral pressure', *Materials and Structures*. Springer Netherlands, 49(6), pp. 2097–2111. doi: 10.1617/s11527-015-0636-0.

Lijina, T. and Jithin, J. . (2018) 'Effect of Steel and Polypropylene Fibre on the Tension Stiffening of Ultra High Performance Concrete', *International Journal of Engineering and Advanced Technology (IJEAT)*, 8(4C).

Lin, H. *et al.* (2019) 'State-of-the-art review on the bond properties of corroded reinforcing steel bar', *Construction and Building Materials*. Elsevier, 213, pp. 216–233. doi: 10.1016/J.CONBUILDMAT.2019.04.077.

Liu, X. and Li, Y. (2018) 'Experimental study of seismic behavior of partially corrosion-

damaged reinforced concrete columns strengthened with FRP composites with large deformability', *Construction and Building Materials*. Elsevier, 191, pp. 1071–1081. doi: 10.1016/J.CONBUILDMAT.2018.10.072.

Lu, C. *et al.* (2016) 'Mechanical properties of corroded steel bars in pre-cracked concrete suffering from chloride attack', *Construction and Building Materials*, 123(123), pp. 649–660. doi: 10.1016/j.conbuildmat.2016.07.032.

Ma, Y., Che, Y. and Gong, J. (2012) 'Behavior of corrosion damaged circular reinforced concrete columns under cyclic loading', *Construction and Building Materials*. Elsevier, 29, pp. 548–556. doi: 10.1016/J.CONBUILDMAT.2011.11.002.

El Maaddawy, T. A. and Soudki, K. A. (2003) 'Effectiveness of Impressed Current Technique to Simulate Corrosion of Steel Reinforcement in Concrete', *Journal of Materials in Civil Engineering*, 15(1), pp. 41–47. doi: 10.1061/(ASCE)0899-1561(2003)15:1(41).

Mangat, P. S. and Elgarf, M. S. (1999) 'Bond characteristics of corrding reinforcement in concrete beams', *Materials and Structures*. Kluwer Academic Publishers, 32(2), pp. 89–97. doi: 10.1007/BF02479434.

Mangat, Pritpal S. and Elgarf, M. S. (1999) 'Flexural Strength of Concrete Beams with Corroding Reinforcement', *ACI Structural Journal*, 96(1), pp. 149–158. doi: 10.14359/606.

Martín Pérez, B. M. (1999) *Service life modelling of R.C. highway structures exposed to chlorides*. University of Toronto. Available at: https://books.google.ca/books/about/Service_Life_Modelling_of_R_C_Highway_St.html?id=qQiGtgAACAAJ&redir_esc=y (Accessed: 14 February 2019).

Meda, A. *et al.* (2014) 'Experimental evaluation of the corrosion influence on the cyclic behaviour of RC columns', *Engineering Structures*. Elsevier, 76, pp. 112–123. doi: 10.1016/J.ENGSTRUCT.2014.06.043.

Mehta, P. K. (1991) 'Durability of Concrete--Fifty Years of Progress?', *Special Publication*, 126, pp. 1–32. doi: 10.14359/1998.

Menengotto, M. and Pinto, P. E. (1973) 'Method o f Analysis for Cyclically Loaded Reinforced Concrete Plane Frames Including Changes in Geometry and Nonelastic Behavior of Elements

under Combined Normal Force and Bending', in *IABSE Symposium on Resistance and Ultimate Deformability of Structures Acted on*. Lisbon.

Molaioni, F., Carlo, F. Di and Rinaldi, Z. (2021) 'Modelling Strategies for the Numerical Simulation of the Behaviour of Corroded RC Columns under Cyclic Loads', *Applied Sciences 2021, Vol. 11, Page 9761*. Multidisciplinary Digital Publishing Institute, 11(20), p. 9761. doi: 10.3390/APP11209761.

Ou, Y.-C. and Chen, H.-H. (2014) 'Cyclic Behavior of Reinforced Concrete Beams with Corroded Transverse Steel Reinforcement', *Journal of Structural Engineering*, 140(9), p. 04014050. doi: 10.1061/(ASCE)ST.1943-541X.0000932.

Palsson, R. and Mirza, M. S. (2002a) 'Mechanical response of corroded steel reinforcement of abandoned concrete bridge', *ACI Structural Journal*, 99(2), pp. 157–162. doi: 10.14359/11538.

Palsson, R. and Mirza, M. S. (2002b) 'Mechanical Response of Corroded Steel Reinforcement of Abandoned Concrete Bridge', *ACI Structural Journal*, 99(2), pp. 157–162. doi: 10.14359/11538.

Pantazopoulou, S. J. *et al.* (2001) *REPAIR OF CORROSION-DAMAGED COLUMNS WITH FRP WRAPS, JOURNAL OF COMPOSITES FOR CONSTRUCTION*. Available at: http://pubs.asce.org/copyright (Accessed: 23 July 2019).

Pantazopoulou, S. J. *et al.* (2019) 'The performance of corroded lap splices in reinforced concrete beams', *Corrosion Reviews*. De Gruyter, 37(1), pp. 31–44. doi: 10.1515/corrrev-2017-0086.

Papakonstantinou, C. G., Balaguru, P. N. and Auyeung, Y. (2011) 'Influence of FRP confinement on bond behavior of corroded steel reinforcement', *Cement and Concrete Composites*. Elsevier, 33(5), pp. 611–621. doi: 10.1016/J.CEMCONCOMP.2011.02.006.

Pardalopoulos, S. I., Pantazopoulou, S. J. and Lekidis, V. A. (2017) 'Simplified method for rapid seismic assessment of older R.C. buildings'. doi: 10.1016/j.engstruct.2017.10.052.

Pardalopoulos, S. I., Pantazopoulou, S. J. and Lekidis, V. A. (2018) 'Simplified method for rapid seismic assessment of older R.C. buildings', *Engineering Structures*. Elsevier Ltd, 154, pp. 10–22. doi: 10.1016/j.engstruct.2017.10.052.

Pardalopoulos, S. J., Thermou, G. E. and Pantazopoulou, S. J. (2013) 'Screening criteria to identify brittle R.C. structural failures in earthquakes', *Bulletin of Earthquake Engineering*, 11(2), pp. 607–636. doi: 10.1007/s10518-012-9390-7.

Parulekar, Y. M. *et al.* (2020) 'Performance Assessment of Corroded Reinforced Concrete Structure Considering Bond Deterioration', *Journal of Performance of Constructed Facilities*. American Society of Civil Engineers, 34(2), p. 04020009. doi: 10.1061/(ASCE)CF.1943-5509.0001411.

Paul, Suvash CZijl, G. Van (2014) 'Cracked and uncracked SHCC specimens under different exposure conditions', in *Strain Hardening Cementitious Composites 3 (SHCC3)*. Dordrecht, pp. 25–32.

Pourbaix, M. (1974) *Atlas of electrochemical equilibria in aqueous solutions*. National Association of Corrosion Engineers. Available at: https://books.google.ca/books?id=iiLRvQEACAAJ&dq=9780915567980&hl=en&sa=X&ved=0ahUKEwivreD28rfgAhVi6IMKHQm4Dn4Q6AEIKjAA (Accessed: 12 February 2019).

Prieto, M., Tanner, P. and Andrade, C. (2011) 'Bond response in structural concrete with corroded steel bars. experimental results', *RILEM Bookseries*. Springer, Dordrecht, 5, pp. 231–241. doi: 10.1007/978-94-007-0677-4_16.

Rajput, A. S. and Sharma, U. K. (2018) 'Corroded reinforced concrete columns under simulated seismic loading', *Engineering Structures*. Elsevier, 171, pp. 453–463. doi: 10.1016/J.ENGSTRUCT.2018.05.097.

Raza, S. *et al.* (2019) 'Strengthening and Repair of Reinforced Concrete Columns by Jacketing: State-of-the-Art Review', *Sustainability*. MDPI AG, 11(11), p. 3208. doi: 10.3390/su11113208.

Robuschi, S. *et al.* (2020) 'Bond of naturally corroded, plain reinforcing bars in concrete', *Structure and Infrastructure Engineering*. Taylor and Francis Ltd., pp. 1–17. doi: 10.1080/15732479.2020.1768273.

Rodriguez, J. and Ortega, J. C. (1994) 'Corrosion of reinforcing bars and service life of reinforced concrete structures: corrosion and bond deterioration', in *International Conference on Concrete across Borders*. Odense, Denmark, pp. 315–326.

Semendary, A. A. and Svecova, D. (2020) ‘Factors affecting bond between precast concrete and cast in place ultra high performance concrete (UHPC)’, *Engineering Structures*. Elsevier, 216, p. 110746. doi: 10.1016/J.ENGSTRUCT.2020.110746.

Sezen, H. and Moehle, J. P. (2004) ‘Shear Strength Model for Lightly Reinforced Concrete Columns’, *Journal of Structural Engineering*. American Society of Civil Engineers, 130(11), pp. 1692–1703. doi: 10.1061/(ASCE)0733-9445(2004)130:11(1692).

Soudki, K. and Sherwood, T. (2003) ‘Bond Behavior of Corroded Steel Reinforcement in Concrete Wrapped with Carbon Fiber Reinforced Polymer Sheets’, *Journal of Materials in Civil Engineering*, 15(4), pp. 358–370. doi: 10.1061/(ASCE)0899-1561(2003)15:4(358).

Stanish, K., Hooton, R. D. and Pantazopoulou, S. J. (1999) ‘Corrosion Effects on Bond Strength in Reinforced Concrete’, *ACI Structural Journal*, 96(6), pp. 915–921. doi: 10.14359/765.

Suffern, C., El-Sayed, A. and Soudki, K. (2010) ‘Shear strength of disturbed regions with corroded stirrups in reinforced concrete beams’, *Canadian Journal of Civil Engineering*, 37(8), pp. 1045–1056. doi: 10.1139/L10-031.

Takuya, K., Ryuta, I. and Masayuki, T. (2020) ‘Prediction of Hydrogen Embrittlement of Reinforcing Steel Bars in Concrete Poles | NTT Technical Review’, *NTT Technical Review*, 18(11). Available at: https://www.ntt-review.jp/archive/ntttechnical.php?contents=ntr202011ra1.html (Accessed: 16 April 2022).

Tastani, S. P. and Pantazopoulou, S. J. (2007) ‘Behavior of Corroded Bar Anchorages’, *ACI Structural Journal*, 104(6), pp. 756–766. doi: 10.14359/18958.

Tastani, S. and Pantazopoulou, S. J. (2005) ‘Recovery of seismic resistance in corrosion-damaged reinforced concrete through FRP jacketing’, *International Journal of Materials and Product Technology*, 23(3/4), p. 389. doi: 10.1504/IJMPT.2005.007737.

Tayeh, B. A., Abu Bakar, B. H. and Megat Johari, M. A. (2013) ‘Characterization of the interfacial bond between old concrete substrate and ultra high performance fiber concrete repair composite’, *Materials and Structures/Materiaux et Constructions*. Springer, 46(5), pp. 743–753. doi: 10.1617/S11527-012-9931-1/FIGURES/13.

Tepfers, R. (1979) ‘Cracking of concrete cover along anchored deformed reinforcing bars’,

Magazine of Concrete Research. Thomas Telford Ltd , 31(106), pp. 3–12. doi: 10.1680/macr.1979.31.106.3.

Tondolo, F. (2015) 'Bond behaviour with reinforcement corrosion', *Construction and Building Materials*. Elsevier, 93, pp. 926–932. doi: 10.1016/J.CONBUILDMAT.2015.05.067.

Torres-Acosta, A. A., Navarro-Gutierrez, S. and Terán-Guillén, J. (2007) 'Residual flexure capacity of corroded reinforced concrete beams', *Engineering Structures*. Elsevier, 29(6), pp. 1145–1152. doi: 10.1016/J.ENGSTRUCT.2006.07.018.

Tuutti, K. (1982) *Corrosion of steel in concrete*. Swedish Cement and Concrete Research Institute, Stockholm. Available at: https://portal.research.lu.se/portal/en/publications/corrosion-of-steel-in-concrete(e97795b5-7f3a-4994-8beb-9438f5a51571).html (Accessed: 6 July 2020).

Valikhani, A. *et al.* (2020) 'Experimental evaluation of concrete-to-UHPC bond strength with correlation to surface roughness for repair application', *Construction and Building Materials*. Elsevier, 238, p. 117753. doi: 10.1016/J.CONBUILDMAT.2019.117753.

Vecchio, F. J. and Collins, M. P. (1986) 'MODIFIED COMPRESSION-FIELD THEORY FOR REINFORCED CONCRETE ELEMENTS SUBJECTED TO SHEAR.', *Journal of the American Concrete Institute*, 83(2), pp. 219–231. doi: 10.14359/10416.

Vu, N. S. and Li, B. (2018) 'Seismic Performance of Flexural Reinforced Concrete Columns with Corroded Reinforcement', *ACI Structural Journal*, 115(5), pp. 1253–1266. doi: 10.14359/51702372.

Vu, N. S., Yu, B. and Li, B. (2016) 'Prediction of strength and drift capacity of corroded reinforced concrete columns', *Construction and Building Materials*. Elsevier, 115, pp. 304–318. doi: 10.1016/J.CONBUILDMAT.2016.04.048.

Wang, L. *et al.* (2015) 'Effects of stirrup and inclined bar corrosion on shear behavior of RC beams', *Construction and Building Materials*. Elsevier, 98, pp. 537–546. doi: 10.1016/J.CONBUILDMAT.2015.07.077.

Xia, J., Jin, W. and Li, L. (2011) 'Shear performance of reinforced concrete beams with corroded stirrups in chloride environment', *Corrosion Science*. Pergamon, 53(5), pp. 1794–1805. doi: 10.1016/J.CORSCI.2011.01.058.

Xu, S. L. and Cai, X. H. (2010) *Bond behavior of corroded reinforcing bar and ultra high toughness cementitious composites (UHTCC)*. Available at: https://framcos.org/FraMCoS-7/06-04.pdf (Accessed: 8 July 2019).

Yang, S.-Y. *et al.* (2016) 'Experimental research on hysteretic behaviors of corroded reinforced concrete columns with different maximum amounts of corrosion of rebar', *Construction and Building Materials*. Elsevier, 121, pp. 319–327. doi: 10.1016/J.CONBUILDMAT.2016.06.002.

Yuan, W., Guo, A. and Li, H. (2017) 'Experimental investigation on the cyclic behaviors of corroded coastal bridge piers with transfer of plastic hinge due to non-uniform corrosion', *Soil Dynamics and Earthquake Engineering*. Elsevier, 102, pp. 112–123. doi: 10.1016/J.SOILDYN.2017.08.019.

Zhang, R., Castel, A. and François, R. (2009) 'The corrosion pattern of reinforcement and its influence on serviceability of reinforced concrete members in chloride environment', *Cement and Concrete Research*. Pergamon, 39(11), pp. 1077–1086. doi: 10.1016/J.CEMCONRES.2009.07.025.

Zhang, W. *et al.* (2012) 'Tensile and fatigue behavior of corroded rebars', *Construction and Building Materials*. Elsevier, 34, pp. 409–417. doi: 10.1016/J.CONBUILDMAT.2012.02.071.

Zhao, Y. *et al.* (2013) 'Bond behaviour of normal/recycled concrete and corroded steel bars', *Construction and Building Materials*. Elsevier, 48, pp. 348–359. doi: 10.1016/J.CONBUILDMAT.2013.06.091.

Zhu, W. *et al.* (2013) 'Effect of corrosion of reinforcement on the mechanical behaviour of highly corroded RC beams', *Engineering Structures*. Elsevier, 56, pp. 544–554. doi: 10.1016/J.ENGSTRUCT.2013.04.017.

Zhu, W. and François, R. (2014) 'Experimental investigation of the relationships between residual cross-section shapes and the ductility of corroded bars', *Construction and Building Materials*, 69(69), pp. 335–345. doi: 10.1016/j.conbuildmat.2014.07.059.

Van Zijl, G. P. A. G. *et al.* (2012) 'Durability of strain-hardening cement-based composites (SHCC)', *Materials and Structures/Materiaux et Constructions*. Springer, 45(10), pp. 1447–1463. doi: 10.1617/s11527-012-9845-y.

4. Effectiveness of UHPC Cover in Delaying Bar Corrosion

4.1. Introduction

Corrosion of reinforcement is the predominant and most crucial deteriorating mechanism of concrete structures, as has been previously demonstrated in this dissertation. Different retrofitting methods have been adopted for corrosion damaged structures, encompassing a range of advanced technologies and material applications. For recovery of structural integrity, retrofitting techniques were summarized in Chapter 2, including either patch repairs or jacketing with reinforced concrete, steel shells, TRMs, externally bonded FRP wraps and near surface mounted FRP laminates (Raza *et al.*, 2019). While these methods may restore structural strength, stiffness and ductility, nevertheless, they do not provide a solution for prevention or delay of corrosion. FRP jacketing, once thought a promising method in mitigating corrosion, has been questioned repeatedly in recent years, for the risk trapping moisture in the structural element, thereby allowing un-aerobic corrosion to continue (Pantazopoulou *et al.*, 2001). A more recent effort has focused on the effectiveness of fiber-reinforced cementitious jackets as a corrosion-mitigating solution when considered with a range of strain hardening cementitious composites (SHCC) reinforced with synthetic fibers. However results were not as promising as was initially anticipated, not supporting evidence for full mitigation (Van Zijl *et al.*, 2012; Paul, Suvash CZijl, 2014; Fakhri, Ragalwar and Ranade, 2019); therefore, a comparative investigation is needed to assess the relationship between mechanical characteristics and composition of the SHCC to its effectiveness in mitigating or delaying corrosion.

Reinforcement embedded in concrete is initially protected by a passive film produced by the alkalinity of concrete ($pH \geq 12$). However, this film begins to deteriorate when concrete is exposed to CO_2 because carbonation reduces the concrete's pH. The protective film can also be locally penetrated once in contact with chlorides; these two mechanisms are chemically very different and therefore they result in two different types of corrosion: general corrosion (owing to carbonation) and pitting corrosion (owing to chlorides) (Andrade and González, 1978; Alonso *et al.*, 1998; ACI 222R-19, 2019). Permeability of concrete plays a significant role in the corrosion process. The higher its value, the easier it is for corrosive agents to be transported and reach the steel-concrete interface. Corrosion initiation in itself brings along a self-sustained cycle leading to further increase of corrosion rate. This is owing to the fact that corrosive byproducts occupy a volume that

is two to six times greater than that of pristine steel, thus exerting a bursting radial pressure on the concrete cover (Tastani and Pantazopoulou, 2007). Once the radial pressure exceeds the tensile strength of concrete, cover cracking and spalling takes place, further increasing the corrosion rate.

Repair materials should satisfy certain characteristics in order to act as physical and chemical barriers against ingress of corrosive agents. Ultra-High Performance Fiber-Reinforced Concrete (UHPC) and Engineered Cementitious Composites (ECC), both having high density, low permeability, and advanced mechanical characteristics, are materials of interest for new construction, but also for repair and rehabilitation. The viability of using these materials to prolong the service life of concrete structures highly exposed to corrosive agents, especially in marine environments, is the motivating concept of the present chapter. Objective of the investigation is to evaluate the efficiency of cracked and uncracked UHPC and ECC in mitigating reinforcement corrosion. Additional variables studied were, concrete cover thickness and pre-existing crack widths in order to form a better understanding of the potential compromise in the effectiveness of this technology imparted by pre-existing service cracks; and the simultaneous action of constant tensile stress on the reinforcement during the corrosion process with the purpose of exploring the effect of stress on corrosion rate.

4.2. Materials, Specimens and Preparations

4.2.1. Material Properties

Two types of high-performance fiber reinforced concrete (UHPC) were used in the experimental study to test the effectiveness of these materials in mitigating corrosion. The same, prepackaged dry cementitious mix was used in both mixes (Densit® Inducast TT-5) which acted as the cementitious matrix, while fiber reinforcement varied in type: either Steel fibers or PVA fibers were considered for comparison. Both mixes were reinforced with 2% (by volume) of fibers, of either type. In the remainder of this paper, the mix containing steel fibers is referred to as UHPC, whereas the mix containing PVA fibers is referred to as ECC. UHPC mix proportions by mass are shown in Table 4-1.

Table 4-1. Mix Proportions by Mass (Densit contains a mix of cement and bauxite sand)

UHPC			ECC		
Dry Mix	Water	Steel Fibers	Dry Mix	Water	PVA Fibers
1	0.13	0.066	1	0.16	9.307 E^{-3}

Six cylinders 75x150mm were cast together with the specimens of each mix. Compressive strengths of the two materials at 28 days are given in Table 4-2.

Table 4-2. Average Compressive Strength of UHPC Materials at 28 Days

Mix ID	*UHPC*			*ECC*		
Cylinder ID	C1	C2	C3	C1	C2	C3
Compressive Strength (MPa)	148	164	152	59	55	65
Average Compressive Strength (MPa)	155			60		

4.2.2. Specimen Fabrication and Test Variables

Fifteen 100mm cylindrical specimens were cast per mixture (i.e a total of 30 specimens), reinforced with a 15M steel bar (16mm diameter) passing through the mid-height of the cylinder along a diameter. Two concrete cover thicknesses were adopted, i.e., one and two multiples of the bar diameter D_b (i.e., cover was 16mm and 32mm), in order to study the effect of concrete cover on corrosion rate. As shown in Figure 4-1, the two specimen thickness values were 80mm and 50 mm respectively.

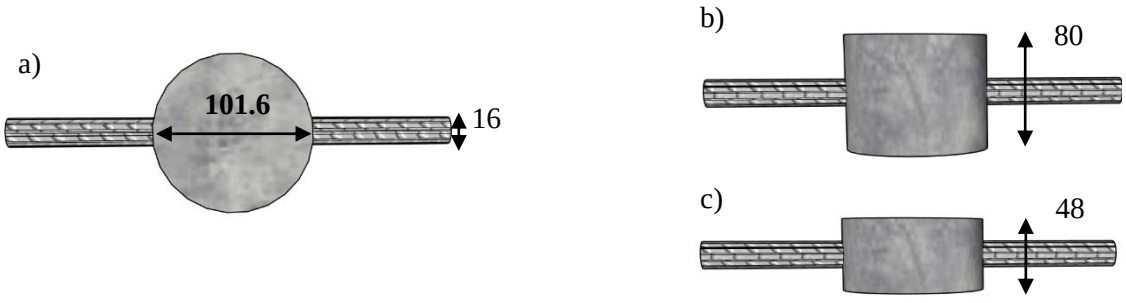

Figure 4-1. Specimen Dimensions in mm. a) Top Cross-section. b) Side View of Thick Specimens. c) Side View of Thin Specimens.

Aside from concrete cover and fiber type, an important variable included in the study was the presence or not of a pre-existing diametric crack intersecting the bar at the mid-point of the bonded length; the crack width was a variable of study.

It has been reported that small transversal cracks lead to pitting corrosion while larger cracks cause uniform corrosion. According to Zhang et al. (2009), the critical widths for pitting corrosion were between 0.5 mm and 1.5 mm (Zhang, Castel and François, 2009) whereas others report that pitting occurs at crack widths as small as 0.25mm-0.3mm (Kondratova, Montes and Bremner, 2000; Civjan *et al.*, 2005); however, other studies suggest that corrosion was not influenced by crack widths below 0.5mm (François and Arliguie, 1998).

In the present work, two crack widths were considered to represent the performance benchmarks at service and limit states, at 0.5mm and 2mm. For relevance with the actual working conditions of a reinforcing bar, it was necessary to apply a sustained, constant tensile stress during corrosion conditioning. Thus, reinforcement was stressed in tension reaching 30% of the bar's axial yield strength. Details on the stressing mechanism adopted are presented in Section 4.3.1.

Table 4-3. Specimen ID's and Test Variables.

		ECC		*UHPC*	
	Crack Width	Number of specimens	Specimen ID	Number of specimens	Specimen ID
1 d_b	0	2	#-P-0	2	#-S-0
	0.5 mm	3	#-P-0.5	3	#-S-0.5
	2 mm	2	#-P-2	2	#-S-2
2 d_b	0	2	#-PT-0	2	#-ST-0
	0.5 mm	2	#-PT-0.5	2	#-ST-0.5
	2 mm	2	#-PT-2	2	#-ST-2
1 d_b	0	1	#-NS-P-0	1	#-NS-S-0
2 d_b	0	1	#-NS-PT-0	1	#-NS-ST-0

*NS denotes non-stressed; # is a numeral identifying a specimen's sequence number.

Thirty specimens were cast and cured for 28 days prior to initiating the corrosion process. Of these, 26 were stressed in tension during the accelerated corrosion process whereas 4 specimens were

left unstressed and served as control specimens. Table 4-3 includes the nomenclature of specimens and their parametric values.

For example, specimen 2-ST-0.5 is the 2nd sample from a group of identical specimens. S refers to the type of fibers present in the specimen (S for steel, P for PVA), T indicates that it is a thick specimen (the absence of T indicates it is a thin specimen). Numeral 0.5 designates the crack width in mm (0 means there is no crack and 2 refers to 2mm cracked specimens).

Pre-cracking of specimens was achieved by conducting a standard splitting test on the cylinders using an MTS machine under displacement control. Load was applied while crack widths were continuously monitored with the help of two linear displacement transducers until their width stabilized to the desired value. Note that due to the presence of fibers and the steel bar crossing the crack, cracks were constantly closing after unloading. Thus, several loading cycles were applied in order to finally reach the target residual crack width after unloading. Pre-cracking instrumentation is depicted in Figure 4-2.

Figure 4-2. Specimen Pre-Cracking Splitting Setup and Instrumentation. Rust stains were caused by oxidation of steel fibers during the curing period and not from accelerated corrosion which followed this stage.

4.3. Accelerated Corrosion Conditioning

4.3.1. Test Preparation

A self-reacting frame was designed to accommodate the constant tensile stress applied on bars, as depicted in Figure 4-3. Each frame comprised two vertical 2”x 4” wood studs on the two sides of each specimen, clamped between two steel C-channels that served as bearing beams each with a central hole slightly larger than the bar diameter. The bar was held inside the frame by nuts above and below to the two C-channels. The nuts, bearing on the C-channels, were used to apply the

tensile stress on the bars through toque. A digital torque wrench was used to accurately apply the suitable torque magnitude that leads to the desired tensile stress in the bar . Torque magnitudes were inspected weekly in order to correct for the loss in tensile strengths due to creep in wood

Bars' ends had been threaded to the appropriate thread size and spacing using a LATHE machine in order to accommodate the nuts. Specimens' sides and exposed bars' surfaces were carefully sealed using epoxy coating to avoid water seepage through the sides of specimens, also to eliminate the occurrence of short-circuits and to keep a uniformly controlled travel path for water and chlorides.

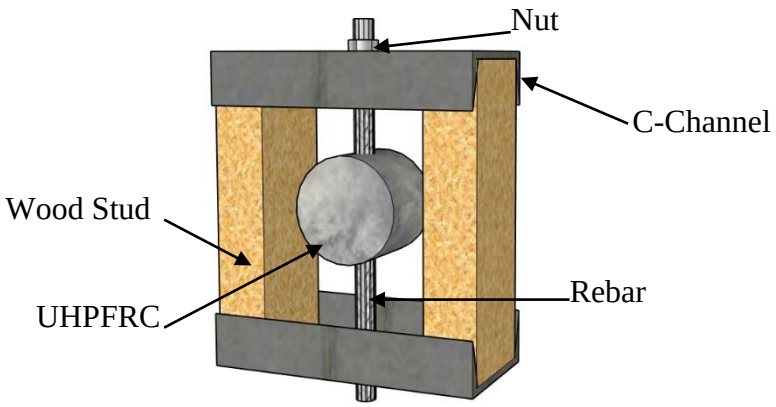

Figure 4-3. Individual-Bar Self-Reacting Frame Setup

4.3.2. Accelerated Corrosion Technique

Accelerated corrosion was achieved through the application of a constant voltage between the ends of a conductive cell, placing the bar in the role of the anode, whereas an external stainless steel mesh acted as a cathode. The circuit was completed through a 3% NaCl solution in which the specimens were periodically immersed. This method allows different specimens to corrode at different rates depending on their individual resistivity, as opposed to the use of constant current which results in the same amount of corrosion throughout all specimens regardless of the crack width, concrete cover or fiber reinforcement type.

A (+/-)24V DC voltage source was used as a power source. Specimens were connected through a breadboard in parallel.

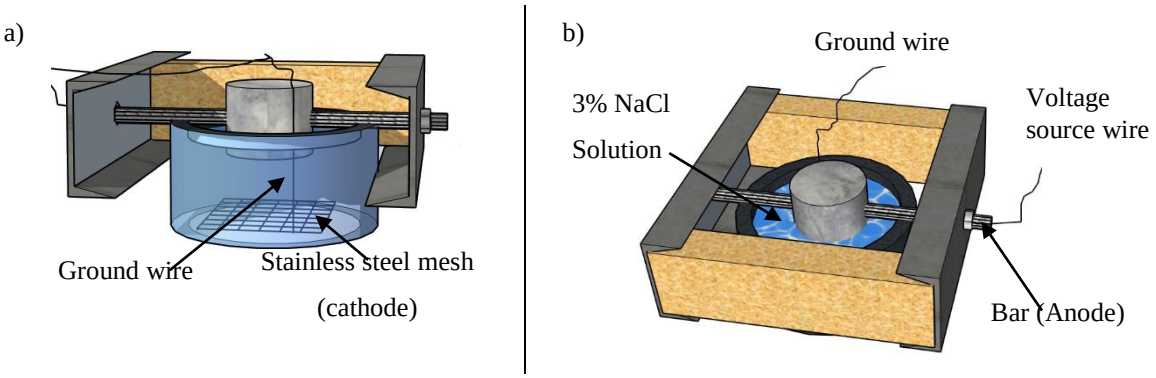

Figure 4-4. Sketch of the Adopted Accelerated Corrosion Setup: a) Side view with cathode mesh. b) Top view showing specimen arrangement in the wet part of the cycle.

Specimens were partially immersed in 3% NaCl solution. One surface of the specimens was exposed to the salt water solution as illustrated in Figure 4-4. They went through a wetting/drying cycle of 1:3 wet/dry ratio of exposure time in hours. This ratio was adopted to ensure complete oxidation of the corrosion byproducts. Prior to each wetting cycle, distilled water was added to the basins to account for evaporated water; This was done in order to maintain a constant concentration of 3% NaCl throughout the conditioning process. Twenty-five cycles were achieved accounting for a total of 600 hours of applied voltage. Potentials were gradually increased to prevent exceeding a current density of 200 µA/cm^2 which is the upper threshold of current density of a corroding bar found in nature (Andrade, Alonso and Gonzalez, 1990). Potentials used throughout the experiment were, 1.05V, 5.89V and 10V for a duration of 24, 224 and 354 hours respectively. Figure 4-5 depicts the applied voltage with respect to time.

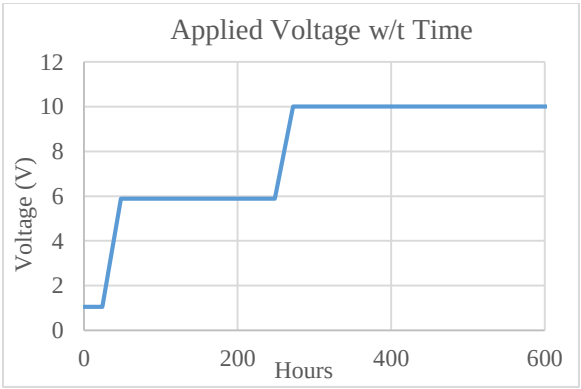

Figure 4-5. Voltage with Respect to Time

Current readings were collected using a multi meter and were taken at the beginning and the end of each wetting cycle. The average of the two readings represented the current in a 24hrs wet period.

4.3.3. Results of the Accelerated Corrosion Phase

Figure 4-6 plots recorded currents (in Amps) with respect to time (hours). Specimens have been grouped into separate graphs based on crack width and concrete cover thickness in order to facilitate comparisons between groups. Mass loss was calculated based on Faraday's law following Equations (4-1) and (4-2).

$$\Delta m\ (grams) = \frac{t * i * M}{z * F} \tag{4-1}$$

$$Mass\ Loss\ (\%) = \frac{\Delta m}{m_0} * 100 \tag{4-2}$$

In Equations. (4-1) and (4-2), *t* is the exposure time (in *s*); *I* is the current (Amperes); *M* is the atomic weight of iron (taken *M=55.847 g/mol*); *z* is the ion charge (2 moles of electrons); *F* is Faraday's Constant representing the amount of electrical charge in *1* mole of electron (taken *F=96,487 C/mol*). Δm and m_o are the mass loss (in grams) and the original mass, respectively.

From Figure 4-6 it is observed that thick specimens showed minimal differences between specimens of identical variables. Specimen NS-P-0 had an unusual behavior in terms of current through time, indicating a much faster rate of corrosion than its other counterparts in the group. This was attributed to the formation of a crack caused by corrosion taking place at the bar-concrete interface at the exterior boundary of the specimen. Results of that specimen were excluded from further analysis.

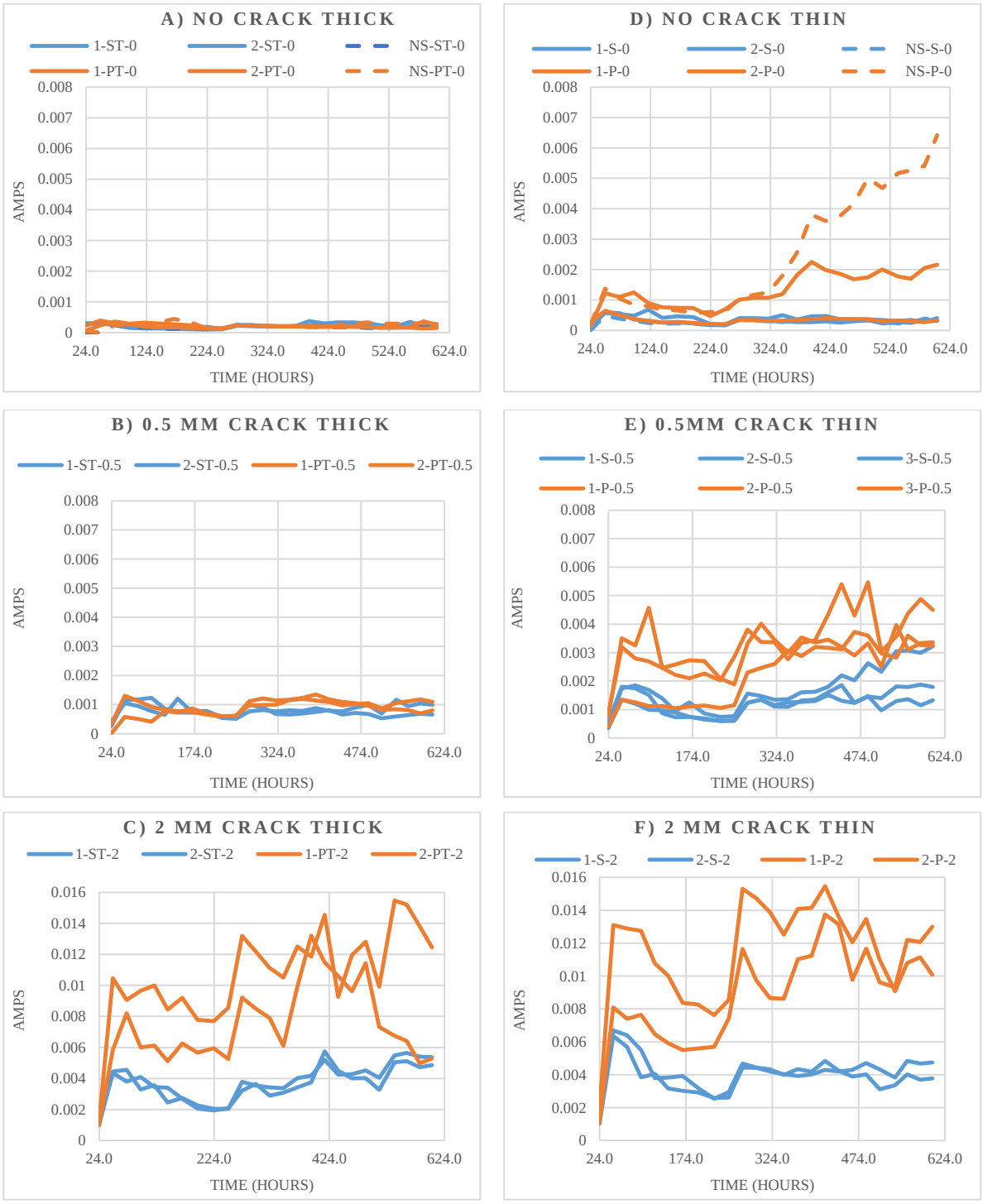

Figure 4-6. Current Readings Through Time of Specimens with Similar Thicknesses and increasing crack widths (from top down)

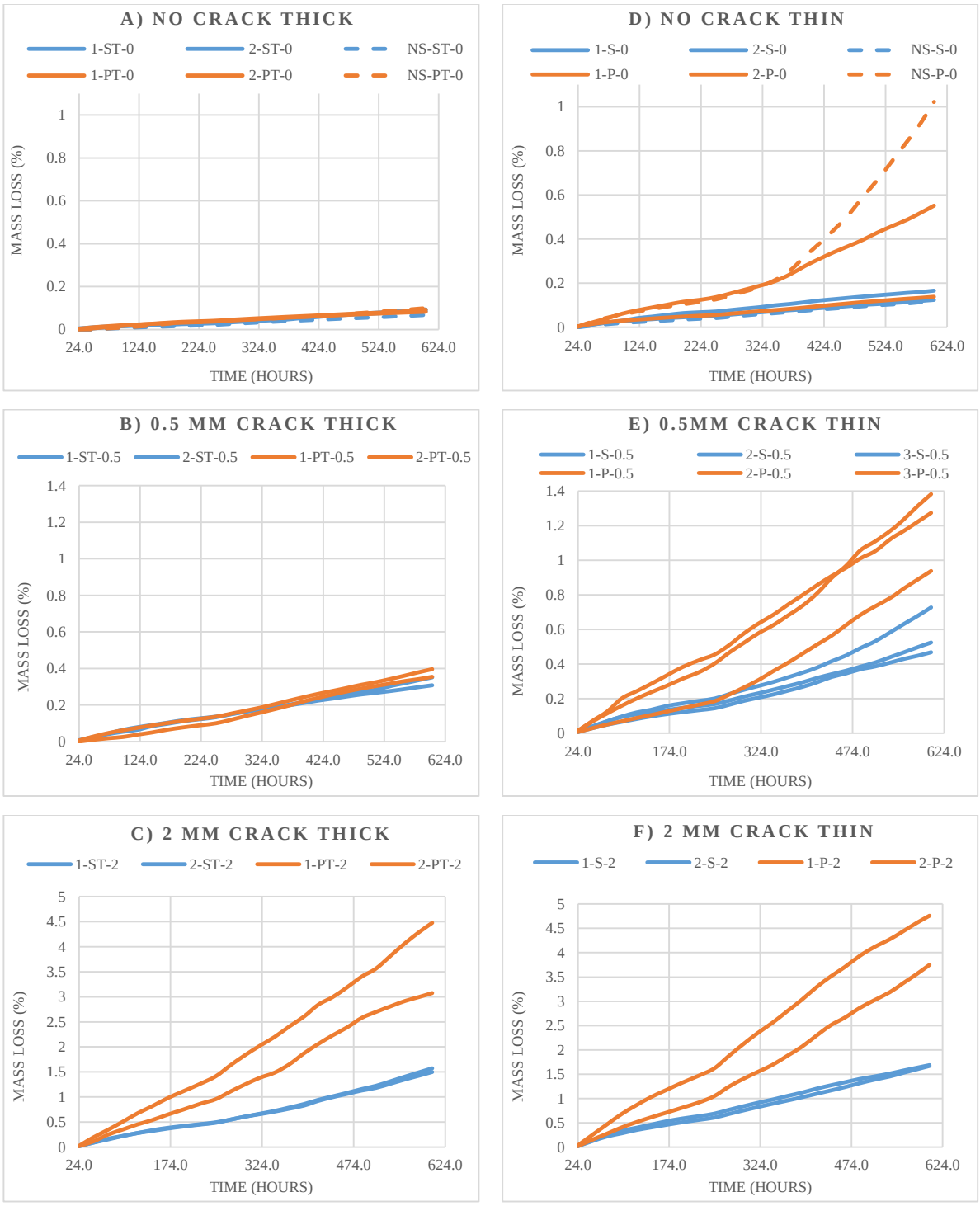

Figure 4-7. Mass Loss of Specimens of Similar Thicknesses Through Time

Specimens 1-P-2 and 1-PT-2, during the initial stage of cracking, formed a diametric crack that propagated throughout their thicknesses. The rest of the specimens formed a crack only towards the exposed surface. It was observed that these two specimens had a higher current compared to

their pairs. This was attributed to the easier access of water to the bar formed through capillary action. It was observed that, in the presence of cracks, ECC specimens showed higher current reading compared to their UHPC counterparts. This was attributed to the hydrophilic nature of PVA fibers, which absorbed and stored water during the wetting part of the conditioning cycle, lowering the effective resistivity of concrete.

Figure 4-7 shows the percentage of mass loss accumulation through time. Graphs obtained from specimens with similar crack widths were plotted to the same scale in order to facilitate comparison between specimens of different thicknesses. It was observed that for uncracked and 0.5mm cracked thick specimens [Figure 4-7 (a) and (b)], fiber type had no influence on mass loss. Irrespective of mix type, specimens were able to effectively mitigate corrosion. These specimens had accumulated mass losses of 0.09% for uncracked thick and 0.35% for 0.5mm cracked thick specimens.

Uncracked and 0.5mm cracked thin ECC specimens [Figures 4-7(d) and (e)] showed a higher mass loss ratio as compared to the UHPC specimens. This is attributed to the hydrophilic characteristic of PVA as mentioned earlier. PVA surrounding the bar may have allowed the passage of water from beneath the bar to its whole perimeter, in turn lowering the resistivity and enabling a higher current.

Concrete cover had an important role in corrosion suppression especially in the case of 0.5 mm cracked specimens. Figures 4-7(b) and (e) demonstrate that 0.5mm cracked thick specimens were less prone to corrosion in contrast to 0.5mm cracked thin specimens.

From Figures 4-7(a) and (d), it was observed that uncracked thin ECC specimens showed higher mass losses than uncracked thick ECC specimens, whereas in the case of uncracked UHPC specimens, concrete cover thickness did not make a difference in mass loss accumulation – practically negligible corrosion was observed in these cases. Table 4-4 displays the average mass loss in percent of every type of specimen. It is noted that the presence of the working level of tensile stress in the bars had no effect on the attained corrosion rate.

Table 4-4. Average Specimen Mass Loss in Percent

	Thin		*Thick*	
	UHPC Specimens	ECC Specimens	UHPC Specimens	ECC Specimens
No Crack	0.102	0.345	0.083	0.091
0.5mm Crack	0.573	1.2	0.329	0.375
2mm Crack	1.678	4.25	1.536	3.777

Specimen NS-P-0 was excluded from the average mass loss calculation

Under the last two columns in Table 4-4 (thick specimens) mass losses for uncracked and 0.5mm cracked specimens are listed. Values reported were practically identical between UHPC and ECC specimens. Fiber type only influenced mass losses of cracked specimens with 2mm cracks. Table 4-4 also shows that for thin specimens, the fiber type influenced the corrosion rate regardless of the presence of cracks or crack widths. UHPC specimens accumulated markedly lower mass loss as opposed to ECC specimens.

Comparing specimens having 2mm crack widths, it was observed that specimens composed of the same concrete had similar levels of mass loss, so the observed results were repeatable.

4.4. Material Effectiveness in Mitigating Corrosion

Previous test results conducted on combinations of concrete or SHCC specimens have shown that upon accelerated corrosion conditioning, the SHCC was able to decrease significantly the rate of corrosion (Fakhri, Ragalwar and Ranade, 2019). Figure 4-8 plots the mass loss (percent) with respect to exposure time (hours).

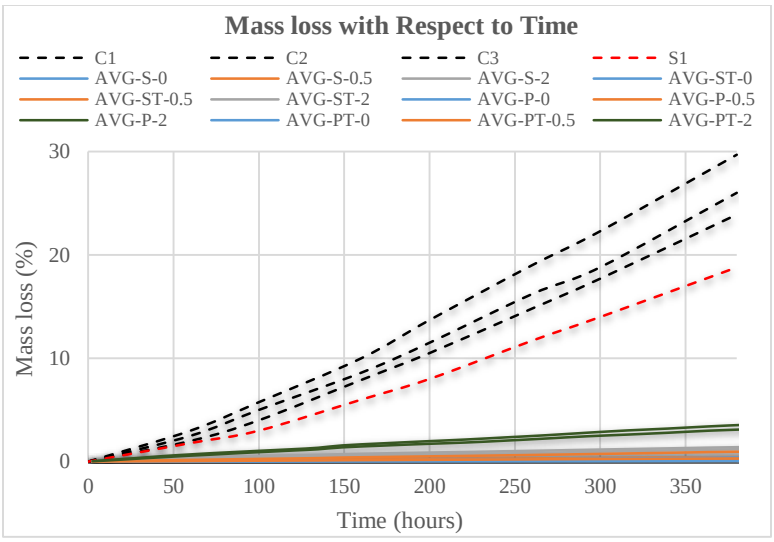

Figure 4-8. Mass Loss with Time of Bars in Various Cementitious Materials

S1 is the average of three full SHCC specimens. C1,C2 and C3 are three normal concrete specimens; data of these specimens were obtained from (Fakhri, Ragalwar and Ranade, 2019). The rest of the plotted data are obtained from the present study. Only the average values of similar specimens was used in order to reduce the scatter of information. Since in the present study three different potentials were used (1.05V, 5.89V and 10V), a modification to the time axis was made in order to render the results of this project comparable with those of Fakhri *et al*. (2019). The time scale reduced by the ratio of the applied potential to 10V; so the first 24hrs were considered 24*1.05/10=2.52 hrs and the 224 hours of applied 5.89V potential were considered as 224*5.89/10=132 hours. It was observed that UHPC and ECC served as a better corrosion-protective medium than both SHCC and concrete even in the presence of 2mm cracks.

4.4.1. Bar Preparation and Cleaning Method

Specimens were tested in tension using a servo-controlled hydraulic press under displacement control, in order to evaluate experimentally the tension stiffening performance of the corroded bar-cover assembly. After the mechanical tests were completed (these are presented in the next chapter), the specimens were bust open using a hydraulic press, reinforcement was then extracted for inspection of their condition. The bar cleaning method adopted was through sandblasting as this is considered to be the most reliable method according to (Fernandez, Lundgren and Zandi, 2018). Sandblasting was performed in a special chamber at a pressure of 6 bar. Sand used for rust

removal was silica sand and each bar's cleansing process required approximately 2-3 minutes of sandblasting.

4.4.2. Type of Corrosion

After the removal of concrete and cleaning of reinforcement bars, rebars were physically inspected in order to further investigate the effect of the several present parameters (crack widths, concrete cover thickness, fiber type etc.) on the type of corrosion. Table 4-5 summarizes the findings of the study.

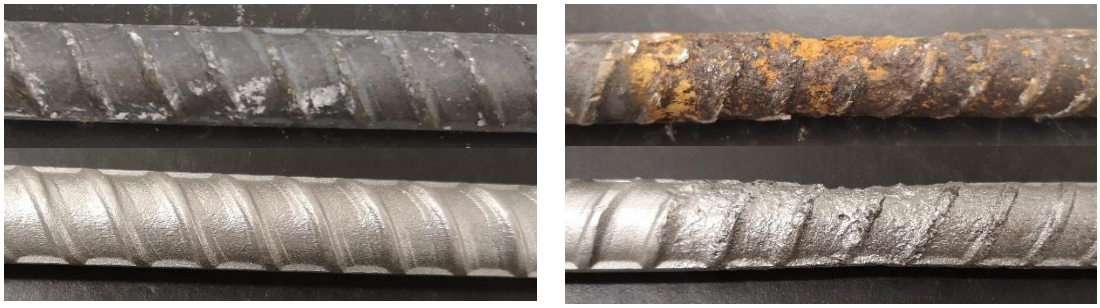

a) 2-PT-0 b) 1-P-2

Figure 4-9. Bars Before and After Cleaning

Bars were inspected prior to and after cleaning; it was observed that most bars of uncracked specimens did not develop any rust along the embedded portion of the bar as depicted in Figure 4-9(a). Figure 4-9(b) shows the condition of specimen 1-P-2's bar which had suffered 4.7 % mass loss.

After a thorough inspection of the bars, it was observed that the reduction in rib height was greater and more catastrophic than the reduction in bar diameter. It was observed that majority of bars of specimens with 0.5mm crack widths had only the exposed side of the bar being corroded while bars of specimens with 2mm crack widths developed corrosion around the perimeter of the bar. These results were reported in Table 4-5 under the column denoted as 'affected sides' where 0 indicates that no corrosion was observed, 1 indicates only the exposed surface was corroded and 2 indicates that the whole perimeter was corroded. This could be attributed to the fact that specimens with 0.5 mm crack widths did not reach as significant mass losses as specimens with 2mm cracks did.

Table 4-5. Corroded Bar Conditions

Specimen ID	*Average Current Density μA/cm²*	*Mass Loss (%)*	*External Corrosion*	*Affected Sides*	*Type of Corrosion*	*Pit*		
						Depth (mm)	**Width (mm)**	**Length (mm)**
1-S-0	7.92	0.166	Yes	0	-	-	-	-
2-S-0	5.92	0.124	No	0	-	-	-	-
NS-S-0	5.73	0.119	No	0	-	-	-	-
1-S-0.5	35.02	0.726	Yes	2	General	-	-	-
2-S-0.5	25.17	0.524	No	1	General	-	-	-
3-S-0.5	22.45	0.468	Yes	1	General	-	-	-
1-S-2	80.60	1.688	No	1	Gen-Pit	0.5	4	4.5
2-S-2	79.86	1.667	No	2	Pit	1.3	2.1	8
1-P-0	6.64	0.139	No	0	-	-	-	-
2-P-0	26.59	0.552	No	1	-	-	-	
NS-P-0	49.71	1.022	No	1	Pit	2	5	5.5
1-P-0.5	45.19	0.938	No	1	Pit	1.7	4	6
2-P-0.5	66.40	1.383	Yes	2	Pit	1.6	1.4	4
3-P-0.5	60.78	1.274	Yes	2	General + Pit	1.2	1.4	2.1
1-P-2	227.38	4.759	No	2	General + Pit	2	4.5	15
2-P-2	180.15	3.751	No	2	General + Pit	-	-	-
1-ST-0	4.52	0.093	Yes	0	-	-	-	-
2-ST-0	4.14	0.086	Yes	0	-	-	-	-
NS-ST-0	3.27	0.068	Yes	0	-	-	-	-
1-ST-0.5	16.75	0.350	Yes	1	General	-	-	-
2-ST-0.5	14.63	0.307	Yes	1	General	-	-	-
1-ST-2	71.91	1.498	No	2	General + Pit	0.3	1.5	1.6
2-ST-2	75.56	1.574	No	2	General + Pit	0.2	1.1	1.5
1-PT-0	4.40	0.092	Yes	0	-	-	-	-
2-PT-0	3.92	0.082	Yes	0	-	-	-	-
NS-PT-0	4.77	0.099	Yes	0	-	-	-	-
1-PT-0.5	18.93	0.395	No	1	Pit	0.7	2	4.3
2-PT-0.5	16.89	0.354	No	1	General + Pit	0.7	2	2.8
1-PT-2	213.94	4.476	No	2	Pit	0.9	4	7
2-PT-2	146.51	3.077	No	2	General	0.4	4	3.5

Types of corrosion were also reported and documented in Table 4-5 under the column denoted as ‘type of corrosion’, where “General” identifies general/uniform corrosion and “Pit” denotes pitting corrosion. In the cases where the type of corrosion was in-between the general and pitting corrosion

types, “General + Pit” was recorded. No clear correlation was made with regards to crack width, and concrete cover thickness with respect to the type of corrosion (General, Pitting).

It was found that some specimens developed some corrosive byproducts/pits on the exposed portion of the bar, at the external point of intersection of bar and concrete. These external corrosion reactions explain the presence of recorded currents passing through uncracked specimens while after cleansing, the bars showed no evidence of corrosion in the embedded segment. All specimens which had external corrosion were documented in Table 4-5 under the column ‘external corrosion’. Pit depths, widths and lengths were also included in Table 4-5.

4.5. Conclusions

Two groups of specimens, the first comprising UHPC cover, the second having an ECC cover, underwent accelerated corrosion through application of a fixed potential. Wetting and drying cycles were adopted in order to guarantee complete oxidization of corrosion-byproducts with a total wet duration of 600 hours. Variables in the study were, fiber type (Steel or PVA) as the dry mix was the same, concrete cover thickness, and diametric crack width (no crack, 0.5mm crack, and 2mm crack). Current was monitored continuously throughout the wetting period; this data was used in calculating mass loss ratio using Faraday’s law. The following conclusions were drawn based on accelerated corrosion data:

- For concrete covers of thickness equal to $1 \cdot d_b$, UHPC showed greater mitigation qualities over ECC, especially in the presence of cracks. This was attributed to the hydrophilic properties of PVA fibers used with the ECC; The presence of water facilitates the passage of current. For covers equal to $2 \cdot d_b$, UHPC only showed improved mitigation qualities over ECC in the presence of 2mm cracks whereas for smaller crack widths both sets of specimens had low levels of accumulated mass loss of similar magnitude.
- Concrete cover had a significant influence on corrosion rate especially for specimens with a 0.5 mm crack width. A 42% reduction in mass loss was observed for UHPC specimens going from $1d_b$ to $2d_b$ cover thickness, whereas the corresponding reduction in ECC specimens was as high as 68%. At 2mm crack width, concrete cover thickness was not as effective in reducing the corrosion rates where a reduction by 8% and 12% was observed for UHPC and ECC respectively by doubling the cover thickness.

- In uncracked cases, for UHPC specimens of both concrete cover thicknesses did not show any mass loss. In ECC cases only the thick uncracked specimens did not show any mass loss.
- No direct correlation was found between crack width and type of corrosion (pitting vs general corrosion)
- Corrosion mitigation characteristics of UHPC and ECC from the present study were compared to those of normal concrete and SHCC from a different study. It was found that UHPC/ECC offered orders of magnitude more protection than both normal concrete and SHCC.
- Tensile stress application on reinforcement did not show any influence on corrosion rate.
- For field practice, a concrete cover of $2d_b$ of UHPC is recommended for corrosion mitigation and for prolonging the service life of structural components.

4.6. References

ACI-374 (2016) *ACI 374 - Guide to Nonlinear Modeling Parameters for Earthquake-Resistant Structures*. Available at: www.concrete.org (Accessed: 27 March 2022).

ACI 222R-19 (2019) 'Guide to Protection of Reinforcing Steel in Concrete Against Corrosion', *American Concrete Institute*, pp. 1–65.

Al-Saidy, A. H. *et al.* (2016) 'Structural behavior of corroded RC beams with/without stirrups repaired with CFRP sheets', *Materials and Structures*. Springer Netherlands, 49(9), pp. 3733–3747. doi: 10.1617/s11527-015-0751-y.

Al-Sulaimani, G. J. *et al.* (1990) 'Influence of corrosion and cracking on bond behavior and strength of reinforced concrete members', *ACI Structural Journal*, 87(2), pp. 220–231. doi: 10.14359/2732.

Alaskar, A. (2013) 'Shear Behaviour of Slender RC Beams with Corroded Web Reinforcement'. University of Waterloo. Available at: https://uwspace.uwaterloo.ca/handle/10012/7472 (Accessed: 15 July 2019).

Allamt, I. M. *et al.* (1994) *Influence of atmospheric corrosion on the mechanical properties of reinforcing steel, Construction and Building Materials*.

Almusallam, A. A. *et al.* (1996) ‘Effect of reinforcement corrosion on bond strength’, *Construction and Building Materials*. Elsevier, 10(2), pp. 123–129. doi: 10.1016/0950-0618(95)00077-1.

Almusallam, A. A. (2001a) ‘Effect of degree of corrosion on the properties of reinforcing steel bars’, *Construction and Building Materials*. Elsevier, 15(8), pp. 361–368. doi: 10.1016/S0950-0618(01)00009-5.

Almusallam, A. A. (2001b) ‘Effect of degree of corrosion on the properties of reinforcing steel bars’, *Construction and Building Materials*. Elsevier, 15(8), pp. 361–368. doi: 10.1016/S0950-0618(01)00009-5.

Alonso, C. *et al.* (1998) ‘Factors controlling cracking of concrete affected by reinforcement corrosion’, *Materials and Structures*. Kluwer Academic Publishers, 31(7), pp. 435–441. doi: 10.1007/BF02480466.

American Road & Transportation Builders Association (2020) *ARTBA Bridge Report*. Available at: https://artbabridgereport.org/ (Accessed: 6 July 2020).

Amleh, L., Mirza, M. and Ahwazi, B. (2000) ‘Bond deterioration of reinforcing steel in concrete due to corrosion’. Available at: https://books.google.com/books?hl=en&lr=&id=F8HosZdH8BUC&oi=fnd&pg=PA247&ots=Iq_HHO_T-s&sig=3ytv3HtTEhxTvU9yTJRyH6PPLrk (Accessed: 5 July 2019).

Andrade, C., Alonso, M. C. and Gonzalez, J. A. (1990) ‘Initial effort to use the corrosion rate measurements for estimating rebar durability’, *ASTM Special Technical Publication*. ASTM International, (1065), pp. 29–37. doi: 10.1520/stp25013s.

Andrade, C. and González, J. A. (1978) ‘Quantitative measurements of corrosion rate of reinforcing steels embedded in concrete using polarization resistance measurements’, *Materials and Corrosion*, 29(8), pp. 515–519. doi: 10.1002/maco.19780290804.

Apostolopoulos, C. A. (2007) ‘Mechanical behavior of corroded reinforcing steel bars S500s tempcore under low cycle fatigue’, *Construction and Building Materials*. Elsevier, 21(7), pp. 1447–1456. doi: 10.1016/J.CONBUILDMAT.2006.07.008.

Apostolopoulos, C. A. and Papadakis, V. G. (2008) ‘Consequences of steel corrosion on the

ductility properties of reinforcement bar', *Construction and Building Materials*. Elsevier, 22(12), pp. 2316–2324. doi: 10.1016/J.CONBUILDMAT.2007.10.006.

Apostolopoulos, C., Drakakaki, A. and Basdeki, M. (2019) 'Seismic assessment of RC column under seismic loads', *International Journal of Structural Integrity*. Emerald Publishing Limited , 10(1), pp. 41–54. doi: 10.1108/IJSI-02-2018-0013.

ASCE 41 (2017) *Seismic Evaluation and Retrofit of Existing Buildings, Seismic Evaluation and Retrofit of Existing Buildings*. American Society of Civil Engineers. doi: 10.1061/9780784414859.

Azad, A. K., Ahmad, S. and Al-Gohi, B. H. A. (2010) 'Flexural strength of corroded reinforced concrete beams', *Magazine of Concrete Research*. Thomas Telford Ltd , 62(6), pp. 405–414. doi: 10.1680/macr.2010.62.6.405.

Berra, M., Castellani, A. and Coronelli, D. (1997) 'Bond in reinforced concrete and corrosion of bars', in *Structural Faults and Repair*. Edinburgh, UK, pp. 349–357.

Berrocal, C. G. *et al.* (2017) 'Corrosion-induced cracking and bond behaviour of corroded reinforcement bars in SFRC', *Composites Part B: Engineering*. Elsevier, 113, pp. 123–137. doi: 10.1016/J.COMPOSITESB.2017.01.020.

Blaber, J., Adair, & B. and Antoniou, & A. (no date) 'Ncorr: Open-Source 2D Digital Image Correlation Matlab Software'. doi: 10.1007/s11340-015-0009-1.

Cairns, J., Du, Y. and Law, D. (2008) 'Structural performance of corrosion-damaged concrete beams', *Magazine of Concrete Research*. Thomas Telford Ltd , 60(5), pp. 359–370. doi: 10.1680/macr.2007.00102.

Di Carlo, F., Meda, A. and Rinaldi, Z. (2017) 'Numerical cyclic behaviour of un-corroded and corroded RC columns reinforced with HPFRC jacket', *Composite Structures*. Elsevier, 163, pp. 432–443. doi: 10.1016/J.COMPSTRUCT.2016.12.038.

Castel, A., François, R. and Arliguie, G. (2000) 'Mechanical behaviour of corroded reinforced concrete beams—Part 1: Experimental study of corroded beams', *Materials and Structures*. Kluwer Academic Publishers, 33(9), pp. 539–544. doi: 10.1007/BF02480533.

CEN (2005) *EN 1998 - 3 Eurocode 8-Design of structures for earthquake resistance-Part 3: Assessment and retrofitting of buildings*.

Cervenka Consulting (2007) 'ATENA Program Documentation'. Prague, Czech Republic.

Civjan, S. A. *et al.* (2005) 'Effectiveness of corrosion inhibiting admixture combinations in structural concrete', *Cement and Concrete Composites*. Elsevier, 27(6), pp. 688–703. doi: 10.1016/J.CEMCONCOMP.2004.07.007.

Coronelli, D. and Gambarova, P. (2004) 'Structural Assessment of Corroded Reinforced Concrete Beams: Modeling Guidelines', *Journal of Structural Engineering*. American Society of Civil Engineers, 130(8), pp. 1214–1224. doi: 10.1061/(ASCE)0733-9445(2004)130:8(1214).

Coronelli, D., Hanjari, K. Z. and Lundgren, K. (2013) 'Severely Corroded RC with Cover Cracking', *Journal of Structural Engineering*, 139(2), pp. 221–232. doi: 10.1061/(ASCE)ST.1943-541X.0000633.

Dang, V. H. and François, R. (2013) 'Influence of long-term corrosion in chloride environment on mechanical behaviour of RC beam', *Engineering Structures*. Elsevier, 48, pp. 558–568. doi: 10.1016/j.engstruct.2012.09.021.

Darwin, D. and Pecknold, D. (1974) *INELASTIC MODEL FOR CYCLIC BIAXIAL LOADING OF REINFORCED CONCRETE*. Illinois, Urbana. Available at: https://www.semanticscholar.org/paper/INELASTIC-MODEL-FOR-CYCLIC-BIAXIAL-LOADING-OF-Darwin-Pecknold/5d1fb39809798f4c65b2dfa0fad5c06dd82e2a6f (Accessed: 20 July 2022).

Du, Y., Clark, L. A. and Chan, A. H. C. (2007) 'Impact of Reinforcement Corrosion on Ductile Behavior of Reinforced Concrete Beams', *ACI Structural Journal*, 104(3), pp. 285–293. doi: 10.14359/18618.

Du, Y. G., Clark, L. A. and Chan, A. H. C. (2005) 'Residual capacity of corroded reinforcing bars', *Magazine of Concrete Research*. Thomas Telford Ltd , 57(3), pp. 135–147. doi: 10.1680/macr.2005.57.3.135.

El-Joukhadar, N., Tsiotsias, K. and Pantazopoulou, S. (2019) 'Consideration of the state of corrosion in seismic assessment of columns', *International Journal of Structural Integrity*.

Emerald Group Publishing Ltd. doi: 10.1108/IJSI-07-2019-0065.

Fakhri, H., Ragalwar, K. A. and Ranade, R. (2019) 'On the use of Strain-Hardening Cementitious Composite covers to mitigate corrosion in reinforced concrete structures', *Construction and Building Materials*. Elsevier Ltd, 224, pp. 850–862. doi: 10.1016/j.conbuildmat.2019.07.052.

Fang, C. *et al.* (2004) 'Corrosion influence on bond in reinforced concrete', *Cement and Concrete Research*. Pergamon, 34(11), pp. 2159–2167. doi: 10.1016/J.CEMCONRES.2004.04.006.

Farhan, N. A., Sheikh, M. N. and Hadi, M. N. S. (2018) 'Experimental Investigation on the Effect of Corrosion on the Bond Between Reinforcing Steel Bars and Fibre Reinforced Geopolymer Concrete', *Structures*. Elsevier, 14, pp. 251–261. doi: 10.1016/J.ISTRUC.2018.03.013.

Fernandez, I. *et al.* (2018) 'Ultimate Capacity of Corroded Statically Indeterminate Reinforced Concrete Members', *International Journal of Concrete Structures and Materials*. Springer Singapore, 12(1), p. 75. doi: 10.1186/s40069-018-0297-9.

Fernandez, I., Bairán, J. M. and Marí, A. R. (2015) 'Corrosion effects on the mechanical properties of reinforcing steel bars. Fatigue and σ–ε behavior', *Construction and Building Materials*. Elsevier, 101, pp. 772–783. doi: 10.1016/J.CONBUILDMAT.2015.10.139.

Fernandez, I. and Berrocal, C. G. (2019) 'Mechanical Properties of 30 Year-Old Naturally Corroded Steel Reinforcing Bars', *International Journal of Concrete Structures and Materials*. Korea Concrete Institute, 13(1), p. 9. doi: 10.1186/s40069-018-0308-x.

Fernandez, I., Lundgren, K. and Zandi, K. (2018) 'Evaluation of corrosion level of naturally corroded bars using different cleaning methods, computed tomography, and 3D optical scanning', *Materials and Structures/Materiaux et Constructions*. Springer Netherlands, 51(3), pp. 1–13. doi: 10.1617/s11527-018-1206-z.

fib-Model Code (2020) 'Model Code 2020, Draft version MC2020', in. fib.

fib bulletin #10 (2000) *Bond of reinforcement in concrete : state-of-art report*. International Federation for Structural Concrete. Available at: https://www.fib-

international.org/publications/fib-bulletins/bond-of-reinforcement-in-concrete-pdf-detail.html (Accessed: 3 July 2019).

fib Model Code (2010) *Fib model code for concrete structures 2010*.

Fischer, C., Ozbolt, J. and Gehlen, C. (2010) 'Numerical investigation on bond behavior of corroded reinforcement', in *7th International Conference on Fracture Mechanics of Concrete and Concrete Structures*. Jeju, Korea, pp. 779–785.

François, R. and Arliguie, G. (1998) 'Influence of Service Cracking on Reinforcement Steel Corrosion', *Journal of Materials in Civil Engineering*, 10(1), pp. 14–20. doi: 10.1061/(ASCE)0899-1561(1998)10:1(14).

François, R., Khan, I. and Dang, V. H. (2013) 'Impact of corrosion on mechanical properties of steel embedded in 27-year-old corroded reinforced concrete beams', *Materials and Structures*. Springer Netherlands, 46(6), pp. 899–910. doi: 10.1617/s11527-012-9941-z.

Fu, C. *et al.* (2017) 'Corrosion characteristics of a 4-year naturally corroded reinforced concrete beam with load-induced transverse cracks', *Corrosion Science*. Pergamon, 117, pp. 11–23. doi: 10.1016/J.CORSCI.2017.01.002.

Ganesh, P. and Ramachandra Murthy, A. (2020) 'Simulation of surface preparations to predict the bond behaviour between normal strength concrete and ultra-high performance concrete', *Construction and Building Materials*. Elsevier, 250, p. 118871. doi: 10.1016/J.CONBUILDMAT.2020.118871.

Gjørv, O. E. (2014) *Durability Design of Concrete Structures in Severe Environments*. CRC Press. doi: 10.1201/b16469.

Goksu, C. and Ilki, A. (2016) 'Seismic Behavior of Reinforced Concrete Columns with Corroded Deformed Reinforcing Bars', *ACI Structural Journal*, 113(5), pp. 1053–1064. doi: 10.14359/51689030.

Haddad, R. H. and Ashteyate, A. M. (2001) 'Role of synthetic fibers in delaying steel corrosion cracks and improving bond with concrete', *Canadian Journal of Civil Engineering*. NRC Research Press Ottawa, Canada , 28(5), pp. 787–793. doi: 10.1139/l01-037.

Hanjari, K. Z., Coronelli, D. and Lundgren, K. (2011) 'Bond capacity of severely corroded bars with corroded stirrups', *Magazine of Concrete Research*. Thomas Telford Ltd , 63(12), pp. 953–968. doi: 10.1680/macr.10.00200.

Harajli, M. H. (2004) 'Comparison of Bond Strength of Steel Bars in Normal- and High-Strength Concrete', *Journal of Materials in Civil Engineering*, 16(4), pp. 365–374. doi: 10.1061/(ASCE)0899-1561(2004)16:4(365).

Higgins, C. and Farrow, W. C. (2006) 'Tests of Reinforced Concrete Beams with Corrosion-Damaged Stirrups', *ACI Structural Journal*, 103(1), pp. 133–141. doi: 10.14359/15094.

Hou, L. *et al.* (2017) 'Effect of corrosion on bond behaviors of rebar embedded in ultra-high toughness cementitious composite', *Construction and Building Materials*. Elsevier, 138, pp. 141–150. doi: 10.1016/J.CONBUILDMAT.2017.02.008.

Hung, C. C., Lee, H. S. and Chan, S. N. (2019) 'Tension-stiffening effect in steel-reinforced UHPC composites: Constitutive model and effects of steel fibers, loading patterns, and rebar sizes', *Composites Part B: Engineering*. Elsevier Ltd, 158, pp. 269–278. doi: 10.1016/j.compositesb.2018.09.091.

Ioannou, A. *et al.* (2022) 'Experimental Testing of ECC Jackets for Repair of Pre-Damaged R . C . Members Experimental Testing of ECC Jackets for Repair of Pre-Damaged R . C . Members under Cyclic Loading', in *12th National Conference on Earthquake Engineering*. Salt Lake City, Utah: Earthquake Engineering Research Institute, pp. 1–5.

Kashani, M. M., Maddocks, J. and Dizaj, E. A. (2019) 'Residual Capacity of Corroded Reinforced Concrete Bridge Components: State-of-the-Art Review', *Journal of Bridge Engineering*, 24(7), p. 03119001. doi: 10.1061/(ASCE)BE.1943-5592.0001429.

Kondratova, I. L., Montes, P. and Bremner, T. W. (2000) 'Accelerated Corrosion Testing Results for Specimens Containing Uncoated Reinforcing Steel and Corrosion Inhibitors', *Special Publication*, 192, pp. 789–806. doi: 10.14359/5785.

Koulouris, K. and Apostolopoulos, C. (2020) 'An Experimental Study on Effects of Corrosion and Stirrups Spacing on Bond Behavior of Reinforced Concrete', *Metals*. MDPI AG, 10(10), p. 1327. doi: 10.3390/met10101327.

Lee, H. S. and Cho, Y. S. (2009) 'Evaluation of the mechanical properties of steel reinforcement embedded in concrete specimen as a function of the degree of reinforcement corrosion', in *International Journal of Fracture*. Springer, pp. 81–88. doi: 10.1007/s10704-009-9334-7.

Li, D. *et al.* (2018) 'Influence of Non-uniform corrosion of steel bars on the seismic behavior of reinforced concrete columns', *Construction and Building Materials*. Elsevier, 167, pp. 20–32. doi: 10.1016/J.CONBUILDMAT.2018.01.149.

Li, J., Gong, J. and Wang, L. (2009) 'Seismic behavior of corrosion-damaged reinforced concrete columns strengthened using combined carbon fiber-reinforced polymer and steel jacket', *Construction and Building Materials*. Elsevier, 23(7), pp. 2653–2663. doi: 10.1016/J.CONBUILDMAT.2009.01.003.

Li, X. *et al.* (2016) 'Effect of loading rate on the bond behaviour of deformed steel bars in concrete subjected to lateral pressure', *Materials and Structures*. Springer Netherlands, 49(6), pp. 2097–2111. doi: 10.1617/s11527-015-0636-0.

Lijina, T. and Jithin, J. . (2018) 'Effect of Steel and Polypropylene Fibre on the Tension Stiffening of Ultra High Performance Concrete', *International Journal of Engineering and Advanced Technology (IJEAT)*, 8(4C).

Lin, H. *et al.* (2019) 'State-of-the-art review on the bond properties of corroded reinforcing steel bar', *Construction and Building Materials*. Elsevier, 213, pp. 216–233. doi: 10.1016/J.CONBUILDMAT.2019.04.077.

Liu, X. and Li, Y. (2018) 'Experimental study of seismic behavior of partially corrosion-damaged reinforced concrete columns strengthened with FRP composites with large deformability', *Construction and Building Materials*. Elsevier, 191, pp. 1071–1081. doi: 10.1016/J.CONBUILDMAT.2018.10.072.

Lu, C. *et al.* (2016) 'Mechanical properties of corroded steel bars in pre-cracked concrete suffering from chloride attack', *Construction and Building Materials*, 123(123), pp. 649–660. doi: 10.1016/j.conbuildmat.2016.07.032.

Ma, Y., Che, Y. and Gong, J. (2012) 'Behavior of corrosion damaged circular reinforced concrete columns under cyclic loading', *Construction and Building Materials*. Elsevier, 29, pp.

548–556. doi: 10.1016/J.CONBUILDMAT.2011.11.002.

El Maaddawy, T. A. and Soudki, K. A. (2003) 'Effectiveness of Impressed Current Technique to Simulate Corrosion of Steel Reinforcement in Concrete', *Journal of Materials in Civil Engineering*, 15(1), pp. 41–47. doi: 10.1061/(ASCE)0899-1561(2003)15:1(41).

Mangat, P. S. and Elgarf, M. S. (1999) 'Bond characteristics of corrding reinforcement in concrete beams', *Materials and Structures*. Kluwer Academic Publishers, 32(2), pp. 89–97. doi: 10.1007/BF02479434.

Mangat, Pritpal S. and Elgarf, M. S. (1999) 'Flexural Strength of Concrete Beams with Corroding Reinforcement', *ACI Structural Journal*, 96(1), pp. 149–158. doi: 10.14359/606.

Martín Pérez, B. M. (1999) *Service life modelling of R.C. highway structures exposed to chlorides*. University of Toronto. Available at: https://books.google.ca/books/about/Service_Life_Modelling_of_R_C_Highway_St.html?id=qQiGtgAACAAJ&redir_esc=y (Accessed: 14 February 2019).

Meda, A. *et al.* (2014) 'Experimental evaluation of the corrosion influence on the cyclic behaviour of RC columns', *Engineering Structures*. Elsevier, 76, pp. 112–123. doi: 10.1016/J.ENGSTRUCT.2014.06.043.

Mehta, P. K. (1991) 'Durability of Concrete--Fifty Years of Progress?', *Special Publication*, 126, pp. 1–32. doi: 10.14359/1998.

Menengotto, M. and Pinto, P. E. (1973) 'Method o f Analysis for Cyclically Loaded Reinforced Concrete Plane Frames Including Changes in Geometry and Nonelastic Behavior of Elements under Combined Normal Force and Bending', in *IABSE Symposium on Resistance and Ultimate Deformability of Structures Acted on*. Lisbon.

Molaioni, F., Carlo, F. Di and Rinaldi, Z. (2021) 'Modelling Strategies for the Numerical Simulation of the Behaviour of Corroded RC Columns under Cyclic Loads', *Applied Sciences 2021, Vol. 11, Page 9761*. Multidisciplinary Digital Publishing Institute, 11(20), p. 9761. doi: 10.3390/APP11209761.

Ou, Y.-C. and Chen, H.-H. (2014) 'Cyclic Behavior of Reinforced Concrete Beams with Corroded Transverse Steel Reinforcement', *Journal of Structural Engineering*, 140(9), p.

04014050. doi: 10.1061/(ASCE)ST.1943-541X.0000932.

Palsson, R. and Mirza, M. S. (2002a) ‘Mechanical response of corroded steel reinforcement of abandoned concrete bridge’, *ACI Structural Journal*, 99(2), pp. 157–162. doi: 10.14359/11538.

Palsson, R. and Mirza, M. S. (2002b) ‘Mechanical Response of Corroded Steel Reinforcement of Abandoned Concrete Bridge’, *ACI Structural Journal*, 99(2), pp. 157–162. doi: 10.14359/11538.

Pantazopoulou, S. J. *et al.* (2001) *REPAIR OF CORROSION-DAMAGED COLUMNS WITH FRP WRAPS, JOURNAL OF COMPOSITES FOR CONSTRUCTION*. Available at: http://pubs.asce.org/copyright (Accessed: 23 July 2019).

Pantazopoulou, S. J. *et al.* (2019) ‘The performance of corroded lap splices in reinforced concrete beams’, *Corrosion Reviews*. De Gruyter, 37(1), pp. 31–44. doi: 10.1515/corrrev-2017-0086.

Papakonstantinou, C. G., Balaguru, P. N. and Auyeung, Y. (2011) ‘Influence of FRP confinement on bond behavior of corroded steel reinforcement’, *Cement and Concrete Composites*. Elsevier, 33(5), pp. 611–621. doi: 10.1016/J.CEMCONCOMP.2011.02.006.

Pardalopoulos, S. I., Pantazopoulou, S. J. and Lekidis, V. A. (2017) ‘Simplified method for rapid seismic assessment of older R.C. buildings’. doi: 10.1016/j.engstruct.2017.10.052.

Pardalopoulos, S. I., Pantazopoulou, S. J. and Lekidis, V. A. (2018) ‘Simplified method for rapid seismic assessment of older R.C. buildings’, *Engineering Structures*. Elsevier Ltd, 154, pp. 10–22. doi: 10.1016/j.engstruct.2017.10.052.

Pardalopoulos, S. J., Thermou, G. E. and Pantazopoulou, S. J. (2013) ‘Screening criteria to identify brittle R.C. structural failures in earthquakes’, *Bulletin of Earthquake Engineering*, 11(2), pp. 607–636. doi: 10.1007/s10518-012-9390-7.

Parulekar, Y. M. *et al.* (2020) ‘Performance Assessment of Corroded Reinforced Concrete Structure Considering Bond Deterioration’, *Journal of Performance of Constructed Facilities*. American Society of Civil Engineers, 34(2), p. 04020009. doi: 10.1061/(ASCE)CF.1943-5509.0001411.

Paul, Suvash CZijl, G. Van (2014) ‘Cracked and uncracked SHCC specimens under different

exposure conditions', in *Strain Hardening Cementitious Composites 3 (SHCC3)*. Dordrecht, pp. 25–32.

Pourbaix, M. (1974) *Atlas of electrochemical equilibria in aqueous solutions*. National Association of Corrosion Engineers. Available at: https://books.google.ca/books?id=iiLRvQEACAAJ&dq=9780915567980&hl=en&sa=X&ved=0ahUKEwivreD28rfgAhVi6IMKHQm4Dn4Q6AEIKjAA (Accessed: 12 February 2019).

Prieto, M., Tanner, P. and Andrade, C. (2011) 'Bond response in structural concrete with corroded steel bars. experimental results', *RILEM Bookseries*. Springer, Dordrecht, 5, pp. 231–241. doi: 10.1007/978-94-007-0677-4_16.

Rajput, A. S. and Sharma, U. K. (2018) 'Corroded reinforced concrete columns under simulated seismic loading', *Engineering Structures*. Elsevier, 171, pp. 453–463. doi: 10.1016/J.ENGSTRUCT.2018.05.097.

Raza, S. *et al.* (2019) 'Strengthening and Repair of Reinforced Concrete Columns by Jacketing: State-of-the-Art Review', *Sustainability*. MDPI AG, 11(11), p. 3208. doi: 10.3390/su11113208.

Robuschi, S. *et al.* (2020) 'Bond of naturally corroded, plain reinforcing bars in concrete', *Structure and Infrastructure Engineering*. Taylor and Francis Ltd., pp. 1–17. doi: 10.1080/15732479.2020.1768273.

Rodriguez, J. and Ortega, J. C. (1994) 'Corrosion of reinforcing bars and service life of reinforced concrete structures: corrosion and bond deterioration', in *International Conference on Concrete across Borders*. Odense, Denmark, pp. 315–326.

Semendary, A. A. and Svecova, D. (2020) 'Factors affecting bond between precast concrete and cast in place ultra high performance concrete (UHPC)', *Engineering Structures*. Elsevier, 216, p. 110746. doi: 10.1016/J.ENGSTRUCT.2020.110746.

Sezen, H. and Moehle, J. P. (2004) 'Shear Strength Model for Lightly Reinforced Concrete Columns', *Journal of Structural Engineering*. American Society of Civil Engineers, 130(11), pp. 1692–1703. doi: 10.1061/(ASCE)0733-9445(2004)130:11(1692).

Soudki, K. and Sherwood, T. (2003) 'Bond Behavior of Corroded Steel Reinforcement in Concrete Wrapped with Carbon Fiber Reinforced Polymer Sheets', *Journal of Materials in Civil*

Engineering, 15(4), pp. 358–370. doi: 10.1061/(ASCE)0899-1561(2003)15:4(358).

Stanish, K., Hooton, R. D. and Pantazopoulou, S. J. (1999) 'Corrosion Effects on Bond Strength in Reinforced Concrete', *ACI Structural Journal*, 96(6), pp. 915–921. doi: 10.14359/765.

Suffern, C., El-Sayed, A. and Soudki, K. (2010) 'Shear strength of disturbed regions with corroded stirrups in reinforced concrete beams', *Canadian Journal of Civil Engineering*, 37(8), pp. 1045–1056. doi: 10.1139/L10-031.

Takuya, K., Ryuta, I. and Masayuki, T. (2020) 'Prediction of Hydrogen Embrittlement of Reinforcing Steel Bars in Concrete Poles | NTT Technical Review', *NTT Technical Review*, 18(11). Available at: https://www.ntt-review.jp/archive/ntttechnical.php?contents=ntr202011ra1.html (Accessed: 16 April 2022).

Tastani, S. P. and Pantazopoulou, S. J. (2007) 'Behavior of Corroded Bar Anchorages', *ACI Structural Journal*, 104(6), pp. 756–766. doi: 10.14359/18958.

Tastani, S. and Pantazopoulou, S. J. (2005) 'Recovery of seismic resistance in corrosion-damaged reinforced concrete through FRP jacketing', *International Journal of Materials and Product Technology*, 23(3/4), p. 389. doi: 10.1504/IJMPT.2005.007737.

Tayeh, B. A., Abu Bakar, B. H. and Megat Johari, M. A. (2013) 'Characterization of the interfacial bond between old concrete substrate and ultra high performance fiber concrete repair composite', *Materials and Structures/Materiaux et Constructions*. Springer, 46(5), pp. 743–753. doi: 10.1617/S11527-012-9931-1/FIGURES/13.

Tepfers, R. (1979) 'Cracking of concrete cover along anchored deformed reinforcing bars', *Magazine of Concrete Research*. Thomas Telford Ltd , 31(106), pp. 3–12. doi: 10.1680/macr.1979.31.106.3.

Tondolo, F. (2015) 'Bond behaviour with reinforcement corrosion', *Construction and Building Materials*. Elsevier, 93, pp. 926–932. doi: 10.1016/J.CONBUILDMAT.2015.05.067.

Torres-Acosta, A. A., Navarro-Gutierrez, S. and Terán-Guillén, J. (2007) 'Residual flexure capacity of corroded reinforced concrete beams', *Engineering Structures*. Elsevier, 29(6), pp. 1145–1152. doi: 10.1016/J.ENGSTRUCT.2006.07.018.

Tuutti, K. (1982) *Corrosion of steel in concrete*. Swedish Cement and Concrete Research Institute, Stockholm. Available at: https://portal.research.lu.se/portal/en/publications/corrosion-of-steel-in-concrete(e97795b5-7f3a-4994-8beb-9438f5a51571).html (Accessed: 6 July 2020).

Valikhani, A. *et al.* (2020) 'Experimental evaluation of concrete-to-UHPC bond strength with correlation to surface roughness for repair application', *Construction and Building Materials*. Elsevier, 238, p. 117753. doi: 10.1016/J.CONBUILDMAT.2019.117753.

Vecchio, F. J. and Collins, M. P. (1986) 'MODIFIED COMPRESSION-FIELD THEORY FOR REINFORCED CONCRETE ELEMENTS SUBJECTED TO SHEAR.', *Journal of the American Concrete Institute*, 83(2), pp. 219–231. doi: 10.14359/10416.

Vu, N. S. and Li, B. (2018) 'Seismic Performance of Flexural Reinforced Concrete Columns with Corroded Reinforcement', *ACI Structural Journal*, 115(5), pp. 1253–1266. doi: 10.14359/51702372.

Vu, N. S., Yu, B. and Li, B. (2016) 'Prediction of strength and drift capacity of corroded reinforced concrete columns', *Construction and Building Materials*. Elsevier, 115, pp. 304–318. doi: 10.1016/J.CONBUILDMAT.2016.04.048.

Wang, L. *et al.* (2015) 'Effects of stirrup and inclined bar corrosion on shear behavior of RC beams', *Construction and Building Materials*. Elsevier, 98, pp. 537–546. doi: 10.1016/J.CONBUILDMAT.2015.07.077.

Xia, J., Jin, W. and Li, L. (2011) 'Shear performance of reinforced concrete beams with corroded stirrups in chloride environment', *Corrosion Science*. Pergamon, 53(5), pp. 1794–1805. doi: 10.1016/J.CORSCI.2011.01.058.

Xu, S. L. and Cai, X. H. (2010) *Bond behavior of corroded reinforcing bar and ultra high toughness cementitious composites (UHTCC)*. Available at: https://framcos.org/FraMCoS-7/06-04.pdf (Accessed: 8 July 2019).

Yang, S.-Y. *et al.* (2016) 'Experimental research on hysteretic behaviors of corroded reinforced concrete columns with different maximum amounts of corrosion of rebar', *Construction and Building Materials*. Elsevier, 121, pp. 319–327. doi: 10.1016/J.CONBUILDMAT.2016.06.002.

Yuan, W., Guo, A. and Li, H. (2017) 'Experimental investigation on the cyclic behaviors of

corroded coastal bridge piers with transfer of plastic hinge due to non-uniform corrosion', *Soil Dynamics and Earthquake Engineering*. Elsevier, 102, pp. 112–123. doi: 10.1016/J.SOILDYN.2017.08.019.

Zhang, R., Castel, A. and François, R. (2009) 'The corrosion pattern of reinforcement and its influence on serviceability of reinforced concrete members in chloride environment', *Cement and Concrete Research*. Pergamon, 39(11), pp. 1077–1086. doi: 10.1016/J.CEMCONRES.2009.07.025.

Zhang, W. *et al.* (2012) 'Tensile and fatigue behavior of corroded rebars', *Construction and Building Materials*. Elsevier, 34, pp. 409–417. doi: 10.1016/J.CONBUILDMAT.2012.02.071.

Zhao, Y. *et al.* (2013) 'Bond behaviour of normal/recycled concrete and corroded steel bars', *Construction and Building Materials*. Elsevier, 48, pp. 348–359. doi: 10.1016/J.CONBUILDMAT.2013.06.091.

Zhu, W. *et al.* (2013) 'Effect of corrosion of reinforcement on the mechanical behaviour of highly corroded RC beams', *Engineering Structures*. Elsevier, 56, pp. 544–554. doi: 10.1016/J.ENGSTRUCT.2013.04.017.

Zhu, W. and François, R. (2014) 'Experimental investigation of the relationships between residual cross-section shapes and the ductility of corroded bars', *Construction and Building Materials*, 69(69), pp. 335–345. doi: 10.1016/j.conbuildmat.2014.07.059.

Van Zijl, G. P. A. G. *et al.* (2012) 'Durability of strain-hardening cement-based composites (SHCC)', *Materials and Structures/Materiaux et Constructions*. Springer, 45(10), pp. 1447–1463. doi: 10.1617/s11527-012-9845-y.

5. Tension Stiffening of UHPC Cover of Corroded Reinforcement

5.1 Introduction

As was established in Chapter 4, materials such as UHPC and ECC have exceptional mechanical properties and durability characteristics that make them materials of choice when it comes to repair and rehabilitation. UHPC and ECC, both encompassing high tensile strain capacity compared to other cementitious materials, contribute to the tensile strength and strain resilience of structural members through tension-stiffening—a mechanism considered trivial when dealing with cracked conventional concrete, but significant due to high bond stresses that develop in the case of High Performance Fiber Reinforced Concrete (HPFRC) materials. Several tests have been conducted investigating the tension stiffening behavior of HPFRC materials (Lijina and Jithin, 2018; Hung, Lee and Chan, 2019). In this chapter, the effects of corrosion, crack widths, concrete cover and fiber type (Steel or PVA) on tension stiffening were explored experimentally, whereas the mechanical properties that quantify this effect were determined using inverse analysis with the help of a finite element model.

5.2 Specimen Shape Validation

An initial investigation was carried out in order to study the possibility of the specimen shape affecting the results; thus a comparative evaluation between cylindrical and rectangular shaped specimens in terms of principal stresses was conducted. Finite element models were created using ATENA 3D, and were tested under a simulated tensile test as was done in the actual tests. Details on finite element modeling are included in Section 5.4. Figures 5-1(a) & (b) show the principal stresses of a circular specimen and a square specimen having the same material properties at 90KN load. It is observed from the principal stress diagrams shown, that the circular shaped specimen leads to similar results as the rectangular shaped specimen.

a) Circular Specimen b) rectangle Specimen

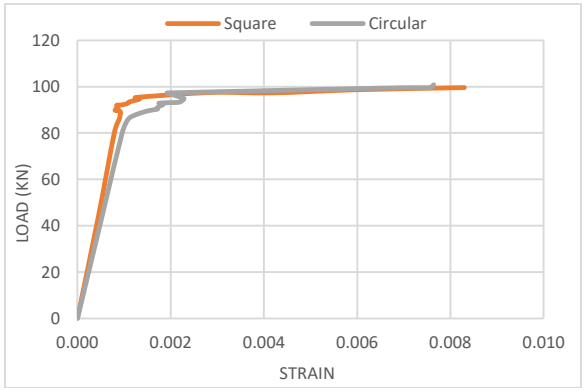

c)

Figure 5-1. (a) and (b) Principal Stress distribution of circular and rectangular specimen shapes. (c) Axial Load-strain Diagram of Rectangular and Circular Shaped Specimens

Figure 5-1(c) displays axial load-strain diagrams of the rectangular and circular models. After a thorough sensitivity analysis, it was found that circular specimens' gauge length should be 50mm in length in order to yield the same load-strain results as rectangular specimens of 100mm gauge length. Strains for circular model were calculated using the relative displacement of two points 50mm apart (+/- 25mm from the centerline) as shown in Figure 5-2(a), and 100mm apart (+/- 50mm from the centerline) for rectangular specimens.

5.3 Test setup and Instrumentation

Figure 5-2(b) shows the tensile test setup adopted while testing. The 600 KN MTS universal testing machine was used for testing, where specimens were loaded in monotonic tension under displacement control at a rate of 0.3 mm/min. Load was measured through the machine's load cell while displacements were measured through digital image correlation (DIC) using the open source software Ncorr (Blaber, Adair and Antoniou, nd). Specimens were prepared by painting the exposed surface with white paint to enhance contrast and speckling over it with black paint. A

sample of a speckled specimen is shown in Figure 5-2(a). Specimens were loaded until reaching 100 KN load as necking would localize outside of the specimen at higher loads. Three bare steel bars, obtained from the same batch as the embedded bars in specimens, were tested in the same universal testing machine. A 50mm extensometer was used to measure strains. The average load-strain data of the three bars was used as a reference point for tension stiffening analysis of specimens.

a) 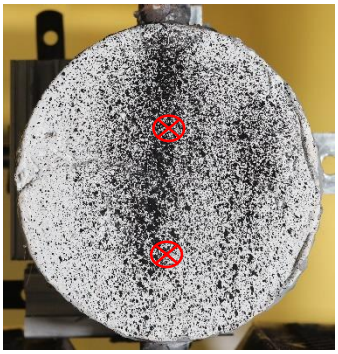 b) 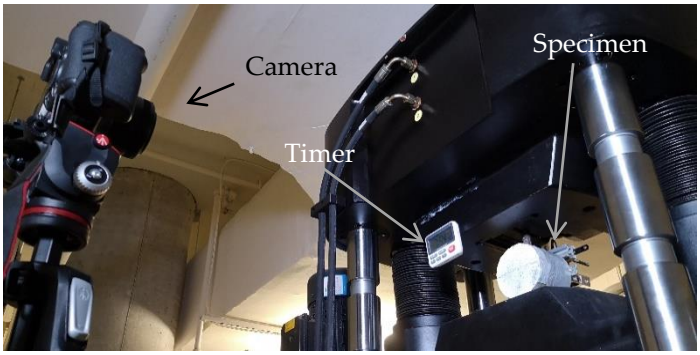

Figure 5-2. a) Sample Speckled Specimen b) Tension Stiffening Test Setup

5.3.1 Digital Image Correlation (DIC)

Displacement monitoring was achieved through digital image correlation using an open source software called Ncorr. Two points (red indicators shown in Figure 5-2(a)) were used as monitoring points in order to calculate strains. Gauge length was 50mm as was found appropriate in the preliminary finite element analysis. Subset radius selection varied between 45 to 60 with spacing between 4 to 8 depending on the image and speckling qualities. The multithread option was incorporated with 2 threads. High strain analysis and subset truncation were utilized in order to take crack formation into consideration. Displacements were then calculated according to true dimensions; strains were calculated with a radius of 5 in order to minimize errors.

5.4 Tension Stiffening Results

5.4.1 Load-Strain Diagrams

Figures 5-3 and 5-4 below show load-strain diagrams of tested specimens. It is noted that specimens having similar variables, mass loss and load-strain behavior were averaged and are represented in a single curve. The averaged specimens are denoted as AVG (UHPC or ECC). The load-strain curve of a bare steel bar was included as benchmark.

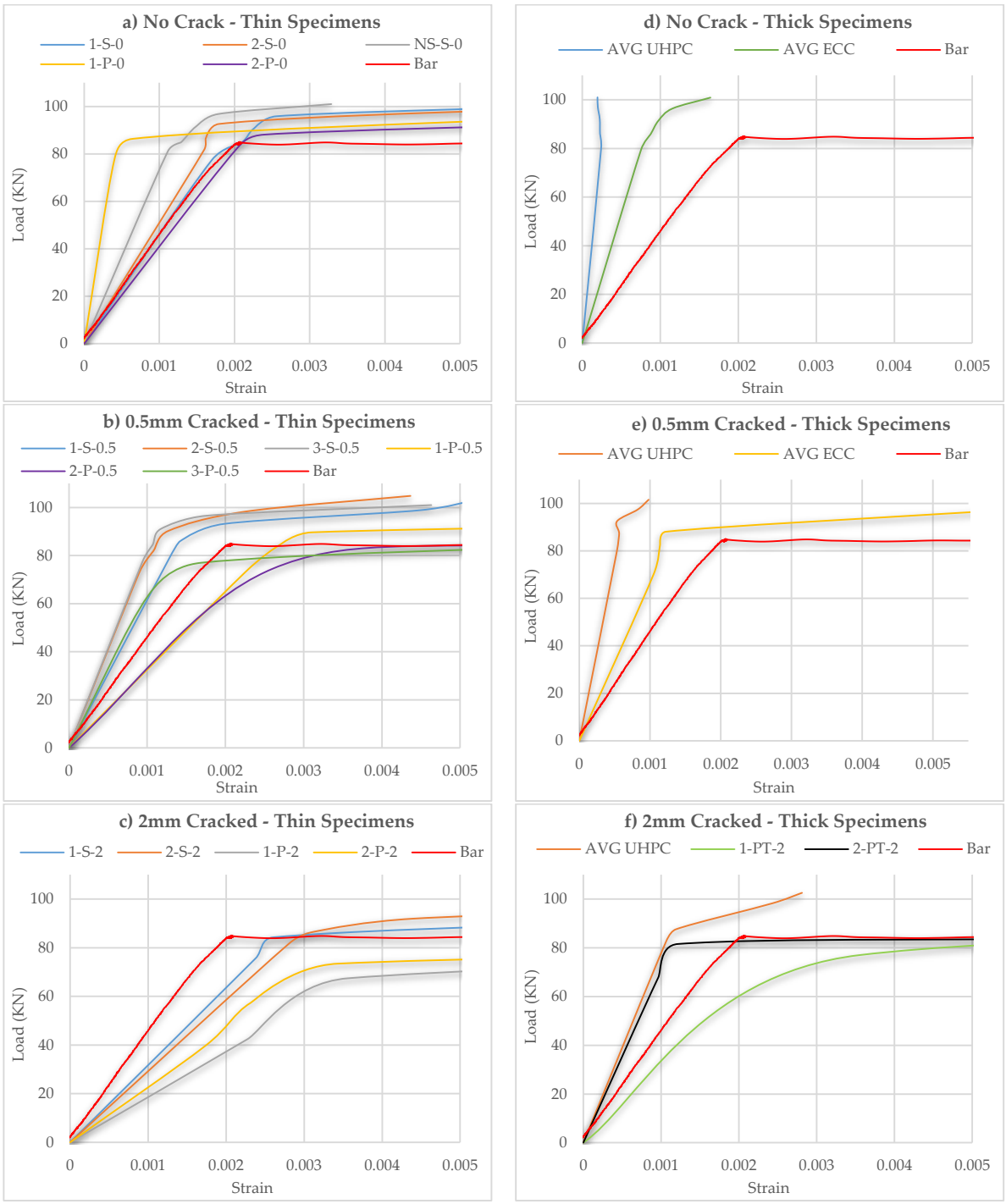

Figure 5-3. Load-Strain Diagrams between strains 0 and 0.005

From Figures 5-3(a) and 5-4(a) (uncracked thin specimens) it is observed that both sets of specimens developed tension stiffening response as they were able to undergo high tensile loads while maintaining relatively small axial strains. UHPC specimens developed smaller strains relative to otherwise identical ECC specimens, although 1-P-0 showed a higher stiffness which surpassed that of the corresponding UHPC specimens. Specimens 1-P-0 and 2-P-0 had two different corrosion percentages (0.1 and 0.5% respectively). The occurrence of corrosion was manifested with a reduction in the stiffness of ECC.

From Figures 5-3(b) and 5-4(b) (0.5mm cracked thin specimens) it is observed that the presence of a 0.5mm crack in UHPC along with corrosion, did not deteriorate its tension-stiffening properties. In fact, an increase in stiffness was observed (see Figure 5-3(b)), a result that could be attributed to the increase in bond strength due to the slight amount of corrosion that had developed (0.5% mass loss). On the contrary, in the presence of a 0.5mm crack together with corrosion (average of 1.2% mass loss), ECC showed a significant reduction in stiffness, and a significant increase in axial strain. Specimens 2-P-0.5 and 3-P-0.5 showed little tension stiffening effect. It is concluded that interaction of bar with the ECC cover had degraded on account of corrosion (1.2% mass loss). Specimen 1-P-0.5 showed a better tension stiffening effect, which is consistent with the previous finding, since this specimen had suffered less damage in terms of mass loss (0.9%).

Figures 5-3(c) and 5-4(c) show load-strain diagrams of the thin specimens with the 2mm crack width. The penetration of corrosion through the 2mm cracks affected drastically the stiffness of all specimens. UHPC however, was able to retain tension stiffening strength beyond yielding.

From Figures 5-3(d) and 5-4(d) it is seen that both UHPC and ECC specimens did not reach the bar's yielding strain ($\varepsilon_y = 0.002$) at 100 KN in tension. UHPC specimens, developed 12% of the bare bar's strain while the ECC specimens reached 38% of the bare bar's axial strain. It should be noted that two out of three thick UHPC specimens showed negative strains; this at first may seem peculiar, however, the reason is explained in the finite element analysis Section 5.4

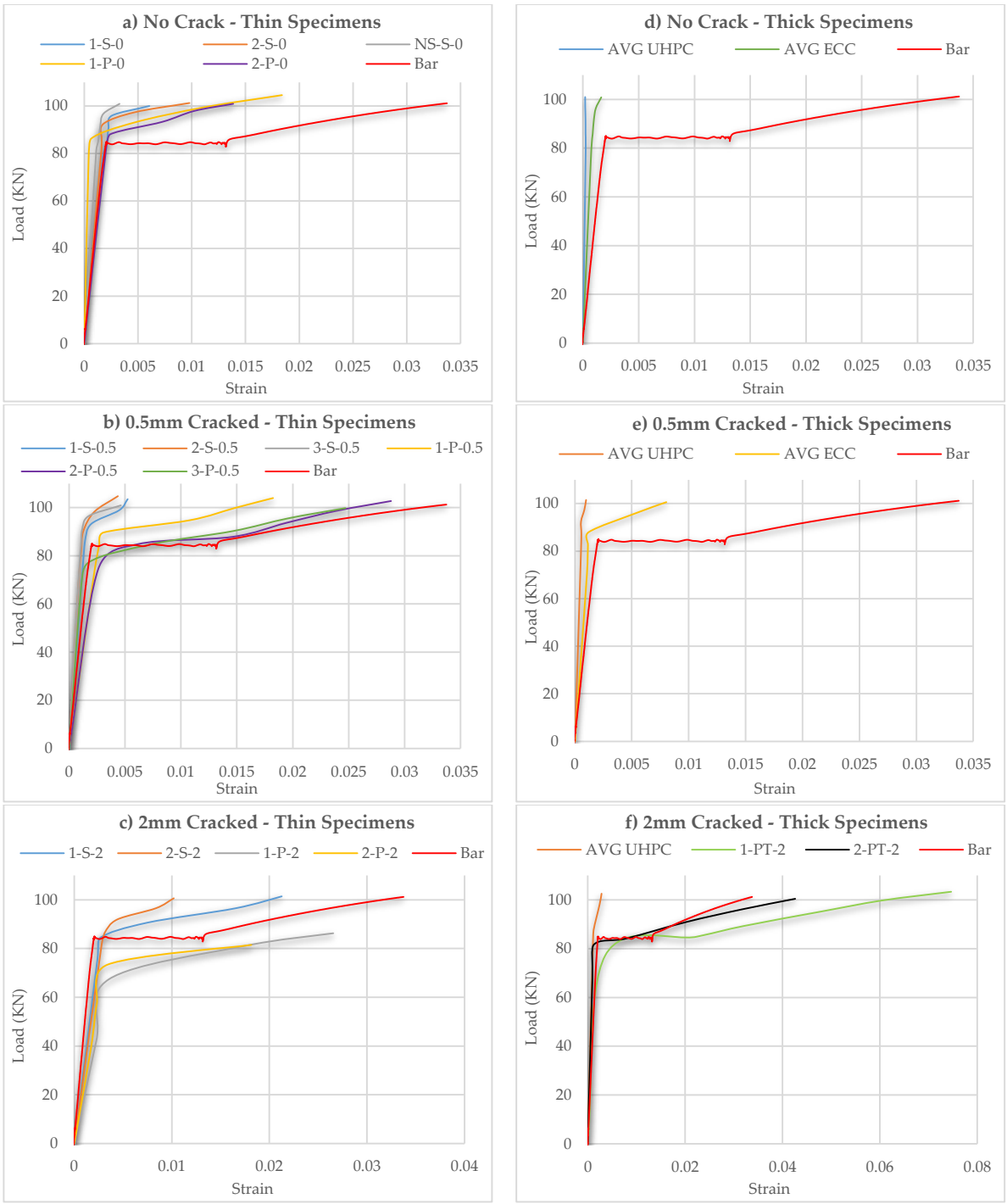

Figure 5-4. Complete Load-Strain Diagrams

Figures 5-3(e) and 5-4(e) show the response of thick specimens having 0.5mm pre-cracks. UHPC showed a very stiff response and developed very small strains (the strain at 100KN was 3% of the bar's strain). ECC specimens also showed a stiff elastic response, however, the strain at 100KN was 24% of the bar's strain.

Figures 5-3(f) and 5-4(f) show thick specimens having 2mm pre-cracks. Even though UHPC specimens suffered from a large crack and mass loss of 1.5%, they were still able to provide tension stiffening after the bar yielding point. UHPC specimens also developed a relatively low strain magnitude of 8.5% of the bar's strain at a load of 100KN. ECC specimens 1-PT-2 and 2-PT-2 had undergone different mass loss ratios (4.47% and 3% respectively) thus exhibited different tension stiffening behavior. Specimen 2-PT-2 showed improved tension-stiffening response as compared with 1-PT-2, although neither specimen had any substantial tension stiffening effects.

5.4.2 Tension Stiffening Contribution

Tension stiffening diagrams shown in Figure 5-5 were divided into three categories depending on the crack width. Tension stiffening was calculated by subtracting the load taken by the specimen from the load taken by the bar at specific strain levels. An averaged load-strain curve for specimens was used in the process, in order to reduce data clatter. For example, the representative thin UHPC specimen in Figure 5-5(a) was determined by using the average load-strain relationships of 1-S-0, 2-S-0 and 3-S-0.

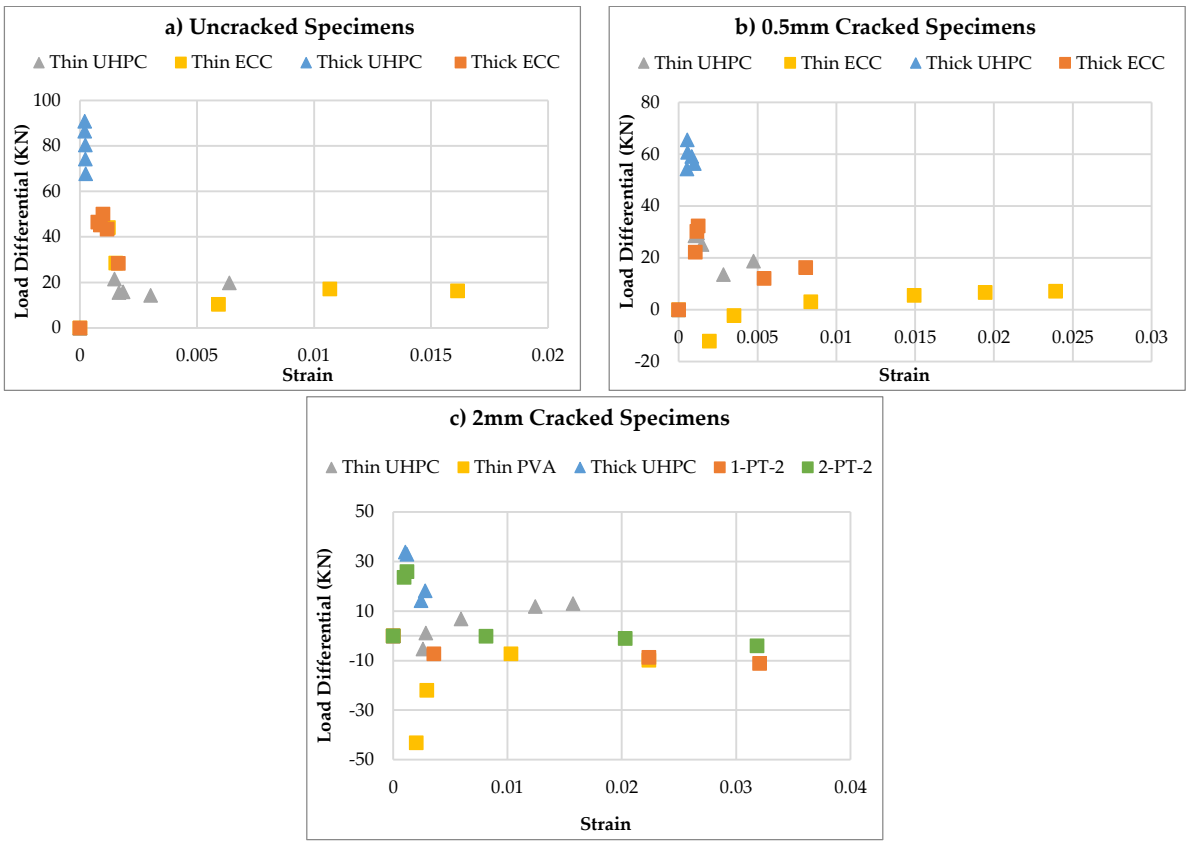

Figure 5-5. Tension-Stiffening Diagrams

UHPC specimens showed a significantly greater tension stiffening capacity as compared to ECC, especially for thick UHPC specimens. From Figure 5-5(a) it could be seen that thick UHPC specimens withstood 90% of the imposed load (90KN). Tensile strength of thick UHPC could be approximately calculated through inverse analysis, assuming the stress distribution is nearly rectangular (uniform), so that the tensile strength is = 90000 / (100*80) = 11.25 MPa. ECC specimens however, showed larger ductility than UHPC specimens, consistent with what has been observed in the literature (Lijina and Jithin, 2018; Hung, Lee and Chan, 2019). Uncracked thick ECC specimens developed 8 times the strain measured in the uncracked thick UHPC specimens. Similarly, uncracked thin ECC specimens developed 2.5 times the strain magnitudes that were recorded in uncracked thin UHPC specimens. Concrete cover thickness had a significant effect on the tension stiffening contribution. It is noted that thick UHPC specimens developed 4.5 times the tension stiffening force magnitude that was sustained by thin UHPC specimens in the uncracked state. Thick uncracked ECC specimens developed 2.5 times the tension stiffening force that was sustained by thin uncracked ECC specimens.

The presence of cracks did not eliminate tension stiffening as would be the case for normal concrete. For 0.5mm cracks (see Figure 5-5(b)), tension stiffening for thick UHPC specimens was lowered by 30% from the reference uncracked value; the reduction was 37% for thick ECC specimens and 58% for thin ECC specimens. However, thin UHPC specimens experienced an increase in the tension stiffening amount by as much as 50%. Clearly, more tests should be conducted to verify this behavior. The amount of tension stiffening developed in thick 0.5mm-cracked UHPC specimens was twice as large as was observed in the companion thick ECC specimens. The tension stiffening contribution of thin UHPC specimens (with 0.5mm cracks) was 4 times larger than that of the companion thin ECC specimens.

5.4.3 Strain Distribution and Crack Patterns

Longitudinal and transverse strains were documented while analyzing the specimens through DIC. Four types of strain distributions were observed, of which a sample of each type is shown in Figure 5-6. Strain and crack patterns depended on the concrete cover, fiber type and crack width. Specimen crack patterns are shown in Table 5. It should be noted that crack pattern 0 indicates no cracks were formed, crack pattern 1, 2 and 3 are shown in Figure 5-6 and 3* signifies that the crack

developed initially by widening the existing crack and then was localized in a different region as shown in Figure 5-6.

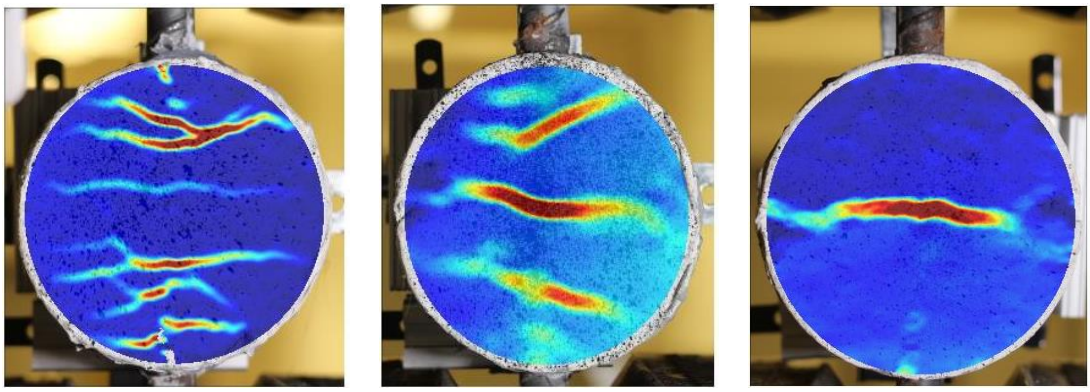

a) Crack Pattern 1 b) Crack Pattern 2 c) Crack Pattern 3

Figure 5-6. Strain Distribution Profile-Crack Pattern

It was observed that uncracked thin specimens, both UHPC and ECC, developed multiple cracks, though none localized in the center (along the diameter). Thick uncracked specimens however, with the exception of 1-PT-0, did not form any cracks. Certain specimens having 0.5mm initial crack width were able to develop multiple transverse cracks as can be seen in Figure 5-6(b) representative of Specimen 3-S-0.5 at 100KN tensile load. The rest of the specimens tended to localize and widen the pre-crack. Even though specimens had similar crack patterns, crack widths and longitudinal strains were not in the same order of magnitude. UHPC specimens developed smaller strains and crack widths, especially in the case of specimens having a 2mm pre-crack where ECC specimens ended up with full discontinuity after splitting of the specimen.

An interesting mechanism was observed while testing specimen 1-ST-0.5 where crack widening was initially localized at the pre-crack as can be seen in Figure 5-7(a). However, at higher loads the crack stopped widening (Figure 5-7(b)) and another crack localized at a different location, as may be seen in Figure 5-7(c).

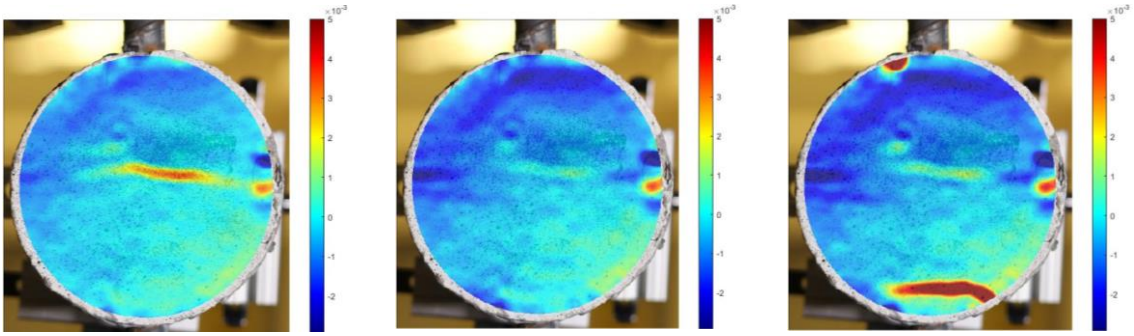

Tensile Load: 85 KN Tensile Load: 95.2 KN Tensile Load: 99.7 KN

Figure 5-7. Axial Strain Profile of 1-ST-0.5 at three Incremental Load steps.

5.5 Finite Element Modeling

To better understand the tension-stiffening behavior, cracking pattern and interface properties (bond properties) of UHPC, finite element analysis was implemented using ATENA 3D software (Cervenka Consulting, 2007). Two models were analyzed, one representing a thin UHPC specimen and another representing a thick UHPC specimen.

5.5.1 Macro-Elements and Material Properties

Taking advantage of symmetry, a quarter of specimens were modeled in order to reduce computational time. Bars were modeled as a 3D macro-element and were assigned '3D Bilinear Steel Von Mises' material. Material properties of the modeled bar were validated with the behavior of the real steel bar as seen in Figure 5-8. Elastic modulus assigned was E_s = 220000 MPa, yield strength f_y= 450 MPa and Hardening Modulus H = 3500 MPa.

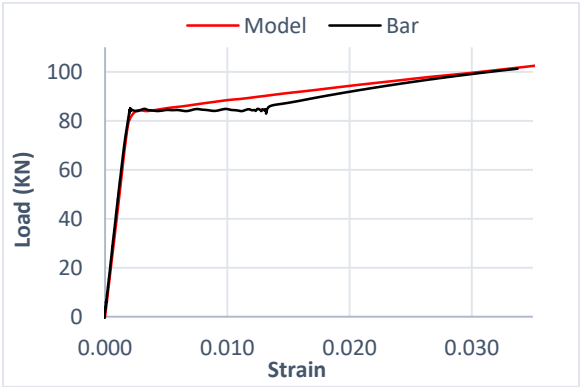

Figure 5-8. Load-Strain Diagram of Modeled Bar and Tested Bar

UHPC was modeled as a cylindrical macro-element using the '3D Nonlinear Cementitious 2 User' material. Tensile strength given was $f_t = 13$ MPa, whereas the tensile stress-strain model of UHPC is shown in Figure 5-9.

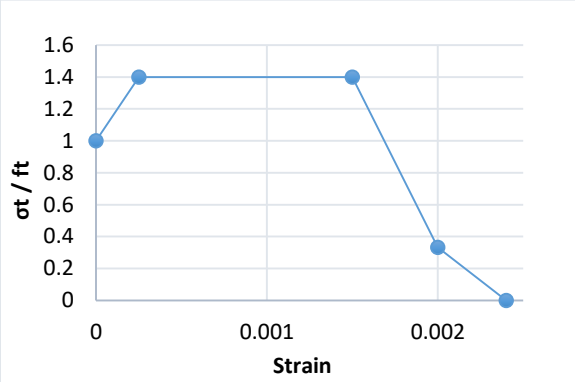

Figure 5-9. UHPC Tensile Constitutive Model

Support conditions were imposed on appropriate surfaces, while loading was applied through prescribed incremental deformations of 0.2 mm per step. A sensitivity analysis was carried out for mesh generation, resulting in a 25 mm tetrahedral mesh with an 8mm refinement on contact surfaces between reinforcement and UHPC. Interface property was assigned on all shared surfaces between UHPC and the bar. It was found that UHPC had a very high bond strength and could be considered to be in perfect connection with the bar for the purposes of modeling. Values assigned to the interface properties are as follows; Normal stiffness K_{nn} = 2 E7 MPa, Tangential stiffness K_{tt} = 2 E8 MPa, Tensile Strength normal to the interface f_t = 3 MPa, Cohesion 20 MPa, Frictional Coefficient = 1. The Cohesion softening function is shown in Figure 5-10.

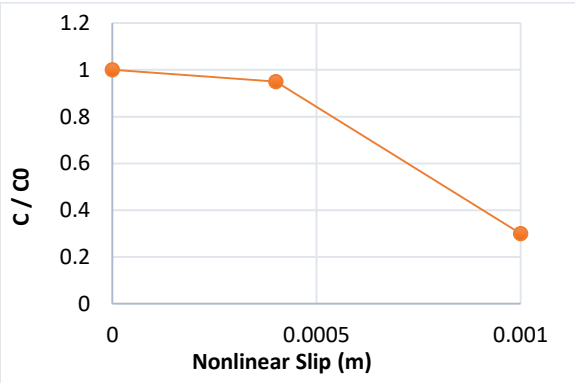

Figure 5-10. Interface Material Cohesion Function

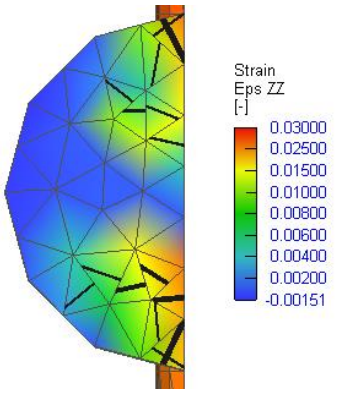

a) Thin UHPC Model

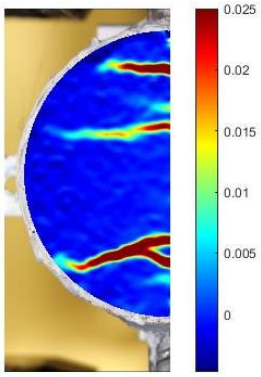

b) Specimen 2-S-0

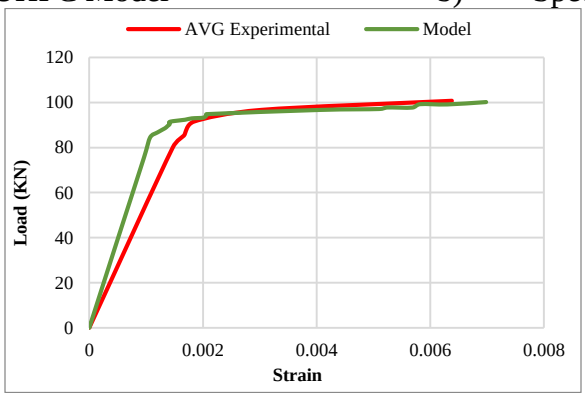

c) Load-Strain Diagrams of Model and Average of Experimental Tests

Figure 5-11. Strain Distribution, Crack Distribution and Load-Strain Diagram Correlation Between Model and Tested Specimen

Figure 5-11(a) and (b) compare the strain distribution of the model and of Specimen 2-S-0. It is observed that the model approximated well the behavior of the specimen in terms of strain and crack pattern. Figure 5-11(c) plots the load-strain diagrams of the model as well as the average of tested experiments. It is noted that the model presented a stiffer response but its overall behavior was similar to that of the tested specimens.

An uncracked thick UHPC model was also simulated under the tension test, as depicted in Figure 5-12. The schematic shows the estimated strain and crack distribution at a load of 100KN. It was observed that although UHPC at the concrete-bar interface experiences tensile stresses, due to the crack formations at the ends of the specimen, concrete at the surface experiences compressive strains. It was also observed that cracks had formed and progressed from the bar's surface towards the concrete's surface, however, they did not reach the free surface of the specimen, which explains why thick specimens did not form any cracks.

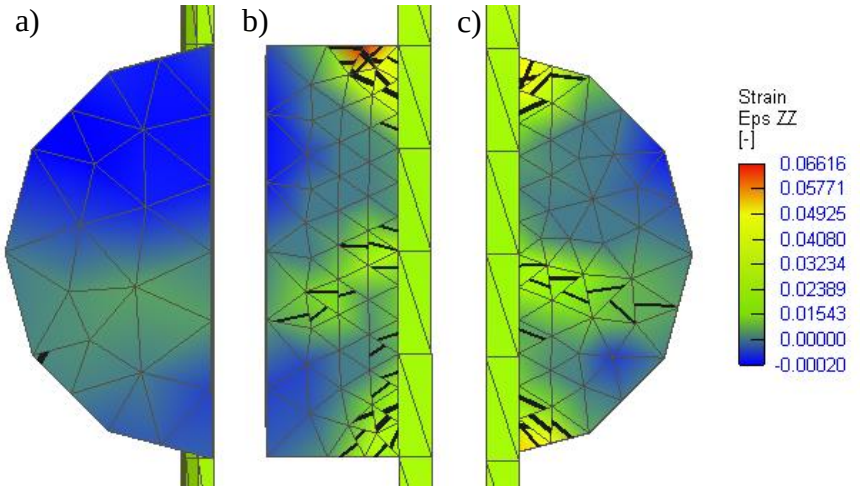

Figure 5-12. Strain and Crack Distribution of a Sample Thick UHPC Specimen. a) Front View b) Side view c) Back view

5.6 Conclusions

Two groups of bar specimens embedded in concrete discs through a centroidal diametric axis were tested in tension to establish the tension stiffening behavior of the cover. The first group was fabricated using aUHPC material for concrete cover, whereas the second comprised an ECC matrix. Prior to testing in tension, the specimens had been subjected to accelerated corrosion through application of a fixed potential; this phase of the test which was meant to illustrate the reduction of the corrosion rate in bars embedded in UHPC was presented in Chapter 4. This chapter summarizes the mechanical tests that followed after the completion of the corrosion process. The bars were pulled in direct tension, and the objective was to to study the tension-stiffening behavior of cracked and un-cracked UHPC and ECC bar cover in the presence of corrosion. The following conclusions were drawn based on load-strain diagrams of tested specimens:

- Uncracked UHPC and ECC specimens showed significant tension-stiffening properties. Specimens developed minimal surface tensile strains even when loaded up to 100 KN in tension (i.e. a load that exceeds the 83KN yielding force of the bar, and carries in well into the strain hardening range). Strains in UHPC reached 12% of the bar's strain, whereas the ECC strain magnitudes were 38% of the bar's strain.

- Concrete cover thickness had a significant effect on tension-stiffening capacity of the specimens. Doubling the concrete cover in the absence of cracks increased tension stiffening amount by four times for UHPC specimens and twice for ECC specimens.
- ECC showed a more ductile behavior than UHPC; However, the latter showed greater tension-stiffening capacity due to its superior tensile strength.
- The presence of pre-existing 0.5mm wide cracks had a more unfavorable effect on ECC specimens as compared to the UHPC specimens.
- All pre cracked specimens with a 2mm-wide crack, with the exception of thick UHPC specimens, lost all tension stiffening contribution. It is recommended to neglect tension stiffening strength in the presence of significant crack widths in assessment calculations.
- UHPC was able to stabilize the pre-existing crack width progression and to form multiple cracks in different locations.
- A UHPC tensile constitutive model and commensurate interface material properties were used in this work and were validated through comparison with the experimental evidence.

5.7 References

ACI-374 (2016) *ACI 374 - Guide to Nonlinear Modeling Parameters for Earthquake-Resistant Structures*. Available at: www.concrete.org (Accessed: 27 March 2022).

ACI 222R-19 (2019) 'Guide to Protection of Reinforcing Steel in Concrete Against Corrosion', *American Concrete Institute*, pp. 1–65.

Al-Saidy, A. H. *et al.* (2016) 'Structural behavior of corroded RC beams with/without stirrups repaired with CFRP sheets', *Materials and Structures*. Springer Netherlands, 49(9), pp. 3733–3747. doi: 10.1617/s11527-015-0751-y.

Al-Sulaimani, G. J. *et al.* (1990) 'Influence of corrosion and cracking on bond behavior and strength of reinforced concrete members', *ACI Structural Journal*, 87(2), pp. 220–231. doi: 10.14359/2732.

Alaskar, A. (2013) 'Shear Behaviour of Slender RC Beams with Corroded Web Reinforcement'. University of Waterloo. Available at: https://uwspace.uwaterloo.ca/handle/10012/7472 (Accessed: 15 July 2019).

Allamt, I. M. *et al.* (1994) *Influence of atmospheric corrosion on the mechanical properties of*

reinforcing steel, *Construction and Building Materials*.

Almusallam, A. A. *et al.* (1996) 'Effect of reinforcement corrosion on bond strength', *Construction and Building Materials*. Elsevier, 10(2), pp. 123–129. doi: 10.1016/0950-0618(95)00077-1.

Almusallam, A. A. (2001a) 'Effect of degree of corrosion on the properties of reinforcing steel bars', *Construction and Building Materials*. Elsevier, 15(8), pp. 361–368. doi: 10.1016/S0950-0618(01)00009-5.

Almusallam, A. A. (2001b) 'Effect of degree of corrosion on the properties of reinforcing steel bars', *Construction and Building Materials*. Elsevier, 15(8), pp. 361–368. doi: 10.1016/S0950-0618(01)00009-5.

Alonso, C. *et al.* (1998) 'Factors controlling cracking of concrete affected by reinforcement corrosion', *Materials and Structures*. Kluwer Academic Publishers, 31(7), pp. 435–441. doi: 10.1007/BF02480466.

American Road & Transportation Builders Association (2020) *ARTBA Bridge Report*. Available at: https://artbabridgereport.org/ (Accessed: 6 July 2020).

Amleh, L., Mirza, M. and Ahwazi, B. (2000) 'Bond deterioration of reinforcing steel in concrete due to corrosion'. Available at: https://books.google.com/books?hl=en&lr=&id=F8HosZdH8BUC&oi=fnd&pg=PA247&ots=Iq_HHO_T-s&sig=3ytv3HtTEhxTvU9yTJRyH6PPLrk (Accessed: 5 July 2019).

Andrade, C., Alonso, M. C. and Gonzalez, J. A. (1990) 'Initial effort to use the corrosion rate measurements for estimating rebar durability', *ASTM Special Technical Publication*. ASTM International, (1065), pp. 29–37. doi: 10.1520/stp25013s.

Andrade, C. and González, J. A. (1978) 'Quantitative measurements of corrosion rate of reinforcing steels embedded in concrete using polarization resistance measurements', *Materials and Corrosion*, 29(8), pp. 515–519. doi: 10.1002/maco.19780290804.

Apostolopoulos, C. A. (2007) 'Mechanical behavior of corroded reinforcing steel bars S500s tempcore under low cycle fatigue', *Construction and Building Materials*. Elsevier, 21(7), pp. 1447–1456. doi: 10.1016/J.CONBUILDMAT.2006.07.008.

Apostolopoulos, C. A. and Papadakis, V. G. (2008) ‘Consequences of steel corrosion on the ductility properties of reinforcement bar’, *Construction and Building Materials*. Elsevier, 22(12), pp. 2316–2324. doi: 10.1016/J.CONBUILDMAT.2007.10.006.

Apostolopoulos, C., Drakakaki, A. and Basdeki, M. (2019) ‘Seismic assessment of RC column under seismic loads’, *International Journal of Structural Integrity*. Emerald Publishing Limited , 10(1), pp. 41–54. doi: 10.1108/IJSI-02-2018-0013.

ASCE 41 (2017) *Seismic Evaluation and Retrofit of Existing Buildings*, *Seismic Evaluation and Retrofit of Existing Buildings*. American Society of Civil Engineers. doi: 10.1061/9780784414859.

Azad, A. K., Ahmad, S. and Al-Gohi, B. H. A. (2010) ‘Flexural strength of corroded reinforced concrete beams’, *Magazine of Concrete Research*. Thomas Telford Ltd , 62(6), pp. 405–414. doi: 10.1680/macr.2010.62.6.405.

Berra, M., Castellani, A. and Coronelli, D. (1997) ‘Bond in reinforced concrete and corrosion of bars’, in *Structural Faults and Repair*. Edinburgh, UK, pp. 349–357.

Berrocal, C. G. *et al.* (2017) ‘Corrosion-induced cracking and bond behaviour of corroded reinforcement bars in SFRC’, *Composites Part B: Engineering*. Elsevier, 113, pp. 123–137. doi: 10.1016/J.COMPOSITESB.2017.01.020.

Blaber, J., Adair, & B. and Antoniou, & A. (no date) ‘Ncorr: Open-Source 2D Digital Image Correlation Matlab Software’. doi: 10.1007/s11340-015-0009-1.

Cairns, J., Du, Y. and Law, D. (2008) ‘Structural performance of corrosion-damaged concrete beams’, *Magazine of Concrete Research*. Thomas Telford Ltd , 60(5), pp. 359–370. doi: 10.1680/macr.2007.00102.

Di Carlo, F., Meda, A. and Rinaldi, Z. (2017) ‘Numerical cyclic behaviour of un-corroded and corroded RC columns reinforced with HPFRC jacket’, *Composite Structures*. Elsevier, 163, pp. 432–443. doi: 10.1016/J.COMPSTRUCT.2016.12.038.

Castel, A., François, R. and Arliguie, G. (2000) ‘Mechanical behaviour of corroded reinforced concrete beams—Part 1: Experimental study of corroded beams’, *Materials and Structures*. Kluwer Academic Publishers, 33(9), pp. 539–544. doi: 10.1007/BF02480533.

CEN (2005) *EN 1998 - 3 Eurocode 8-Design of structures for earthquake resistance-Part 3: Assessment and retrofitting of buildings*.

Cervenka Consulting (2007) 'ATENA Program Documentation'. Prague, Czech Republic.

Civjan, S. A. *et al.* (2005) 'Effectiveness of corrosion inhibiting admixture combinations in structural concrete', *Cement and Concrete Composites*. Elsevier, 27(6), pp. 688–703. doi: 10.1016/J.CEMCONCOMP.2004.07.007.

Coronelli, D. and Gambarova, P. (2004) 'Structural Assessment of Corroded Reinforced Concrete Beams: Modeling Guidelines', *Journal of Structural Engineering*. American Society of Civil Engineers, 130(8), pp. 1214–1224. doi: 10.1061/(ASCE)0733-9445(2004)130:8(1214).

Coronelli, D., Hanjari, K. Z. and Lundgren, K. (2013) 'Severely Corroded RC with Cover Cracking', *Journal of Structural Engineering*, 139(2), pp. 221–232. doi: 10.1061/(ASCE)ST.1943-541X.0000633.

Dang, V. H. and François, R. (2013) 'Influence of long-term corrosion in chloride environment on mechanical behaviour of RC beam', *Engineering Structures*. Elsevier, 48, pp. 558–568. doi: 10.1016/j.engstruct.2012.09.021.

Darwin, D. and Pecknold, D. (1974) *INELASTIC MODEL FOR CYCLIC BIAXIAL LOADING OF REINFORCED CONCRETE*. Illinois, Urbana. Available at: https://www.semanticscholar.org/paper/INELASTIC-MODEL-FOR-CYCLIC-BIAXIAL-LOADING-OF-Darwin-Pecknold/5d1fb39809798f4c65b2dfa0fad5c06dd82e2a6f (Accessed: 20 July 2022).

Du, Y., Clark, L. A. and Chan, A. H. C. (2007) 'Impact of Reinforcement Corrosion on Ductile Behavior of Reinforced Concrete Beams', *ACI Structural Journal*, 104(3), pp. 285–293. doi: 10.14359/18618.

Du, Y. G., Clark, L. A. and Chan, A. H. C. (2005) 'Residual capacity of corroded reinforcing bars', *Magazine of Concrete Research*. Thomas Telford Ltd , 57(3), pp. 135–147. doi: 10.1680/macr.2005.57.3.135.

El-Joukhadar, N., Tsiotsias, K. and Pantazopoulou, S. (2019) 'Consideration of the state of corrosion in seismic assessment of columns', *International Journal of Structural Integrity*. Emerald Group Publishing Ltd. doi: 10.1108/IJSI-07-2019-0065.

Fakhri, H., Ragalwar, K. A. and Ranade, R. (2019) 'On the use of Strain-Hardening Cementitious Composite covers to mitigate corrosion in reinforced concrete structures', *Construction and Building Materials*. Elsevier Ltd, 224, pp. 850–862. doi: 10.1016/j.conbuildmat.2019.07.052.

Fang, C. *et al.* (2004) 'Corrosion influence on bond in reinforced concrete', *Cement and Concrete Research*. Pergamon, 34(11), pp. 2159–2167. doi: 10.1016/J.CEMCONRES.2004.04.006.

Farhan, N. A., Sheikh, M. N. and Hadi, M. N. S. (2018) 'Experimental Investigation on the Effect of Corrosion on the Bond Between Reinforcing Steel Bars and Fibre Reinforced Geopolymer Concrete', *Structures*. Elsevier, 14, pp. 251–261. doi: 10.1016/J.ISTRUC.2018.03.013.

Fernandez, I. *et al.* (2018) 'Ultimate Capacity of Corroded Statically Indeterminate Reinforced Concrete Members', *International Journal of Concrete Structures and Materials*. Springer Singapore, 12(1), p. 75. doi: 10.1186/s40069-018-0297-9.

Fernandez, I., Bairán, J. M. and Marí, A. R. (2015) 'Corrosion effects on the mechanical properties of reinforcing steel bars. Fatigue and σ–ε behavior', *Construction and Building Materials*. Elsevier, 101, pp. 772–783. doi: 10.1016/J.CONBUILDMAT.2015.10.139.

Fernandez, I. and Berrocal, C. G. (2019) 'Mechanical Properties of 30 Year-Old Naturally Corroded Steel Reinforcing Bars', *International Journal of Concrete Structures and Materials*. Korea Concrete Institute, 13(1), p. 9. doi: 10.1186/s40069-018-0308-x.

Fernandez, I., Lundgren, K. and Zandi, K. (2018) 'Evaluation of corrosion level of naturally corroded bars using different cleaning methods, computed tomography, and 3D optical scanning', *Materials and Structures/Materiaux et Constructions*. Springer Netherlands, 51(3), pp. 1–13. doi: 10.1617/s11527-018-1206-z.

fib-Model Code (2020) 'Model Code 2020, Draft version MC2020', in. fib.

fib bulletin #10 (2000) *Bond of reinforcement in concrete : state-of-art report*. International Federation for Structural Concrete. Available at: https://www.fib-international.org/publications/fib-bulletins/bond-of-reinforcement-in-concrete-pdf-detail.html (Accessed: 3 July 2019).

fib Model Code (2010) *Fib model code for concrete structures 2010*.

Fischer, C., Ozbolt, J. and Gehlen, C. (2010) 'Numerical investigation on bond behavior of corroded reinforcement', in *7th International Conference on Fracture Mechanics of Concrete and Concrete Structures*. Jeju, Korea, pp. 779–785.

François, R. and Arliguie, G. (1998) 'Influence of Service Cracking on Reinforcement Steel Corrosion', *Journal of Materials in Civil Engineering*, 10(1), pp. 14–20. doi: 10.1061/(ASCE)0899-1561(1998)10:1(14).

François, R., Khan, I. and Dang, V. H. (2013) 'Impact of corrosion on mechanical properties of steel embedded in 27-year-old corroded reinforced concrete beams', *Materials and Structures*. Springer Netherlands, 46(6), pp. 899–910. doi: 10.1617/s11527-012-9941-z.

Fu, C. *et al.* (2017) 'Corrosion characteristics of a 4-year naturally corroded reinforced concrete beam with load-induced transverse cracks', *Corrosion Science*. Pergamon, 117, pp. 11–23. doi: 10.1016/J.CORSCI.2017.01.002.

Ganesh, P. and Ramachandra Murthy, A. (2020) 'Simulation of surface preparations to predict the bond behaviour between normal strength concrete and ultra-high performance concrete', *Construction and Building Materials*. Elsevier, 250, p. 118871. doi: 10.1016/J.CONBUILDMAT.2020.118871.

Gjørv, O. E. (2014) *Durability Design of Concrete Structures in Severe Environments*. CRC Press. doi: 10.1201/b16469.

Goksu, C. and Ilki, A. (2016) 'Seismic Behavior of Reinforced Concrete Columns with Corroded Deformed Reinforcing Bars', *ACI Structural Journal*, 113(5), pp. 1053–1064. doi: 10.14359/51689030.

Haddad, R. H. and Ashteyate, A. M. (2001) 'Role of synthetic fibers in delaying steel corrosion cracks and improving bond with concrete', *Canadian Journal of Civil Engineering*. NRC Research Press Ottawa, Canada , 28(5), pp. 787–793. doi: 10.1139/l01-037.

Hanjari, K. Z., Coronelli, D. and Lundgren, K. (2011) 'Bond capacity of severely corroded bars with corroded stirrups', *Magazine of Concrete Research*. Thomas Telford Ltd , 63(12), pp. 953–968. doi: 10.1680/macr.10.00200.

Harajli, M. H. (2004) ‘Comparison of Bond Strength of Steel Bars in Normal- and High-Strength Concrete’, *Journal of Materials in Civil Engineering*, 16(4), pp. 365–374. doi: 10.1061/(ASCE)0899-1561(2004)16:4(365).

Higgins, C. and Farrow, W. C. (2006) ‘Tests of Reinforced Concrete Beams with Corrosion-Damaged Stirrups’, *ACI Structural Journal*, 103(1), pp. 133–141. doi: 10.14359/15094.

Hou, L. *et al.* (2017) ‘Effect of corrosion on bond behaviors of rebar embedded in ultra-high toughness cementitious composite’, *Construction and Building Materials*. Elsevier, 138, pp. 141–150. doi: 10.1016/J.CONBUILDMAT.2017.02.008.

Hung, C. C., Lee, H. S. and Chan, S. N. (2019) ‘Tension-stiffening effect in steel-reinforced UHPC composites: Constitutive model and effects of steel fibers, loading patterns, and rebar sizes’, *Composites Part B: Engineering*. Elsevier Ltd, 158, pp. 269–278. doi: 10.1016/j.compositesb.2018.09.091.

Ioannou, A. *et al.* (2022) ‘Experimental Testing of ECC Jackets for Repair of Pre-Damaged R . C . Members Experimental Testing of ECC Jackets for Repair of Pre-Damaged R . C . Members under Cyclic Loading’, in *12th National Conference on Earthquake Engineering*. Salt Lake City, Utah: Earthquake Engineering Research Institute, pp. 1–5.

Kashani, M. M., Maddocks, J. and Dizaj, E. A. (2019) ‘Residual Capacity of Corroded Reinforced Concrete Bridge Components: State-of-the-Art Review’, *Journal of Bridge Engineering*, 24(7), p. 03119001. doi: 10.1061/(ASCE)BE.1943-5592.0001429.

Kondratova, I. L., Montes, P. and Bremner, T. W. (2000) ‘Accelerated Corrosion Testing Results for Specimens Containing Uncoated Reinforcing Steel and Corrosion Inhibitors’, *Special Publication*, 192, pp. 789–806. doi: 10.14359/5785.

Koulouris, K. and Apostolopoulos, C. (2020) ‘An Experimental Study on Effects of Corrosion and Stirrups Spacing on Bond Behavior of Reinforced Concrete’, *Metals*. MDPI AG, 10(10), p. 1327. doi: 10.3390/met10101327.

Blaber, J., Adair, & B. and Antoniou, & A. (no date) ‘Ncorr: Open-Source 2D Digital Image Correlation Matlab Software’. doi: 10.1007/s11340-015-0009-1.

Lee, H. S. and Cho, Y. S. (2009) 'Evaluation of the mechanical properties of steel reinforcement embedded in concrete specimen as a function of the degree of reinforcement corrosion', in *International Journal of Fracture*. Springer, pp. 81–88. doi: 10.1007/s10704-009-9334-7.

Li, D. *et al.* (2018) 'Influence of Non-uniform corrosion of steel bars on the seismic behavior of reinforced concrete columns', *Construction and Building Materials*. Elsevier, 167, pp. 20–32. doi: 10.1016/J.CONBUILDMAT.2018.01.149.

Li, J., Gong, J. and Wang, L. (2009) 'Seismic behavior of corrosion-damaged reinforced concrete columns strengthened using combined carbon fiber-reinforced polymer and steel jacket', *Construction and Building Materials*. Elsevier, 23(7), pp. 2653–2663. doi: 10.1016/J.CONBUILDMAT.2009.01.003.

Li, X. *et al.* (2016) 'Effect of loading rate on the bond behaviour of deformed steel bars in concrete subjected to lateral pressure', *Materials and Structures*. Springer Netherlands, 49(6), pp. 2097–2111. doi: 10.1617/s11527-015-0636-0.

Lijina, T. and Jithin, J. . (2018) 'Effect of Steel and Polypropylene Fibre on the Tension Stiffening of Ultra High Performance Concrete', *International Journal of Engineering and Advanced Technology (IJEAT)*, 8(4C).

Lin, H. *et al.* (2019) 'State-of-the-art review on the bond properties of corroded reinforcing steel bar', *Construction and Building Materials*. Elsevier, 213, pp. 216–233. doi: 10.1016/J.CONBUILDMAT.2019.04.077.

Liu, X. and Li, Y. (2018) 'Experimental study of seismic behavior of partially corrosion-damaged reinforced concrete columns strengthened with FRP composites with large deformability', *Construction and Building Materials*. Elsevier, 191, pp. 1071–1081. doi: 10.1016/J.CONBUILDMAT.2018.10.072.

Lu, C. *et al.* (2016) 'Mechanical properties of corroded steel bars in pre-cracked concrete suffering from chloride attack', *Construction and Building Materials*, 123(123), pp. 649–660. doi: 10.1016/j.conbuildmat.2016.07.032.

Ma, Y., Che, Y. and Gong, J. (2012) 'Behavior of corrosion damaged circular reinforced concrete columns under cyclic loading', *Construction and Building Materials*. Elsevier, 29, pp. 548–556. doi: 10.1016/J.CONBUILDMAT.2011.11.002.

El Maaddawy, T. A. and Soudki, K. A. (2003) ‘Effectiveness of Impressed Current Technique to Simulate Corrosion of Steel Reinforcement in Concrete’, *Journal of Materials in Civil Engineering*, 15(1), pp. 41–47. doi: 10.1061/(ASCE)0899-1561(2003)15:1(41).

Mangat, P. S. and Elgarf, M. S. (1999) ‘Bond characteristics of corrding reinforcement in concrete beams’, *Materials and Structures*. Kluwer Academic Publishers, 32(2), pp. 89–97. doi: 10.1007/BF02479434.

Mangat, Pritpal S. and Elgarf, M. S. (1999) ‘Flexural Strength of Concrete Beams with Corroding Reinforcement’, *ACI Structural Journal*, 96(1), pp. 149–158. doi: 10.14359/606.

Martín Pérez, B. M. (1999) *Service life modelling of R.C. highway structures exposed to chlorides*. University of Toronto. Available at: https://books.google.ca/books/about/Service_Life_Modelling_of_R_C_Highway_St.html?id=qQiGtgAACAAJ&redir_esc=y (Accessed: 14 February 2019).

Meda, A. *et al.* (2014) ‘Experimental evaluation of the corrosion influence on the cyclic behaviour of RC columns’, *Engineering Structures*. Elsevier, 76, pp. 112–123. doi: 10.1016/J.ENGSTRUCT.2014.06.043.

Mehta, P. K. (1991) ‘Durability of Concrete--Fifty Years of Progress?’, *Special Publication*, 126, pp. 1–32. doi: 10.14359/1998.

Menengotto, M. and Pinto, P. E. (1973) ‘Method o f Analysis for Cyclically Loaded Reinforced Concrete Plane Frames Including Changes in Geometry and Nonelastic Behavior of Elements under Combined Normal Force and Bending’, in *IABSE Symposium on Resistance and Ultimate Deformability of Structures Acted on*. Lisbon.

Molaioni, F., Carlo, F. Di and Rinaldi, Z. (2021) ‘Modelling Strategies for the Numerical Simulation of the Behaviour of Corroded RC Columns under Cyclic Loads’, *Applied Sciences 2021, Vol. 11, Page 9761*. Multidisciplinary Digital Publishing Institute, 11(20), p. 9761. doi: 10.3390/APP11209761.

Ou, Y.-C. and Chen, H.-H. (2014) ‘Cyclic Behavior of Reinforced Concrete Beams with Corroded Transverse Steel Reinforcement’, *Journal of Structural Engineering*, 140(9), p. 04014050. doi: 10.1061/(ASCE)ST.1943-541X.0000932.

Palsson, R. and Mirza, M. S. (2002a) ‘Mechanical response of corroded steel reinforcement of

abandoned concrete bridge', *ACI Structural Journal*, 99(2), pp. 157–162. doi: 10.14359/11538.

Palsson, R. and Mirza, M. S. (2002b) 'Mechanical Response of Corroded Steel Reinforcement of Abandoned Concrete Bridge', *ACI Structural Journal*, 99(2), pp. 157–162. doi: 10.14359/11538.

Pantazopoulou, S. J. *et al.* (2001) *REPAIR OF CORROSION-DAMAGED COLUMNS WITH FRP WRAPS, JOURNAL OF COMPOSITES FOR CONSTRUCTION*. Available at: http://pubs.asce.org/copyright (Accessed: 23 July 2019).

Pantazopoulou, S. J. *et al.* (2019) 'The performance of corroded lap splices in reinforced concrete beams', *Corrosion Reviews*. De Gruyter, 37(1), pp. 31–44. doi: 10.1515/corrrev-2017-0086.

Papakonstantinou, C. G., Balaguru, P. N. and Auyeung, Y. (2011) 'Influence of FRP confinement on bond behavior of corroded steel reinforcement', *Cement and Concrete Composites*. Elsevier, 33(5), pp. 611–621. doi: 10.1016/J.CEMCONCOMP.2011.02.006.

Pardalopoulos, S. I., Pantazopoulou, S. J. and Lekidis, V. A. (2017) 'Simplified method for rapid seismic assessment of older R.C. buildings'. doi: 10.1016/j.engstruct.2017.10.052.

Pardalopoulos, S. I., Pantazopoulou, S. J. and Lekidis, V. A. (2018) 'Simplified method for rapid seismic assessment of older R.C. buildings', *Engineering Structures*. Elsevier Ltd, 154, pp. 10–22. doi: 10.1016/j.engstruct.2017.10.052.

Pardalopoulos, S. J., Thermou, G. E. and Pantazopoulou, S. J. (2013) 'Screening criteria to identify brittle R.C. structural failures in earthquakes', *Bulletin of Earthquake Engineering*, 11(2), pp. 607–636. doi: 10.1007/s10518-012-9390-7.

Parulekar, Y. M. *et al.* (2020) 'Performance Assessment of Corroded Reinforced Concrete Structure Considering Bond Deterioration', *Journal of Performance of Constructed Facilities*. American Society of Civil Engineers, 34(2), p. 04020009. doi: 10.1061/(ASCE)CF.1943-5509.0001411.

Paul, Suvash CZijl, G. Van (2014) 'Cracked and uncracked SHCC specimens under different exposure conditions', in *Strain Hardening Cementitious Composites 3 (SHCC3)*. Dordrecht, pp. 25–32.

Pourbaix, M. (1974) *Atlas of electrochemical equilibria in aqueous solutions*. National

Association of Corrosion Engineers. Available at: https://books.google.ca/books?id=iiLRvQEACAAJ&dq=9780915567980&hl=en&sa=X&ved=0ahUKEwivreD28rfgAhVi6IMKHQm4Dn4Q6AEIKjAA (Accessed: 12 February 2019).

Prieto, M., Tanner, P. and Andrade, C. (2011) 'Bond response in structural concrete with corroded steel bars. experimental results', *RILEM Bookseries*. Springer, Dordrecht, 5, pp. 231–241. doi: 10.1007/978-94-007-0677-4_16.

Rajput, A. S. and Sharma, U. K. (2018) 'Corroded reinforced concrete columns under simulated seismic loading', *Engineering Structures*. Elsevier, 171, pp. 453–463. doi: 10.1016/J.ENGSTRUCT.2018.05.097.

Raza, S. *et al.* (2019) 'Strengthening and Repair of Reinforced Concrete Columns by Jacketing: State-of-the-Art Review', *Sustainability*. MDPI AG, 11(11), p. 3208. doi: 10.3390/su11113208.

Robuschi, S. *et al.* (2020) 'Bond of naturally corroded, plain reinforcing bars in concrete', *Structure and Infrastructure Engineering*. Taylor and Francis Ltd., pp. 1–17. doi: 10.1080/15732479.2020.1768273.

Rodriguez, J. and Ortega, J. C. (1994) 'Corrosion of reinforcing bars and service life of reinforced concrete structures: corrosion and bond deterioration', in *International Conference on Concrete across Borders*. Odense, Denmark, pp. 315–326.

Semendary, A. A. and Svecova, D. (2020) 'Factors affecting bond between precast concrete and cast in place ultra high performance concrete (UHPC)', *Engineering Structures*. Elsevier, 216, p. 110746. doi: 10.1016/J.ENGSTRUCT.2020.110746.

Sezen, H. and Moehle, J. P. (2004) 'Shear Strength Model for Lightly Reinforced Concrete Columns', *Journal of Structural Engineering*. American Society of Civil Engineers, 130(11), pp. 1692–1703. doi: 10.1061/(ASCE)0733-9445(2004)130:11(1692).

Soudki, K. and Sherwood, T. (2003) 'Bond Behavior of Corroded Steel Reinforcement in Concrete Wrapped with Carbon Fiber Reinforced Polymer Sheets', *Journal of Materials in Civil Engineering*, 15(4), pp. 358–370. doi: 10.1061/(ASCE)0899-1561(2003)15:4(358).

Stanish, K., Hooton, R. D. and Pantazopoulou, S. J. (1999) 'Corrosion Effects on Bond Strength in Reinforced Concrete', *ACI Structural Journal*, 96(6), pp. 915–921. doi: 10.14359/765.

Suffern, C., El-Sayed, A. and Soudki, K. (2010) ‘Shear strength of disturbed regions with corroded stirrups in reinforced concrete beams’, *Canadian Journal of Civil Engineering*, 37(8), pp. 1045–1056. doi: 10.1139/L10-031.

Takuya, K., Ryuta, I. and Masayuki, T. (2020) ‘Prediction of Hydrogen Embrittlement of Reinforcing Steel Bars in Concrete Poles | NTT Technical Review’, *NTT Technical Review*, 18(11). Available at: https://www.ntt-review.jp/archive/ntttechnical.php?contents=ntr202011ra1.html (Accessed: 16 April 2022).

Tastani, S. P. and Pantazopoulou, S. J. (2007) ‘Behavior of Corroded Bar Anchorages’, *ACI Structural Journal*, 104(6), pp. 756–766. doi: 10.14359/18958.

Tastani, S. and Pantazopoulou, S. J. (2005) ‘Recovery of seismic resistance in corrosion-damaged reinforced concrete through FRP jacketing’, *International Journal of Materials and Product Technology*, 23(3/4), p. 389. doi: 10.1504/IJMPT.2005.007737.

Tayeh, B. A., Abu Bakar, B. H. and Megat Johari, M. A. (2013) ‘Characterization of the interfacial bond between old concrete substrate and ultra high performance fiber concrete repair composite’, *Materials and Structures/Materiaux et Constructions*. Springer, 46(5), pp. 743–753. doi: 10.1617/S11527-012-9931-1/FIGURES/13.

Tepfers, R. (1979) ‘Cracking of concrete cover along anchored deformed reinforcing bars’, *Magazine of Concrete Research*. Thomas Telford Ltd , 31(106), pp. 3–12. doi: 10.1680/macr.1979.31.106.3.

Tondolo, F. (2015) ‘Bond behaviour with reinforcement corrosion’, *Construction and Building Materials*. Elsevier, 93, pp. 926–932. doi: 10.1016/J.CONBUILDMAT.2015.05.067.

Torres-Acosta, A. A., Navarro-Gutierrez, S. and Terán-Guillén, J. (2007) ‘Residual flexure capacity of corroded reinforced concrete beams’, *Engineering Structures*. Elsevier, 29(6), pp. 1145–1152. doi: 10.1016/J.ENGSTRUCT.2006.07.018.

Tuutti, K. (1982) *Corrosion of steel in concrete*. Swedish Cement and Concrete Research Institute, Stockholm. Available at: https://portal.research.lu.se/portal/en/publications/corrosion-of-steel-in-concrete(e97795b5-7f3a-4994-8beb-9438f5a51571).html (Accessed: 6 July 2020).

Valikhani, A. *et al.* (2020) ‘Experimental evaluation of concrete-to-UHPC bond strength with correlation to surface roughness for repair application’, *Construction and Building Materials*.

Elsevier, 238, p. 117753. doi: 10.1016/J.CONBUILDMAT.2019.117753.

Vecchio, F. J. and Collins, M. P. (1986) 'MODIFIED COMPRESSION-FIELD THEORY FOR REINFORCED CONCRETE ELEMENTS SUBJECTED TO SHEAR.', *Journal of the American Concrete Institute*, 83(2), pp. 219–231. doi: 10.14359/10416.

Vu, N. S. and Li, B. (2018) 'Seismic Performance of Flexural Reinforced Concrete Columns with Corroded Reinforcement', *ACI Structural Journal*, 115(5), pp. 1253–1266. doi: 10.14359/51702372.

Vu, N. S., Yu, B. and Li, B. (2016) 'Prediction of strength and drift capacity of corroded reinforced concrete columns', *Construction and Building Materials*. Elsevier, 115, pp. 304–318. doi: 10.1016/J.CONBUILDMAT.2016.04.048.

Wang, L. *et al.* (2015) 'Effects of stirrup and inclined bar corrosion on shear behavior of RC beams', *Construction and Building Materials*. Elsevier, 98, pp. 537–546. doi: 10.1016/J.CONBUILDMAT.2015.07.077.

Xia, J., Jin, W. and Li, L. (2011) 'Shear performance of reinforced concrete beams with corroded stirrups in chloride environment', *Corrosion Science*. Pergamon, 53(5), pp. 1794–1805. doi: 10.1016/J.CORSCI.2011.01.058.

Xu, S. L. and Cai, X. H. (2010) *Bond behavior of corroded reinforcing bar and ultra high toughness cementitious composites (UHTCC)*. Available at: https://framcos.org/FraMCoS-7/06-04.pdf (Accessed: 8 July 2019).

Yang, S.-Y. *et al.* (2016) 'Experimental research on hysteretic behaviors of corroded reinforced concrete columns with different maximum amounts of corrosion of rebar', *Construction and Building Materials*. Elsevier, 121, pp. 319–327. doi: 10.1016/J.CONBUILDMAT.2016.06.002.

Yuan, W., Guo, A. and Li, H. (2017) 'Experimental investigation on the cyclic behaviors of corroded coastal bridge piers with transfer of plastic hinge due to non-uniform corrosion', *Soil Dynamics and Earthquake Engineering*. Elsevier, 102, pp. 112–123. doi: 10.1016/J.SOILDYN.2017.08.019.

Zhang, R., Castel, A. and François, R. (2009) 'The corrosion pattern of reinforcement and its influence on serviceability of reinforced concrete members in chloride environment', *Cement and Concrete Research*. Pergamon, 39(11), pp. 1077–1086. doi:

10.1016/J.CEMCONRES.2009.07.025.

Zhang, W. *et al.* (2012) ‘Tensile and fatigue behavior of corroded rebars’, *Construction and Building Materials*. Elsevier, 34, pp. 409–417. doi: 10.1016/J.CONBUILDMAT.2012.02.071.

Zhao, Y. *et al.* (2013) ‘Bond behaviour of normal/recycled concrete and corroded steel bars’, *Construction and Building Materials*. Elsevier, 48, pp. 348–359. doi: 10.1016/J.CONBUILDMAT.2013.06.091.

Zhu, W. *et al.* (2013) ‘Effect of corrosion of reinforcement on the mechanical behaviour of highly corroded RC beams’, *Engineering Structures*. Elsevier, 56, pp. 544–554. doi: 10.1016/J.ENGSTRUCT.2013.04.017.

Zhu, W. and François, R. (2014) ‘Experimental investigation of the relationships between residual cross-section shapes and the ductility of corroded bars’, *Construction and Building Materials*, 69(69), pp. 335–345. doi: 10.1016/j.conbuildmat.2014.07.059.

Van Zijl, G. P. A. G. *et al.* (2012) ‘Durability of strain-hardening cement-based composites (SHCC)’, *Materials and Structures/Materiaux et Constructions*. Springer, 45(10), pp. 1447–1463. doi: 10.1617/s11527-012-9845-y.

6. Main Experimental Program – Specimen Preparations

6.1. Design of Experimental Program and Specimen Characteristics

The objective of this experiment was to investigate the effect of corrosion on the seismic behavior of lap-spliced columns designed according to pre-1970 design recommendations and to study the efficiency of UHPC jacketing as a repair (post-earthquake) or retrofitting (pre-earthquake) material. The experimental program comprised six previously corroded column specimens, of which four were tested twice (i.e., before and after retroffiting), so that a total of ten column experiments were conducted as outlined in Table 6-1: specimens marked as "Corroded" were tested after completion of the corrosion conditioning; "Post-Testing Repaired" are columns that were first tested under mechanical load and then repaired with UHPC jacketing, and last, "Strengthened" are columns that have been jacketed immediately after completion of the conditioning cycle and then tested under mechanical load.

Lap splice length was taken according to ACI 318-63 where the required lap length was only, $l_p = 24D_b$. Stirrups used were 8mm in diameter and were spaced at 250mm along the shear span of the column as shown in Figure 6-1, concrete cover was taken to be c_c=25mm. Variables of study were the bar diameter and the column length which affected the flexural demand to supply ratio, and the repair/retrofit strategy used after the desired level of reinforcement corrosion was imparted on the columns through accelerated conditioning. Columns were either reinforced with 4-20M bars or with 6-15M longitudinal bars. Both of these alternative reinforcement arrangements correspond to the same area of reinforcement $A_s = 1256mm^2$, the only difference being the number of bars and the bar diameter used. These variables were introduced in order to understand the implications of having different bar sizes for the same amount of reinforcement in a corrosive environment.

Four of the columns had a shear span of 1.45m and two had a shear span of 0.85m; this variable was introduced in order to study the effect of corrosion on lap-spliced columns that are short and stocky (i.e., having a relatively low aspect ratio).

Two of the long columns were subjected to a simulated seismic load after the accelerated corrosion process and were subsequently repaired with a thin UHPC jacketing and retested. This was done in order to study the effectiveness of the repair scheme in a post-earthquake disaster situation. The remainder of the columns were retrofitted immediately after the accelerated corrosion procedure

and then tested under simulated seismic load. This facilitated the comparison between corroded, repaired, and retrofitted columns.

Table 6-1. Specimen details

Column ID	*Longitudinal Reinforcement*	*Lap Length*	*Shear Span Length (L_s)*	*Testing Methodology*
L-20-Cor	4 – 20M	480 mm	1.45 m	Corroded
L-20-Rep	4 – 20M	480 mm	1.45 m	Post-testing Repaired
L-20-Str	4 – 20M	480 mm	1.45 m	Strengthened
S-20-Cor	4 – 20M	480 mm	0.85 m	Corroded
S-20-Rep	4 – 20M	480 mm	0.85 m	Post-testing Repaired
L-15-Cor	6 – 15M	360 mm	1.45 m	Corroded
L-15-Rep	6 – 15M	360 mm	1.45 m	Post-testing Repaired
L-15-Str	6 – 15M	360 mm	1.45 m	Strengthened
S-15-Cor	6 – 15M	360 mm	0.85 m	Corroded
S-15-Rep	6 – 15M	360 mm	0.85 m	Post-testing Repaired

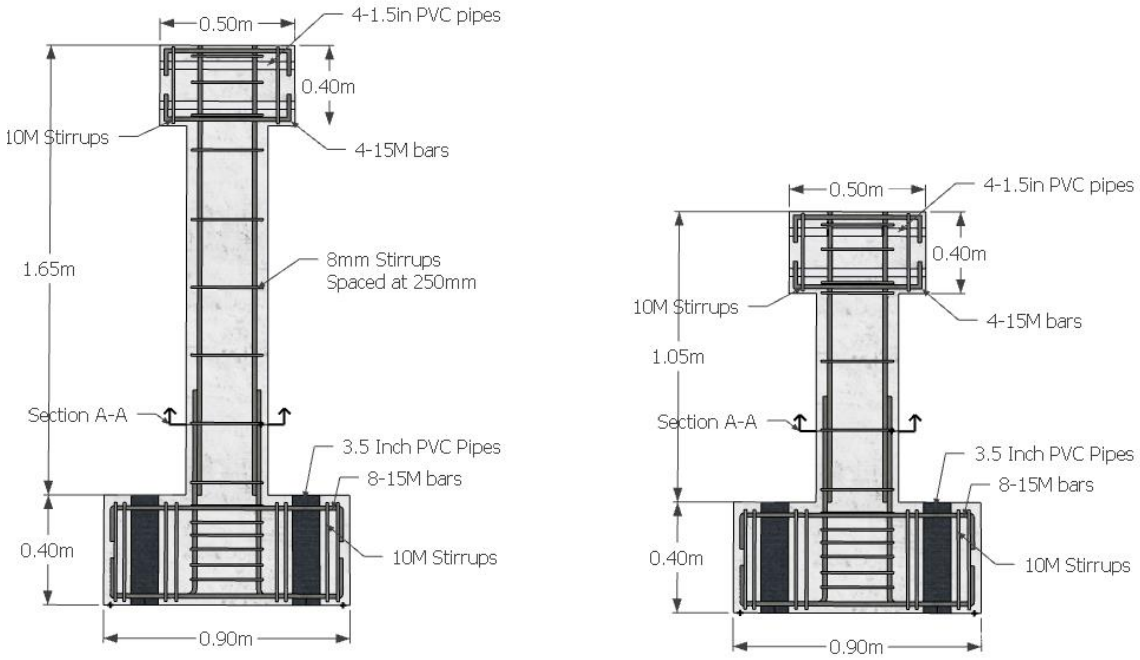

Figure 6-1. Standard column detailing for tall and short columns.

6.2. Formwork and Reinforcing Cage Fabrication

Formwork design and fabrication was accomplished in-house. No contractors were involved in the process. The formwork was made up out of ½ in plywood and 2x2" wooden studs.

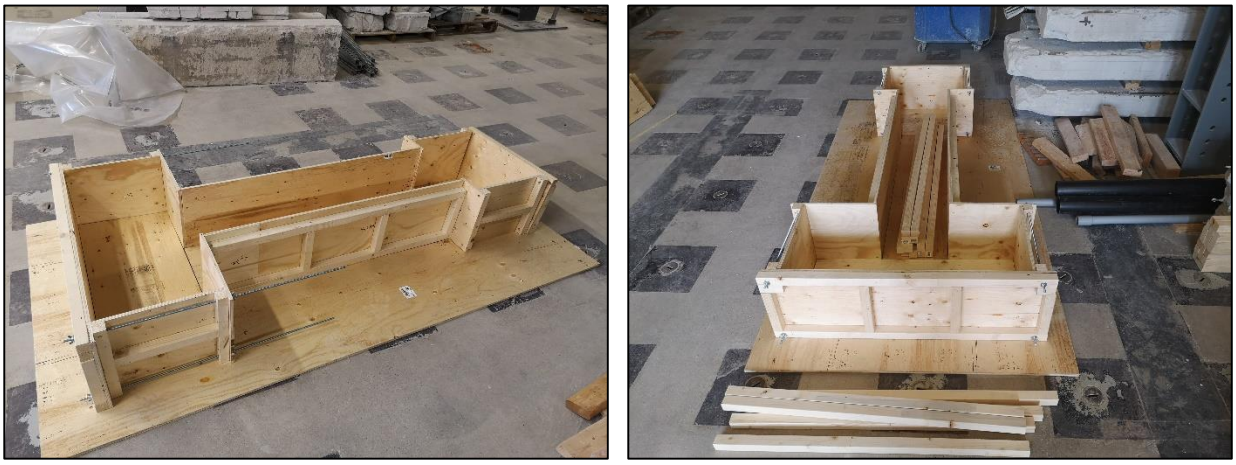

Figure 6-2. Photos of column formwork

Tilt-up construction method was chosen for the column fabrication in order to cast each specimen at once eliminating several casts per specimen.

Reinforcement was also cut and bent in-house using a rebar bending machine. Ribbed stirrups, 8mm in diameter and bent at 135^{o} were used to confine the column's longitudinal reinforcement in the foundation and cap beam. In the shear span stirrups constituted of 8mm diameter smooth reinforcement bent at 90^{o} with $6d_b$ hook length as this form of shear reinforcement is more representative of old construction practices. The cap beam was reinforced with 4-15M (evenly divided between top and bottom reinforcement) bars while the foundation was reinforced with 8-15M bars (evenly divided between top and bottom reinforcement). The cap beam and foundation's reinforcement were confined by 10M ribbed stirrups.

Cage Fabrication was carried out in two phases. In the first phase, the foundation cage was prepared including the starter bars (longitudinal reinforcement extending from the footing into the shear span) as shown in Figure 6-3 (right) which was then placed in the formwork. In the next phase the remainder of the reinforcement was introduced in the forms as shown in Figures 6-3 (left) and 6-4 where the rest of the longitudinal reinforcement was connected to the starter bars in addition to the shear span's stirrups. Following cage fabrication, hooks were attached to the cage for lifting of the specimens and finally the formwork was then reinforced to avoid any unwanted

formwork deformation after pouring the concrete. Figure 6-4 shows the state of the specimens awaiting casting.

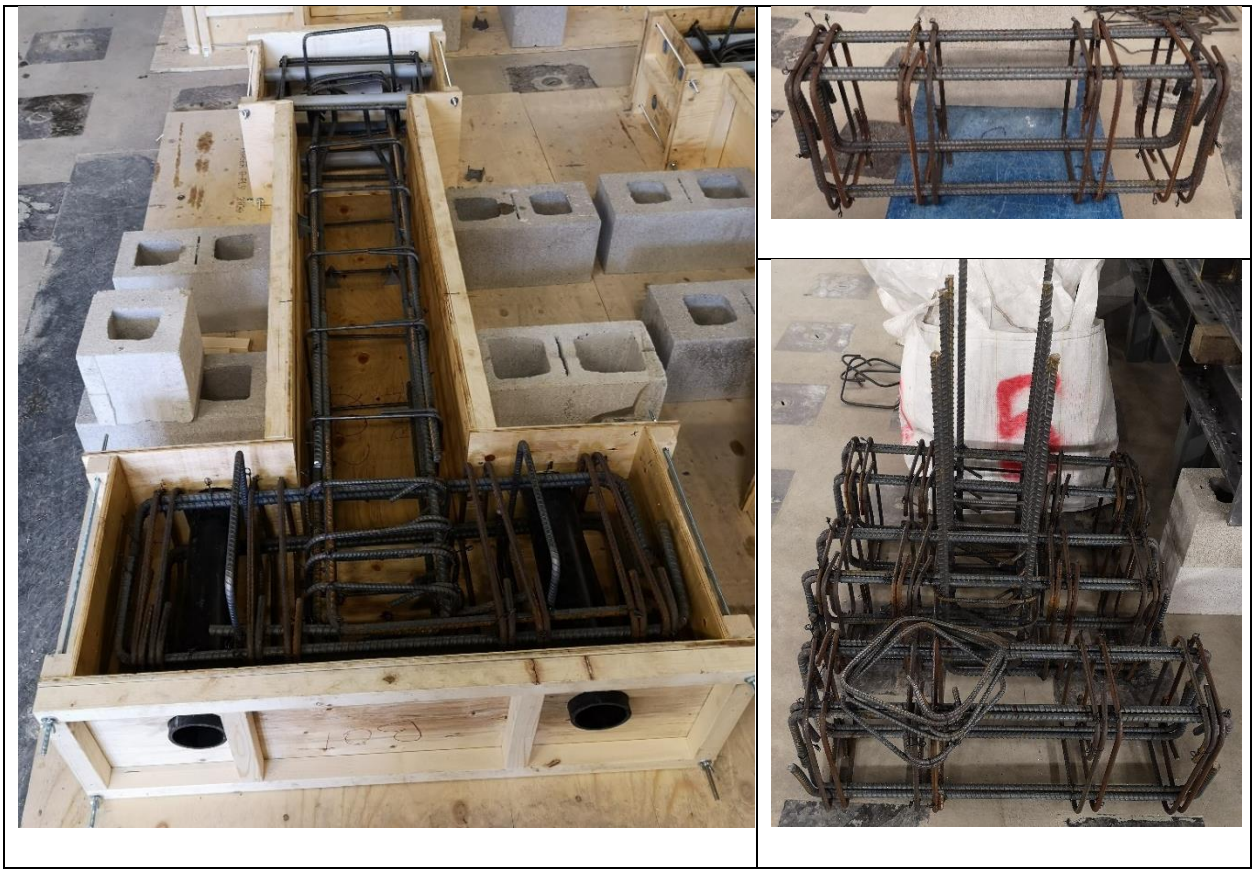

Figure 6-3. Column reinforcement cage preparation. Full column placed in formwork ready for casting (left), footing cage (right)

Once all formworks were stabilized and oiled, a ready mix concrete truck came in and poured the concrete into the formwork through a chute. The specimens were left two days in the formwork to harden and were then demolded and wrapped in burlap and plastic sheeting to cure for 28 days.

Figure 6-4. Specimens ready for casting

6.3. Accelerated Corrosion Procedure

After the curing the specimens, the accelerated corrosion conditioning began. The region of interest was the lap-splice zone thus only 0.6m of the column length was included in the corrosion process. The longitudinal reinforcement of the columns served as the anode while external rebar coupons served as cathodes and were placed on the face of the column as shown in Figure 6-5. Columns were wrapped in burlap in several layers and contained sponges in between the layers for additional water absorption and retention. The current used was 0.7 Amps which was equivalent to a current density of 200 $\mu A/cm^2$ as this was the threshold current density found in a natural corrosive environment (Andrade, Alonso and Gonzalez, 1990). The area steel area calculated to reach 0.7 Amps was the surface area of longitudinal reinforcement in the lap-splice zone as well as the surface area of stirrups present in this region. Specimens were subjected to wetting and drying cycles where the wetting period was one day and the drying period was two days. The drying period was integral to the corrosion conditioning of the specimens as it allowed the corrosion byproducts to oxidize as fully as possible, which leads to an increase in the rust's volume and in turn yields realistic cover cracking. The wetting cycle included covering up the burlap in a plastic sheet and pouring a 3% NaCl solution into the jacket until the burlap and sponges were soaked. Then a rope was used to tighten the ends of the jacket to reduce water evaporation during the wetting cycle. Plastic sheeting was used to protect the top of the foundation from unwanted corrosion as can be seen in Figure 6-6. This method was not as effective as intended, because it was found in the end of the conditioning process that the foundation did experience

some cover cracking. Specimens underwent 57 cycles with a target corrosion level of 5% of reinforcement mass loss. The time needed to reach the target corrosion level was calculated using Faraday's law, shown in Equation (6-1).

$$\Delta m\ (grams) = \frac{t*i*M}{z*F} \tag{6-1}$$

$$Mass\ Loss\ (\%) = \frac{\Delta m}{m_0} * 100 \tag{6-2}$$

Where *t* is the exposure time (*s*); *I* is the current (*Amperes*); *M* is the atomic weight of iron (taken as, *M=55.847 g/mol*); *z* is the ion charge (*2* moles of electrons); *F* is Faraday's Constant representing the amount of electrical charge in 1 mole of electron (taken *F=96,487 C/mol*). Δ_m and m_o are the mass loss (in grams) and the original mass, respectively. The entire corrosion process took nine months to be completed.

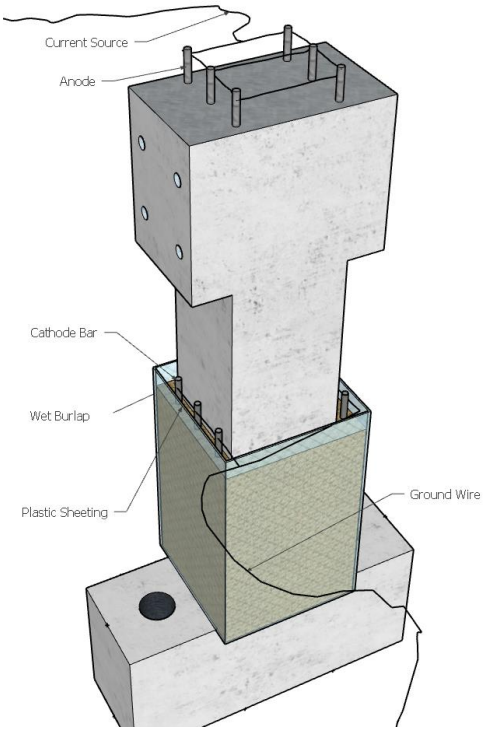

Figure 6-5. Column's accelerated corrosion setup.

Figure 6-6. Photos from the accelerated corrosion program. Short column with cathode bars shown before covering with second layer of burlap and a plastic sheet (left). All columns are shown during a wetting cycle (right).

6.4. Post-Corrosion State of Columns

This section presents the state of the six columns after completion of the accelerated conditioning phase and before mechanical testing.

6.4.1. L-15-Cor Cracking Pattern

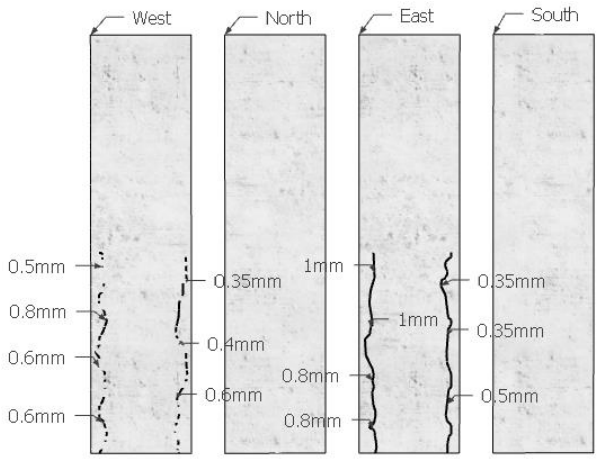

Figure 6-7. Cracking pattern of column L-15-Cor post corrosion

North : South : East : West:

Figure 6-8. State of column L-15-Cor after the accelerated corrosion program

6.4.2. L-20-Cor Cracking Pattern

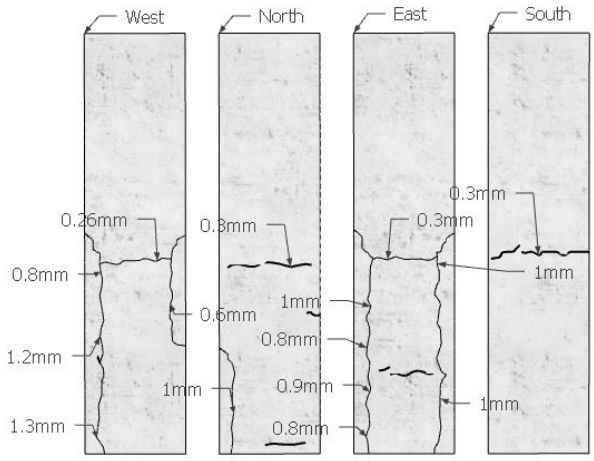

Figure 6-9. Cracking pattern of column L-20-Cor post corrosion

North : South: East: West:

Figure 6-10. State of column L-20-Cor after the accelerated corrosion program

6.4.3. S-15-Cor Cracking Pattern

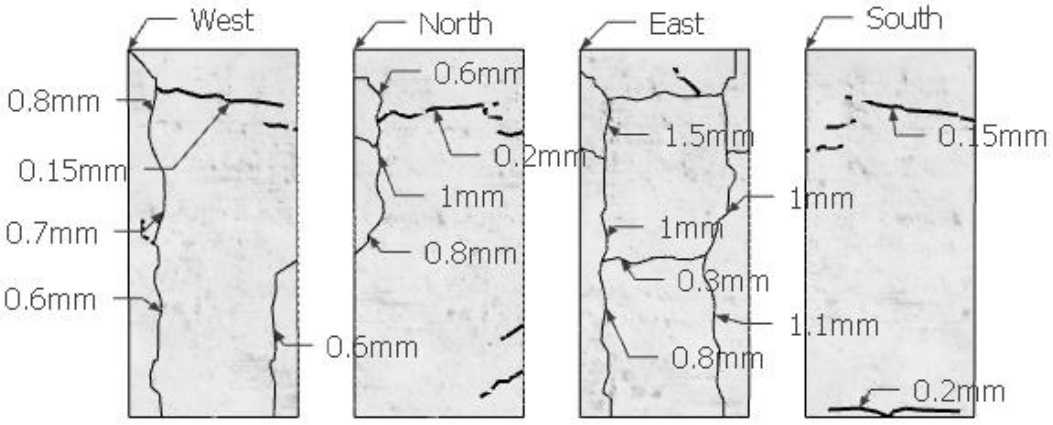

Figure 6-11. Cracking pattern of column S-15-Cor post corrosion

North: South: East: West :

Figure 6-12. State of column S-15-Cor after the accelerated corrosion program

6.4.4. S-20-Cor Cracking Pattern

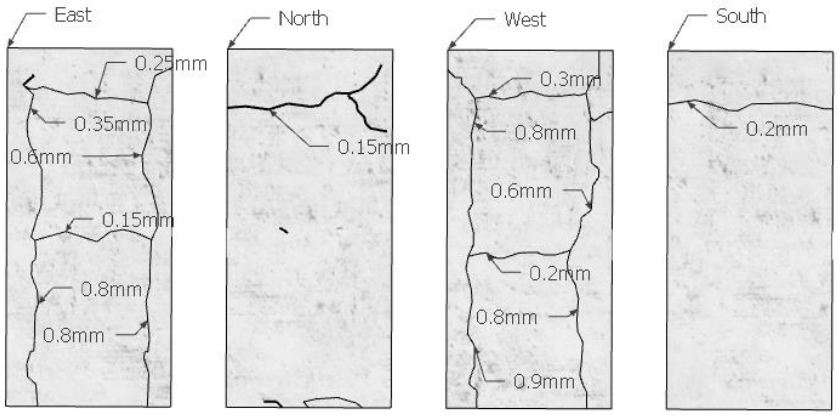

Figure 6-13. Cracking pattern of column S-20-Cor post corrosion

North : South : East : West :

Figure 6-14. State of column S-20-Cor after the accelerated corrosion program

6.4.5. L-15-Str Cracking Pattern

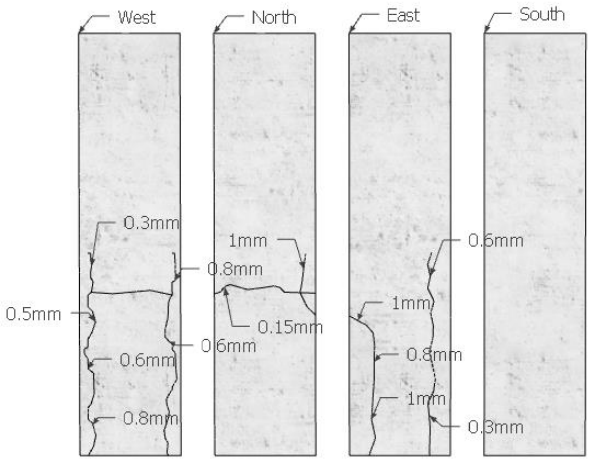

Figure 6-15. Cracking pattern of column L-15-Str post corrosion

North : South : East : West :

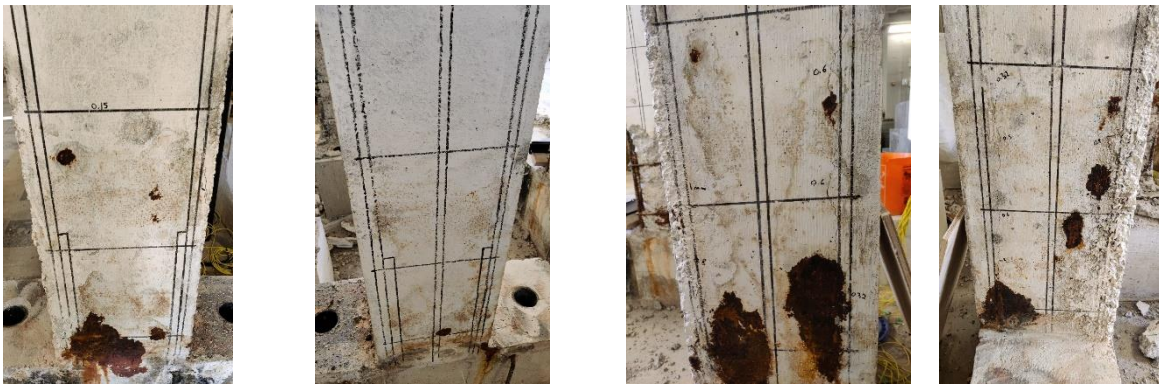

Figure 6-16. State of column L-15-Str after the accelerated corrosion program

6.4.6. L-20-Str Cracking Pattern

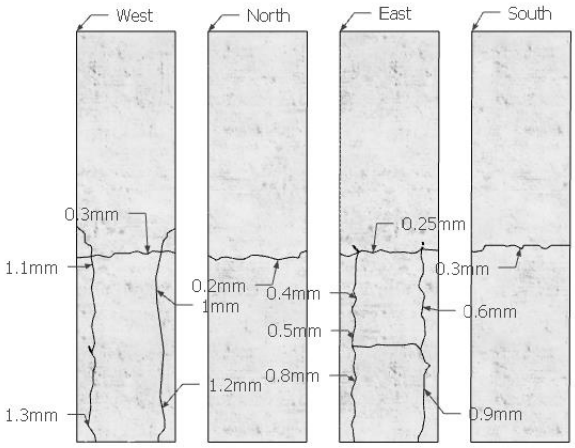

Figure 6-17. Cracking pattern of column L-20-Str post corrosion

North: South: East: West:

Figure 6-18. State of column L-20-Str after the accelerated corrosion program

6.5. Preparations for the Mechanical Testing

Prior to load testing the specimens, certain provisions were made in order to render the specimens ready for testing. The accelerated corrosion process required reinforcement to be extruding from the top of the column's cap. These bars were removed using an angle grinder as can be seen in Figure 6-19. Additionally, plastic pipes extruding from the footing (required to accommodate the anchor rods to fix the specimen on the floor) and from the column's cap (for the rods required to attach the lateral actuator on the specimen) were sawn off manually flush with the concrete surface.

Any contact irregularities at the column bases to the lab floor were corrected by casting a thin plaster filler underneath the column prior to testing in order to ensure that the column was levelled.

Figure 6-19. Removing extruded bars from the top of the columns.

6.5.1. Test Setup

The test setup adopted in this series of experiments consisted of using two actuators, i.e., a vertical actuator for the axial load application and a horizontal actuator for the reversed cyclic lateral displacement application. The vertical actuator, having 1000 KN capacity, was hung off an overhead cantilever which was bolted to the strong-wall. The horizontal actuator, having a 250 KN capacity was mounted on a steel beam that was connected to the orthogonal part of the strong wall, as shown in Figure 6-20.

Figure 6-20. Experimental test setup preparation while mounting the vertical actuator to the supporting cantilever

Column specimens were carefully moved in place and anchored through the strong floor. Two UHPC plates were placed underneath the top washers of the anchor rods, to avoid any local failure in the concrete footings. A sample mounted specimen is shown in Figures 6-21 below. Steel plates were placed at the face of the column's cap in order avoid any local failures while loading/unloading. Additional steel strips were placed underneath the column's cap and were connected to the vertical actuator through threaded rods to avoid slippage between the vertical actuator and the column cap during testing.

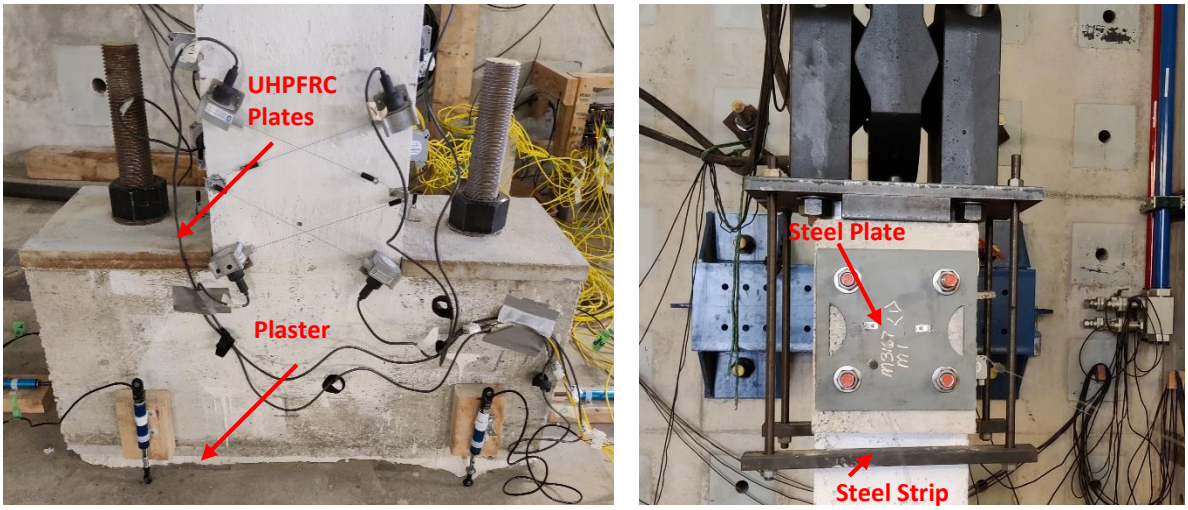

Figure 6-21. Close up on column test preparations. UHPC plates and plastering of the base (left), steel plate and vertical actuator clamp (right).

6.5.2. Instrumentation

This section describes the instrumentation utilized throughout the experimental program. In this series of experiments, two types of instrumentation were used, the first being displacement transducers (DT) and the second being resistive sensor linear position string potentiometers (SP). Table 6-2 displays the legend for the nomenclature of the potentiometers and linear string pots employed during the test.

Table 6-2. Instrumentation name and respective purpose

ID	*Type of Instrument*	*Purpose of Use*
VR1, VR2, VR3, VL1, VL2, VL3	SP	SPs were placed on both the flexural and compressive faces of the column at set gauges (15cm). Measurements were used to calculate the curvature of the section in three intervals along the plastic hinge region.
XM, XN, XO, XP	SP	SPs were placed in an X shape at set gauges (15cm vertically and 28cm horizontally). The measurements were used to calculate shear drifts.
UR, UL	DT	DTs were placed at the front face of the column at the location of the anchors to measure uplift.
HR, HL	DT	DTs were placed horizontally at the base of the column to measure slip.
LTR, LTL	SP	Two SPs were attached to the cap of the column to measure both lateral displacement and torsion (in case it happened).
LM	SP	One SP was used to measure the lateral displacement of the middle of the column.
VTOP	SP	One SP was used to measure the vertical displacement of the column in order to calculate axial strains.

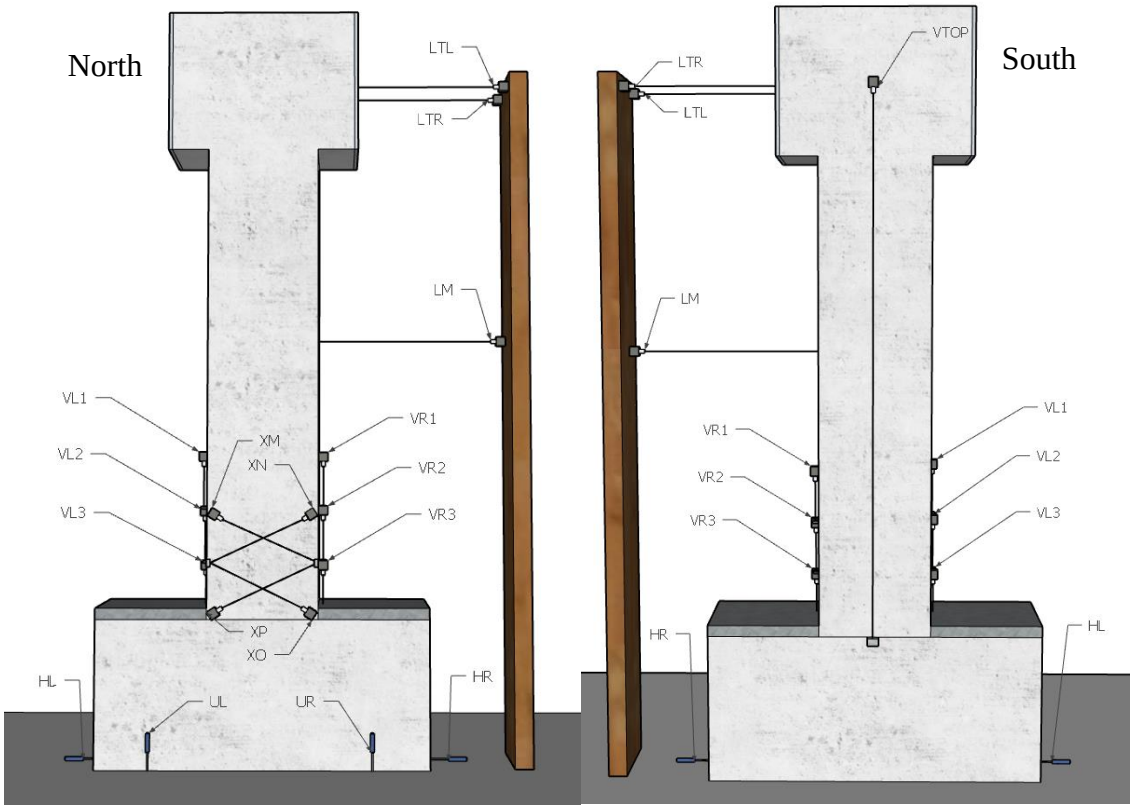

Figure 6-22. Instrumentation setup diagram

The adopted loading protocol shown in Figure 6-22 was chosen based on ACI 374.2R-13 Recommendations. Three cycles per drift level were adopted in order to fully exhaust the bond capacity of the lapped reinforcement.

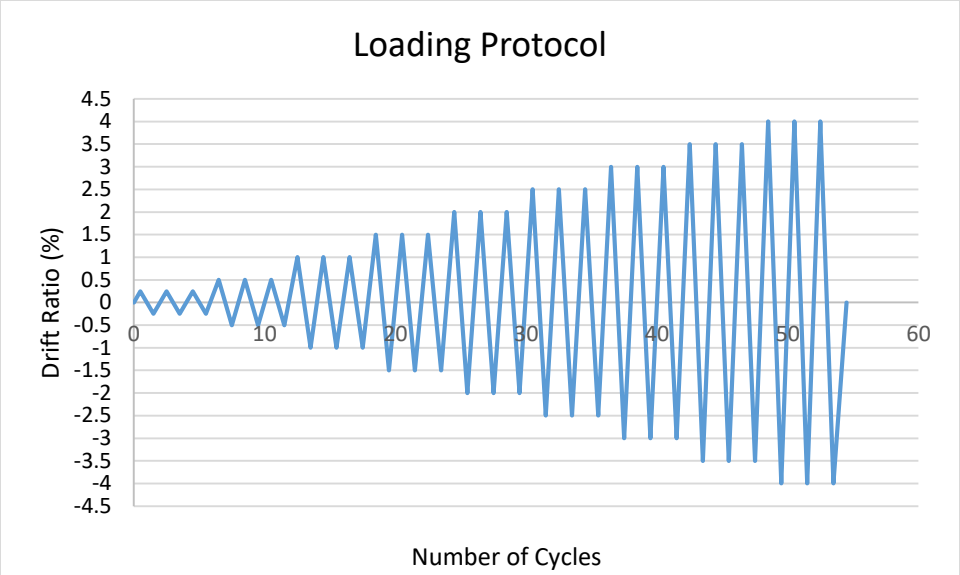

Figure 6-23. Loading protocol adopted in the experimental program

The loading protocol was controlled by the lateral displacement of the column cap (D_{top}) adjusted for slippage at the base of the specimen. The displacement was calculated using Equation (6-3).

$$D_{top} = \frac{LTR+LTL}{2} - HR \tag{6-3}$$

The drift ratio θ_{chord} of the column which represents the inclination of the chord from its tangent at the column base was calculated using Equation(6-4):

$$\theta_{chord} = \frac{D_{top}}{L_s} \tag{6-4}$$

6.6. Repair and Strengthening of Columns Using UHPC

After the first phase of testing the first set of columns (Columns with IDs that include the nomenclature 'Cor' from Table 6-1), a jackhammer was used to remove the concrete cover and a portion of the core concrete. The repair strategy was implemented as follows: in all cases the depth of the cover material removed, up to a depth of $1D_b$ into the core measured from the inner longitudinal bar. This was done in order to ensure full bond in the retrofitted specimen between the longitudinal reinforcement and the UHPC jacket. Where the concrete in the plastic hinge region had completely disintegrated, the fragmented core was removed and replaced with UHPC material.

Table 6-3 displays which columns were only repaired by cover replacement and which had also the core replaced.

Table 6-3. Type of repair strategy adopted for each column

Column ID	***Testing Methodology***	***Repair Strategy***
L-20-Rep	Post-testing Repaired	Core Removal
L-20-Str	Strengthened	Perimeter removal
S-20-Rep	Post-testing Repaired	Core Removal
L-15-Rep	Post-testing Repaired	Perimeter removal
L-15-Str	Strengthened	Perimeter removal
S-15-Rep	Post-testing Repaired	Core Removal

The repair work extended into the footing to a depth of 5-10 cm in order to mitigate failure at the column-footing interface. Figures 6-24 show a sample of the repair work.

Figure 6-24. Sample of the state of the columns after concrete removal during the repair/strengthening process

After concrete removal, the corroded reinforcement was cleaned using a wire cup brush attached to an angle grinder. Ideally, cleaning would be done using sand blasting, however that was not an

available option. The exposed concrete was then blasted with pressurized air to remove any debris or dust. A special jacketing formwork was designed for the repair work with two slanted openings to facilitate pouring of the UHPC material into the thin layers of the cover over the entire length of the repaired region. Where the length of cover replacement was large, intermediate openings in the formwork were used for pouring at two levels; when the fluid concrete reached the level of the lower opening it was sealed and then pouring was continued from the upper opening. Figure 6-25 shows two formworks in use after casting UHPC.

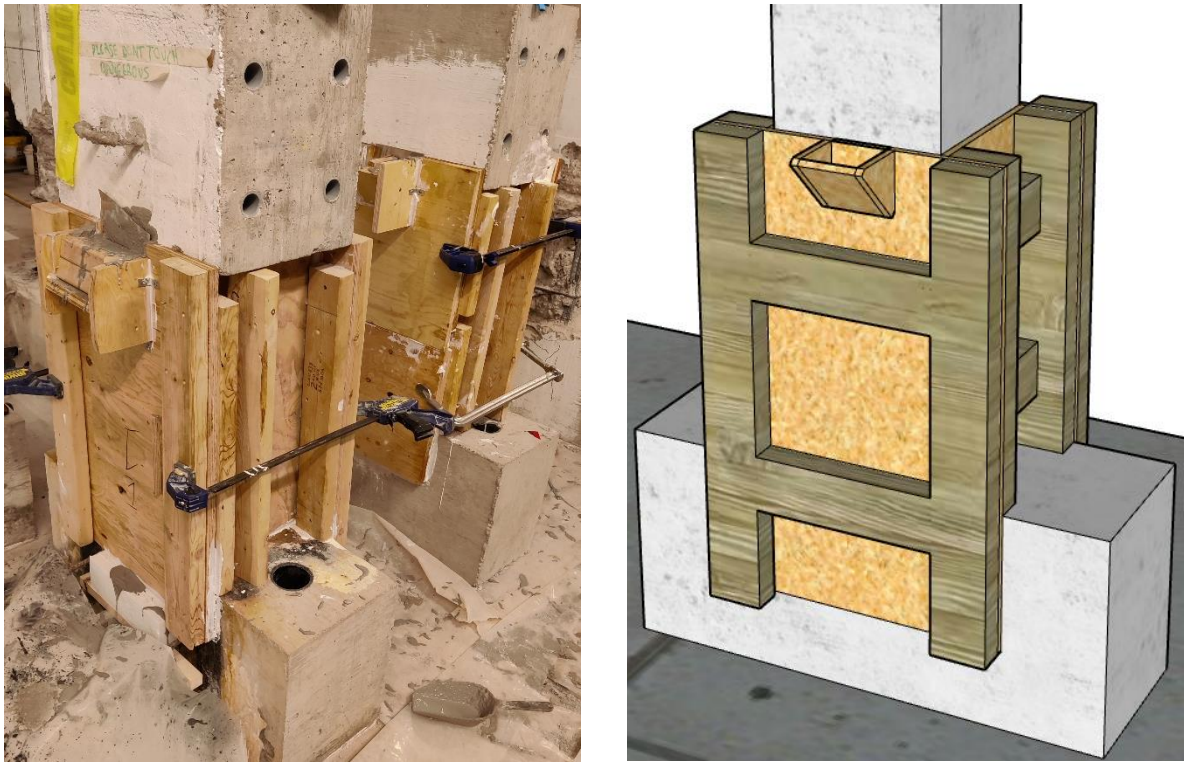

Figure 6-25. Sample of formwork used during the repair/strengthening process

Formwork was demolded after two days from casting in order to ensure hardening of UHPC, the jacket was then wrapped with wet burlap and a plastic sheet (to minimize water evaporation) for 28 days.

7. Experimental Results and Discussion

7.1. Material Properties

Samples of reinforcement used in the construction of the columns were tested in tension to determine the material's properties. Table 7-1 shows the material properties of reinforcement used in the experimental program.

Table 7-1. Reinforcement material properties

Bar Size	f_y	f_u	ε_u
15M bars	425	570	0.2
20M bars	400	535	0.2
8mm Stirrups	300	415	0.2

Concrete was provided by a ready-mix concrete producer with the specifications of having a 21 MPa 28-day compressive strength and a maximum aggregate side of 15mm. UHPC materials were cast in-house. The mix design of the prepackaged material is the same as described in Chapter 4: it consists of mixing 1 unit of mass of dry-mix Densit Inducast TT-5® with 0.13 units of water, and 0.066 units of mass of straight steel fibers (2% by volume steel fibers). Straight brass coated Dramix® were used having 13mm length and 0.2mm diameter The material was very flowable with the 2 min spread reaching 210 mm as shown in Figure 7-1.

Figure 7-1. UHPC flow test

Three concrete cylinders obtained from each casting were tested in the same day as the column testing. Table 7-2 shows the concrete compressive strength of each batch, obtained as the average of three samples. Tensile strength of normal concrete was assumed to be 10% of its compressive strength, while for UHPC, thin prisms (referred to in this work as Graybeal-type of specimens)

were cast with the cylinders and were also tested in direct tension in the MTS Universal Test Frame to accurately determine the material's tensile stress-strain response. Tension specimens were cast from one end, for optimal fiber orientation. Figure 7-2 shows the UHPC's tensile stress with respect to the actuator's displacement

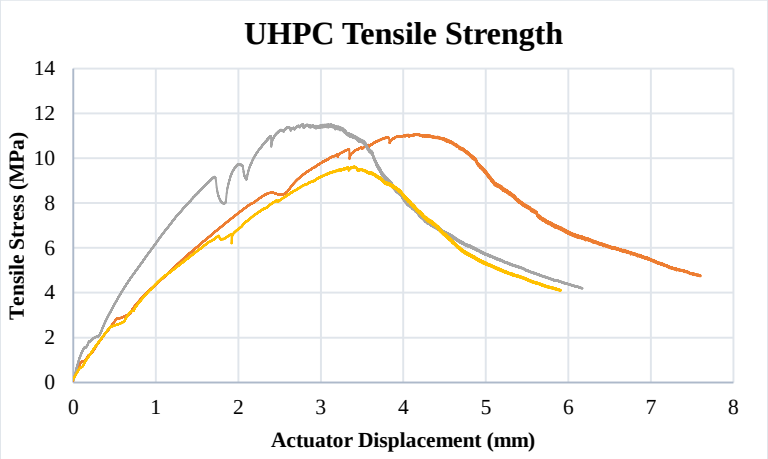

Figure 7-2. UHPC Graybeal-type tensile tests

Table 7-2. Concrete material properties

Column Specimen Type	*Compressive Strength f'_c*	*Tensile Strength f_t*
Tall Columns with 15M Bars	20 MPa	2 MPa
Tall Columns with 20M Bars	24 MPa	2.4 MPa
Short Columns	28 MPa	2.8 MPa
UHPC material in jackets	160 MPa	11 MPa

7.2. Hysteretic Response of Columns

Column specimens were tested under cyclic displacement reversals following the loading protocol shown in Figure 6-23. During these tests, failure was defined when the lateral load capacity (V) dropped to 80% of the maximum lateral load capacity (V_{max}) after correcting for P-Delta. Yielding deformation was determined by drawing a secant to intersect the load-drift curve at 75% of the maximum lateral capacity (V_{max}) as suggested by Sezen and Moehle, (2004), and is also recommended in ASCE/SEI 41 (2017). Tables 7-3 and 7-4 summarize the results related to the mechanical properties of the columns and the increase in strength and deformation capacities between concrete and repaired/strengthened columns. The following paragraphs discuss experimental observations in the tests. In the following discussion, positive is considered the direction of loading away from the wall (where the piston head bears on the beam cap), and

negative is pulling towards the wall (in this case the load was transferred to the specimen through the back plate on the beam cap, through tension of the threaded rods.

7.2.1. Short Concrete Columns

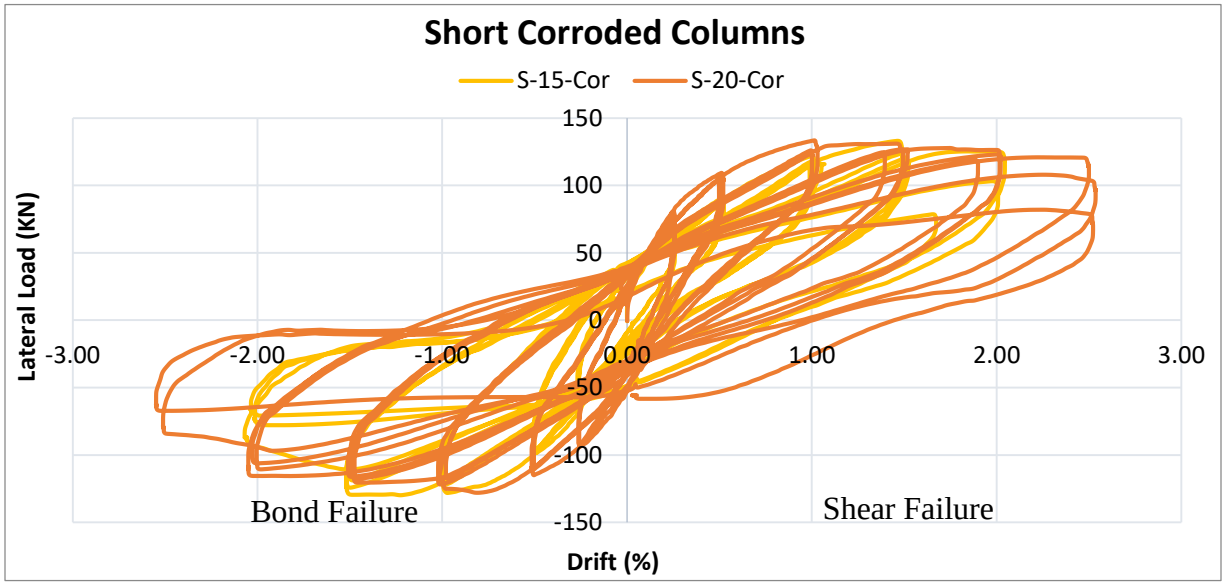

Figure 7-3. Hysteretic response of short corroded columns

Figure 7-3 shows the hysteretic response of the short corroded columns, S-20-Cor and S-15-Cor. Axial load applied on the short columns was P = 380KN. For column S-20-Cor , yield strength in the positive direction was V_y^+=109KN, and it was attained at a drift of θ_y^+ = 0.55%, whereas in the negative direction, the yield strength was V_y^-= -106KN, attained at a drift of θ_y^- = -0.38%. Maximum lateral strength recorded in the positive direction was V_{max}^+=133KN, attained at a drift of $\theta^+{}_{max}$ = 1%, whereas in the negative direction, V_{max}^-= -128KN, attained at θ_{max}^-= -0.98%. The ultimate drift in the positive direction was θ_u^+= 2.5% whereas in the negative direction it was θ_u^-= -2%.

For column S-15-Con, the yield strength in the positive direction was V_y^+=113KN attained at a drift of θ_y^+= 0.8%, whereas in the negative direction, the yield strength was V_y^-=-111KN attained at a drift of θ_y^- = -0.6%. Maximum lateral strength recorded in the positive direction was $V^+{}_{max}$=133KN attained at a drift of attained θ_{max}^+ = 1.5%; in the negative direction V_{max}^- = -130KN attained at θ_{max}^-= -1.2%. The ultimate drift in the positive direction was θ_u^+ = 2% whereas in the negative direction it was θ_u^- = -1.8%.

Lateral strength in column S-20-Cor was maintained between cycles until reaching a drift of 2.5% where the recorded reduction in lateral strength reached 60% between the first and third cycle. Column S-15-Cor experienced a 30% reduction in lateral strength between the first and third cycle at 2% drift whereas the drop in lateral capacity of column S-20-Cor at the same drift level was only 4%.

S-20-Cor displayed a favorable behavior relative to column S-15-Cor by maintaining its strength between cycles at similar drifts levels and by reaching a higher ultimate drift capacity.

Two failure modes were observed in both columns. One column side's failure was dominated by lap-splice (bond) failure, which was observed in the negative drift region of Figure 7-3 (column moving towards the strong wall), where a significant degradation in strength is observed with increasing drift level on one side of the column. The other side of the column experiences a shear failure, which is evident by the pinching of the hysteretic loops and is confirmed by the crack pattern on the column as is observed in Figure 7-4. The side views (left) of both S-25-Cor and S-20-Cor columns show the pre-existing longitudinal cracks caused by corrosion without a significant increase in crack width and that is because shear failure dominated the response when the column was pushed in that direction. Side views (right) on the other hand show significant increase in longitudinal crack width or total cover delamination due to bond failure.

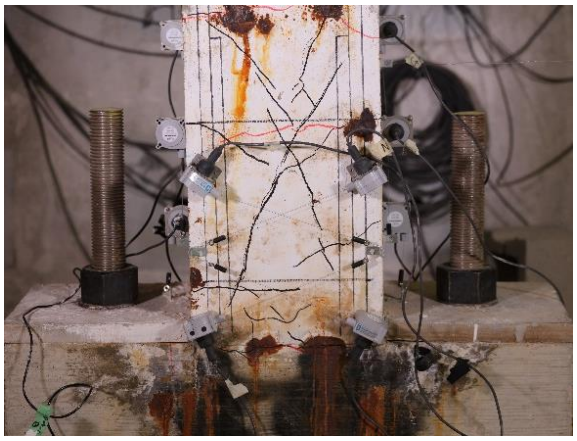

a) S-20-Cor Front View

b) S-20-Cor Side View

c) S-20-Cor Side View

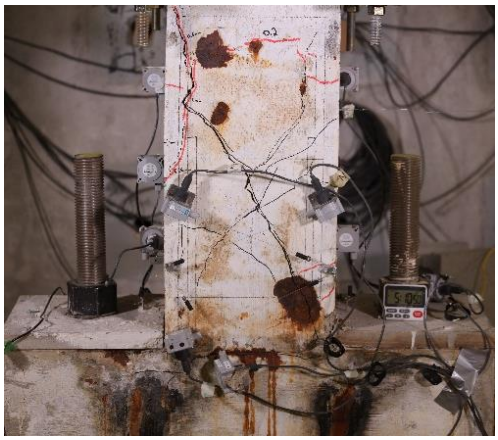

d) S-15-Cor Front View

e) S-15-Cor Side View

f) S-15-Cor Side View

Figure 7-4. Final state of short concrete columns after testing.

7.2.2. Repaired Short Corroded Columns

After repair, the short columns showed a significant improvement in performance. Both columns had almost identical behavior, in terms of stiffness and lateral load carrying capacity as can be seen in Figure 7-5. A limitation in the test was exceeding 4% drift for the short columns due to the vertical actuator's inability to deflect further in the lateral direction.

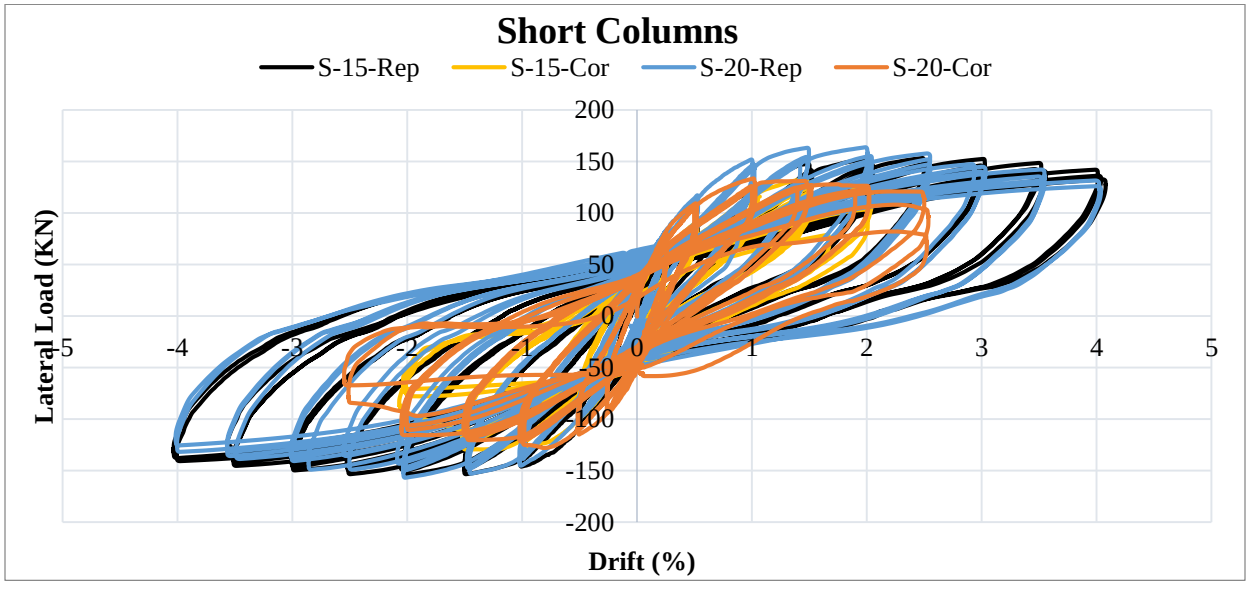

Figure 7-5. Hysteretic response of short corroded and repaired columns

Column S-20-Rep showed a 28% increase in yield strength in both directions, V^{+}_{y}=140KN from V_y^+=109KN and V_y^-=-136KN from V_y^-=-106KN. The yield drifts also increased by 45% in the

positive direction and 137% in the negative direction. An increase of 23% was recorded in the maximum lateral capacity, V_{max}^{+}=163KN from V_{max}^{+}=133KN and V_{max}^{-}=157KN from V_{max}^{-} =128KN. Similarly, the drift at maximum deformation was increased by 50% in the positive direction and 104% in the negative direction. Ultimate drift capacity also showed a significant improvement, however due to the fact that testing limitation in the level of deformation was imposed on the testing regime, the increase in ultimate deformation was limited to a certain level corresponding to 4% drift. The increase in ultimate deformation in the positive direction was greater than 60% whereas in the negative direction was greater than 100%. It is noted that this was the direction where for the initial testing of S-15-Cor and S-20-Cor bond failure had occurred in the reinforcement; this bond failure had occurred after strain penetration from the critical section towards both the shear span and the footing.

The yield strength of column S-15-Rep showed an 18% was increased in both directions, with V_{y}^{+}=133KN from V_{y}^{+}=113KN and V_{y}^{-}=-130KN from V_{y}^{-}=-111KN. The yield drifts also increased by 50% in the positive direction and 17% in the negative direction. An increase of 15% was recorded in the positive maximum lateral capacity, V_{max}^{+}=163KN from V_{max}^{+}=133KN and 18% in the negative maximum lateral capacity, V_{max}^{-}=157KN from V_{max}^{-}=128KN. An increase in the drift at maximum lateral capacity $\theta_{\max}$ by 33% in the positive direction and 25% in the negative direction. The increase in ultimate deformation in the positive direction was greater than 100% whereas in the negative direction was greater than 120%.

No damage was recorded in the repaired segment of the column's shear span, aside from hairline cracks as can be seen in Figure 7-6. Plastic hinge localization was moved from the shear span into the joint (foundation/column connection) and occurred primarily in the form of strain penetration. Therefore, the increase in strength and ductility was not controlled by the UHPC-strengthened column, but by the joint's moment and rotation capacity, the latter of which was a function of pullout slip of the reinforcement from the foundation. The repair method, using UHPC, was successful in altering the failure mode from a semi-brittle shear failure/bond failure to a ductile flexural failure, however, in light of the pre-existing damage along the anchorages, a significant part of the existing compliance was not affected by the repair. Towards the end of the testing some slidding occurred along a concave cracked surface below the repaired length inside the footing which is depicted clearly in Fig. 7-4 (Right).

Figure 7-6. Final state of repaired columns after testing. S-20-Rep (left) and S-15-Rep (Right).

7.2.3. Tall Concrete Columns

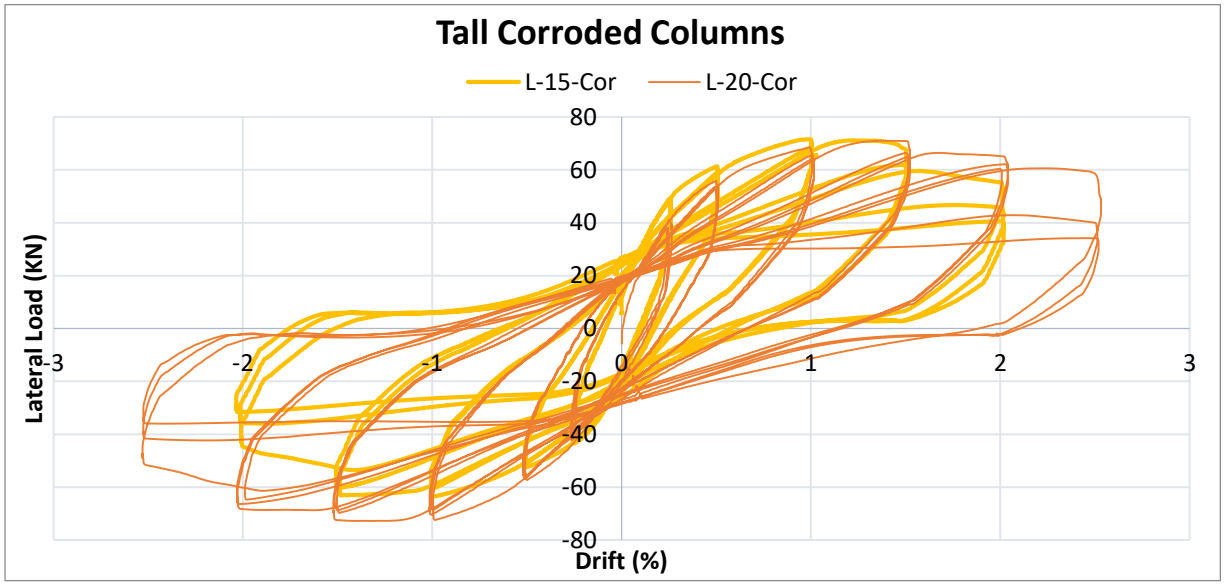

Figure 7-7. Hysteretic response of tall corroded columns

Axial load applied on the tall 15M columns was P = 270KN whereas the axial load applied on the tall 20M columns was P = 330KN. Figure 7-7 shows the hysteretic response of tall corroded columns. For column L-20-Cor, yield strength in the positive direction was V_y^+=57.5KN attained at a drift of θ_y^+= 0.55%, in the negative direction, the yield strength was V_y^-=-60KN attained at a drift of θ_y^- = -0.6%. Maximum lateral strength recorded in the positive direction was V_{max}^+=71KN attained at a drift of θ_{max}^+ = 1.3%, in the negative direction V_{max}^- = -72.8KN attained at θ_{max}^- = -1%. The ultimate drift in the positive direction was θ_u^+ = 2.5% whereas in the negative direction it was θ_u^-= -2.5%.

For column L-15-Cor , yield strength in the positive direction was V_y^+=59KN attained at a drift of θ_y^+ = 0.4%, in the negative direction, the yield strength was V_y^-=-51KN attained at a drift of θ_y^-= -0.5%. Maximum lateral strength recorded in the positive direction was V_{max}^+=71.5KN reached at a drift of θ_{max}^+ = 1%, in the negative direction V_{max}^- = -63.7KN attained at θ_{max}^- = -1%. The ultimate drift in the positive direction was θ_u^+ = 1.8% whereas in the negative direction it was θ_u^- = -1.6%.

Lateral strength in column L-20-Cor was maintained between cycles until reaching a drift of 2.5% where recorded drops in lateral strength reached 45%. Column L-15-Cor experienced a 30% drop in lateral strength between the first and third cycle at 2% drift whereas the drop in lateral capacity of column S-20-Cor at the same drift was only 8%.

L-20-Cor displayed a favorable behavior relative to column L-15-Cor by maintaining strength between cycles at similar drifts levels and by having a higher ultimate drift capacity.

Columns' behavior was predominantly controlled by flexural strength of the columns, however with increasing drift demand, bond became the controlling factor of the column's behavior and that is evident in the significant degradation in strength with increasing drift. This phenomenon was more obvious in the case of the 15M columns as opposed to the 20M columns, due to the higher bond strength that comes with larger bar sizes. Figure 7-8 shows the final state of the columns. It was noticed that flexural and shear cracks were limited in width with increasing drift demand. Pre-existing longitudinal cracks caused by corrosion were widening with increased drift, which explains why the flexural cracks were limited.

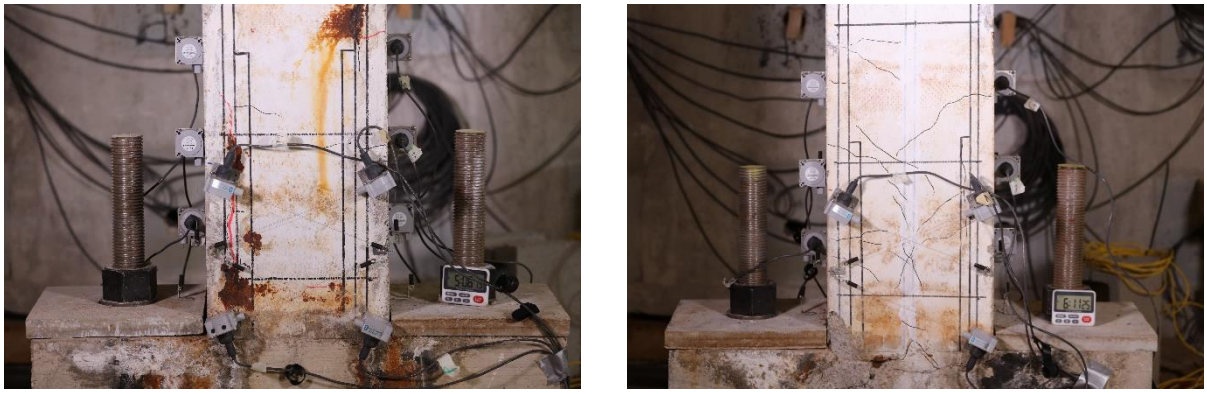

Figure 7-8. Final state of columns after testing. L-20-Cor (left) L-15-Cor (right).

7.2.4. Repaired and Retrofitted Tall Columns

Repaired tall columns, similar to the repaired short columns, showed a significant improvement in performance compared to corroded columns. It should be noted that, due to technical limitations, tall columns' imposed deformation was limited to 3.5% drift whereas the columns themselves were able to sustain higher deformations.

An increase in strength and ductility was recorded in repaired and retrofitted 15M and 20M columns (L-15-Rep, L-15-Str, L-20-Rep, L-20-Str). Tall repaired and strengthened columns, similar to short repaired columns, shifted the plastic hinge location from the base of the column into the column-footing joint, thus the strength of the column was governed by the moment capacity of the joint. That explains the high correlation shown in Figures 7-9 and 7-10 between hysteretic responses of L-15-Rep, L-15-Str, L-20-Rep, L-20-Str specimens.

Column L-20-Rep showed a 27% increase in yield strength in the positive direction, V_y^+=73KN from V_y^+=57.5KN and an increase of 32% in the negative direction V_y^-=-79KN from V_y^-=-60KN. The yield drifts also increased by 100% in the positive direction and 67% in the negative direction. An increase of 24% was recorded in the positive maximum lateral capacity, V_{max}^+=88KN from V_{max}^+=71KN and 28% in the negative direction V_{max}^-=-93KN from V_{max}^-=-73KN. While also increasing the drift at maximum load by 54% in the positive direction and 100% in the negative direction. Ultimate drift capacity also showed a significant improvement, in the positive direction the recorded increase was greater than 40% whereas in the negative direction was greater than 60%.

Column L-20-Str showed a 39% increase in yield strength in the positive direction, V_y^+=80KN from V_y^+=57.5KN and an increase of 27% in the negative direction V_y^-=-76KN from V_y^-=-60KN. The yield drifts also increased by 155% in the positive direction and 83% in the negative direction. An increase of 23% was recorded in the positive maximum lateral capacity, V_{max}^+=87.2KN from V_{max}^+=71KN and 27% in the negative direction V_{max}^-=-92.6KN from V_{max}^-=-73KN. While also increasing the drift at maximum load by 54% in the positive direction and 50% in the negative direction. Ultimate drift capacity also showed a significant improvement, in the positive direction the recorded increase was greater than 40% whereas in the negative direction was greater than

60%.

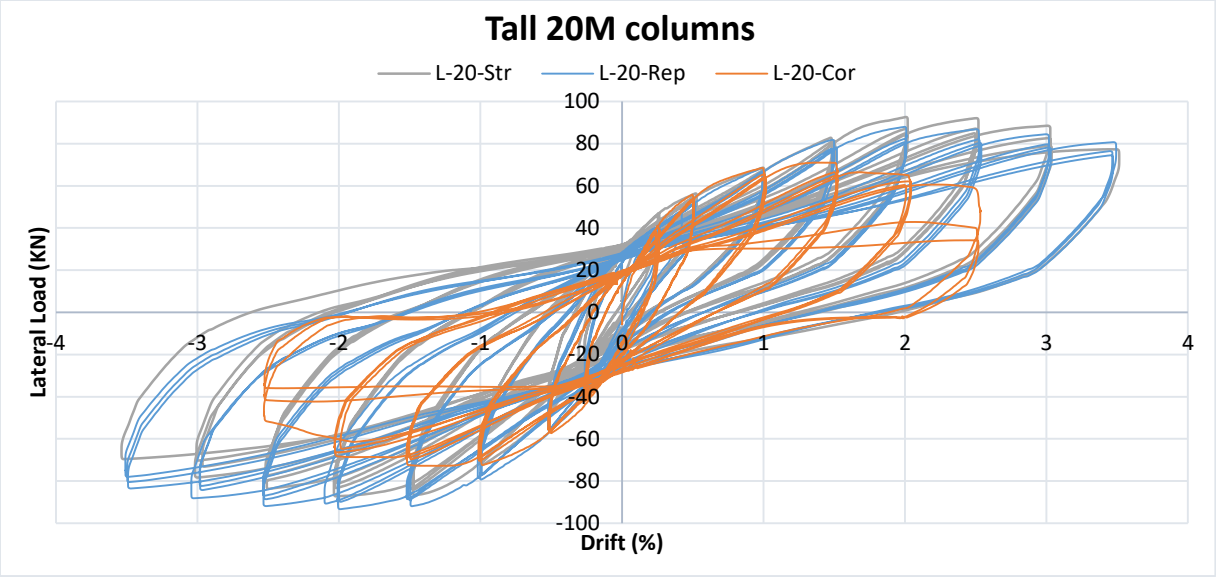

Figure 7-9. Hysteretic response of tall columns reinforced with 20M bars.

Column L-15-Rep showed a 37% increase in yield strength in both directions, V_y^+=81KN from V_y^+=59KN and V_y^-=-70KN from V_y^-=-51KN. The yield drifts also increased by 100% in the both directions. An increase of 35% was recorded in the positive maximum lateral capacity, V_{max}^+=96.5KN from V_{max}^+=71.5KN and 29% in the negative direction V_{max}^-=-82.2KN from V_{max}^-=-63.7KN. While also increasing the drift at maximum load by 54% in the positive direction and 100% in the negative direction. Ultimate drift capacity also showed a significant improvement, in the positive direction the recorded increase was greater than 94% whereas in the negative direction was greater than 119%.

Column L-15-Rep showed a 37% increase in yield strength in both directions, V_y^+=80KN from V_y^+=59KN and V_y^-=-70KN from V_y^-=-51KN. The yield drifts also increased by 100% in the positive direction and by 50% in the negative direction. An increase of 37% was recorded in the positive maximum lateral capacity, V_{max}^+=97.8KN from V_{max}^+=71.5KN and 32% in the negative direction V_{max}^-= -84.1KN from V_{max}^-= -63.7KN. While also increasing the drift at maximum load by 100% in the positive direction and 50% in the negative direction. Ultimate drift capacity also

showed a significant improvement, in the positive direction the recorded increase was greater than 94% whereas in the negative direction was greater than 119%.

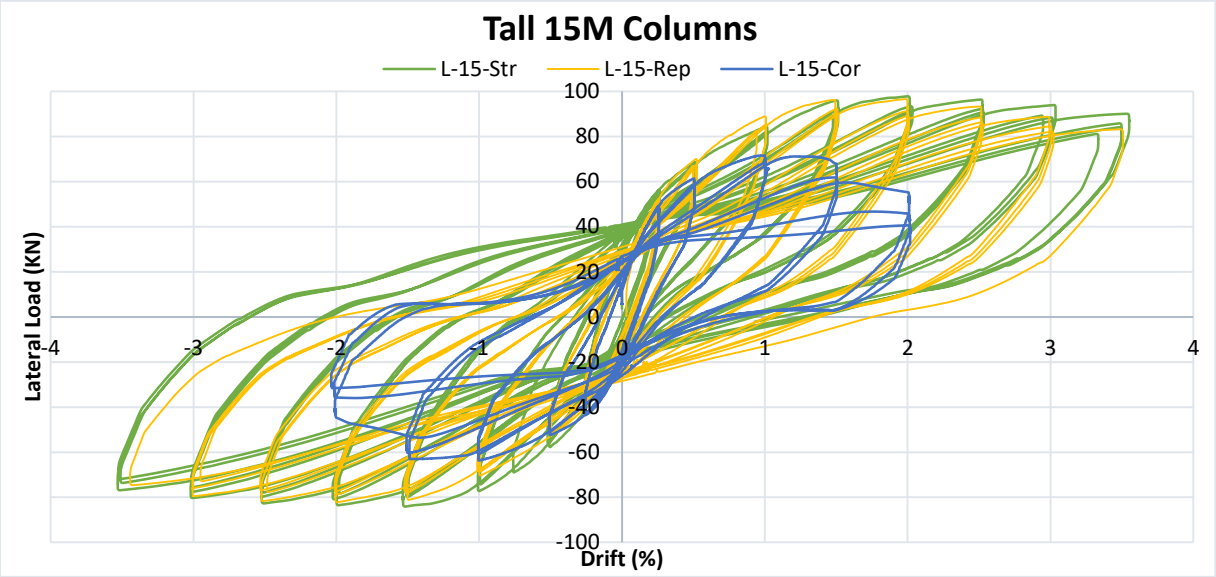

Figure 7-10. Hysteretic response of columns reinforced with 15M bars.

Figure 7-11 displays the final state of tall repaired and strengthened columns. Damage in the shear span was limited to hairline cracks whereas the footing experienced all the damage. Especially along the UHPC-Concrete interface.

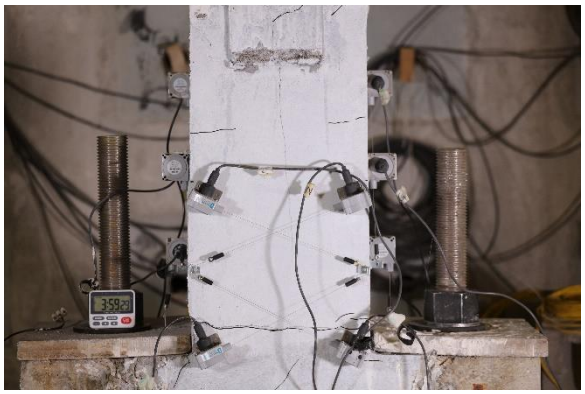

L-15-Rep

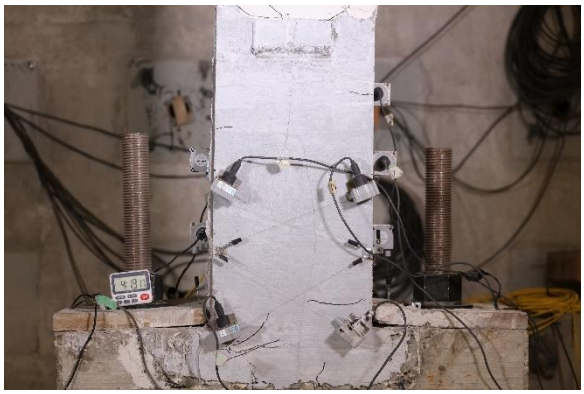

L-15-Str

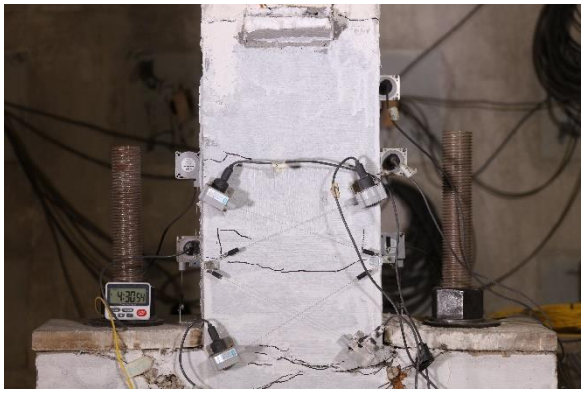

L-20-Rep

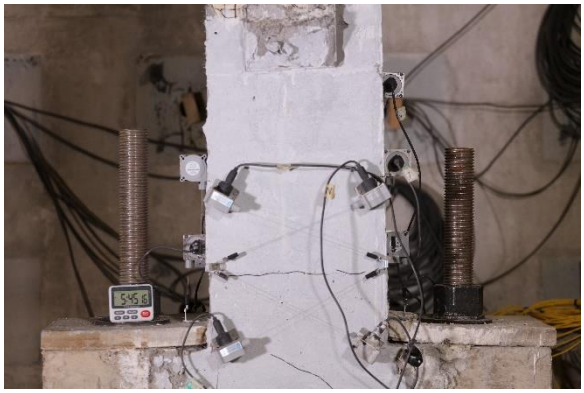

L-20-Str

Figure 7-11. Final state of tall repaired and strengthened columns.

Table 7-3. Mechanical properties of tested columns

	Yield Strength (KN)		*Yield Drift (%)*		*Maximum Strength (KN)*		*Maximum Drift (%)*		*Ultimate Drift (%)*	
ID	V_y^+	V_y^-	θ_y^+	θ_y^-	V_{max}^+	V_{max}^-	θ_{max}^+	θ_{max}^-	θ_u^+	θ_u^-
S-15-Cor	113	-111	0.8	-0.6	133.1	-129.9	1.5	-1.2	2	-1.8
S-15-Rep	133	-130	1.2	-0.7	153.2	-153.7	2	-1.5	>4	<-4
S-20-Cor	109	-106	0.55	-0.38	133.4	-128	1	-0.98	2.5	-2
S-20-Rep	140	-136	0.8	-0.9	163.6	-156.9	1.5	-2	4	-4
L-15-Cor	59	-51	0.4	-0.5	71.5	-63.7	1	-1	1.8	-1.6
L-15-Rep	81	-70	0.8	-1	96.5	-82.2	1.5	-2	>3.5	<-3.5
L-15-Str	80	-70	0.8	-0.8	97.8	-84.1	2	-1.5	>3.5	<-3.5
L-20-Cor	57.5	-60	0.55	-0.6	71	-72.8	1.3	-1	2.5	-2.2
L-20-Rep	73	-79	1.1	-1	87.93	-93.32	2	-2	>3.5	<-3.5
L-20-Str	80	-76	1.4	-1.1	87.24	-92.61	2	-1.5	3.5	-3.5

Table 7-4. Recorded increase (percent change) in strength and deformation capacity of tested columns

	ΔV_y (%)		$\Delta\theta_y$		ΔV_{max}		$\Delta\theta_{max}$		$\Delta\theta_u$	
ID	+	-	+	-	+	-	+	-	+	-
S-15-Cor	NA	NA	NA	NA	NA	NA	NA	NA	NA	NA
S-15-Rep	18%	17%	50%	17%	15%	18%	33%	25%	100%	122%
S-20-Cor	NA	NA	NA	NA	NA	NA	NA	NA	NA	NA
S-20-Rep	28%	28%	45%	137%	23%	23%	50%	104%	60%	100%
L-15-Cor	NA	NA	NA	NA	NA	NA	NA	NA	NA	NA
L-15-Rep	37%	37%	100%	100%	35%	29%	50%	100%	94%	119%
L-15-Str	36%	37%	100%	60%	37%	32%	100%	50%	94%	119%
L-20-Cor	NA	NA	NA	NA	NA	NA	NA	NA	NA	NA
L-20-Rep	27%	32%	100%	67%	24%	28%	54%	100%	40%	59%
L-20-Str	39%	27%	155%	83%	23%	27%	54%	50%	40%	59%

Table 7-3 documents key mechanical properties of the tested columns in both directions

7.3. Curvature Distribution in Columns

Curvature distribution was calculated using string pot instrumentation shown in Chapter 6. Measurements were taken in three intervals spaced at 15cm along the shear span of the columns. Curvature was calculated using Equation (7-1).

$$\phi = \frac{\Delta_t - \Delta_c}{h_c l_c} \tag{7-1}$$

Where ϕ is the curvature, Δ_t and Δ_c are the measured displacements by the string pots in the tensile and compressive zones respectively. h_c is the center to center horizontal distance between string pots and l_c is the vertical gauge length.

Figures 7-12 to 7-15 plot the curvature diagrams of the specimens along the height (450mm) where instrumentation was placed. The figures show the curvature profiles of columns before and after the repair, the strengthened columns' data was excluded to reduce the data clutter in the diagrams. Curvature diagrams are representative of two different drift levels, the first at drifts of ±0.5% and the second at drifts of ±2%. It should be noted that the curvature segment along the height from 0 to 150mm also includes the effect of reinforcement pull-out between the column and the foundation.

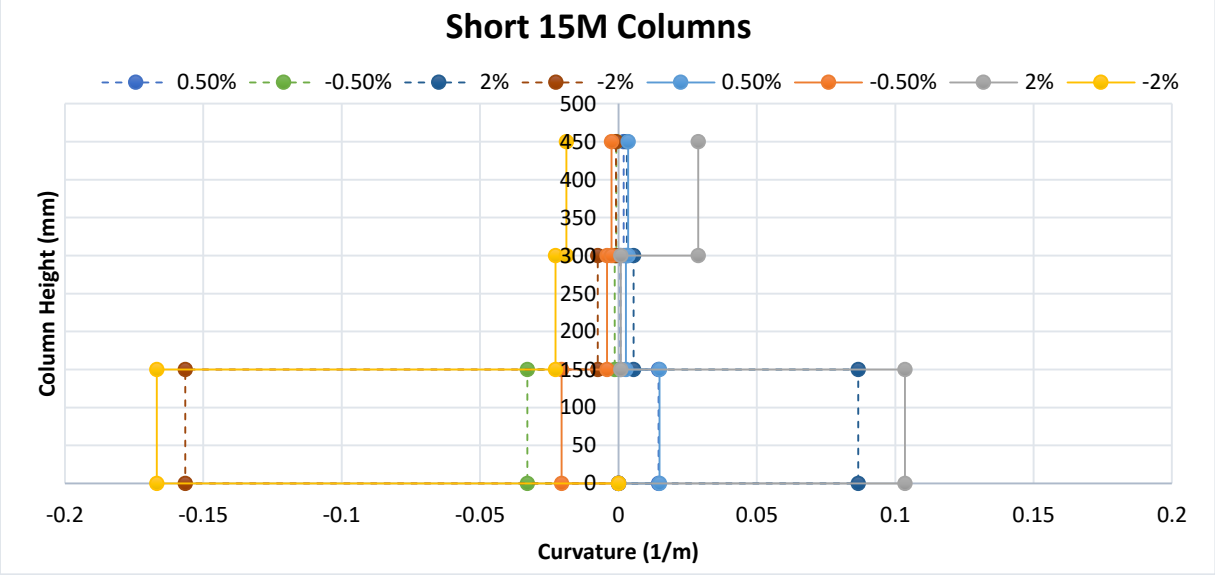

Figure 7-12. Curvature profile of columns S-15-Cor (straight lines) and S-15-Rep (Dashed lines)

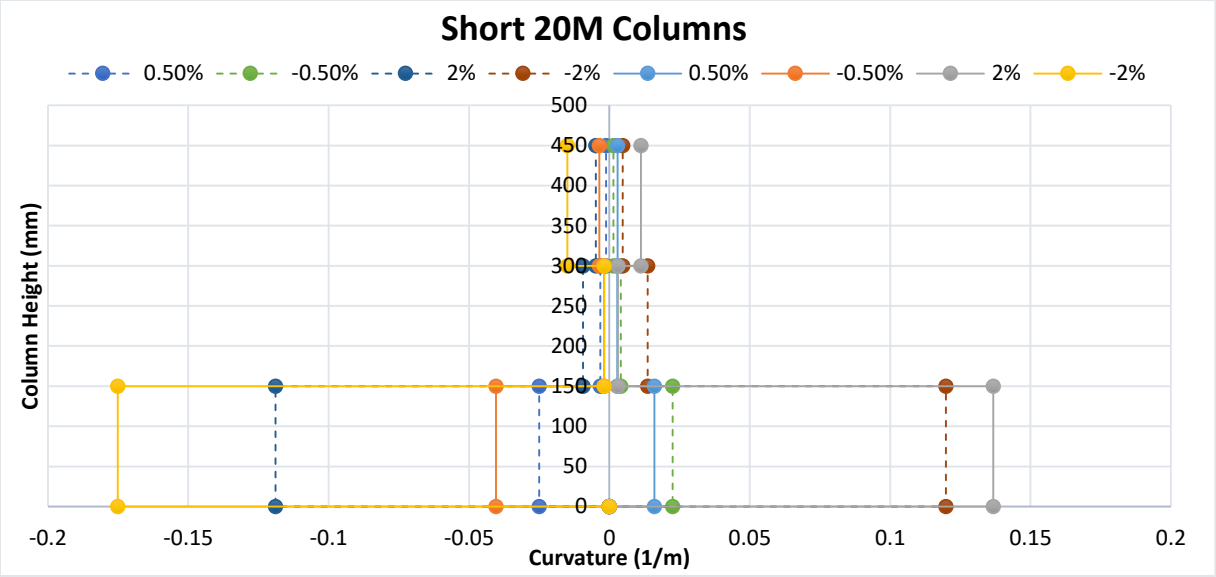

Figure 7-13. Curvature profile of columns L-20-Cor (straight lines) and L-20-Rep (Dashed lines)

Curvature diagrams for short columns pre-repair (straight lines) clearly capture the two failure modes experienced (see Figures 7-12 and 7-13). The negative drift region shows higher curvature as opposed to the positive drift region because the negative drift region experienced bond-failure whereas the positive drift region experienced shear failure which does not demand higher curvatures.

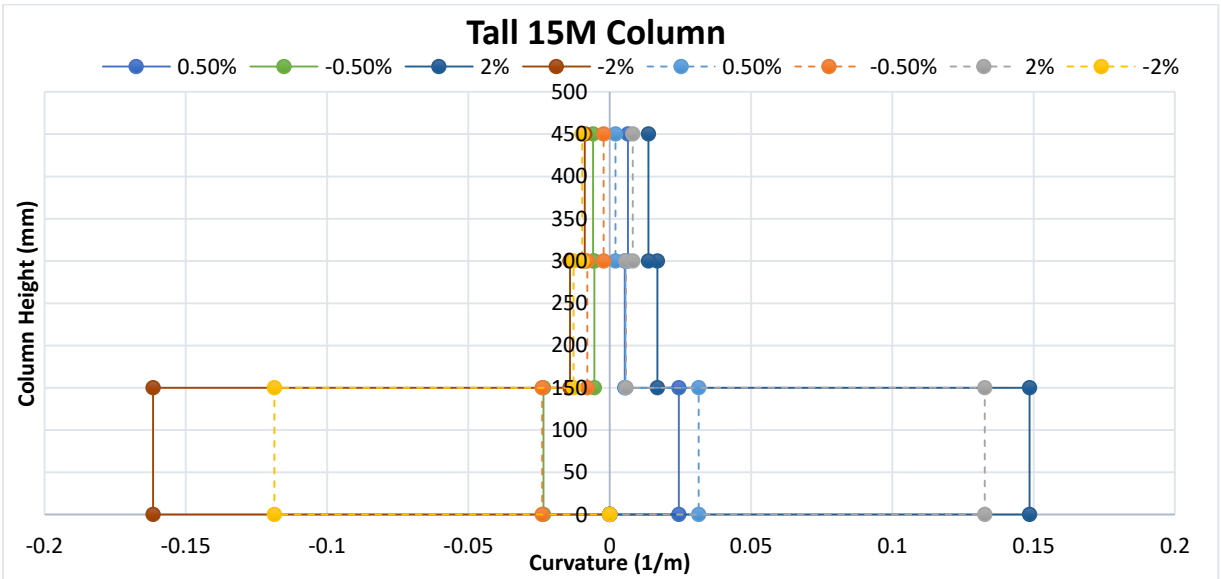

Figure 7-14. Curvature profile of columns L-15-Cor (straight lines) and L-15-Rep (Dashed lines)

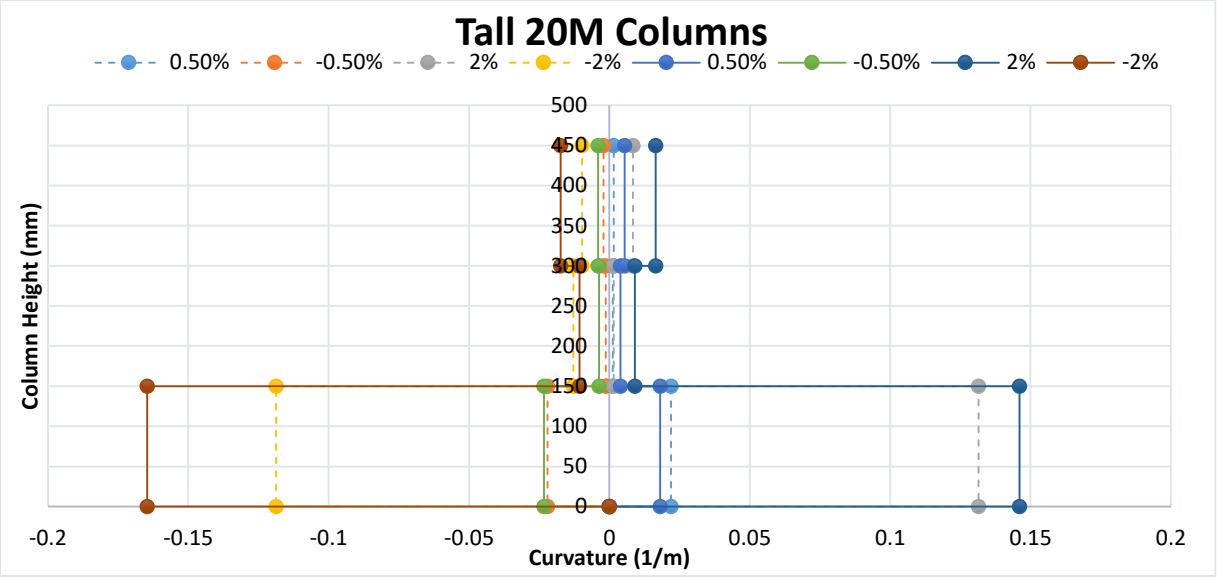

Figure 7-15. Curvature profile of columns S-20-Cor (straight lines) and S-20-Rep (Dashed lines)

Tall columns, unlike the short columns, symmetrical curvature profiles as can be seen in Figures 7-14 and 7-15. This is due to the fact that tall columns either failed in bond (concrete columns) or in flexure (repaired columns) both of which demand higher curvatures.

It can be observed that in all cases, at higher drift demands, curvature of repaired columns in the critical region was reduced. The reduction varied between 6 to 30% in the critical region, the middle region had alternating curvatures, where the repaired and concrete columns had close curvatures. In the region between the heights of 300mm and 450mm, the reduction in curvature was between 40% and 100%.

7.4. Shear-Strain Demand in Columns

Shear strains were calculated using measurements from string pots (XM, XN, XO and XP) shown in Chapter 6. The shear strain was calculated using Equation (7-2), from which the shear drift was calculated using Equation (7-3)

$$\varepsilon_{shear} = \frac{x_2 - x_1}{\sqrt{L_2^2 + L_1^2}} \tag{7-2}$$

Where x_1 and x_2 are diagonal measurements taken by linear string pots. L_1 and L_2 are the vertical and horizontal distanced respectively, between instruments. For a clearer understanding see Figure 7-16.

$$\theta_{shear} = \frac{\varepsilon_{shear} * L_1}{L_s} * 100 \quad (7\text{-}3)$$

Where ε_{shear} is the shear strain, L_1 is the vertical gauge length and L_s is the shear span. Using Equation (7-3) the shear drift in the two gauges was calculated, the first being $\theta_{shr,1}$ and the second being $\theta_{shr,2}$.

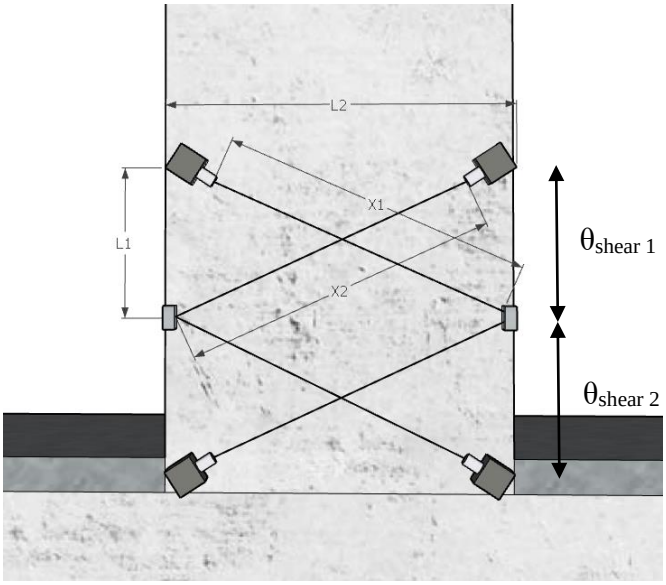

Figure 7-16. Instrumentation for shear strain measurements

The drift caused by shear $\theta_{shr,tot}$ is the summation of $\theta_{shr,1}$ and $\theta_{shr,2}$. Figure 7-17 plots the calculated shear drifts of the columns with increasing total drift demand. It should be noted that the data of column L-20-Cor was disregarded due to the poor quality of measurement during the testing of the said column.

Figure 7-17 plots the drift caused by shear with respect to the total applied drift on the columns. Dashed lines represent concrete columns (pre-repair) while straight lines represent repaired and strengthened columns. It can be observed, that un-strengthened specimens endured large shear drift demands as opposed to repaired and strengthened specimens. Column L-15-Rep had the largest shear drift amongst repaired/strengthened columns reaching a drift demand of 0.037% while the rest of the strengthened specimens had a maximum shear drift between 0.005% and 0.01%.

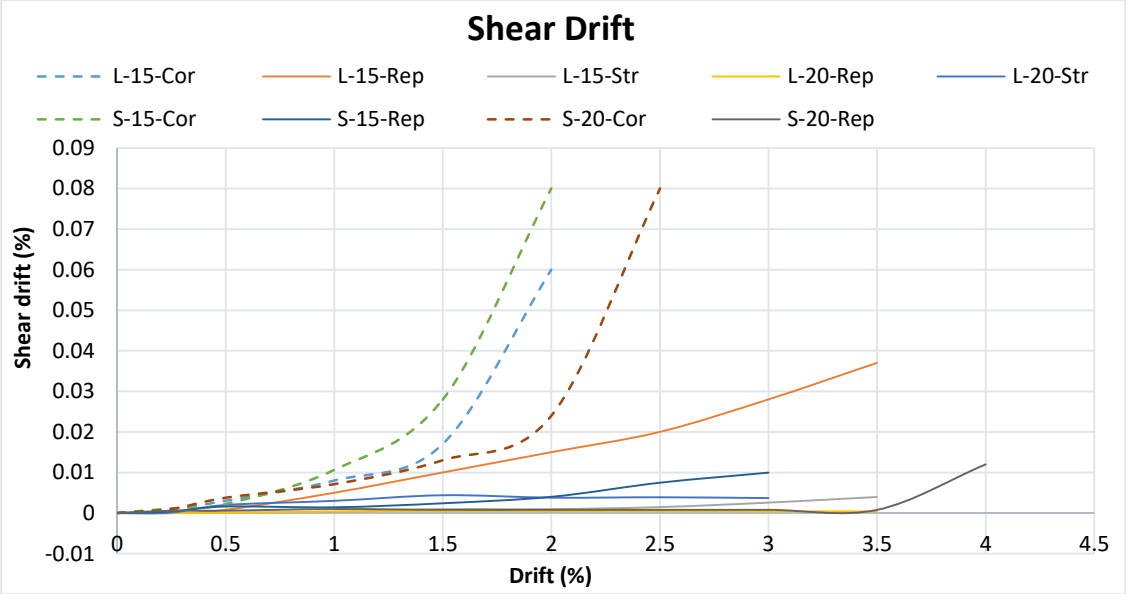

Figure 7-17. Shear drift of columns with increasing drift demand.

7.5. Conclusions

Six lap-spliced columns designed based on pre-1970s design standards were constructed having a lap length of $l_p = 24D_b$. Specimens underwent accelerated corrosion conditioning reaching a level of 5% mass loss according to Faraday's law. A portion of the specimens were subjected to cyclic loading prior to strengthening in order to simulate repairing seismically damaged columns post-earthquakes while the rest of the columns were strengthened prior to testing. The strengthening strategy implemented entails either completely replacing the core concrete with UHPC or only replacing the perimeter of the section at a specified depth making sure the reinforcement was embedded in UHPC. Conclusion drawn from this experiment are as follows:

- Pre-1970 design standards are not resilient to earthquake loading.
- UHPC jacketing by cover replacement improved the strength and ductility of the corroded columns.
- UHPC jacketing changed the failure mode from either shear failure or bond failure to a ductile flexural failure. However, at the point of termination of the repair jacket in the footing a sliding cradle developed at the interface with the existing concrete, where

significant amount of slippage of reinforcement from the previously damaged anchorage occurred, controlling the response at advanced levels of lateral drift.

- Complete removal of the concrete core did not have an improved performance compared to specimens with only the perimeter concrete removed.
- Repaired columns (post-earthquake) had an identical behavior to strengthened columns (pre-earthquake).
- UHPC cover replacement also showed a reduction in curvature in the strengthened segment of the columns.
- UHPC cover replacement significantly suppressed shear strain in the critical region.

7.6. References

ACI-374 (2016) *ACI 374 - Guide to Nonlinear Modeling Parameters for Earthquake-Resistant Structures*. Available at: www.concrete.org (Accessed: 27 March 2022).

ACI 222R-19 (2019) 'Guide to Protection of Reinforcing Steel in Concrete Against Corrosion', *American Concrete Institute*, pp. 1–65.

Al-Saidy, A. H. *et al.* (2016) 'Structural behavior of corroded RC beams with/without stirrups repaired with CFRP sheets', *Materials and Structures*. Springer Netherlands, 49(9), pp. 3733–3747. doi: 10.1617/s11527-015-0751-y.

Al-Sulaimani, G. J. *et al.* (1990) 'Influence of corrosion and cracking on bond behavior and strength of reinforced concrete members', *ACI Structural Journal*, 87(2), pp. 220–231. doi: 10.14359/2732.

Alaskar, A. (2013) 'Shear Behaviour of Slender RC Beams with Corroded Web Reinforcement'. University of Waterloo. Available at: https://uwspace.uwaterloo.ca/handle/10012/7472 (Accessed: 15 July 2019).

Allamt, I. M. *et al.* (1994) *Influence of atmospheric corrosion on the mechanical properties of reinforcing steel, Construction and Building Materials*.

Almusallam, A. A. *et al.* (1996) 'Effect of reinforcement corrosion on bond strength', *Construction and Building Materials*. Elsevier, 10(2), pp. 123–129. doi: 10.1016/0950-0618(95)00077-1.

Almusallam, A. A. (2001a) ‘Effect of degree of corrosion on the properties of reinforcing steel bars’, *Construction and Building Materials*. Elsevier, 15(8), pp. 361–368. doi: 10.1016/S0950-0618(01)00009-5.

Almusallam, A. A. (2001b) ‘Effect of degree of corrosion on the properties of reinforcing steel bars’, *Construction and Building Materials*. Elsevier, 15(8), pp. 361–368. doi: 10.1016/S0950-0618(01)00009-5.

Alonso, C. *et al.* (1998) ‘Factors controlling cracking of concrete affected by reinforcement corrosion’, *Materials and Structures*. Kluwer Academic Publishers, 31(7), pp. 435–441. doi: 10.1007/BF02480466.

American Road & Transportation Builders Association (2020) *ARTBA Bridge Report*. Available at: https://artbabridgereport.org/ (Accessed: 6 July 2020).

Amleh, L., Mirza, M. and Ahwazi, B. (2000) ‘Bond deterioration of reinforcing steel in concrete due to corrosion’. Available at: https://books.google.com/books?hl=en&lr=&id=F8HosZdH8BUC&oi=fnd&pg=PA247&ots=Iq_HHO_T-s&sig=3ytv3HtTEhxTvU9yTJRyH6PPLrk (Accessed: 5 July 2019).

Andrade, C., Alonso, M. C. and Gonzalez, J. A. (1990) ‘Initial effort to use the corrosion rate measurements for estimating rebar durability’, *ASTM Special Technical Publication*. ASTM International, (1065), pp. 29–37. doi: 10.1520/stp25013s.

Andrade, C. and González, J. A. (1978) ‘Quantitative measurements of corrosion rate of reinforcing steels embedded in concrete using polarization resistance measurements’, *Materials and Corrosion*, 29(8), pp. 515–519. doi: 10.1002/maco.19780290804.

Apostolopoulos, C. A. (2007) ‘Mechanical behavior of corroded reinforcing steel bars S500s tempcore under low cycle fatigue’, *Construction and Building Materials*. Elsevier, 21(7), pp. 1447–1456. doi: 10.1016/J.CONBUILDMAT.2006.07.008.

Apostolopoulos, C. A. and Papadakis, V. G. (2008) ‘Consequences of steel corrosion on the ductility properties of reinforcement bar’, *Construction and Building Materials*. Elsevier, 22(12), pp. 2316–2324. doi: 10.1016/J.CONBUILDMAT.2007.10.006.

Apostolopoulos, C., Drakakaki, A. and Basdeki, M. (2019) ‘Seismic assessment of RC column

under seismic loads', *International Journal of Structural Integrity*. Emerald Publishing Limited , 10(1), pp. 41–54. doi: 10.1108/IJSI-02-2018-0013.

ASCE 41 (2017) *Seismic Evaluation and Retrofit of Existing Buildings, Seismic Evaluation and Retrofit of Existing Buildings*. American Society of Civil Engineers. doi: 10.1061/9780784414859.

Azad, A. K., Ahmad, S. and Al-Gohi, B. H. A. (2010) 'Flexural strength of corroded reinforced concrete beams', *Magazine of Concrete Research*. Thomas Telford Ltd , 62(6), pp. 405–414. doi: 10.1680/macr.2010.62.6.405.

Berra, M., Castellani, A. and Coronelli, D. (1997) 'Bond in reinforced concrete and corrosion of bars', in *Structural Faults and Repair*. Edinburgh, UK, pp. 349–357.

Berrocal, C. G. *et al.* (2017) 'Corrosion-induced cracking and bond behaviour of corroded reinforcement bars in SFRC', *Composites Part B: Engineering*. Elsevier, 113, pp. 123–137. doi: 10.1016/J.COMPOSITESB.2017.01.020.

Blaber, J., Adair, & B. and Antoniou, & A. (no date) 'Ncorr: Open-Source 2D Digital Image Correlation Matlab Software'. doi: 10.1007/s11340-015-0009-1.

Cairns, J., Du, Y. and Law, D. (2008) 'Structural performance of corrosion-damaged concrete beams', *Magazine of Concrete Research*. Thomas Telford Ltd , 60(5), pp. 359–370. doi: 10.1680/macr.2007.00102.

Di Carlo, F., Meda, A. and Rinaldi, Z. (2017) 'Numerical cyclic behaviour of un-corroded and corroded RC columns reinforced with HPFRC jacket', *Composite Structures*. Elsevier, 163, pp. 432–443. doi: 10.1016/J.COMPSTRUCT.2016.12.038.

Castel, A., François, R. and Arliguie, G. (2000) 'Mechanical behaviour of corroded reinforced concrete beams—Part 1: Experimental study of corroded beams', *Materials and Structures*. Kluwer Academic Publishers, 33(9), pp. 539–544. doi: 10.1007/BF02480533.

CEN (2005) *EN 1998 - 3 Eurocode 8-Design of structures for earthquake resistance-Part 3: Assessment and retrofitting of buildings*.

Cervenka Consulting (2007) 'ATENA Program Documentation'. Prague, Czech Republic.

Civjan, S. A. *et al.* (2005) 'Effectiveness of corrosion inhibiting admixture combinations in structural concrete', *Cement and Concrete Composites*. Elsevier, 27(6), pp. 688–703. doi: 10.1016/J.CEMCONCOMP.2004.07.007.

Coronelli, D. and Gambarova, P. (2004) 'Structural Assessment of Corroded Reinforced Concrete Beams: Modeling Guidelines', *Journal of Structural Engineering*. American Society of Civil Engineers, 130(8), pp. 1214–1224. doi: 10.1061/(ASCE)0733-9445(2004)130:8(1214).

Coronelli, D., Hanjari, K. Z. and Lundgren, K. (2013) 'Severely Corroded RC with Cover Cracking', *Journal of Structural Engineering*, 139(2), pp. 221–232. doi: 10.1061/(ASCE)ST.1943-541X.0000633.

Dang, V. H. and François, R. (2013) 'Influence of long-term corrosion in chloride environment on mechanical behaviour of RC beam', *Engineering Structures*. Elsevier, 48, pp. 558–568. doi: 10.1016/j.engstruct.2012.09.021.

Darwin, D. and Pecknold, D. (1974) *INELASTIC MODEL FOR CYCLIC BIAXIAL LOADING OF REINFORCED CONCRETE*. Illinois, Urbana. Available at: https://www.semanticscholar.org/paper/INELASTIC-MODEL-FOR-CYCLIC-BIAXIAL-LOADING-OF-Darwin-Pecknold/5d1fb39809798f4c65b2dfa0fad5c06dd82e2a6f (Accessed: 20 July 2022).

Du, Y., Clark, L. A. and Chan, A. H. C. (2007) 'Impact of Reinforcement Corrosion on Ductile Behavior of Reinforced Concrete Beams', *ACI Structural Journal*, 104(3), pp. 285–293. doi: 10.14359/18618.

Du, Y. G., Clark, L. A. and Chan, A. H. C. (2005) 'Residual capacity of corroded reinforcing bars', *Magazine of Concrete Research*. Thomas Telford Ltd , 57(3), pp. 135–147. doi: 10.1680/macr.2005.57.3.135.

El-Joukhadar, N., Tsiotsias, K. and Pantazopoulou, S. (2019) 'Consideration of the state of corrosion in seismic assessment of columns', *International Journal of Structural Integrity*. Emerald Group Publishing Ltd. doi: 10.1108/IJSI-07-2019-0065.

Fakhri, H., Ragalwar, K. A. and Ranade, R. (2019) 'On the use of Strain-Hardening Cementitious Composite covers to mitigate corrosion in reinforced concrete structures',

Construction and Building Materials. Elsevier Ltd, 224, pp. 850–862. doi: 10.1016/j.conbuildmat.2019.07.052.

Fang, C. *et al.* (2004) 'Corrosion influence on bond in reinforced concrete', *Cement and Concrete Research*. Pergamon, 34(11), pp. 2159–2167. doi: 10.1016/J.CEMCONRES.2004.04.006.

Farhan, N. A., Sheikh, M. N. and Hadi, M. N. S. (2018) 'Experimental Investigation on the Effect of Corrosion on the Bond Between Reinforcing Steel Bars and Fibre Reinforced Geopolymer Concrete', *Structures*. Elsevier, 14, pp. 251–261. doi: 10.1016/J.ISTRUC.2018.03.013.

Fernandez, I. *et al.* (2018) 'Ultimate Capacity of Corroded Statically Indeterminate Reinforced Concrete Members', *International Journal of Concrete Structures and Materials*. Springer Singapore, 12(1), p. 75. doi: 10.1186/s40069-018-0297-9.

Fernandez, I., Bairán, J. M. and Marí, A. R. (2015) 'Corrosion effects on the mechanical properties of reinforcing steel bars. Fatigue and σ–ε behavior', *Construction and Building Materials*. Elsevier, 101, pp. 772–783. doi: 10.1016/J.CONBUILDMAT.2015.10.139.

Fernandez, I. and Berrocal, C. G. (2019) 'Mechanical Properties of 30 Year-Old Naturally Corroded Steel Reinforcing Bars', *International Journal of Concrete Structures and Materials*. Korea Concrete Institute, 13(1), p. 9. doi: 10.1186/s40069-018-0308-x.

Fernandez, I., Lundgren, K. and Zandi, K. (2018) 'Evaluation of corrosion level of naturally corroded bars using different cleaning methods, computed tomography, and 3D optical scanning', *Materials and Structures/Materiaux et Constructions*. Springer Netherlands, 51(3), pp. 1–13. doi: 10.1617/s11527-018-1206-z.

fib-Model Code (2020) 'Model Code 2020, Draft version MC2020', in. fib.

fib bulletin #10 (2000) *Bond of reinforcement in concrete : state-of-art report*. International Federation for Structural Concrete. Available at: https://www.fib-international.org/publications/fib-bulletins/bond-of-reinforcement-in-concrete-pdf-detail.html (Accessed: 3 July 2019).

fib Model Code (2010) *Fib model code for concrete structures 2010*.

Fischer, C., Ozbolt, J. and Gehlen, C. (2010) ‘Numerical investigation on bond behavior of corroded reinforcement’, in *7th International Conference on Fracture Mechanics of Concrete and Concrete Structures*. Jeju, Korea, pp. 779–785.

François, R. and Arliguie, G. (1998) ‘Influence of Service Cracking on Reinforcement Steel Corrosion’, *Journal of Materials in Civil Engineering*, 10(1), pp. 14–20. doi: 10.1061/(ASCE)0899-1561(1998)10:1(14).

François, R., Khan, I. and Dang, V. H. (2013) ‘Impact of corrosion on mechanical properties of steel embedded in 27-year-old corroded reinforced concrete beams’, *Materials and Structures*. Springer Netherlands, 46(6), pp. 899–910. doi: 10.1617/s11527-012-9941-z.

Fu, C. *et al.* (2017) ‘Corrosion characteristics of a 4-year naturally corroded reinforced concrete beam with load-induced transverse cracks’, *Corrosion Science*. Pergamon, 117, pp. 11–23. doi: 10.1016/J.CORSCI.2017.01.002.

Ganesh, P. and Ramachandra Murthy, A. (2020) ‘Simulation of surface preparations to predict the bond behaviour between normal strength concrete and ultra-high performance concrete’, *Construction and Building Materials*. Elsevier, 250, p. 118871. doi: 10.1016/J.CONBUILDMAT.2020.118871.

Gjørv, O. E. (2014) *Durability Design of Concrete Structures in Severe Environments*. CRC Press. doi: 10.1201/b16469.

Goksu, C. and Ilki, A. (2016) ‘Seismic Behavior of Reinforced Concrete Columns with Corroded Deformed Reinforcing Bars’, *ACI Structural Journal*, 113(5), pp. 1053–1064. doi: 10.14359/51689030.

Haddad, R. H. and Ashteyate, A. M. (2001) ‘Role of synthetic fibers in delaying steel corrosion cracks and improving bond with concrete’, *Canadian Journal of Civil Engineering*. NRC Research Press Ottawa, Canada , 28(5), pp. 787–793. doi: 10.1139/l01-037.

Hanjari, K. Z., Coronelli, D. and Lundgren, K. (2011) ‘Bond capacity of severely corroded bars with corroded stirrups’, *Magazine of Concrete Research*. Thomas Telford Ltd , 63(12), pp. 953–968. doi: 10.1680/macr.10.00200.

Harajli, M. H. (2004) ‘Comparison of Bond Strength of Steel Bars in Normal- and High-Strength

Concrete', *Journal of Materials in Civil Engineering*, 16(4), pp. 365–374. doi: 10.1061/(ASCE)0899-1561(2004)16:4(365).

Higgins, C. and Farrow, W. C. (2006) 'Tests of Reinforced Concrete Beams with Corrosion-Damaged Stirrups', *ACI Structural Journal*, 103(1), pp. 133–141. doi: 10.14359/15094.

Hou, L. *et al.* (2017) 'Effect of corrosion on bond behaviors of rebar embedded in ultra-high toughness cementitious composite', *Construction and Building Materials*. Elsevier, 138, pp. 141–150. doi: 10.1016/J.CONBUILDMAT.2017.02.008.

Hung, C. C., Lee, H. S. and Chan, S. N. (2019) 'Tension-stiffening effect in steel-reinforced UHPC composites: Constitutive model and effects of steel fibers, loading patterns, and rebar sizes', *Composites Part B: Engineering*. Elsevier Ltd, 158, pp. 269–278. doi: 10.1016/j.compositesb.2018.09.091.

Ioannou, A. *et al.* (2022) 'Experimental Testing of ECC Jackets for Repair of Pre-Damaged R . C . Members Experimental Testing of ECC Jackets for Repair of Pre-Damaged R . C . Members under Cyclic Loading', in *12th National Conference on Earthquake Engineering*. Salt Lake City, Utah: Earthquake Engineering Research Institute, pp. 1–5.

Kashani, M. M., Maddocks, J. and Dizaj, E. A. (2019) 'Residual Capacity of Corroded Reinforced Concrete Bridge Components: State-of-the-Art Review', *Journal of Bridge Engineering*, 24(7), p. 03119001. doi: 10.1061/(ASCE)BE.1943-5592.0001429.

Kondratova, I. L., Montes, P. and Bremner, T. W. (2000) 'Accelerated Corrosion Testing Results for Specimens Containing Uncoated Reinforcing Steel and Corrosion Inhibitors', *Special Publication*, 192, pp. 789–806. doi: 10.14359/5785.

Koulouris, K. and Apostolopoulos, C. (2020) 'An Experimental Study on Effects of Corrosion and Stirrups Spacing on Bond Behavior of Reinforced Concrete', *Metals*. MDPI AG, 10(10), p. 1327. doi: 10.3390/met10101327.

Lee, H. S. and Cho, Y. S. (2009) 'Evaluation of the mechanical properties of steel reinforcement embedded in concrete specimen as a function of the degree of reinforcement corrosion', in *International Journal of Fracture*. Springer, pp. 81–88. doi: 10.1007/s10704-009-9334-7.

Li, D. *et al.* (2018) 'Influence of Non-uniform corrosion of steel bars on the seismic behavior of

reinforced concrete columns', *Construction and Building Materials*. Elsevier, 167, pp. 20–32. doi: 10.1016/J.CONBUILDMAT.2018.01.149.

Li, J., Gong, J. and Wang, L. (2009) 'Seismic behavior of corrosion-damaged reinforced concrete columns strengthened using combined carbon fiber-reinforced polymer and steel jacket', *Construction and Building Materials*. Elsevier, 23(7), pp. 2653–2663. doi: 10.1016/J.CONBUILDMAT.2009.01.003.

Li, X. *et al.* (2016) 'Effect of loading rate on the bond behaviour of deformed steel bars in concrete subjected to lateral pressure', *Materials and Structures*. Springer Netherlands, 49(6), pp. 2097–2111. doi: 10.1617/s11527-015-0636-0.

Lijina, T. and Jithin, J. . (2018) 'Effect of Steel and Polypropylene Fibre on the Tension Stiffening of Ultra High Performance Concrete', *International Journal of Engineering and Advanced Technology (IJEAT)*, 8(4C).

Lin, H. *et al.* (2019) 'State-of-the-art review on the bond properties of corroded reinforcing steel bar', *Construction and Building Materials*. Elsevier, 213, pp. 216–233. doi: 10.1016/J.CONBUILDMAT.2019.04.077.

Liu, X. and Li, Y. (2018) 'Experimental study of seismic behavior of partially corrosion-damaged reinforced concrete columns strengthened with FRP composites with large deformability', *Construction and Building Materials*. Elsevier, 191, pp. 1071–1081. doi: 10.1016/J.CONBUILDMAT.2018.10.072.

Lu, C. *et al.* (2016) 'Mechanical properties of corroded steel bars in pre-cracked concrete suffering from chloride attack', *Construction and Building Materials*, 123(123), pp. 649–660. doi: 10.1016/j.conbuildmat.2016.07.032.

Ma, Y., Che, Y. and Gong, J. (2012) 'Behavior of corrosion damaged circular reinforced concrete columns under cyclic loading', *Construction and Building Materials*. Elsevier, 29, pp. 548–556. doi: 10.1016/J.CONBUILDMAT.2011.11.002.

El Maaddawy, T. A. and Soudki, K. A. (2003) 'Effectiveness of Impressed Current Technique to Simulate Corrosion of Steel Reinforcement in Concrete', *Journal of Materials in Civil Engineering*, 15(1), pp. 41–47. doi: 10.1061/(ASCE)0899-1561(2003)15:1(41).

Mangat, P. S. and Elgarf, M. S. (1999) ‘Bond characteristics of corrding reinforcement in concrete beams’, *Materials and Structures*. Kluwer Academic Publishers, 32(2), pp. 89–97. doi: 10.1007/BF02479434.

Mangat, Pritpal S. and Elgarf, M. S. (1999) ‘Flexural Strength of Concrete Beams with Corroding Reinforcement’, *ACI Structural Journal*, 96(1), pp. 149–158. doi: 10.14359/606.

Martín Pérez, B. M. (1999) *Service life modelling of R.C. highway structures exposed to chlorides*. University of Toronto. Available at: https://books.google.ca/books/about/Service_Life_Modelling_of_R_C_Highway_St.html?id=qQiGtgAACAAJ&redir_esc=y (Accessed: 14 February 2019).

Meda, A. *et al.* (2014) ‘Experimental evaluation of the corrosion influence on the cyclic behaviour of RC columns’, *Engineering Structures*. Elsevier, 76, pp. 112–123. doi: 10.1016/J.ENGSTRUCT.2014.06.043.

Mehta, P. K. (1991) ‘Durability of Concrete--Fifty Years of Progress?’, *Special Publication*, 126, pp. 1–32. doi: 10.14359/1998.

Menengotto, M. and Pinto, P. E. (1973) ‘Method o f Analysis for Cyclically Loaded Reinforced Concrete Plane Frames Including Changes in Geometry and Nonelastic Behavior of Elements under Combined Normal Force and Bending’, in *IABSE Symposium on Resistance and Ultimate Deformability of Structures Acted on*. Lisbon.

Molaioni, F., Carlo, F. Di and Rinaldi, Z. (2021) ‘Modelling Strategies for the Numerical Simulation of the Behaviour of Corroded RC Columns under Cyclic Loads’, *Applied Sciences 2021, Vol. 11, Page 9761*. Multidisciplinary Digital Publishing Institute, 11(20), p. 9761. doi: 10.3390/APP11209761.

Ou, Y.-C. and Chen, H.-H. (2014) ‘Cyclic Behavior of Reinforced Concrete Beams with Corroded Transverse Steel Reinforcement’, *Journal of Structural Engineering*, 140(9), p. 04014050. doi: 10.1061/(ASCE)ST.1943-541X.0000932.

Palsson, R. and Mirza, M. S. (2002a) ‘Mechanical response of corroded steel reinforcement of abandoned concrete bridge’, *ACI Structural Journal*, 99(2), pp. 157–162. doi: 10.14359/11538.

Palsson, R. and Mirza, M. S. (2002b) ‘Mechanical Response of Corroded Steel Reinforcement of

Abandoned Concrete Bridge', *ACI Structural Journal*, 99(2), pp. 157–162. doi: 10.14359/11538.

Pantazopoulou, S. J. *et al.* (2001) *REPAIR OF CORROSION-DAMAGED COLUMNS WITH FRP WRAPS, JOURNAL OF COMPOSITES FOR CONSTRUCTION*. Available at: http://pubs.asce.org/copyright (Accessed: 23 July 2019).

Pantazopoulou, S. J. *et al.* (2019) 'The performance of corroded lap splices in reinforced concrete beams', *Corrosion Reviews*. De Gruyter, 37(1), pp. 31–44. doi: 10.1515/corrrev-2017-0086.

Papakonstantinou, C. G., Balaguru, P. N. and Auyeung, Y. (2011) 'Influence of FRP confinement on bond behavior of corroded steel reinforcement', *Cement and Concrete Composites*. Elsevier, 33(5), pp. 611–621. doi: 10.1016/J.CEMCONCOMP.2011.02.006.

Pardalopoulos, S. I., Pantazopoulou, S. J. and Lekidis, V. A. (2017) 'Simplified method for rapid seismic assessment of older R.C. buildings'. doi: 10.1016/j.engstruct.2017.10.052.

Pardalopoulos, S. I., Pantazopoulou, S. J. and Lekidis, V. A. (2018) 'Simplified method for rapid seismic assessment of older R.C. buildings', *Engineering Structures*. Elsevier Ltd, 154, pp. 10–22. doi: 10.1016/j.engstruct.2017.10.052.

Pardalopoulos, S. J., Thermou, G. E. and Pantazopoulou, S. J. (2013) 'Screening criteria to identify brittle R.C. structural failures in earthquakes', *Bulletin of Earthquake Engineering*, 11(2), pp. 607–636. doi: 10.1007/s10518-012-9390-7.

Parulekar, Y. M. *et al.* (2020) 'Performance Assessment of Corroded Reinforced Concrete Structure Considering Bond Deterioration', *Journal of Performance of Constructed Facilities*. American Society of Civil Engineers, 34(2), p. 04020009. doi: 10.1061/(ASCE)CF.1943-5509.0001411.

Paul, Suvash CZijl, G. Van (2014) 'Cracked and uncracked SHCC specimens under different exposure conditions', in *Strain Hardening Cementitious Composites 3 (SHCC3)*. Dordrecht, pp. 25–32.

Pourbaix, M. (1974) *Atlas of electrochemical equilibria in aqueous solutions*. National Association of Corrosion Engineers. Available at: https://books.google.ca/books?id=iiLRvQEACAAJ&dq=9780915567980&hl=en&sa=X&ved=0

ahUKEwivreD28rfgAhVi6IMKHQm4Dn4Q6AEIKjAA (Accessed: 12 February 2019).

Prieto, M., Tanner, P. and Andrade, C. (2011) 'Bond response in structural concrete with corroded steel bars. experimental results', *RILEM Bookseries*. Springer, Dordrecht, 5, pp. 231–241. doi: 10.1007/978-94-007-0677-4_16.

Rajput, A. S. and Sharma, U. K. (2018) 'Corroded reinforced concrete columns under simulated seismic loading', *Engineering Structures*. Elsevier, 171, pp. 453–463. doi: 10.1016/J.ENGSTRUCT.2018.05.097.

Raza, S. *et al.* (2019) 'Strengthening and Repair of Reinforced Concrete Columns by Jacketing: State-of-the-Art Review', *Sustainability*. MDPI AG, 11(11), p. 3208. doi: 10.3390/su11113208.

Robuschi, S. *et al.* (2020) 'Bond of naturally corroded, plain reinforcing bars in concrete', *Structure and Infrastructure Engineering*. Taylor and Francis Ltd., pp. 1–17. doi: 10.1080/15732479.2020.1768273.

Rodriguez, J. and Ortega, J. C. (1994) 'Corrosion of reinforcing bars and service life of reinforced concrete structures: corrosion and bond deterioration', in *International Conference on Concrete across Borders*. Odense, Denmark, pp. 315–326.

Semendary, A. A. and Svecova, D. (2020) 'Factors affecting bond between precast concrete and cast in place ultra high performance concrete (UHPC)', *Engineering Structures*. Elsevier, 216, p. 110746. doi: 10.1016/J.ENGSTRUCT.2020.110746.

Sezen, H. and Moehle, J. P. (2004) 'Shear Strength Model for Lightly Reinforced Concrete Columns', *Journal of Structural Engineering*. American Society of Civil Engineers, 130(11), pp. 1692–1703. doi: 10.1061/(ASCE)0733-9445(2004)130:11(1692).

Soudki, K. and Sherwood, T. (2003) 'Bond Behavior of Corroded Steel Reinforcement in Concrete Wrapped with Carbon Fiber Reinforced Polymer Sheets', *Journal of Materials in Civil Engineering*, 15(4), pp. 358–370. doi: 10.1061/(ASCE)0899-1561(2003)15:4(358).

Stanish, K., Hooton, R. D. and Pantazopoulou, S. J. (1999) 'Corrosion Effects on Bond Strength in Reinforced Concrete', *ACI Structural Journal*, 96(6), pp. 915–921. doi: 10.14359/765.

Suffern, C., El-Sayed, A. and Soudki, K. (2010) 'Shear strength of disturbed regions with

corroded stirrups in reinforced concrete beams', *Canadian Journal of Civil Engineering*, 37(8), pp. 1045–1056. doi: 10.1139/L10-031.

Takuya, K., Ryuta, I. and Masayuki, T. (2020) 'Prediction of Hydrogen Embrittlement of Reinforcing Steel Bars in Concrete Poles | NTT Technical Review', *NTT Technical Review*, 18(11). Available at: https://www.ntt-review.jp/archive/ntttechnical.php?contents=ntr202011ra1.html (Accessed: 16 April 2022).

Tastani, S. P. and Pantazopoulou, S. J. (2007) 'Behavior of Corroded Bar Anchorages', *ACI Structural Journal*, 104(6), pp. 756–766. doi: 10.14359/18958.

Tastani, S. and Pantazopoulou, S. J. (2005) 'Recovery of seismic resistance in corrosion-damaged reinforced concrete through FRP jacketing', *International Journal of Materials and Product Technology*, 23(3/4), p. 389. doi: 10.1504/IJMPT.2005.007737.

Tayeh, B. A., Abu Bakar, B. H. and Megat Johari, M. A. (2013) 'Characterization of the interfacial bond between old concrete substrate and ultra high performance fiber concrete repair composite', *Materials and Structures/Materiaux et Constructions*. Springer, 46(5), pp. 743–753. doi: 10.1617/S11527-012-9931-1/FIGURES/13.

Tepfers, R. (1979) 'Cracking of concrete cover along anchored deformed reinforcing bars', *Magazine of Concrete Research*. Thomas Telford Ltd , 31(106), pp. 3–12. doi: 10.1680/macr.1979.31.106.3.

Tondolo, F. (2015) 'Bond behaviour with reinforcement corrosion', *Construction and Building Materials*. Elsevier, 93, pp. 926–932. doi: 10.1016/J.CONBUILDMAT.2015.05.067.

Torres-Acosta, A. A., Navarro-Gutierrez, S. and Terán-Guillén, J. (2007) 'Residual flexure capacity of corroded reinforced concrete beams', *Engineering Structures*. Elsevier, 29(6), pp. 1145–1152. doi: 10.1016/J.ENGSTRUCT.2006.07.018.

Tuutti, K. (1982) *Corrosion of steel in concrete*. Swedish Cement and Concrete Research Institute, Stockholm. Available at: https://portal.research.lu.se/portal/en/publications/corrosion-of-steel-in-concrete(e97795b5-7f3a-4994-8beb-9438f5a51571).html (Accessed: 6 July 2020).

Valikhani, A. *et al.* (2020) 'Experimental evaluation of concrete-to-UHPC bond strength with correlation to surface roughness for repair application', *Construction and Building Materials*.

Elsevier, 238, p. 117753. doi: 10.1016/J.CONBUILDMAT.2019.117753.

Vecchio, F. J. and Collins, M. P. (1986) 'MODIFIED COMPRESSION-FIELD THEORY FOR REINFORCED CONCRETE ELEMENTS SUBJECTED TO SHEAR.', *Journal of the American Concrete Institute*, 83(2), pp. 219–231. doi: 10.14359/10416.

Vu, N. S. and Li, B. (2018) 'Seismic Performance of Flexural Reinforced Concrete Columns with Corroded Reinforcement', *ACI Structural Journal*, 115(5), pp. 1253–1266. doi: 10.14359/51702372.

Vu, N. S., Yu, B. and Li, B. (2016) 'Prediction of strength and drift capacity of corroded reinforced concrete columns', *Construction and Building Materials*. Elsevier, 115, pp. 304–318. doi: 10.1016/J.CONBUILDMAT.2016.04.048.

Wang, L. *et al.* (2015) 'Effects of stirrup and inclined bar corrosion on shear behavior of RC beams', *Construction and Building Materials*. Elsevier, 98, pp. 537–546. doi: 10.1016/J.CONBUILDMAT.2015.07.077.

Xia, J., Jin, W. and Li, L. (2011) 'Shear performance of reinforced concrete beams with corroded stirrups in chloride environment', *Corrosion Science*. Pergamon, 53(5), pp. 1794–1805. doi: 10.1016/J.CORSCI.2011.01.058.

Xu, S. L. and Cai, X. H. (2010) *Bond behavior of corroded reinforcing bar and ultra high toughness cementitious composites (UHTCC)*. Available at: https://framcos.org/FraMCoS-7/06-04.pdf (Accessed: 8 July 2019).

Yang, S.-Y. *et al.* (2016) 'Experimental research on hysteretic behaviors of corroded reinforced concrete columns with different maximum amounts of corrosion of rebar', *Construction and Building Materials*. Elsevier, 121, pp. 319–327. doi: 10.1016/J.CONBUILDMAT.2016.06.002.

Yuan, W., Guo, A. and Li, H. (2017) 'Experimental investigation on the cyclic behaviors of corroded coastal bridge piers with transfer of plastic hinge due to non-uniform corrosion', *Soil Dynamics and Earthquake Engineering*. Elsevier, 102, pp. 112–123. doi: 10.1016/J.SOILDYN.2017.08.019.

Zhang, R., Castel, A. and François, R. (2009) 'The corrosion pattern of reinforcement and its influence on serviceability of reinforced concrete members in chloride environment', *Cement*

and Concrete Research. Pergamon, 39(11), pp. 1077–1086. doi: 10.1016/J.CEMCONRES.2009.07.025.

Zhang, W. *et al.* (2012) 'Tensile and fatigue behavior of corroded rebars', *Construction and Building Materials*. Elsevier, 34, pp. 409–417. doi: 10.1016/J.CONBUILDMAT.2012.02.071.

Zhao, Y. *et al.* (2013) 'Bond behaviour of normal/recycled concrete and corroded steel bars', *Construction and Building Materials*. Elsevier, 48, pp. 348–359. doi: 10.1016/J.CONBUILDMAT.2013.06.091.

Zhu, W. *et al.* (2013) 'Effect of corrosion of reinforcement on the mechanical behaviour of highly corroded RC beams', *Engineering Structures*. Elsevier, 56, pp. 544–554. doi: 10.1016/J.ENGSTRUCT.2013.04.017.

Zhu, W. and François, R. (2014) 'Experimental investigation of the relationships between residual cross-section shapes and the ductility of corroded bars', *Construction and Building Materials*, 69(69), pp. 335–345. doi: 10.1016/j.conbuildmat.2014.07.059.

Van Zijl, G. P. A. G. *et al.* (2012) 'Durability of strain-hardening cement-based composites (SHCC)', *Materials and Structures/Materiaux et Constructions*. Springer, 45(10), pp. 1447–1463. doi: 10.1617/s11527-012-9845-y.

8. Finite Element Analysis of Columns

The reinforcement in the tests was corroded, therefore, it was not possible to attach strain gauges along the length of bars so as to study the behavior in detail within the critical regions. Yet, it is important to obtain insights regarding the response of the column pointwise in order to better understand the effectiveness of the retrofitting approach that has been tested in the experimental investigation. Detailed behavior of the specimens can be explored and better understood with the help of nonlinear finite element simulation, provided that the global response characteristics and damage patterns are reproduced successfully. In this chapter, results from finite element analysis of the tested lap-spliced columns are correlated with calculated values obtained from detailed modeling, and subsequently analyzed to understand critical variables such as the spread of strain penetration and the definition of plastic hinge in the presence of UHPC jacketing. The modeling framework developed in Chapter 3 to model corroded columns was implemented in the present investigation to also model the specimens of the experimental program, using the finite element software GiD and ATENA Studio. However, an additional section was included, in order to develop the data and corroborate modeling of the UHPC-Concrete interface.

8.1. UHPC-Concrete Interface Failure envelope.

Interaction at the interface between the roughened concrete surface (after knocking off of the cracked cover) and the casted jacket occurs mostly by friction under the normal confining pressure exerted by the jacket on the encased core. Past work has illustrated that the source of that confining pressure as illustrated in Figure 8-1 is owing to the postcracking tensile strength of the UHPC jacket (see for example, Ioannou *et al.,* (2022) who observed similar action in an ECC jacket application over conventional concrete). Some cohesion also exists between the concrete and the jacket, however its magnitude is negligible – this was confirmed through tension tests on the interface. To better understand and quantify the interface properties between UHPC and concrete, a small experimental investigation was carried out and is presented in the following sections. A Mohr-Coulomb type of failure envelope was calibrated with the experimental results and was subsequently implemented in the finite element model in order to better simulate the jacketing function.

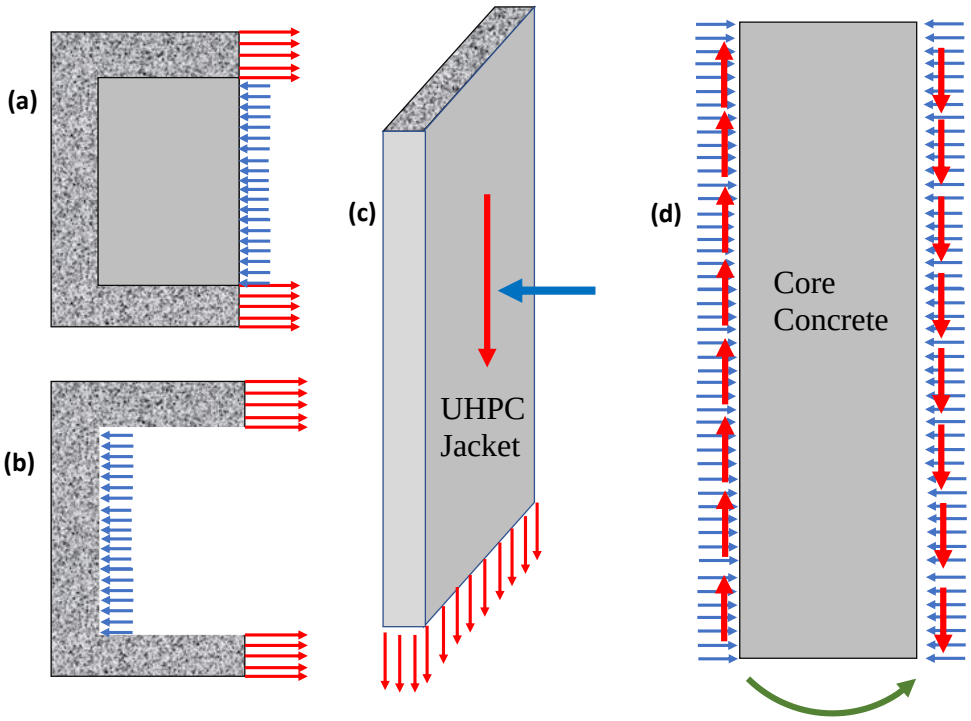

Figure 8-1. Function of the jacket - concrete interface, transferring forces between the UHPC shell and the encased core: Normal pressure at the interface enables mechanical interlock and frictional action.

8.1.1. Material Properties:

Normal Concrete (NC) was cast in the lab having the mix proportions as shown in Table 8-1. The proportions are given in content ratio by weight. For example, for 1Kg of cement, 0.79kg of water was added, with 2.5kg of coarse aggregates and 3.1 kg of fine aggregates. The compressive strength of concrete at the day of testing was 24 MPa.

Table 8-1. Normal concrete mix proportions

	Water	**Cement**	**Coarse Aggregates**	**Fine Aggregates**
Content Ratio	0.79	1	2.5	3.1

The UHPC material was made using the same prepackaged material that was also used throughout the experimental programs of the present thesis (Densit Inducast TT-5®). The mix proportions are given in Chapter 4. At the day of testing, the UHPC material had a compressive strength of 165 MPa measured on 75 mm x 150 mm cylinders and a tensile strength of 10 MPa measured on prismatic specimens (25 mm x 50 mm prisms under direct tension).

8.1.2. Specimens

To study the interaction at the interface, a series of slanted shear tests were conducted on specially fabricated prismatic specimens, which contained an interface plane at an angle with respect to the longitudinal axis of the prisms. Thus, each prism contained normal concrete in 50% of its volume. After casting normal concrete in the prismatic molds that were open at the top up to midheight, and while the concrete was fresh, the specimens were placed on shelves having three different inclinations to the horizontal plane so as to generate a free surface at an angle with the longitudinal axis. The concrete portions of the specimens were cured for 28 days. The free surface was then roughened with a maximum depth of 2mm as seen in Figure 8-2 and cleaned using pressurized air. Then the molds were filled with UHPC, this time standing on flat ground so that the free surface at the top of the mold would be horizontal and the resulting specimen would be a prism having cross sectional dimensions of 100 mm x 100 mm and a varying height depending on the angle of inclination of the interface. Prior to casting the UHPC, the roughened surfaces of the concrete were sprayed with water so as to increase the bonding strength between the two materials.

Angles of inclination considered were, (30˚, 45˚ and 60˚), in order to produce an adequate number of normal stress vs shear stress pairs at failure so as to support the derivation of a failure criterion. The collection of specimens also included tensile splitting tests along the interface. Specimens used for tension were 100x100x100mm cubes where half of the material was UHPC and the other half was normal concrete (NC); the latter material was cast first, and then the mold was laid flat on ground in order to generate a free surface at 90^{o} with respect to the side of the specimens. Figure 8-3 illustrates the different variations in specimens made. Three specimens of each variation were fabricated.

Figure 8-2. Interface surface prior to UHPC addition

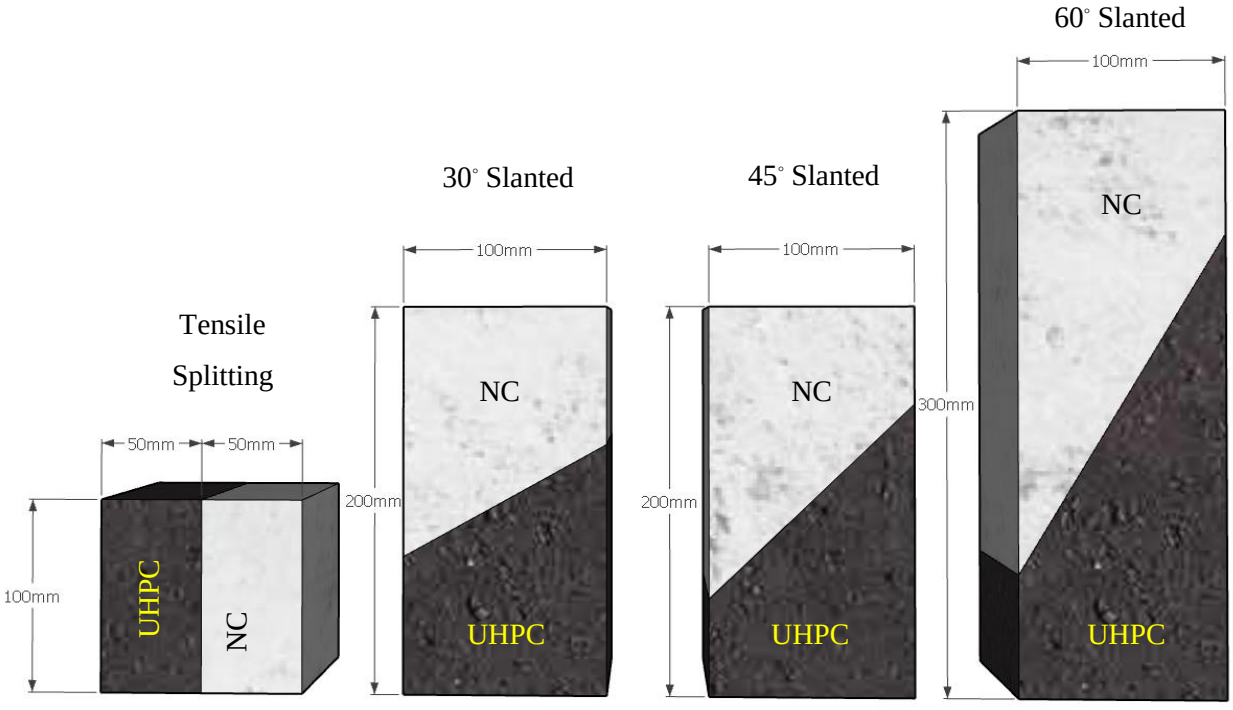

Figure 8-3. Slanted shear test and tensile splitting test specimens

8.1.3. Testing and Results

Slanted shear and splitting tensile specimens were tested under uni-axial compression loading. Analysis of the data is shown in Figure 8-4, test setup of both slanted shear tests and splitting tensile tests are shown in Figure 8-5 and the test results are given in Table 8-2.

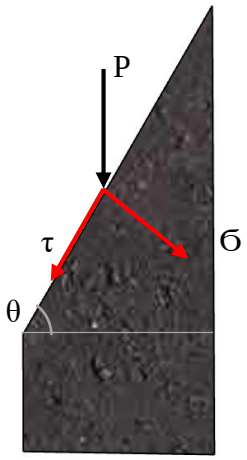

Figure 8-4. Free body diagram of a sample specimen.

The normal stresses were calculated using Equation 8-1 and the shear stresses were calculated using Equation 8-2.

$$б = \frac{P}{A}(\cos\theta)^2 \tag{8-1}$$

$$\tau = \frac{P}{A}\cos\theta\sin\theta \tag{8-2}$$

Where P is the applied load in KN, A is the cross sectional area of the specimen and θ is the angle between the inclined plane and the horizontal.

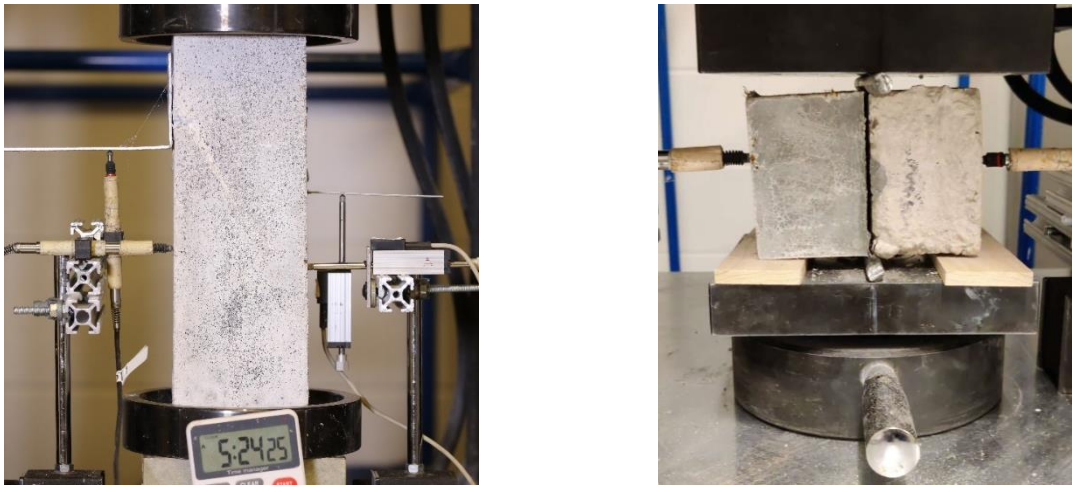

a) Slanted Shear Test b) Splitting Tensile Test

Figure 8-5. Test setup for slanted shear tests (a) and splitting tensile tests (b).

Results are summarized in Table 8-2. It is noted that in all cases failure occurred either at the interface or inside the normal concrete part of the specimen. For this reason, all values were

normalized with respect to the compressive strength of normal concrete, (f'_c = 24 MPa) and then plotted in Figure 8-6. The trend line of the data points shown defines the envelope of the normal and shear stress combinations at the point of prism failure (attainment of peak load). It should be noted that the sign convention used assumes negative values for compression and positive values for tension.

Table 8-2. Slanted shear and splitting tensile test results

		V_{max} (KN)	**Shear Stress τ (MPa)**	**Normal Stress σ (MPa)**
30 Degree Slant	Sample 1	209	9.06	15.7
	Sample 2	212	9.18	15.9
	Sample 3	206	8.92	15.45
	Average	209	9.06	15.68
45 Degree Slant	Sample 1	194	9.7	9.7
	Sample 2	203	10.15	10.15
	Sample 3	191	9.55	9.55
	Average	196	9.8	9.8
60 Degree Slant	Sample 1	154	6.68	3.83
	Sample 2	NA	NA	NA
	Sample 3	147	6.38	3.65
	Average	150.5	6.5	3.74
Splitting Tensile	Sample 1	15	0	0.95
	Sample 2	17	0	1.08
	Sample 3	15.4	0	0.98
	Average	15.8	0	1

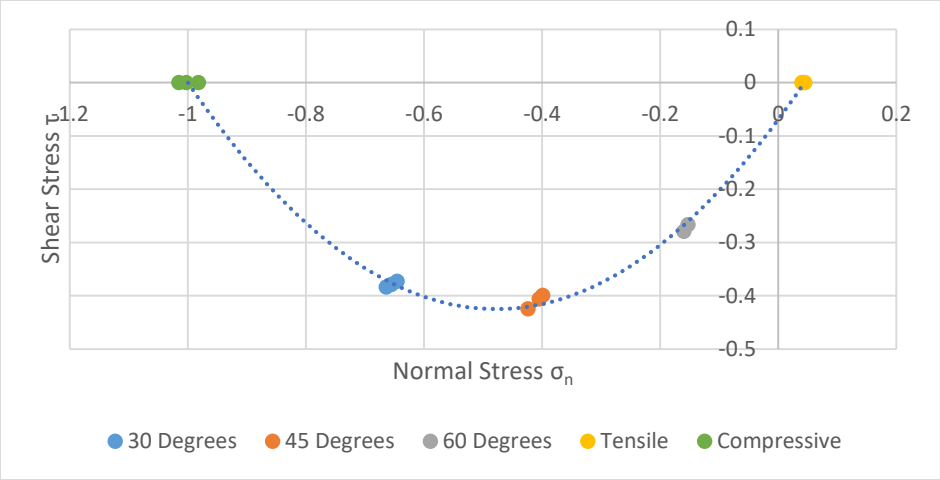

Figure 8-6. Failure envelope of UHPC-NC interface strength of current experiment.

Results of slanted shear, pure shear and splitting tests obtained from the literature (Tayeh, Abu Bakar and Johari, 2013; Ganesh and Murthy, 2020; Semendary and Svecova, 2020; Valikhani *et al.*, 2020) were added to this experimental investigation's database for verification of the findings. Figure 8-7 plots the additional data points to the previously shown data given in Figure 8-6. Using the experimental results an expression for the envelope in the normal stress – shear stress space was drawn, as shown by the dashed line in Figure 8-6, described by Equation (8-3).

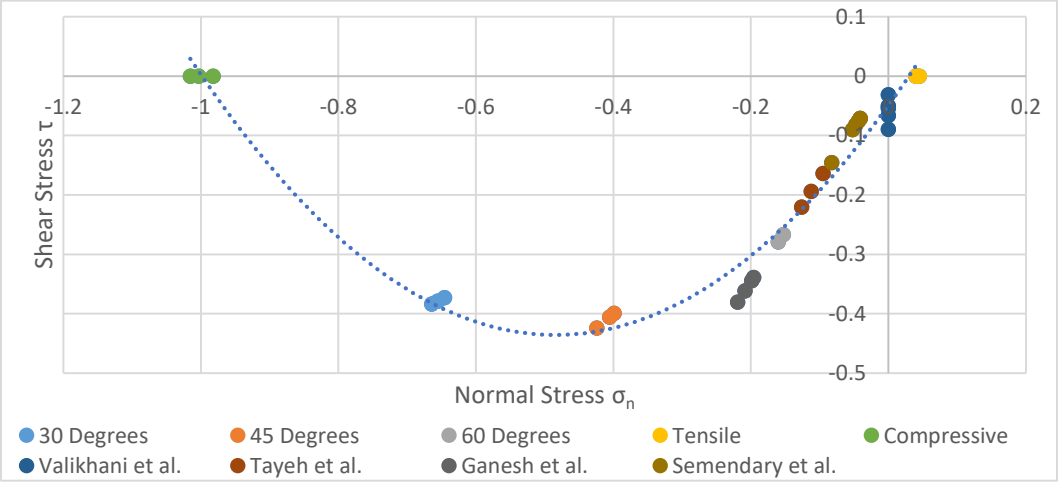

Figure 8-7: Failure envelope of UHPC-NC interface including experimental data from the literature.

$$\frac{\tau}{f_c'} + 0.05 = 1.65\frac{\sigma_n}{f_c'}\left(\frac{\sigma_n}{f_c'} + 1\right) \tag{8-3}$$

Equation 8-3 is a frictional, Mohr-Coulomb type of failure criterion for the interface interaction between normal concrete and UHPC material. As was explained earlier, the criterion is expressed in terms of the compressive strength of the concrete. This τ-σ_n failure envelope will be used in subsequent sections for modeling the interface between UHPC and NC of the tested columns.

8.2. Modeling and Material Selection

A typical FE model of a tall column is shown in Figure 8-8, developed in ATENA-DIC. Specimen Models were discretized into several macro elements in order to assign different material properties or different mesh sizes to the various parts of the column. Taking advantage of symmetry of the cross section in the transverse direction of the typical specimen (i.e. x-z is the plane of symmetry, at y=0), only half of the cantilever cross section was modeled, with the boundary condition that $u_y(x,0,z)=0$. All nodes on the bottom surface of the foundation were restrained from vertical movement ($u_z(x,y,0)=0$). A 50 mm thick plate was used at the top of the cantilever cross section to apply the axial force in the form of distributed constant vertical pressure. Two additional 50 mm thick plates were used at the front and back sides of the column to apply the lateral displacement at the centroid. These auxiliary elements were assigned "3D Elastic Isotropic" steel material, fully bonded on the column at the loading point, in order to enable more uniform spreading of the load in the contact surfaces and to avoid local convergence problems.

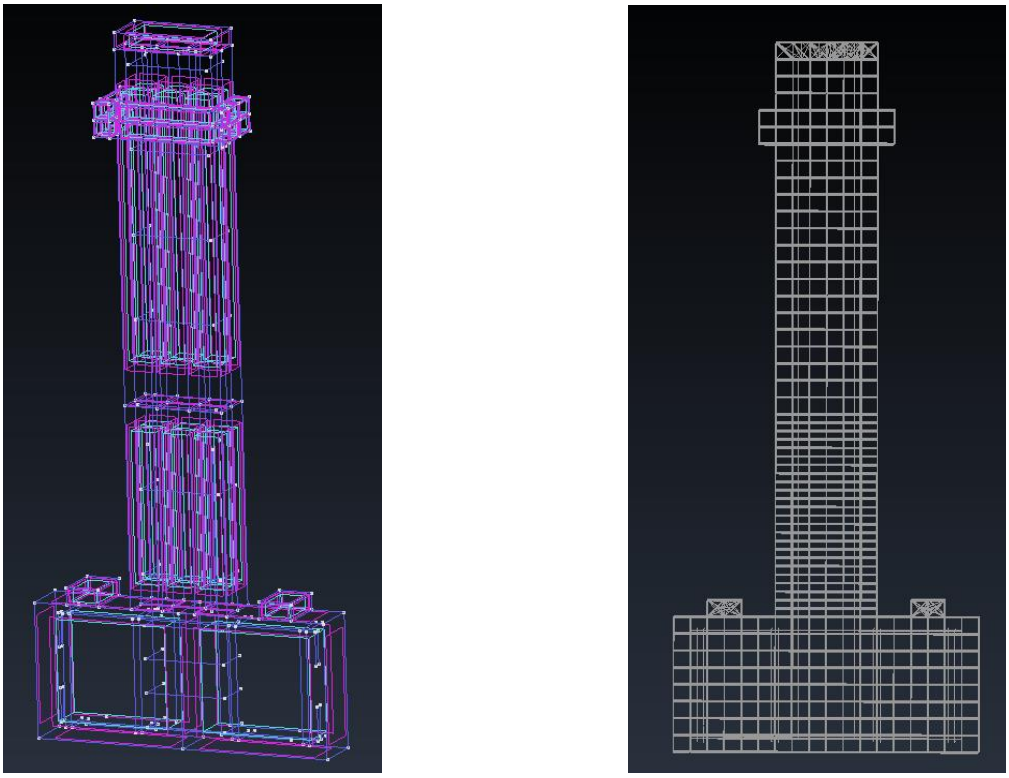

Figure 8-8. Standard finite element model. Column macro elements (left). Column mesh (right).

The column was meshed using 25 mm hexahedral elements for the first 0.5 m for the shear span length where severe inelasticity was expected; the remainder of the shear span was discretized into 50 mm elements. This mesh arrangement was the result of several trials and was used for the main part of the study because it was found to be most efficient discretization in terms of granularity in the results and computational time demand.

The concrete material model implemented in the simulation was "3D Nonlinear Cementitious2", where the biaxial strength failure envelope under plane stress was specified in the input. In this model, the nonlinearity of concrete is dependent on the equivalent uniaxial strain ε^{eq} (a concept originally proposed by Darwin and Pecknold, (1974)). The equivalent uniaxial strain is defined as the strain that is produced by the stress σ_{ci} in a uniaxial test with the modulus E_{ci} in the direction i ($\varepsilon^{eq} = \sigma_{ci}/E_{ci}$). The complete equivalent uniaxial stress-strain diagram for concrete is shown in Chapter 3, Figure 3-7. Concrete compressive strength f_c' of each column was assigned accordingly, whereas tensile strength f_t was taken equal to be 10% of the compressive strength. The concrete fracture energy, *GF*, was determined based on the Model Code 2010 expression: $GF = 73 \cdot (f_c')^{0.18}$. A fully rotated crack model was used, where the axis of the principal stress and principal strain

coincided throughout loading and crack formation in the model, which led to eliminating the development of shear strains along the crack plane. The degradation from the elastic slope in the unloading branch from the compression stress-strain envelope was controlled by the unloading factor f_U which in the model was taken equal to 0.1. This factor ranges between 0-0.99, where 0 corresponds to unloading to the origin while 0.99 corresponds to concrete unloading parallel to the initial stiffness as was explained in Chapter 3, Figure 3-7. Reinforcing bars were modelled as truss elements using the "Cyclic Reinforcement" option, using a *bilinear-with-hardening* type of uniaxial stress-strain behavior, having a steel elastic modulus E_s equal to 200,000 MPa. The rest of the reinforcement input parameters are listed in Table 7-1 of Chapter 7.

Reinforcement bars were investigated during the concrete replacement process discussed in Section 6.6 of Chapter 6. It had been found that, due to the placement of the bars in the lap-splice zone, corrosion did not develop in the contact between reinforcement bars, but rather, it occurred at the reinforcement surfaces that were closest to the exposed concrete surface as is shown in Figure 8-9. Thus, the effects of corrosion were not represented in modeling the bond stress-strain relationship of reinforcement. It was also found that there was no significant corrosion damage in the starter bars extending from the footing. Instead, the corrosion damage predominantly occurred in the reinforcement extending into the shear span. Thus, the reinforcement material properties of the starter bars inside the footing were not modified from their original reference values.

In order to account for the effects of corrosion, several interventions were made in the nonlinear model of the column. Therefore, the reinforcement material properties of reinforcement extending into the shear span were modified according to Equations (3-2, 3-3 and 3-4). Note that bar diameters for both ties and longitudinal reinforcement were not reduced in the model because the effective reduction in bar strength due to corrosion was already accounted for in Equations (3-2, 3-3 and 3-4). The Menegotto-Pinto model (Menengotto and Pinto, 1973) with a Bauschinger R value = 7, C_1 value = 5000 and C_2 value = 20 were used to model the hysteretic response of the reinforcement using Equations(3-8 to 3-11).

Figure 8-9. Reinforcement condition during inspection after concrete removal.

Bond material connecting the steel nodes with spatially coincident nodes in the concrete was assigned to the main reinforcement using the "Bond for Reinforcement" model. Here, the part of reinforcement anchored inside the support footing was considered in perfect contact with the concrete and in pristine condition, for the initial phase of loading of the columns. For the reinforcement in the deformable part of the member, the bond stress-slip law was modelled according to the Model Code 2010, where bond strength of the longitudinal bars was governed by splitting failure. Thus, it was assumed that the corroded columns' bond strength was governed by splitting failure due to pre-existing cover cracking resulting from corrosion accumulation. It should be noted that during the calibration phase of the model, the bond law had the greatest influence in the results and in reproducing the observed behavior of the column. A thorough sensitivity analysis was performed in order to obtain the bond stress-slip relationship adopted in the models.

Figure 8-10 depicts the assumed bond-slip envelopes for longitudinal reinforcement in concrete columns (L-15-Cor and L-20-Cor), where it is illustrated that the peak and degraded values depend on the degree of corrosion. It is noted that the bond model adopted for modeling reinforcement in the shear span has a reduced peak strength and a shallow slope. It was assumed so because the reinforcement in the shear span suffered from corrosion and had spalled the concrete cover, a fact that renders the bond stress-slip behavior more flexible. Alternatively, the starter bars being protected by the reinforcement in the shear span and being deeper into the section, had a stiffer initial slope in their bond stress-slip envelope.

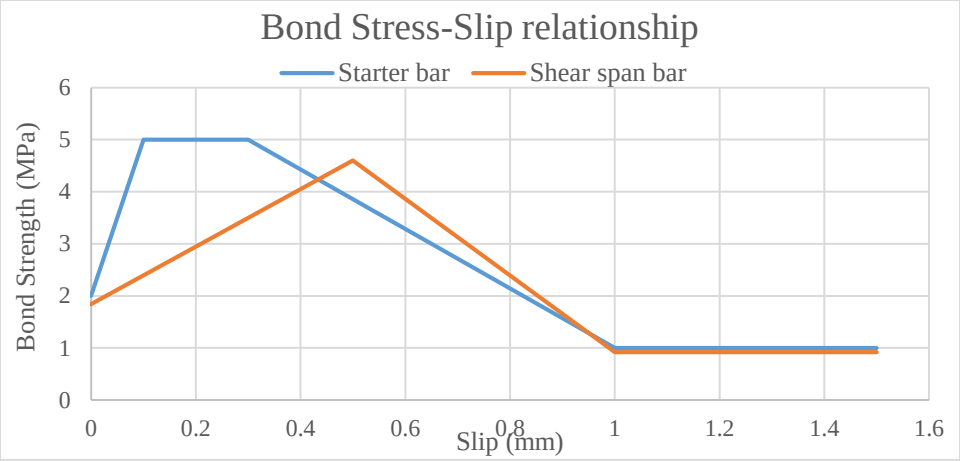

Figure 8-10. Bond stress-slip relationship of starter bars and extension bars in concrete columns.

The bond-slip relationship adopted for the same reinforcement when embedded in the UHPC cover replacing jacket is shown in Figure 8-11.

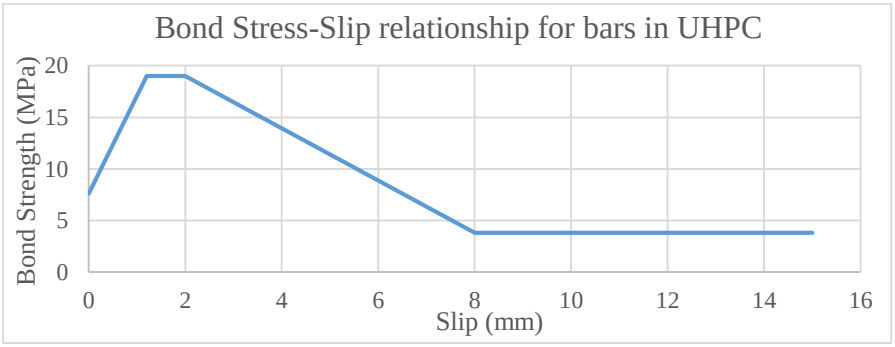

Figure 8-11. Bond stress-slip relationship of reinforcement embedded in UHPC

Concrete cover cracking was accounted for by reducing the compressive and tensile strengths of the concrete cover material; thus, compressive strength was reduced according to Equation (3-6) whereas the tensile strength of normal concrete was assumed to be entirely lost (i.e., neglected).

The Newton-Raphson method was adopted amongst the solution parameters of the analysis with an iteration limit of 200. Band width optimization method was chosen to be 'Sloan' with the stiffness type being 'Elastic Predictor'. The solver used was 'LU' with specific conditional break criteria as recommended by the program.

8.3. Simulation Results and Discussion

8.3.1. Comparison of Calculated and Experimental Hysteretic Responses

Resistance curves obtained from the finite element analysis are shown in Figure 8-13 and are compared with the experimental results that were presented in Chapter 7. The lateral resistance loads for both the experimental results and the numerical results were corrected to account for the P-Δ effect contributed by the applied axial load, so as to eliminate the phenomenological lateral degradation owing to second order effects and the lateral load contribution of the axial load. It is noted that second order effects occur both in the simulation and in the experiment, but they are not mutually equivalent. The values of the lateral resistance load calculated with the finite element model were corrected based on Equation 3-12, since the vertical load produces second order moments with respect to the column base, as it follows the top section of the cantilever model during lateral displacement. At the same time, and with the purpose of taking into account the second order effects on the experimentally tested columns, it was determined that the measured lateral resistance ought to be enhanced so as to account for an additional component contributed by the inclined piston which did not stay vertical during testing, but pivoted with respect to its point of attachment at its upper pin, as it followed the lateral displacement at the top of the cantilever specimen, as shown in Figure 8-12. Therefore, the experimental lateral resistance values were corrected according to Equation 8-4.

$$V_{res} = V_{exp} + P \cdot \theta \cdot \cos\theta + P \cdot sin\theta \quad (8\text{-}4)$$

Figure 8-12. Test setup adopted in the experimental program

Based on the obtained responses, it was concluded that the numerical models were able to replicate with sufficient accuracy the behavior of the experimentally tested columns. Some minor divergences were observed as follows: In the case of specimens L-15-Cor and L-20-Cor, the unloading path of the numerical models did not exhibit early, as was seen in the experiment, the horizontal dragging of the hysteretic loops in the range of low loads (around zero) which is a hallmark of bond degradation. The models eventually successfully replicated the bond-failure in columns L-15-Cor and L-20-Cor at the corresponding drift levels 2% and 2.5% respectively, but relatively later than what was observed and without the evidence of strong pinching. This might be improved with modifications to the residual bond strength of reinforcement. The unloading path of L-15-Str and L-20-Str was much closer to the experiment, since jacketing enabled full bond recovery. One limitation faced while modeling was not being able to model the pre-existing longitudinal cracks in the concrete columns caused by reinforcement corrosion. This limitation affected the cracking pattern of the concrete columns. The finite element analysis showed longitudinal cracking caused by bond failure along the out-of-plane face of the column whereas in the experiments, the longitudinal cracks were along the orthogonal face. Aside from this limitation, the model was able to reproduce a very similar behavior of that of the experiments.

The models of the strengthened columns also successfully replicated the hysteretic behavior of the tested columns, which is a critical attribute for the relevance and quality of the correlation**.** However, in this case, the numerical results showed increased initial stiffness compared to the

experimental results. This discrepancy was also found in a similar study by (Di Carlo, Meda and Rinaldi, 2017), but its magnitude is within the order of experimental error observed in tests of identical specimens, and in this light, the correlation is deemed satisfactory.

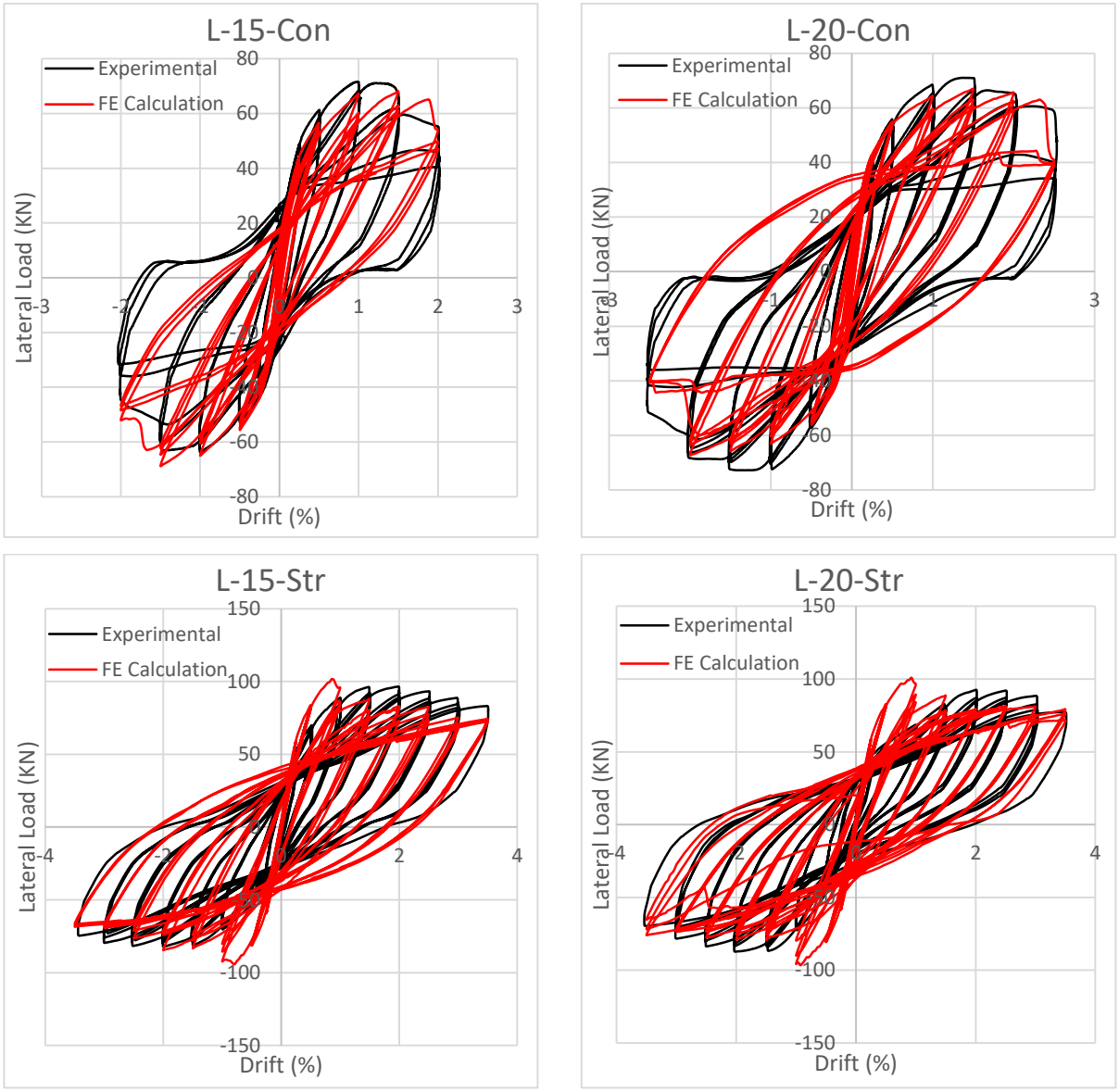

Figure 8-13. Hysteretic response comparison between experimental and numerical results

8.3.2. Cracking Patterns and Concrete Strain Distribution

As was discussed in the previous section, Concrete columns (L-15-Cor and L-20-Cor) exhibited longitudinal cracking along the out-of-plane face of the column while the longitudinal cracking in

the experimental tests was localized along the orthogonal face due their pre-existence from the corrosion conditioning phase. This bias is also responsible for the reduced amount of bond-failure related pinching in the hysteresis loops discussed earlier.

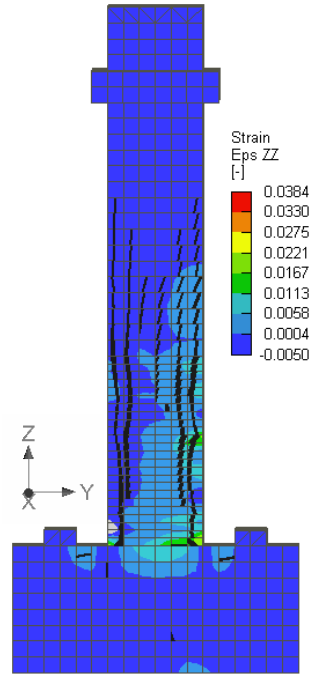

a) ε_{zz} strain of L-15-Cor at 2% Drift

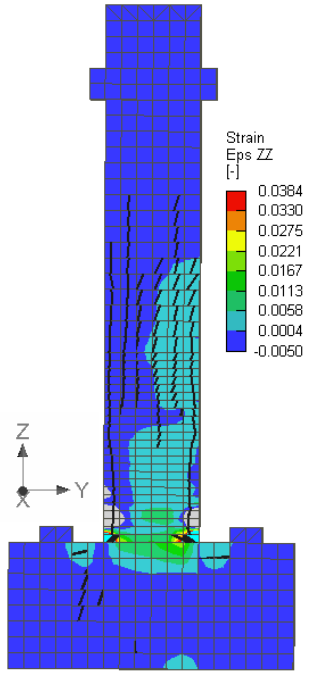

b) ε_{zz} strain of L-20-Cor at 2% Drift

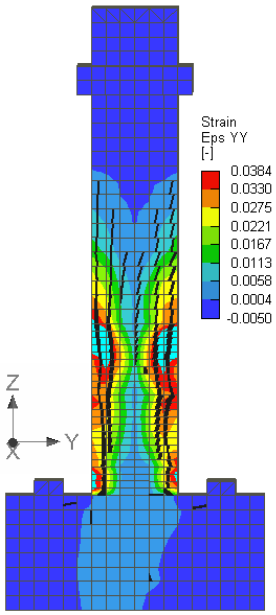

c) ε_{yy} strain of L-15-Cor at 2% Drift

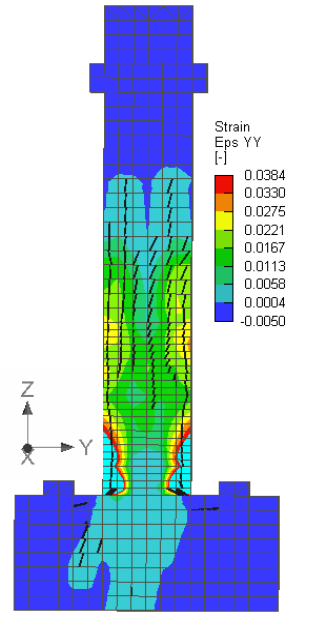

d) ε_{yy} strain of L-20-Cor at 2% Drift

Figure 8-14. Cracking pattern and strain distribution of concrete columns: a) and b) plot the normal strains ε_{zz}; c) and d) plot the normal strains ε_{yy}.

Figure 8-14 shows the cracking patterns at 2% drift for columns L-15-Cor and L-20-Cor respectively. Cracks shown are limited to a 0.1mm width. It may be observed that L-15-Cor had wider crack widths at 2% where it failed in bond, relative to L-20-Cor which failed at 2.5%. The normal (zz) strain distribution is very similar in both columns where strain localization occurred at the column-footing interface, marked by a uniformly distributed strain pattern in the shear span. Normal strains (zz) in column L-15-Cor were somewhat suppressed relative to L-20-Cor at 2%. This could be attributed to the dominant bond failure in L-15-Cor at 2%. This is verified by considering the normal ε_{yy} strain distribution of the two columns shown in Figure 8-14 c) and d): all strains are positive, underscoring the lateral dilation that occurred as a result of the bond damage. It can also be observed that the footing did not suffer extensive damage; instead, the damage was localized in the column's shear span.

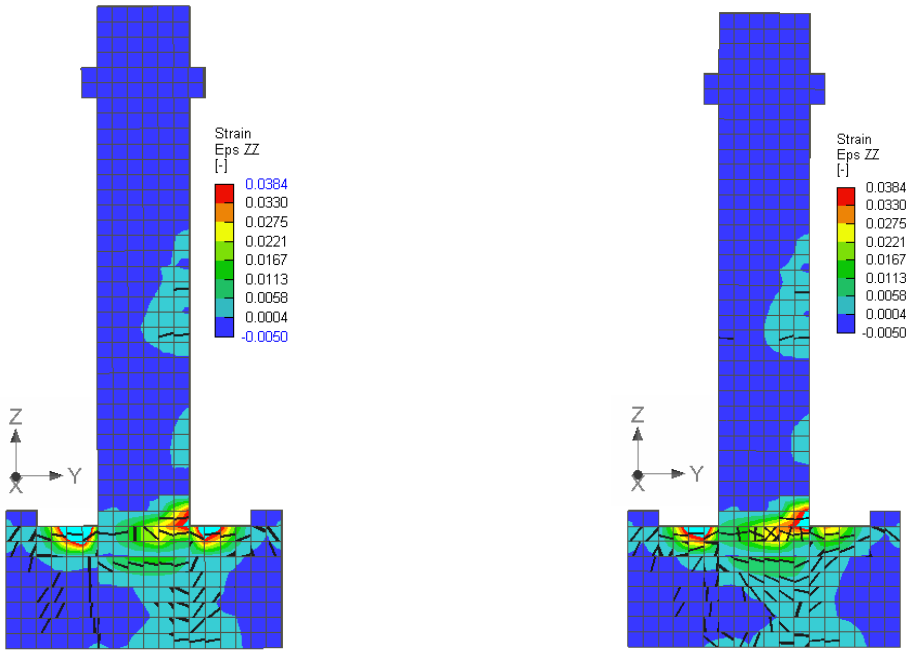

a) L-15-Str b) L-20-Str

Figure 8-15. Cracking pattern and ε_{zz} strain distribution of strengthened columns at 2% lateral drift

Figure 8-15 shows the cracking patterns at 2% drift for columns L-15-Str and L-20-Str respectively. As before, cracks shown are limited to a 0.1mm width. It is observed that both columns developed localized damage in the footing, where the cracking patterns for both columns were almost identical. As was observed in the experiment, the numerical models identify correctly

the formation of a failure surface along the UHPC-NC interface inside the footing. The segment of the shear span strengthened with UHPC did not develop any cracking which is also consistent with the experimental observation. It is clear that the model was able to replicate successfully the behavior and failure mode of the strengthened columns.

8.3.3. Reinforcement Strain Distribution

Reinforcement strain distributions were obtained from the post-processing software of ATENA Studio at different drift levels. Figures 8-16 until 8-19 display the reinforcement strain distribution of columns L-15-Cor, L-15-Str, L-20-Cor and L-20-Str respectively, at different drift levels. The color grading was limited at a strain of 0.002 in order to easily identify yielding in reinforcement.

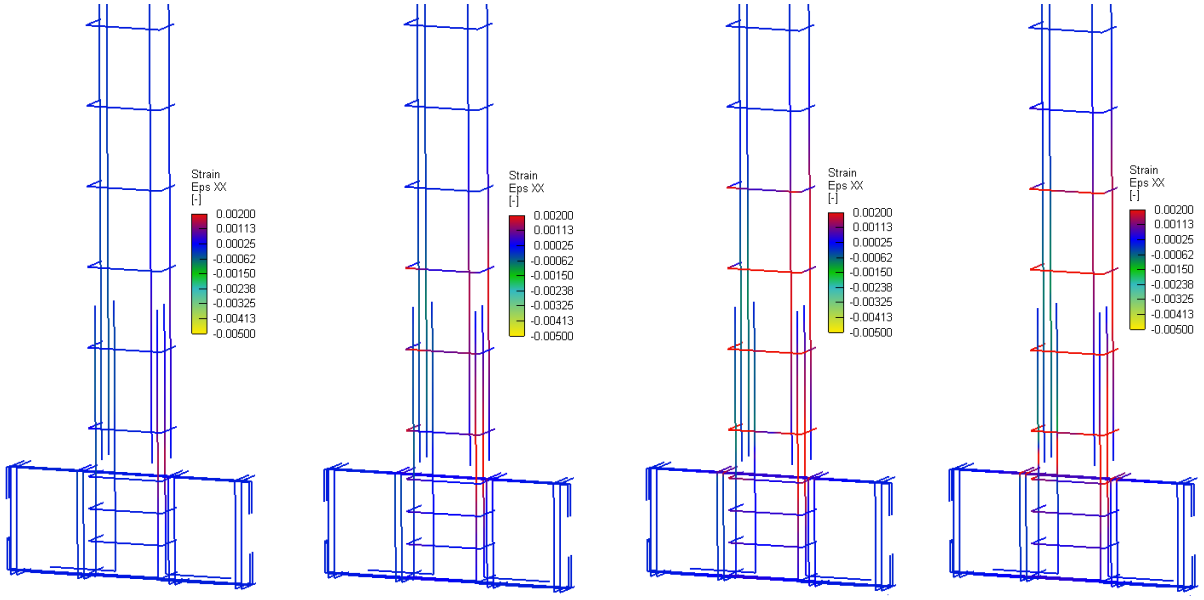

a) 0.5% b) 1% c) 1.5% d) 2%

Figure 8-16. Reinforcement strain distribution of column L-15-Cor at different drift levels

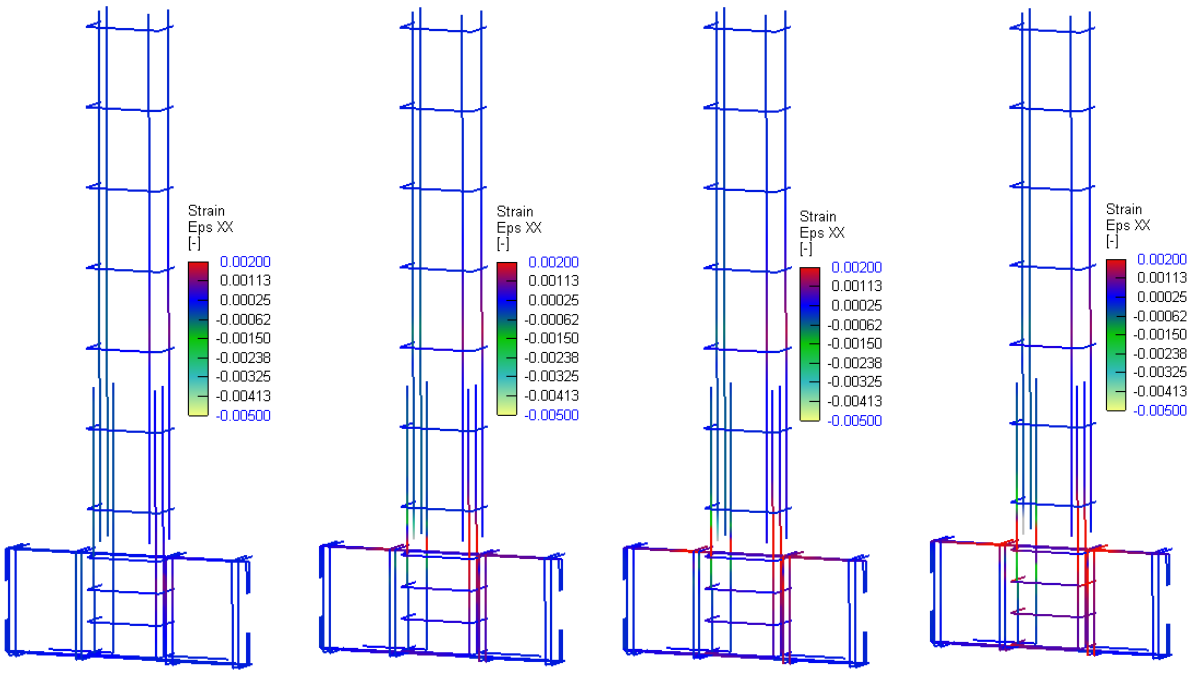

a) 0.5% b) 1% c) 1.5% d) 2%

Figure 8-17. Reinforcement strain distribution of column L-15-Str at different drift levels

From Figure 8-16, it is observed that yielding of the L-15-Cor begun in the starter bars of the lap-pairs, in the column's shear span above the footing. With increasing drift demand, yielding penetrates modestly into the footing and aggressively into the shear span. Reinforcement extending in the shear span experienced significant yielding along its length, until reaching a drift of 2% where bond failure occurred. At higher drift levels, as shown in Figure 8-16, c) and d), it is observed that strains in reinforcement decreased, although the drift ratio increased from 1.5% to 2%. This release in strains validates the fact that the columns failed in bond. Furthermore, it was observed that with increasing drift levels, transverse reinforcement (stirrups) experience significant strain demand. At 1% drift ratio, three stirrups partially experienced yielding whereas at 2% five stirrups were experiencing significant yielding. The significant strains propagating along the reinforcement as bond degraded imposed an ever increasing demand on the stirrups to control the dilation of the specimen and to support the longitudinal bar development through clamping action.

Figure 8-17 displays the reinforcement strain distribution with increasing drifts of column L-15-Str. An immediate comparison between Figures 8-16 and 8-17 illustrates clearly the effect of strengthening with UHPC jacketing. At 0.5% drift ratio, no yielding occurred in the strengthened

column L-15-Str. Yielding occurred in the starter reinforcement at 1% drift ratio, and propagated down into the footing's reinforcement. It is noted that yielding in reinforcement did not significantly penetrate into the shear span, since bond strength was significantly higher on account of the UHPC jacket. Alternatively, yielding significantly localized in the footing almost reaching its full depth. Transverse reinforcement in the shear span did not experience any yielding, as the failure was dominated by flexure and localization in the footing. This highlights that the jacket provides a significant contribution to shear strength in the columns as well as in the bond mechanism of the longitudinal bars; it is noted that some yielding was also observed in the shear span reinforcement above the UHPC-strengthened region.

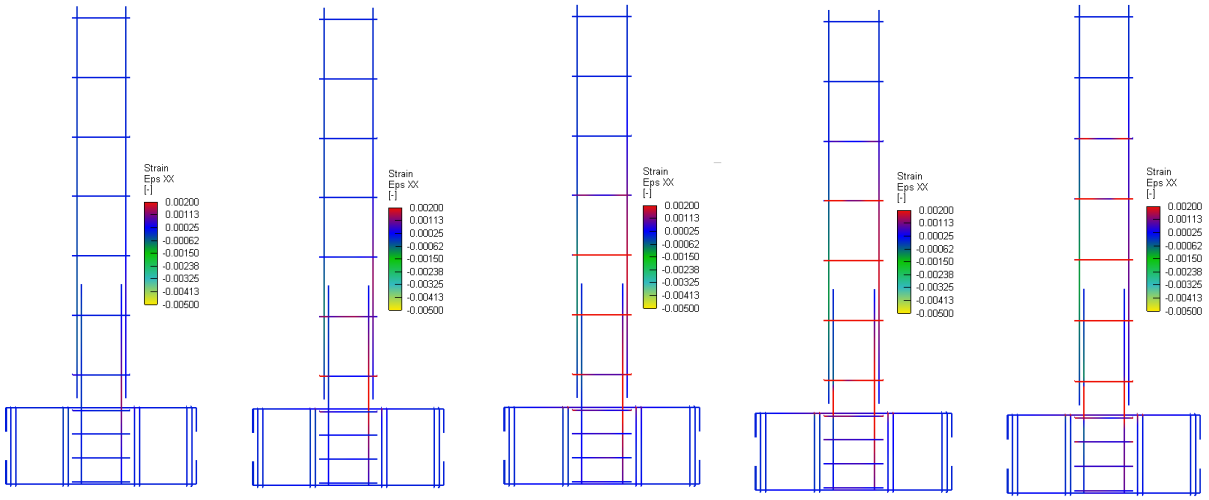

a) 0.5% b) 1% c) 1.5% d) 2% e) 2.5%

Figure 8-18. Reinforcement strain distribution of column L-20-Cor at different drift levels

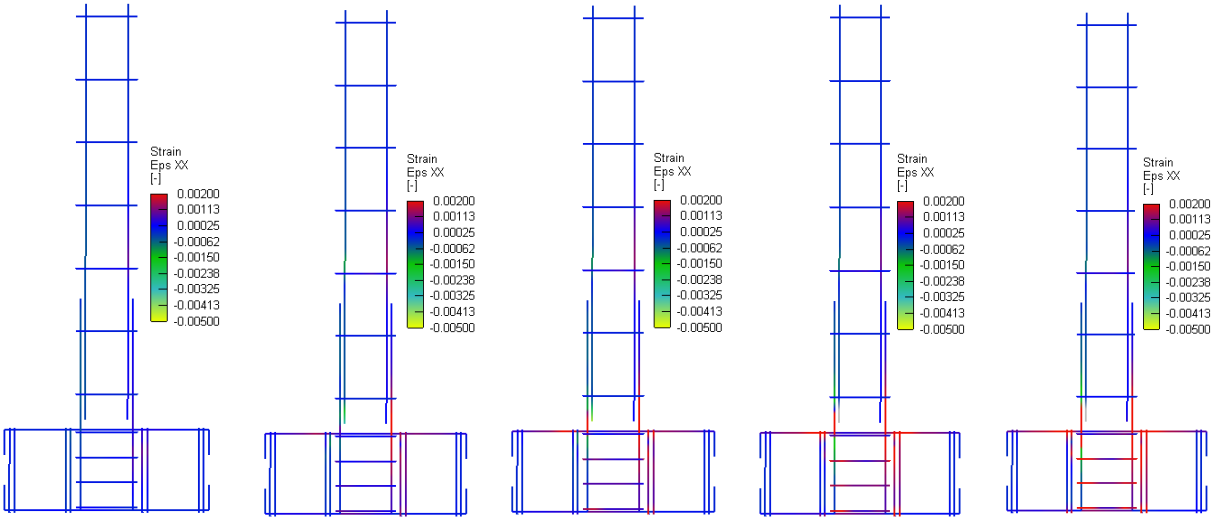

a) 0.5% b) 1% c) 1.5% d) 2% e) 2.5%

Figure 8-19. Reinforcement strain distribution of column L-20-Str at different drift levels

Based on Figures 8-18 and 8-19 which display the reinforcement strain distribution of columns L-20-Cor and L-20-Str similar observations could be made from the comparison between L-15-Cor and L-15-Str. From Figure 8-18, it is noted that reinforcement yielding begins at a drift ratio of 0.5%, and that with increasing drift levels yielding penetrates significantly into the shear span reaching the mid-height of the column. In fact, the extent of yield penetration in both the footing and the shear span for column L-20-Cor exceeded that of L-15-Cor. This could be attributed to the higher forces that develop in the 20M bars which impose a greater demand on the reserves of bond strength. Stirrup engagement was also observed in L-20-Cor, where at a drift ratio of 2.5%, six stirrups in the shear span developed yielding. Strain release before and after bond failure was also noted in column L-20-Cor (see Figure 8-18 d) and e).)

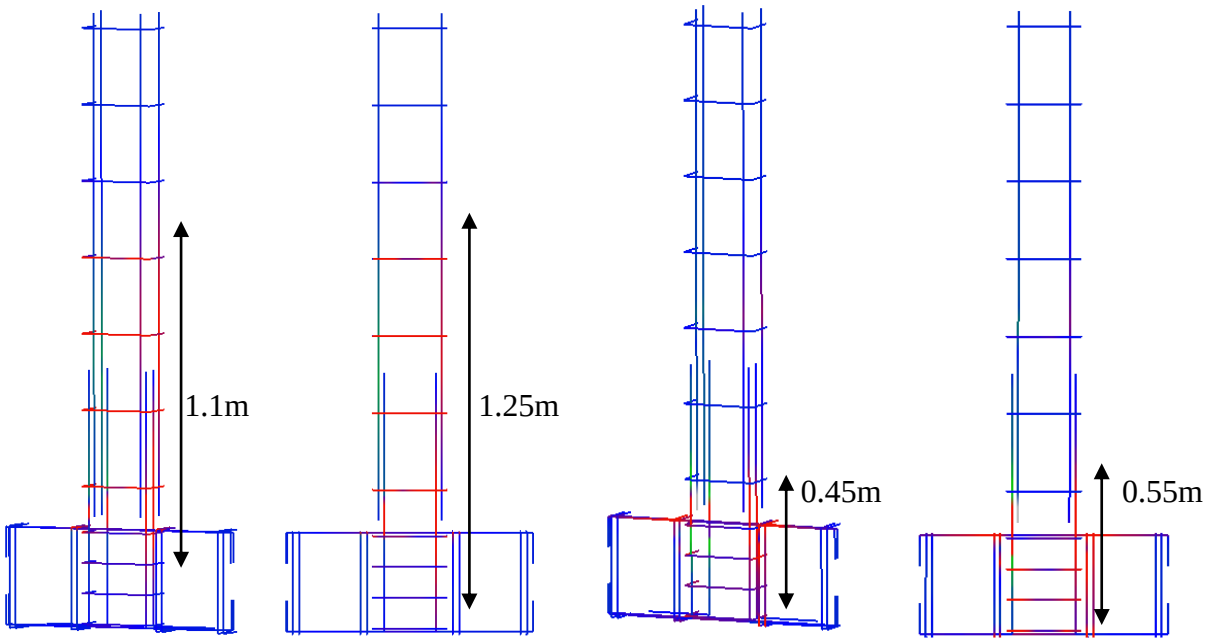

a) L-15-Cor b) L-20-Cor c) L-15-Str d) L-20-Str

Figure 8-20. Plastic reinforcement deformation length along column height

Figure 8-19 depicts the reinforcement strain distribution in the strengthened column L-20-Str. Just as was seen in column L-15-Str, the strengthened component did not experience any yielding at a drift ratio of 0.5%. Yielding was observed onwards from 1% drift ratio, and was also localized in the footing with minimal yield penetration into the shear span, again, due to the significant bond strength increase effected by the addition of the jacket. Clear engagement of the footing

reinforcement was observed with increasing drift demand; thus, the attained strength recorded when testing the columns was controlled by the footing's capacity and not by the UHPC-strengthened member capacity. Figure 8-20 shows the various lengths along the columns where reinforcement strains exceeded 0.002 at 2% drift. It is clear that UHPC strengthened columns had a significantly shorter plastic hinge length as opposed to the original concrete columns. It should be noted that the term plastic hinge in this context refers to the length of reinforcement bar over which yielding had occurred (not calculated from the empirical code expressions). From the same figure, it can be observed that columns reinforced with 20M reinforcement experienced longer plastic hinge length as opposed to columns reinforced with 15M reinforcement, on account of the greater extent of strain penetration that occurs in larger diameter bars. It is noted that stirrups yield over the length of the plastic hinge in all cases examined.

8.4. Conclusions

In this chapter, a numerical investigation into the previously tested lap-spliced tall columns was carried out. Four columns were modeled following the methodology proposed in Chapter 3. Columns selected for detailed analysis were specimens L-15-Cor, L-20-Cor, L-15-Str and L-20-Str. Based on the numerical simulation conducted presented in this chapter, the following conclusions were drawn:

- The modeling procedure for corroded columns, which was proposed in Chapter 3 was validated
- Calibration of the Bond Model was the single most critical step towards accurately reproducing the behavior of the columns
- Some differences in behavior between columns reinforced with 15M and 20M bars were observed even though the total reinforcement area was the same. These differences were:
    - Bond failure in L-15-Cor preceded L-20-Cor (in terms of lateral drift ratio)
    - The strain penetration into the shear span was more intense in the case of bigger diameter bars, leading to a commensurate increase in the plastic hinge length of L-20-Cor as compared to that of L-15-Cor
- Non-strengthened columns experienced increased stress demand in their transverse reinforcement due to bond failure of longitudinal reinforcement; all stirrups over the plastic hinge length defined based on longitudinal bar yield penetration also developed yielding.
- UHPC cover replacement was able to significantly suppress yield penetration into the strengthened region
- UHPC-strengthened columns relieved stress demand off of transverse reinforcement and shifted the stress demand into the footing region
- It is recommended to avoid this damage mode by retrofitting the anchorages in the footing when using this strengthening method.
- At advanced levels of lateral drift, a large part of the response was controlled by rocking over a concave sliding surface created in the footing under the interface between the UHPC jacket and the pre-existing concrete.

8.5. References

ACI-374 (2016) *ACI 374 - Guide to Nonlinear Modeling Parameters for Earthquake-Resistant Structures*. Available at: www.concrete.org (Accessed: 27 March 2022).

ACI 222R-19 (2019) 'Guide to Protection of Reinforcing Steel in Concrete Against Corrosion', *American Concrete Institute*, pp. 1–65.

Al-Saidy, A. H. *et al.* (2016) 'Structural behavior of corroded RC beams with/without stirrups repaired with CFRP sheets', *Materials and Structures*. Springer Netherlands, 49(9), pp. 3733–3747. doi: 10.1617/s11527-015-0751-y.

Al-Sulaimani, G. J. *et al.* (1990) 'Influence of corrosion and cracking on bond behavior and strength of reinforced concrete members', *ACI Structural Journal*, 87(2), pp. 220–231. doi: 10.14359/2732.

Alaskar, A. (2013) 'Shear Behaviour of Slender RC Beams with Corroded Web Reinforcement'. University of Waterloo. Available at: https://uwspace.uwaterloo.ca/handle/10012/7472 (Accessed: 15 July 2019).

Allamt, I. M. *et al.* (1994) *Influence of atmospheric corrosion on the mechanical properties of reinforcing steel, Construction and Building Materials*.

Almusallam, A. A. *et al.* (1996) 'Effect of reinforcement corrosion on bond strength', *Construction and Building Materials*. Elsevier, 10(2), pp. 123–129. doi: 10.1016/0950-0618(95)00077-1.

Almusallam, A. A. (2001a) 'Effect of degree of corrosion on the properties of reinforcing steel bars', *Construction and Building Materials*. Elsevier, 15(8), pp. 361–368. doi: 10.1016/S0950-0618(01)00009-5.

Almusallam, A. A. (2001b) 'Effect of degree of corrosion on the properties of reinforcing steel bars', *Construction and Building Materials*. Elsevier, 15(8), pp. 361–368. doi: 10.1016/S0950-0618(01)00009-5.

Alonso, C. *et al.* (1998) 'Factors controlling cracking of concrete affected by reinforcement corrosion', *Materials and Structures*. Kluwer Academic Publishers, 31(7), pp. 435–441. doi:

10.1007/BF02480466.

American Road & Transportation Builders Association (2020) *ARTBA Bridge Report*. Available at: https://artbabridgereport.org/ (Accessed: 6 July 2020).

Amleh, L., Mirza, M. and Ahwazi, B. (2000) 'Bond deterioration of reinforcing steel in concrete due to corrosion'. Available at: https://books.google.com/books?hl=en&lr=&id=F8HosZdH8BUC&oi=fnd&pg=PA247&ots=Iq_HHO_T-s&sig=3ytv3HtTEhxTvU9yTJRyH6PPLrk (Accessed: 5 July 2019).

Andrade, C., Alonso, M. C. and Gonzalez, J. A. (1990) 'Initial effort to use the corrosion rate measurements for estimating rebar durability', *ASTM Special Technical Publication*. ASTM International, (1065), pp. 29–37. doi: 10.1520/stp25013s.

Andrade, C. and González, J. A. (1978) 'Quantitative measurements of corrosion rate of reinforcing steels embedded in concrete using polarization resistance measurements', *Materials and Corrosion*, 29(8), pp. 515–519. doi: 10.1002/maco.19780290804.

Apostolopoulos, C. A. (2007) 'Mechanical behavior of corroded reinforcing steel bars S500s tempcore under low cycle fatigue', *Construction and Building Materials*. Elsevier, 21(7), pp. 1447–1456. doi: 10.1016/J.CONBUILDMAT.2006.07.008.

Apostolopoulos, C. A. and Papadakis, V. G. (2008) 'Consequences of steel corrosion on the ductility properties of reinforcement bar', *Construction and Building Materials*. Elsevier, 22(12), pp. 2316–2324. doi: 10.1016/J.CONBUILDMAT.2007.10.006.

Apostolopoulos, C., Drakakaki, A. and Basdeki, M. (2019) 'Seismic assessment of RC column under seismic loads', *International Journal of Structural Integrity*. Emerald Publishing Limited , 10(1), pp. 41–54. doi: 10.1108/IJSI-02-2018-0013.

ASCE 41 (2017) *Seismic Evaluation and Retrofit of Existing Buildings, Seismic Evaluation and Retrofit of Existing Buildings*. American Society of Civil Engineers. doi: 10.1061/9780784414859.

Azad, A. K., Ahmad, S. and Al-Gohi, B. H. A. (2010) 'Flexural strength of corroded reinforced concrete beams', *Magazine of Concrete Research*. Thomas Telford Ltd , 62(6), pp. 405–414. doi: 10.1680/macr.2010.62.6.405.

Berra, M., Castellani, A. and Coronelli, D. (1997) 'Bond in reinforced concrete and corrosion of bars', in *Structural Faults and Repair*. Edinburgh, UK, pp. 349–357.

Berrocal, C. G. *et al.* (2017) 'Corrosion-induced cracking and bond behaviour of corroded reinforcement bars in SFRC', *Composites Part B: Engineering*. Elsevier, 113, pp. 123–137. doi: 10.1016/J.COMPOSITESB.2017.01.020.

Blaber, J., Adair, & B. and Antoniou, & A. (no date) 'Ncorr: Open-Source 2D Digital Image Correlation Matlab Software'. doi: 10.1007/s11340-015-0009-1.

Cairns, J., Du, Y. and Law, D. (2008) 'Structural performance of corrosion-damaged concrete beams', *Magazine of Concrete Research*. Thomas Telford Ltd , 60(5), pp. 359–370. doi: 10.1680/macr.2007.00102.

Di Carlo, F., Meda, A. and Rinaldi, Z. (2017) 'Numerical cyclic behaviour of un-corroded and corroded RC columns reinforced with HPFRC jacket', *Composite Structures*. Elsevier, 163, pp. 432–443. doi: 10.1016/J.COMPSTRUCT.2016.12.038.

Castel, A., François, R. and Arliguie, G. (2000) 'Mechanical behaviour of corroded reinforced concrete beams—Part 1: Experimental study of corroded beams', *Materials and Structures*. Kluwer Academic Publishers, 33(9), pp. 539–544. doi: 10.1007/BF02480533.

CEN (2005) *EN 1998 - 3 Eurocode 8-Design of structures for earthquake resistance-Part 3: Assessment and retrofitting of buildings*.

Cervenka Consulting (2007) 'ATENA Program Documentation'. Prague, Czech Republic.

Civjan, S. A. *et al.* (2005) 'Effectiveness of corrosion inhibiting admixture combinations in structural concrete', *Cement and Concrete Composites*. Elsevier, 27(6), pp. 688–703. doi: 10.1016/J.CEMCONCOMP.2004.07.007.

Coronelli, D. and Gambarova, P. (2004) 'Structural Assessment of Corroded Reinforced Concrete Beams: Modeling Guidelines', *Journal of Structural Engineering*. American Society of Civil Engineers, 130(8), pp. 1214–1224. doi: 10.1061/(ASCE)0733-9445(2004)130:8(1214).

Coronelli, D., Hanjari, K. Z. and Lundgren, K. (2013) 'Severely Corroded RC with Cover Cracking', *Journal of Structural Engineering*, 139(2), pp. 221–232. doi:

10.1061/(ASCE)ST.1943-541X.0000633.

Dang, V. H. and François, R. (2013) 'Influence of long-term corrosion in chloride environment on mechanical behaviour of RC beam', *Engineering Structures*. Elsevier, 48, pp. 558–568. doi: 10.1016/j.engstruct.2012.09.021.

Darwin, D. and Pecknold, D. (1974) *INELASTIC MODEL FOR CYCLIC BIAXIAL LOADING OF REINFORCED CONCRETE*. Illinois, Urbana. Available at: https://www.semanticscholar.org/paper/INELASTIC-MODEL-FOR-CYCLIC-BIAXIAL-LOADING-OF-Darwin-Pecknold/5d1fb39809798f4c65b2dfa0fad5c06dd82e2a6f (Accessed: 20 July 2022).

Du, Y., Clark, L. A. and Chan, A. H. C. (2007) 'Impact of Reinforcement Corrosion on Ductile Behavior of Reinforced Concrete Beams', *ACI Structural Journal*, 104(3), pp. 285–293. doi: 10.14359/18618.

Du, Y. G., Clark, L. A. and Chan, A. H. C. (2005) 'Residual capacity of corroded reinforcing bars', *Magazine of Concrete Research*. Thomas Telford Ltd , 57(3), pp. 135–147. doi: 10.1680/macr.2005.57.3.135.

El-Joukhadar, N., Tsiotsias, K. and Pantazopoulou, S. (2019) 'Consideration of the state of corrosion in seismic assessment of columns', *International Journal of Structural Integrity*. Emerald Group Publishing Ltd. doi: 10.1108/IJSI-07-2019-0065.

Fakhri, H., Ragalwar, K. A. and Ranade, R. (2019) 'On the use of Strain-Hardening Cementitious Composite covers to mitigate corrosion in reinforced concrete structures', *Construction and Building Materials*. Elsevier Ltd, 224, pp. 850–862. doi: 10.1016/j.conbuildmat.2019.07.052.

Fang, C. *et al.* (2004) 'Corrosion influence on bond in reinforced concrete', *Cement and Concrete Research*. Pergamon, 34(11), pp. 2159–2167. doi: 10.1016/J.CEMCONRES.2004.04.006.

Farhan, N. A., Sheikh, M. N. and Hadi, M. N. S. (2018) 'Experimental Investigation on the Effect of Corrosion on the Bond Between Reinforcing Steel Bars and Fibre Reinforced Geopolymer Concrete', *Structures*. Elsevier, 14, pp. 251–261. doi:

10.1016/J.ISTRUC.2018.03.013.

Fernandez, I. *et al.* (2018) 'Ultimate Capacity of Corroded Statically Indeterminate Reinforced Concrete Members', *International Journal of Concrete Structures and Materials*. Springer Singapore, 12(1), p. 75. doi: 10.1186/s40069-018-0297-9.

Fernandez, I., Bairán, J. M. and Marí, A. R. (2015) 'Corrosion effects on the mechanical properties of reinforcing steel bars. Fatigue and σ–ε behavior', *Construction and Building Materials*. Elsevier, 101, pp. 772–783. doi: 10.1016/J.CONBUILDMAT.2015.10.139.

Fernandez, I. and Berrocal, C. G. (2019) 'Mechanical Properties of 30 Year-Old Naturally Corroded Steel Reinforcing Bars', *International Journal of Concrete Structures and Materials*. Korea Concrete Institute, 13(1), p. 9. doi: 10.1186/s40069-018-0308-x.

Fernandez, I., Lundgren, K. and Zandi, K. (2018) 'Evaluation of corrosion level of naturally corroded bars using different cleaning methods, computed tomography, and 3D optical scanning', *Materials and Structures/Materiaux et Constructions*. Springer Netherlands, 51(3), pp. 1–13. doi: 10.1617/s11527-018-1206-z.

fib-Model Code (2020) 'Model Code 2020, Draft version MC2020', in. fib.

fib bulletin #10 (2000) *Bond of reinforcement in concrete : state-of-art report*. International Federation for Structural Concrete. Available at: https://www.fib-international.org/publications/fib-bulletins/bond-of-reinforcement-in-concrete-pdf-detail.html (Accessed: 3 July 2019).

fib Model Code (2010) *Fib model code for concrete structures 2010*.

Fischer, C., Ozbolt, J. and Gehlen, C. (2010) 'Numerical investigation on bond behavior of corroded reinforcement', in *7th International Conference on Fracture Mechanics of Concrete and Concrete Structures*. Jeju, Korea, pp. 779–785.

François, R. and Arliguie, G. (1998) 'Influence of Service Cracking on Reinforcement Steel Corrosion', *Journal of Materials in Civil Engineering*, 10(1), pp. 14–20. doi: 10.1061/(ASCE)0899-1561(1998)10:1(14).

François, R., Khan, I. and Dang, V. H. (2013) 'Impact of corrosion on mechanical properties of

steel embedded in 27-year-old corroded reinforced concrete beams', *Materials and Structures*. Springer Netherlands, 46(6), pp. 899–910. doi: 10.1617/s11527-012-9941-z.

Fu, C. *et al.* (2017) 'Corrosion characteristics of a 4-year naturally corroded reinforced concrete beam with load-induced transverse cracks', *Corrosion Science*. Pergamon, 117, pp. 11–23. doi: 10.1016/J.CORSCI.2017.01.002.

Ganesh, P. and Ramachandra Murthy, A. (2020) 'Simulation of surface preparations to predict the bond behaviour between normal strength concrete and ultra-high performance concrete', *Construction and Building Materials*. Elsevier, 250, p. 118871. doi: 10.1016/J.CONBUILDMAT.2020.118871.

Gjørv, O. E. (2014) *Durability Design of Concrete Structures in Severe Environments*. CRC Press. doi: 10.1201/b16469.

Goksu, C. and Ilki, A. (2016) 'Seismic Behavior of Reinforced Concrete Columns with Corroded Deformed Reinforcing Bars', *ACI Structural Journal*, 113(5), pp. 1053–1064. doi: 10.14359/51689030.

Haddad, R. H. and Ashteyate, A. M. (2001) 'Role of synthetic fibers in delaying steel corrosion cracks and improving bond with concrete', *Canadian Journal of Civil Engineering*. NRC Research Press Ottawa, Canada , 28(5), pp. 787–793. doi: 10.1139/l01-037.

Hanjari, K. Z., Coronelli, D. and Lundgren, K. (2011) 'Bond capacity of severely corroded bars with corroded stirrups', *Magazine of Concrete Research*. Thomas Telford Ltd , 63(12), pp. 953–968. doi: 10.1680/macr.10.00200.

Harajli, M. H. (2004) 'Comparison of Bond Strength of Steel Bars in Normal- and High-Strength Concrete', *Journal of Materials in Civil Engineering*, 16(4), pp. 365–374. doi: 10.1061/(ASCE)0899-1561(2004)16:4(365).

Higgins, C. and Farrow, W. C. (2006) 'Tests of Reinforced Concrete Beams with Corrosion-Damaged Stirrups', *ACI Structural Journal*, 103(1), pp. 133–141. doi: 10.14359/15094.

Hou, L. *et al.* (2017) 'Effect of corrosion on bond behaviors of rebar embedded in ultra-high toughness cementitious composite', *Construction and Building Materials*. Elsevier, 138, pp. 141–150. doi: 10.1016/J.CONBUILDMAT.2017.02.008.

Hung, C. C., Lee, H. S. and Chan, S. N. (2019) 'Tension-stiffening effect in steel-reinforced UHPC composites: Constitutive model and effects of steel fibers, loading patterns, and rebar sizes', *Composites Part B: Engineering*. Elsevier Ltd, 158, pp. 269–278. doi: 10.1016/j.compositesb.2018.09.091.

Ioannou, A. *et al.* (2022) 'Experimental Testing of ECC Jackets for Repair of Pre-Damaged R . C . Members Experimental Testing of ECC Jackets for Repair of Pre-Damaged R . C . Members under Cyclic Loading', in *12th National Conference on Earthquake Engineering*. Salt Lake City, Utah: Earthquake Engineering Research Institute, pp. 1–5.

Kashani, M. M., Maddocks, J. and Dizaj, E. A. (2019) 'Residual Capacity of Corroded Reinforced Concrete Bridge Components: State-of-the-Art Review', *Journal of Bridge Engineering*, 24(7), p. 03119001. doi: 10.1061/(ASCE)BE.1943-5592.0001429.

Kondratova, I. L., Montes, P. and Bremner, T. W. (2000) 'Accelerated Corrosion Testing Results for Specimens Containing Uncoated Reinforcing Steel and Corrosion Inhibitors', *Special Publication*, 192, pp. 789–806. doi: 10.14359/5785.

Koulouris, K. and Apostolopoulos, C. (2020) 'An Experimental Study on Effects of Corrosion and Stirrups Spacing on Bond Behavior of Reinforced Concrete', *Metals*. MDPI AG, 10(10), p. 1327. doi: 10.3390/met10101327.

Lee, H. S. and Cho, Y. S. (2009) 'Evaluation of the mechanical properties of steel reinforcement embedded in concrete specimen as a function of the degree of reinforcement corrosion', in *International Journal of Fracture*. Springer, pp. 81–88. doi: 10.1007/s10704-009-9334-7.

Li, D. *et al.* (2018) 'Influence of Non-uniform corrosion of steel bars on the seismic behavior of reinforced concrete columns', *Construction and Building Materials*. Elsevier, 167, pp. 20–32. doi: 10.1016/J.CONBUILDMAT.2018.01.149.

Li, J., Gong, J. and Wang, L. (2009) 'Seismic behavior of corrosion-damaged reinforced concrete columns strengthened using combined carbon fiber-reinforced polymer and steel jacket', *Construction and Building Materials*. Elsevier, 23(7), pp. 2653–2663. doi: 10.1016/J.CONBUILDMAT.2009.01.003.

Li, X. *et al.* (2016) 'Effect of loading rate on the bond behaviour of deformed steel bars in

concrete subjected to lateral pressure', *Materials and Structures*. Springer Netherlands, 49(6), pp. 2097–2111. doi: 10.1617/s11527-015-0636-0.

Lijina, T. and Jithin, J. . (2018) 'Effect of Steel and Polypropylene Fibre on the Tension Stiffening of Ultra High Performance Concrete', *International Journal of Engineering and Advanced Technology (IJEAT)*, 8(4C).

Lin, H. *et al.* (2019) 'State-of-the-art review on the bond properties of corroded reinforcing steel bar', *Construction and Building Materials*. Elsevier, 213, pp. 216–233. doi: 10.1016/J.CONBUILDMAT.2019.04.077.

Liu, X. and Li, Y. (2018) 'Experimental study of seismic behavior of partially corrosion-damaged reinforced concrete columns strengthened with FRP composites with large deformability', *Construction and Building Materials*. Elsevier, 191, pp. 1071–1081. doi: 10.1016/J.CONBUILDMAT.2018.10.072.

Lu, C. *et al.* (2016) 'Mechanical properties of corroded steel bars in pre-cracked concrete suffering from chloride attack', *Construction and Building Materials*, 123(123), pp. 649–660. doi: 10.1016/j.conbuildmat.2016.07.032.

Ma, Y., Che, Y. and Gong, J. (2012) 'Behavior of corrosion damaged circular reinforced concrete columns under cyclic loading', *Construction and Building Materials*. Elsevier, 29, pp. 548–556. doi: 10.1016/J.CONBUILDMAT.2011.11.002.

El Maaddawy, T. A. and Soudki, K. A. (2003) 'Effectiveness of Impressed Current Technique to Simulate Corrosion of Steel Reinforcement in Concrete', *Journal of Materials in Civil Engineering*, 15(1), pp. 41–47. doi: 10.1061/(ASCE)0899-1561(2003)15:1(41).

Mangat, P. S. and Elgarf, M. S. (1999) 'Bond characteristics of corrding reinforcement in concrete beams', *Materials and Structures*. Kluwer Academic Publishers, 32(2), pp. 89–97. doi: 10.1007/BF02479434.

Mangat, Pritpal S. and Elgarf, M. S. (1999) 'Flexural Strength of Concrete Beams with Corroding Reinforcement', *ACI Structural Journal*, 96(1), pp. 149–158. doi: 10.14359/606.

Martín Pérez, B. M. (1999) *Service life modelling of R.C. highway structures exposed to chlorides*. University of Toronto. Available at:

https://books.google.ca/books/about/Service_Life_Modelling_of_R_C_Highway_St.html?id=qQiGtgAACAAJ&redir_esc=y (Accessed: 14 February 2019).

Meda, A. *et al.* (2014) 'Experimental evaluation of the corrosion influence on the cyclic behaviour of RC columns', *Engineering Structures*. Elsevier, 76, pp. 112–123. doi: 10.1016/J.ENGSTRUCT.2014.06.043.

Mehta, P. K. (1991) 'Durability of Concrete--Fifty Years of Progress?', *Special Publication*, 126, pp. 1–32. doi: 10.14359/1998.

Menengotto, M. and Pinto, P. E. (1973) 'Method o f Analysis for Cyclically Loaded Reinforced Concrete Plane Frames Including Changes in Geometry and Nonelastic Behavior of Elements under Combined Normal Force and Bending', in *IABSE Symposium on Resistance and Ultimate Deformability of Structures Acted on*. Lisbon.

Molaioni, F., Carlo, F. Di and Rinaldi, Z. (2021) 'Modelling Strategies for the Numerical Simulation of the Behaviour of Corroded RC Columns under Cyclic Loads', *Applied Sciences 2021, Vol. 11, Page 9761*. Multidisciplinary Digital Publishing Institute, 11(20), p. 9761. doi: 10.3390/APP11209761.

Ou, Y.-C. and Chen, H.-H. (2014) 'Cyclic Behavior of Reinforced Concrete Beams with Corroded Transverse Steel Reinforcement', *Journal of Structural Engineering*, 140(9), p. 04014050. doi: 10.1061/(ASCE)ST.1943-541X.0000932.

Palsson, R. and Mirza, M. S. (2002a) 'Mechanical response of corroded steel reinforcement of abandoned concrete bridge', *ACI Structural Journal*, 99(2), pp. 157–162. doi: 10.14359/11538.

Palsson, R. and Mirza, M. S. (2002b) 'Mechanical Response of Corroded Steel Reinforcement of Abandoned Concrete Bridge', *ACI Structural Journal*, 99(2), pp. 157–162. doi: 10.14359/11538.

Pantazopoulou, S. J. *et al.* (2001) *REPAIR OF CORROSION-DAMAGED COLUMNS WITH FRP WRAPS, JOURNAL OF COMPOSITES FOR CONSTRUCTION*. Available at: http://pubs.asce.org/copyright (Accessed: 23 July 2019).

Pantazopoulou, S. J. *et al.* (2019) 'The performance of corroded lap splices in reinforced concrete beams', *Corrosion Reviews*. De Gruyter, 37(1), pp. 31–44. doi: 10.1515/corrrev-2017-0086.

Papakonstantinou, C. G., Balaguru, P. N. and Auyeung, Y. (2011) 'Influence of FRP confinement on bond behavior of corroded steel reinforcement', *Cement and Concrete Composites*. Elsevier, 33(5), pp. 611–621. doi: 10.1016/J.CEMCONCOMP.2011.02.006.

Pardalopoulos, S. I., Pantazopoulou, S. J. and Lekidis, V. A. (2017) 'Simplified method for rapid seismic assessment of older R.C. buildings'. doi: 10.1016/j.engstruct.2017.10.052.

Pardalopoulos, S. I., Pantazopoulou, S. J. and Lekidis, V. A. (2018) 'Simplified method for rapid seismic assessment of older R.C. buildings', *Engineering Structures*. Elsevier Ltd, 154, pp. 10–22. doi: 10.1016/j.engstruct.2017.10.052.

Pardalopoulos, S. J., Thermou, G. E. and Pantazopoulou, S. J. (2013) 'Screening criteria to identify brittle R.C. structural failures in earthquakes', *Bulletin of Earthquake Engineering*, 11(2), pp. 607–636. doi: 10.1007/s10518-012-9390-7.

Parulekar, Y. M. *et al.* (2020) 'Performance Assessment of Corroded Reinforced Concrete Structure Considering Bond Deterioration', *Journal of Performance of Constructed Facilities*. American Society of Civil Engineers, 34(2), p. 04020009. doi: 10.1061/(ASCE)CF.1943-5509.0001411.

Paul, Suvash CZijl, G. Van (2014) 'Cracked and uncracked SHCC specimens under different exposure conditions', in *Strain Hardening Cementitious Composites 3 (SHCC3)*. Dordrecht, pp. 25–32.

Pourbaix, M. (1974) *Atlas of electrochemical equilibria in aqueous solutions*. National Association of Corrosion Engineers. Available at: https://books.google.ca/books?id=iiLRvQEACAAJ&dq=9780915567980&hl=en&sa=X&ved=0ahUKEwivreD28rfgAhVi6IMKHQm4Dn4Q6AEIKjAA (Accessed: 12 February 2019).

Prieto, M., Tanner, P. and Andrade, C. (2011) 'Bond response in structural concrete with corroded steel bars. experimental results', *RILEM Bookseries*. Springer, Dordrecht, 5, pp. 231–241. doi: 10.1007/978-94-007-0677-4_16.

Rajput, A. S. and Sharma, U. K. (2018) 'Corroded reinforced concrete columns under simulated seismic loading', *Engineering Structures*. Elsevier, 171, pp. 453–463. doi: 10.1016/J.ENGSTRUCT.2018.05.097.

Raza, S. *et al.* (2019) ‘Strengthening and Repair of Reinforced Concrete Columns by Jacketing: State-of-the-Art Review’, *Sustainability*. MDPI AG, 11(11), p. 3208. doi: 10.3390/su11113208.

Robuschi, S. *et al.* (2020) ‘Bond of naturally corroded, plain reinforcing bars in concrete’, *Structure and Infrastructure Engineering*. Taylor and Francis Ltd., pp. 1–17. doi: 10.1080/15732479.2020.1768273.

Rodriguez, J. and Ortega, J. C. (1994) ‘Corrosion of reinforcing bars and service life of reinforced concrete structures: corrosion and bond deterioration’, in *International Conference on Concrete across Borders*. Odense, Denmark, pp. 315–326.

Semendary, A. A. and Svecova, D. (2020) ‘Factors affecting bond between precast concrete and cast in place ultra high performance concrete (UHPC)’, *Engineering Structures*. Elsevier, 216, p. 110746. doi: 10.1016/J.ENGSTRUCT.2020.110746.

Sezen, H. and Moehle, J. P. (2004) ‘Shear Strength Model for Lightly Reinforced Concrete Columns’, *Journal of Structural Engineering*. American Society of Civil Engineers, 130(11), pp. 1692–1703. doi: 10.1061/(ASCE)0733-9445(2004)130:11(1692).

Soudki, K. and Sherwood, T. (2003) ‘Bond Behavior of Corroded Steel Reinforcement in Concrete Wrapped with Carbon Fiber Reinforced Polymer Sheets’, *Journal of Materials in Civil Engineering*, 15(4), pp. 358–370. doi: 10.1061/(ASCE)0899-1561(2003)15:4(358).

Stanish, K., Hooton, R. D. and Pantazopoulou, S. J. (1999) ‘Corrosion Effects on Bond Strength in Reinforced Concrete’, *ACI Structural Journal*, 96(6), pp. 915–921. doi: 10.14359/765.

Suffern, C., El-Sayed, A. and Soudki, K. (2010) ‘Shear strength of disturbed regions with corroded stirrups in reinforced concrete beams’, *Canadian Journal of Civil Engineering*, 37(8), pp. 1045–1056. doi: 10.1139/L10-031.

Takuya, K., Ryuta, I. and Masayuki, T. (2020) ‘Prediction of Hydrogen Embrittlement of Reinforcing Steel Bars in Concrete Poles | NTT Technical Review’, *NTT Technical Review*, 18(11). Available at: https://www.ntt-review.jp/archive/ntttechnical.php?contents=ntr202011ra1.html (Accessed: 16 April 2022).

Tastani, S. P. and Pantazopoulou, S. J. (2007) ‘Behavior of Corroded Bar Anchorages’, *ACI Structural Journal*, 104(6), pp. 756–766. doi: 10.14359/18958.

Tastani, S. and Pantazopoulou, S. J. (2005) 'Recovery of seismic resistance in corrosion-damaged reinforced concrete through FRP jacketing', *International Journal of Materials and Product Technology*, 23(3/4), p. 389. doi: 10.1504/IJMPT.2005.007737.

Tayeh, B. A., Abu Bakar, B. H. and Megat Johari, M. A. (2013) 'Characterization of the interfacial bond between old concrete substrate and ultra high performance fiber concrete repair composite', *Materials and Structures/Materiaux et Constructions*. Springer, 46(5), pp. 743–753. doi: 10.1617/S11527-012-9931-1/FIGURES/13.

Tepfers, R. (1979) 'Cracking of concrete cover along anchored deformed reinforcing bars', *Magazine of Concrete Research*. Thomas Telford Ltd , 31(106), pp. 3–12. doi: 10.1680/macr.1979.31.106.3.

Tondolo, F. (2015) 'Bond behaviour with reinforcement corrosion', *Construction and Building Materials*. Elsevier, 93, pp. 926–932. doi: 10.1016/J.CONBUILDMAT.2015.05.067.

Torres-Acosta, A. A., Navarro-Gutierrez, S. and Terán-Guillén, J. (2007) 'Residual flexure capacity of corroded reinforced concrete beams', *Engineering Structures*. Elsevier, 29(6), pp. 1145–1152. doi: 10.1016/J.ENGSTRUCT.2006.07.018.

Tuutti, K. (1982) *Corrosion of steel in concrete*. Swedish Cement and Concrete Research Institute, Stockholm. Available at: https://portal.research.lu.se/portal/en/publications/corrosion-of-steel-in-concrete(e97795b5-7f3a-4994-8beb-9438f5a51571).html (Accessed: 6 July 2020).

Valikhani, A. *et al.* (2020) 'Experimental evaluation of concrete-to-UHPC bond strength with correlation to surface roughness for repair application', *Construction and Building Materials*. Elsevier, 238, p. 117753. doi: 10.1016/J.CONBUILDMAT.2019.117753.

Vecchio, F. J. and Collins, M. P. (1986) 'MODIFIED COMPRESSION-FIELD THEORY FOR REINFORCED CONCRETE ELEMENTS SUBJECTED TO SHEAR.', *Journal of the American Concrete Institute*, 83(2), pp. 219–231. doi: 10.14359/10416.

Vu, N. S. and Li, B. (2018) 'Seismic Performance of Flexural Reinforced Concrete Columns with Corroded Reinforcement', *ACI Structural Journal*, 115(5), pp. 1253–1266. doi: 10.14359/51702372.

Vu, N. S., Yu, B. and Li, B. (2016) 'Prediction of strength and drift capacity of corroded

reinforced concrete columns', *Construction and Building Materials*. Elsevier, 115, pp. 304–318. doi: 10.1016/J.CONBUILDMAT.2016.04.048.

Wang, L. *et al.* (2015) 'Effects of stirrup and inclined bar corrosion on shear behavior of RC beams', *Construction and Building Materials*. Elsevier, 98, pp. 537–546. doi: 10.1016/J.CONBUILDMAT.2015.07.077.

Xia, J., Jin, W. and Li, L. (2011) 'Shear performance of reinforced concrete beams with corroded stirrups in chloride environment', *Corrosion Science*. Pergamon, 53(5), pp. 1794–1805. doi: 10.1016/J.CORSCI.2011.01.058.

Xu, S. L. and Cai, X. H. (2010) *Bond behavior of corroded reinforcing bar and ultra high toughness cementitious composites (UHTCC)*. Available at: https://framcos.org/FraMCoS-7/06-04.pdf (Accessed: 8 July 2019).

Yang, S.-Y. *et al.* (2016) 'Experimental research on hysteretic behaviors of corroded reinforced concrete columns with different maximum amounts of corrosion of rebar', *Construction and Building Materials*. Elsevier, 121, pp. 319–327. doi: 10.1016/J.CONBUILDMAT.2016.06.002.

Yuan, W., Guo, A. and Li, H. (2017) 'Experimental investigation on the cyclic behaviors of corroded coastal bridge piers with transfer of plastic hinge due to non-uniform corrosion', *Soil Dynamics and Earthquake Engineering*. Elsevier, 102, pp. 112–123. doi: 10.1016/J.SOILDYN.2017.08.019.

Zhang, R., Castel, A. and François, R. (2009) 'The corrosion pattern of reinforcement and its influence on serviceability of reinforced concrete members in chloride environment', *Cement and Concrete Research*. Pergamon, 39(11), pp. 1077–1086. doi: 10.1016/J.CEMCONRES.2009.07.025.

Zhang, W. *et al.* (2012) 'Tensile and fatigue behavior of corroded rebars', *Construction and Building Materials*. Elsevier, 34, pp. 409–417. doi: 10.1016/J.CONBUILDMAT.2012.02.071.

Zhao, Y. *et al.* (2013) 'Bond behaviour of normal/recycled concrete and corroded steel bars', *Construction and Building Materials*. Elsevier, 48, pp. 348–359. doi: 10.1016/J.CONBUILDMAT.2013.06.091.

Zhu, W. *et al.* (2013) 'Effect of corrosion of reinforcement on the mechanical behaviour of

highly corroded RC beams', *Engineering Structures*. Elsevier, 56, pp. 544–554. doi: 10.1016/J.ENGSTRUCT.2013.04.017.

Zhu, W. and François, R. (2014) 'Experimental investigation of the relationships between residual cross-section shapes and the ductility of corroded bars', *Construction and Building Materials*, 69(69), pp. 335–345. doi: 10.1016/j.conbuildmat.2014.07.059.

Van Zijl, G. P. A. G. *et al.* (2012) 'Durability of strain-hardening cement-based composites (SHCC)', *Materials and Structures/Materiaux et Constructions*. Springer, 45(10), pp. 1447–1463. doi: 10.1617/s11527-012-9845-y.

9. Resistance Curve Reduction Factors and Structural System Modelling

Nonlinear seismic evaluation frameworks of reinforced concrete (RC) structures such as those of ASCE/SEI 41 (2017) and EN 1998-III (2005) are considered to be calculation-intensive and difficult to apply, primarily because they demand extensive information of reinforcement ratios and detailing. The aim of these assessment procedures is to compare the seismic demands imparted on the structure by a future seismic event, with the available member deformation capacities that correspond to preselected states of damage which are referred to in earthquake engineering literature as *performance limit states*. By comparing the deformation demands with the deformation capacities the objective is to predict the seismic performance and anticipated damage. It is noted however, that evaluation guidelines do not consider the condition of reinforcement, which was proven to affect the member's residual mechanical properties, the hierarchy of failure modes and the consequences on seismic performance. Considering that the condition of the reinforcement complicates further the problem of seismic assessment, this chapter attempts to settle this deficiency in the seismic evaluation framework by proposing simple modifications to the existing nonlinear assessment procedures in order to account for the effects of corrosion on seismic performance. The chapter also includes a methodology and application example of computational assessment procedures of complete structures, considering corrosion damage in the structural model when conducting nonlinear time history analysis.

Apart from the modifications to the member resistance curves to account for corrosion, which would be useful for a detailed Tier-3 seismic evaluation procedure, additional, simple tools are developed. A Tier-2 assessment procedure for seismic evaluation of structures is a method of lower computational intensity than a full nonlinear evaluation. Tier-2 methods are meant to be relatively straightforward, in order to obtain results rapidly, so as to determine whether a Tier-3 (i.e. detailed nonlinear analysis) is required in order to determine the expected performance at the anticipated hazard level. Past work had led to the development of two criteria (Pardalopoulos et al, 2017) that determine the spectral deformation demand in terms of relative drift ratio, θ_d, at peak response, and the available strength of the individual member at the attainment of that drift demand. In the present investigation the effect of stiffness modification due to corrosion on drift demand is considered in modifying the existing Tier-2 proposal.

It is noted that seismic displacement demand may be approximated from the structural period in the fundamental translational mode of vibration, $T_1(s)$, and the Absolute spectral acceleration $S_a(T_1)$ for the design hazard. Thus, the corresponding relative spectral displacement is equal to $S_d(T_1)=T_1^2 S_a(T_1)/4\pi^2$. The layout of the structural system controls the tendency for localization of deformation demands. This, for the critical storey is quantified by the difference in the relative coordinates in the ends i and j of the member in the fundamental mode of vibration Φ of the structure: i.e., Φ_i-Φ_j.

To preclude structural failure of the critical floor, the drift capacity of the member, θ_c, should exceed the demand, θ_d. Term θ_c is defined as the drift ratio value beyond which, the resistance envelope of the structural member subjected to lateral displacement reversals experiences severe degradation (the convention is to use the value corresponding to a post peak residual resistance equal to 85% of the strength). Several experiments have been conducted to study the effects of reinforcement corrosion on the strength and drift capacity of structural components. Major concerns are, the loss of bar area, the embrittlement of reinforcement and delamination of concrete, and the degradation of bond strength between steel and concrete due to accumulation of rust (Almusallam et al., 1996; Mangat and Elgarf, 1999; Stanish et al. 1999; Tastani and Pantazopoulou, 2007; Zhao et al., 2013). The tests from the literature but also the first phase of the experimental program on columns that was conducted in the present work conclusively illustrated that both response indices are severely impacted (i.e., the stiffness, which determines the period and thereby the drift demand, and the deformation capacity). Most importantly, the sequence of failure modes is often drastically affected, with members originally designed for flexure to be eventually failing by shear or in the anchorages/lap splices as a result of disproportional reduction of the stirrup bar area or of bar ribs (Tastani and Pantazopoulou, 2005).

9.1. Database of Published Test Specimens

To provide a basis for benchmarking the results of the experimental and finite element studies, a database of tests conducted under cyclic displacement reversals that simulated earthquake effects on corroded columns was assembled. Prior to testing, the columns had been corroded to various degrees of mass loss by accelerated corrosion. The acquired data was used to provide a thorough understanding of the mechanical effects of corrosion on columns as corrosion propagates, specifically in order to quantify the degradation in strength and ultimate drift capacity. The

following studies were used in the database (Li et al., 2009; Ma at al., 2012; Meda et al., 2014; Yang et al., 2016; Yuan et al., 2017; Li et al., 2018; Liu and Li, 2018; Rajput and Sharma, 2018; Vu and Li, 2018; Apostolopoulos et al., 2019). More details on the database collected can be found in El-Joukhadar et al. (2019).

9.1.1. Data Analysis and Modelling Parameters for Columns

Columns were divided into two groups according with the magnitude of statically applied, overbearing axial load, N: this is quantified as a normalized ratio ($v=N/A_g f_c'$). Thus, Group #1 comprised columns with an axial load ratio $0 \leq v \leq 0.2$ (i.e. lightly loaded), whereas Group #2 comprised columns bearing a significant amount of axial load acting ($0.2 \leq v \leq 0.4$). In assessing their performance for the needs of the present study, parameters studied for the two groups were as follows: 1) the ultimate drift capacity, θ_u, of the columns when rupture of the column's longitudinal bars occurred, 2) the lateral resistance $V_{cor}(\theta)$ of the columns at drift ratios equal to, θ=0.5% (at about yielding of longitudinal reinforcement), θ=1% and θ=2% (at approximate rotational ductilities, μ_θ, equal to 2 and 4, respectively).

Results are plotted in Figures 9-1 to 9-4 where response indices are normalized with respect to their uncorroded counterpart: Figure 9-1 plots the percent reduction in ultimate drift capacity of specimen groups 1 and 2 against the reported mass loss ratio, x (black and orange points correspond to specimens of Group #1 and #2 respectively; the trend-lines bear the same colour code for easy reference).

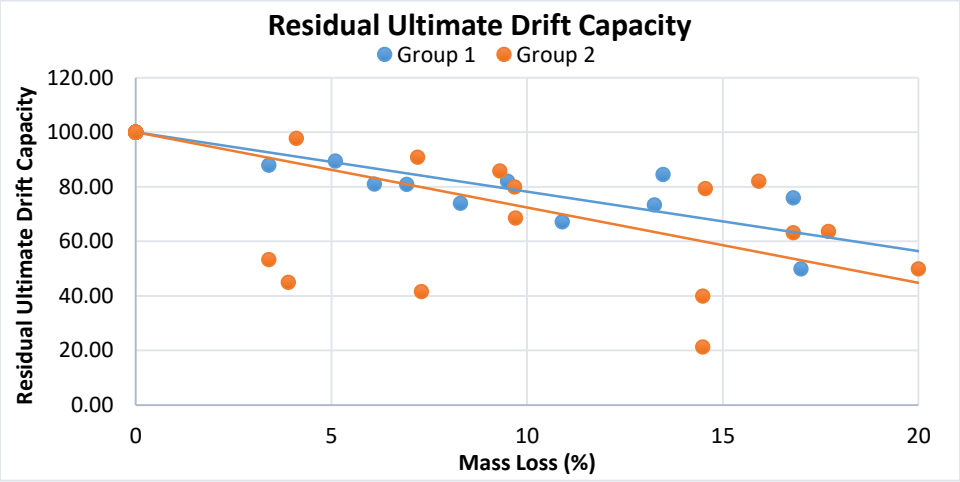

Figure 9-1. Reduction in the Ultimate Drift Capacities of Groups 1 & 2

The steeper trend represents the reduced ultimate drift capacity of Group #2, whereas the line with a milder slope represents that of Group #1. These trends are approximated by the following equations for the reduced drift capacity $\theta_{u,cor}$ given with reference to the uncorroded value $\theta_{u,o}$ as a function of the steel mass loss percent (subscripts 1 and 2 correspond to the two groups):

$$\underline{\text{For Group 1:}} \quad r_{d,1} = \frac{\theta_{u,cor,1}}{\theta_{u,0,1}} = 1 - \frac{2.2x}{100} \tag{9.1}$$

$$\underline{\text{For Group 2:}} \quad r_{d,2} = \frac{\theta_{u,cor,1}}{\theta_{u,0,1}} = 1 - \frac{2.75x}{100} \tag{9.2}$$

Here, r_d is the corroded residual ultimate drift capacity ratio, $\theta_{u,cor}$ is the residual displacement capacity of the corroded member, $\theta_{u,o}$ is the displacement capacity of an otherwise identical uncorroded member, and x is the steel mass loss (Eq. 9-1) (subscripts 1 and 2 correspond to the two groups).

It is observed that the deteriorating effect of corrosion on the ultimate drift capacity is greater in Group # 2 columns, particularly in cases with a higher mass loss. Figures 9-1, 9-2 and 9-3 plot the normalized lateral load capacity of the columns, $V_{u,cor}$, at lateral drift ratios of 0.5%, 1% and 2% respectively (normalization is done with respect to the corresponding uncorroded strength, V_u). For drift ratio equal to 0.5% (approximately onset of yielding), both groups of specimens experience a mild reduction in resistance, with the normalized capacity ratio reaching approximately the value of 90% (on average) for mass losses as high as 20%. It could be argued that no significant decrease in strength is noticeable at this level of drift ratio. For 1% drift, the trends in the values of normalized lateral load resistance became steeper as compared to the 0.5% drift. A target value of 90% in normalized lateral strength occurred at a mass loss value of x=17% for Group #1 columns and 80% residual load for Group #2, at 20% mass loss, and the gap between Groups #1 and #2 became more evident.

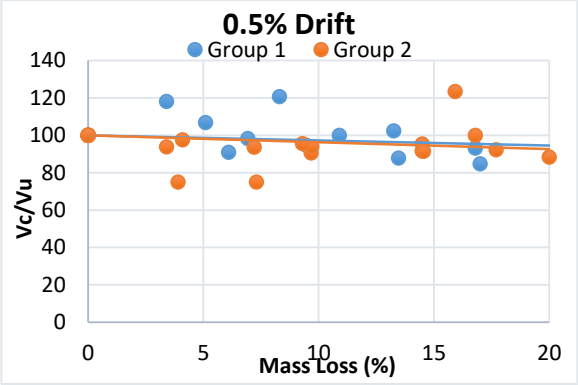

Figure 9-2. Residual Lateral Load Capacity at 0.5% Drift

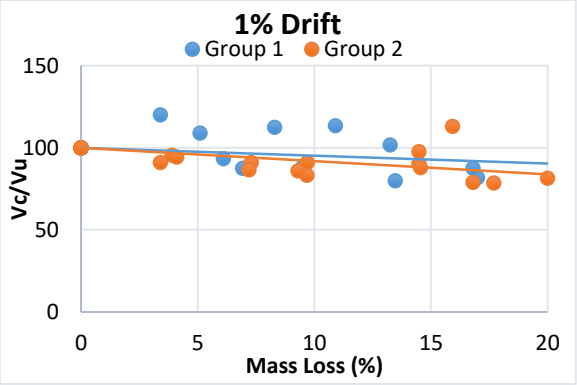

Figure 9-3. Residual Lateral Load Capacity at 1% Drift

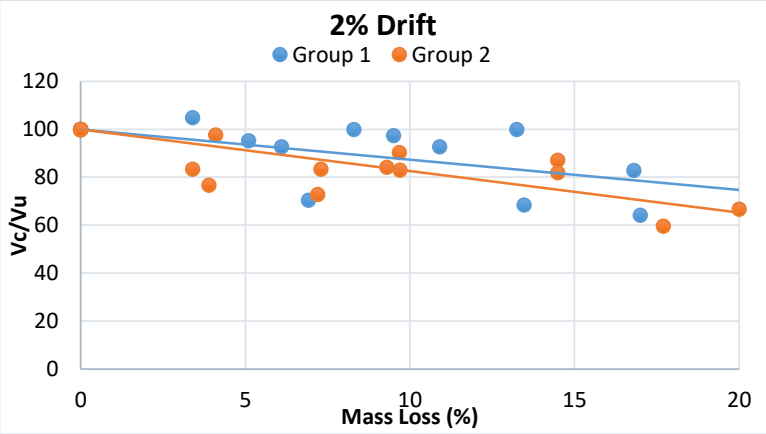

Figure 9-4. Residual Lateral Strength Capacity at 2% Drift

At 2% drift, the reduction in lateral resistance is more evident. Group #1 reaches 80% of residual strength at 17% of mass loss whereas group #2 reaches around 65% of resistance ratio at 20% mass loss.

A parametric equation was formulated to quantify the residual lateral resistance of the columns as a function of the mass loss and drift demand. Equations (6) and (7) describe the observed trends for groups #1 and #2, respectively:

$$\underline{\text{For Group 1:}} \quad r_{v,1} = \frac{V_{cor,1}}{V_{u,1}} = 1 - \frac{0.5 \cdot \theta \cdot x}{100} \tag{9-3}$$

$$\underline{\text{For Group 2:}} \quad r_{v,2} = \frac{V_{cor,2}}{V_{u,2}} = 1 - \frac{0.8 \cdot \theta \cdot x}{100} \tag{9-4}$$

Variable r_v is the corroded lateral resistance ratio, V_{cor} is the lateral resistance of the corroded column at a given level of lateral drift, θ (in percent), and V_u is the corresponding resistance (at the same drift level) of the reference un-corroded column with otherwise identical loading and pristine reinforcing details. Note that the reduction in lateral strength is directly proportional to the reduction in ultimate tensile strength of corroded bars and that the reduced ultimate drift capacity is directly proportional to the reduced maximum elongation of corroded bars owing to the fact that most studied columns failed in flexure instead of shear or anchorage slip.

The stiffness degradation of columns with increasing corrosion-induced reinforcement mass-loss was also studied. Stiffness of each tested column was calculated by dividing the nominal yield force (taken for consistency to be $V_y = 0.85V_{max}$) by the nominal yield drift (taken equal to $\theta_y = 0.5\%$). Stiffness ratios were then calculated by dividing the stiffness of corroded columns by the stiffness of their respective uncorroded column. Figure 9-5 shows the corroded stiffness ratios of Groups 1(a), and 2(b).

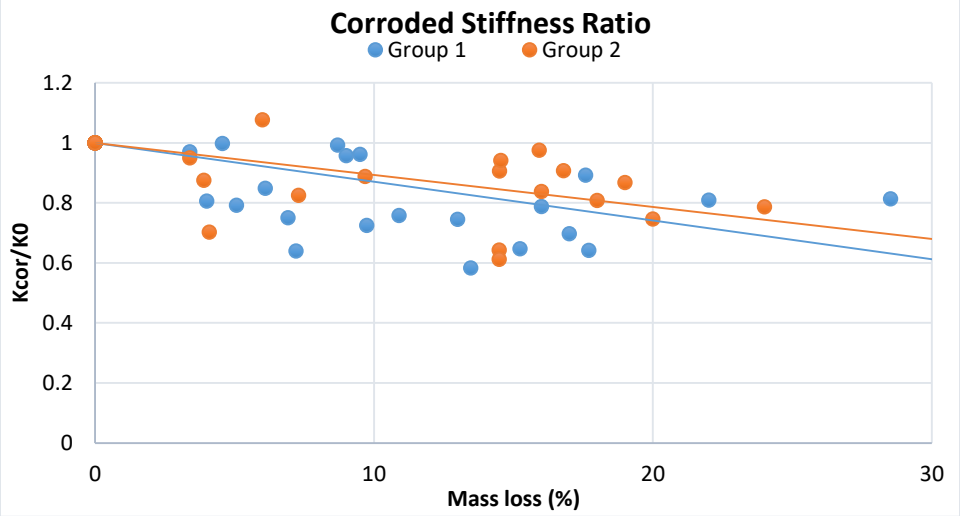

Figure 9-5. Residual stiffness of corroded columns

Equations (9.5-9.6) represent the corroded stiffness ratios for columns in Groups 1 and 2 respectively.

$$\underline{\text{For Group 1:}} \quad r_{k,1} = 1 - \frac{1.29 \cdot x}{100} \tag{9.5}$$

$$\underline{\text{For Group 2:}} \quad r_{k,2} = 1 - \frac{1.07 \cdot x}{100} \tag{9.6}$$

Discrepancies in data are noted between specimens experiencing similar mass losses: this could be attributed to the different test setups, shear reinforcement arrangement and to the current density used in the accelerated corrosion process. Values of current densities ranged from 200 μA/cm^2 to 5000 μA/cm^2 which would yield different corrosive products with different densities of oxides. The difference in corrosive products' densities result in significantly different bond strengths and cracking in the concrete cover (Alonso *et al.*, 1998; El Maaddawy and Soudki, 2003). But the overall behavioral trend of the columns enables the formulation of the above expressions that can be embedded easily in the assessment process by modifying the modeling parameters so as to represent corroded structures.

The above derived expressions (Eqs. 9.1 to 9.6) provide an analytical tool enabling the definition of backbone resistance envelopes of affected structural members from the reference values that ASCE-SEI 41 (2017) recommends for identical components without corrosion:

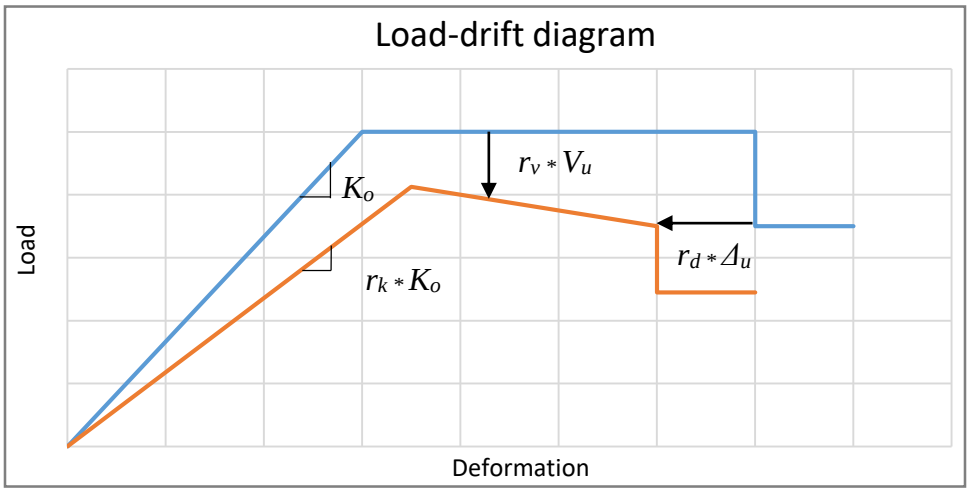

Figure 9-6. Modified resistance envelope for uncorroded and corroded members with otherwise identical properties.

For example, Figure 9-6 plots a backbone envelope prototype that the ASCE/SEI 41 (2017) recommends as *Modelling Parameters* for a column, to be used in nonlinear structural analysis simulations for plastic hinge modelling. In the figure, the blue line represents the response of a pristine component, whereas the orange line represents the modified envelope after degradation for a given level of mass loss. The slope of the ascending branch is thus reduced through multiplier

r_k from the initial reference value (Eq. 9.5, 9.6 and interpolation thereof); similarly, the strength of the load plateau is reduced from its reference value by multiplying with factor r_v (Eq. 9.3, 9.4) and the ultimate drift capacity is reduced by multiplying its reference value by r_d (Eq. 9.1, 9.2).

9.2. Modelling a Structure Example Using SAP2000

To illustrate the relevance of the seismic evaluation procedure with consideration of the corrosion effects, an idealized five-story corroded building (one version with a soft first – storey known as pilotis system, and one without pilotis) was assessed under a time-history analysis. In this investigation, it has been assumed that only the ground floor columns had suffered from corrosion damage. The structure was assessed for a number of ground motion records as listed in Tables 9-2 and 9-3. The records were selected to represent a range of peak ground acceleration intensities from 0.15g to 0.42g. These were further scaled up or down from the recorded peak ground acceleration (pga) value by 0.05g so that a range of plausible ground motions could be considered without employing frequency content of motions out of the range of their intensity. Therefore, for a ground motion with a pga of 0.2g, scaled versions to 0.15g and 0.25g were considered; similarly, for records with a pga of 0.25g, scaling down 0.2g and up to 0.3 was considered. Ground motion time histories are shown in Figure 9-7.

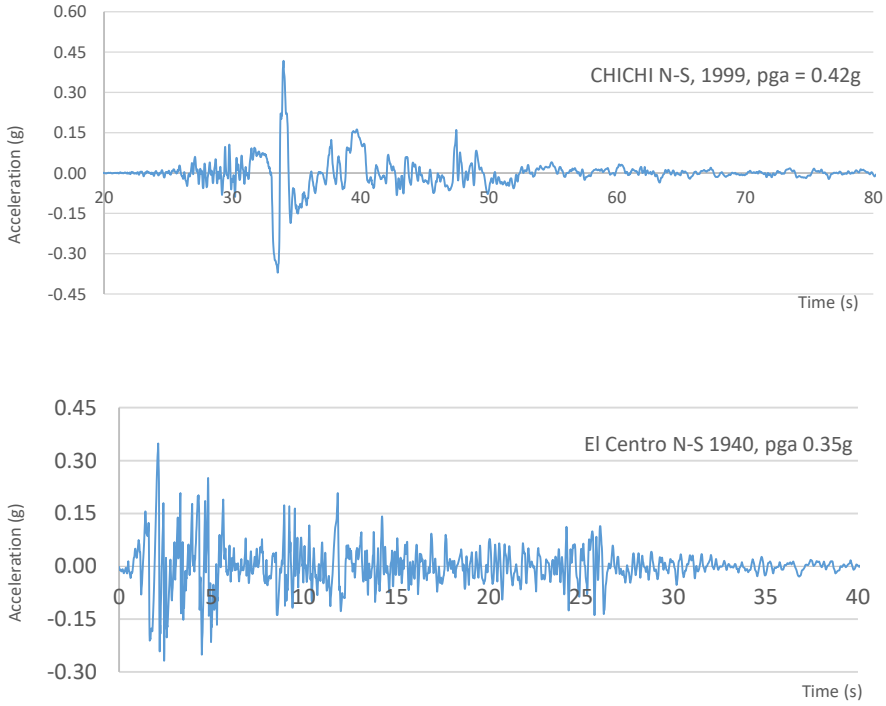

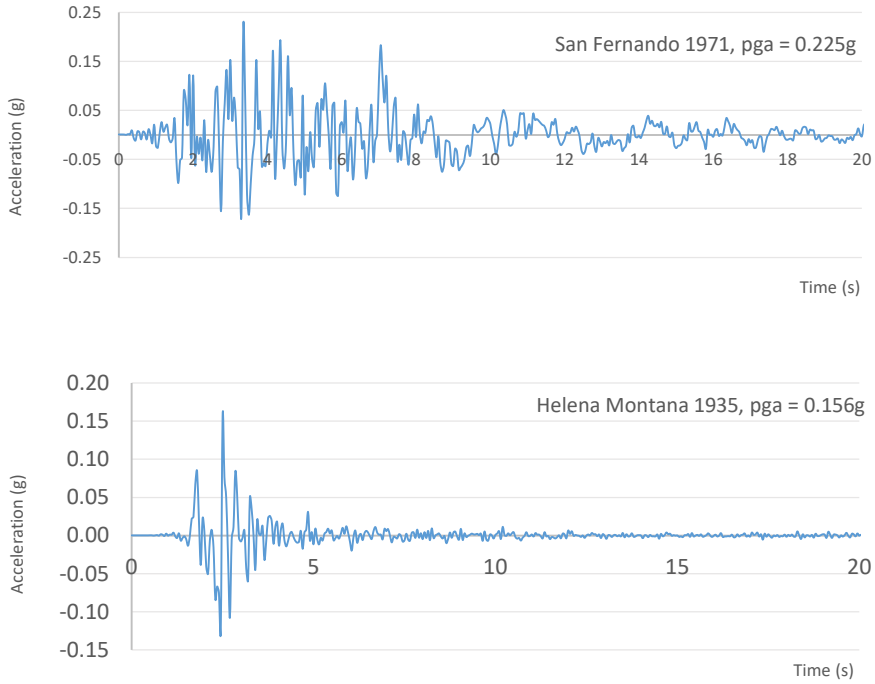

Figure 9-7. Ground motion time histories of: CHICHI 1999, El Centro 1940, San Fernando 1971 and Helena Montana 1935 earthquakes

9.2.1. Model Description

The example model building studied had a regular floor plan as shown in Figure 9-9 with a 2.9 m story height and *6 m* and *5.5 m* spans in the x and y directions, respectively. Columns had square cross-sections of *400*x*400 mm*. All columns were reinforced with *8-20M* bars with f_y = *400* MPa and *10M* bars as perimeter ties spaced at 180mm o.c. with f_{yt} = *220* MPa. Beams had a rectangular cross-section of *250*x*500mm* and were singly reinforced with *3-15M* bars in the tension regions (at the lower part in the mid-span and the top of the section at supports). Monolithically cast slabs, (including a layer of topping) *180 mm* thick with *60mm* of fill on top of it, reinforced with *10M* bars were spaced at *200 mm* top and bottom in both directions. Cross-sectional reinforcing details of the structural members are shown in Figure 9-8.

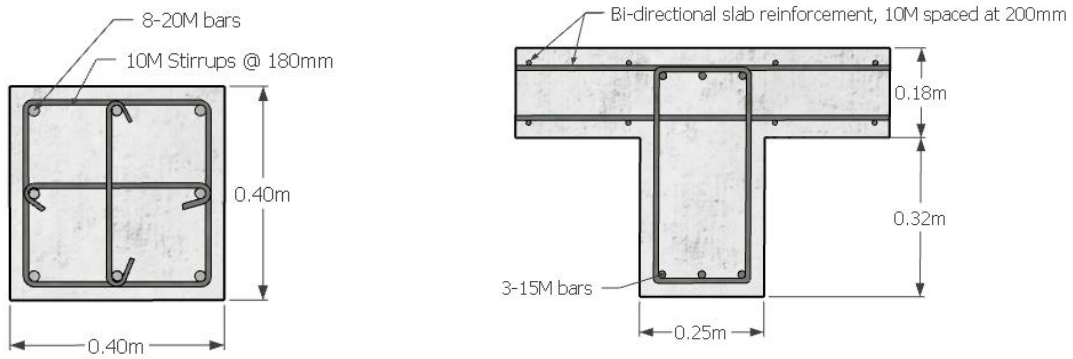

Typical Columns Cross-Section Typical Beam Cross-Section

Figure 9-8. Cross-Sectional detailing of the structure's columns and beams

Concrete compressive strength was taken equal to f'_c = 25 MPa; Concrete cover was c_c = 25 mm. Exterior cladding comprising masonry blocks in the upper floors were replaced by X braces having the same lateral stiffness in order to simplify the modelling process. Two cases of the building were studied, one being in pristine condition, and the second assuming all first storey columns were corroded having 10% in reinforcement mass loss. These two cases were studied for the structure with and without a soft first storey (pilotis); thus a total of four different cases were considered for each ground motion analysis.

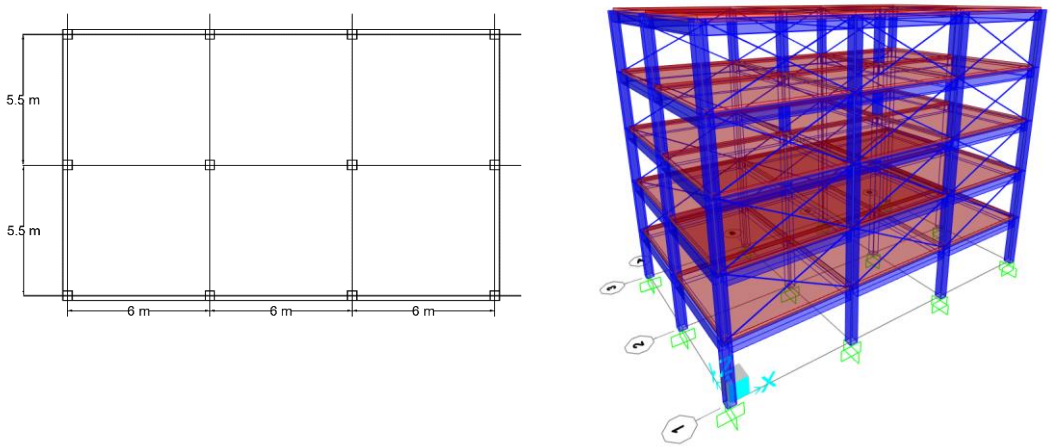

Figure 9-9. Floor plan (left) SAP2000 model of building with pilotis (right)

9.2.2. Model Modifications

In this example only those special modifications to the frame model that are needed for accounting for the effects of corrosion on member properties are discussed. Material properties of steel bars (i.e., the yield and ultimate strengths of both longitudinal and transverse reinforcements) were reduced based on Eqs. (2.3) and were assigned to the corroded columns. To account for the cracking and effective delamination of the concrete cover, section dimensions of corroded columns were reduced to 370 (from 400, therefore, the contribution of cover concrete was neglected in the plastic hinge zone of the corroded members).

Since the columns studied in Section 4 of this paper have identical characteristics as the columns of the building under study, plastic hinge properties assigned were based on the moment vs. plastic rotation values derived according with the backbone curves. In the more general case, plastic hinge characteristics of corroded columns could be defined from the backbone curve of a pristine column using Eqs. (9.1-9.6). Moment-rotation curves of pristine columns can be obtained based on either ASCE 41-17 or Eurocode 8-III (ASCE 41, 2017; EN 1998-3, 2021).

Plastic hinges of columns were modelled as interacting axial-biaxial bending hinges and were deformation controlled. The hinge behavior was specified in terms of moment-rotation backbone envelope with symmetric characteristics about the two principal axes of the column cross sections, as depicted in Figure 9-10. Uncorroded hinges had a yielding moment of *200 KN.m* and a maximum moment of *235 KN.m*. Corroded hinges had a yielding moment of *140 KN.m*. These moment capacities are assigned for the case of pure flexure, and the program then extracts the envelope for higher axial load values.

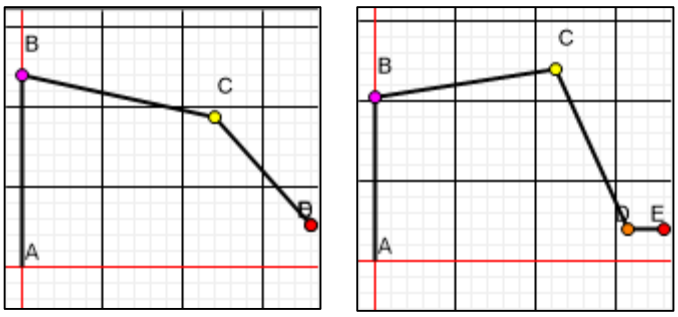

Figure 9-10. Plastic Hinge Properties. Corroded Hinge (left) Uncorroded Hinge (right)

The graphs of Figure 9-10 represent the plastic hinge properties of both corroded and uncorroded columns; the envelopes refer only to the plastic component of the total response (after having subtracted the elastic component, which is defined by the yield moment, M_y and the drift ratio at the onset of yielding, θ_y). The secant to yield elastic stiffness of the members considered was that of the cracked section and was calculated as described in ASCE/SEI 41, 2017, Table 10-5. Corroded stiffness was calculated using Equation 9-7.

$$EI_{cor} = r_{k,1} \cdot EI \tag{9-7}$$

The model was subjected to non-linear time-history analysis with direct time integration. Second order effects were taken into consideration (thus the analysis was preceded with the application of permanent loads). The time step size was set equal to the discretization time step of the ground motion record. 5% damping was assumed. Each story was assigned a rigid diaphragm and the end length rigid zone offsets for the beams and columns was 0.5.

9.2.3. Results and Discussion

Before the time history analysis, modal analysis was conducted using SAP2000, and it was found that corrosion in the bottom floor columns of the structure with pilotis increased the fundamental period of the structure by 28% (from T = 0.7s to T=0.9s.) whereas in the structure without the pilots (this is the bare frame without the cladding to add stiffness to the upper floors) the period was increased by 15% (from T = 0.86s to T = 0.99s).

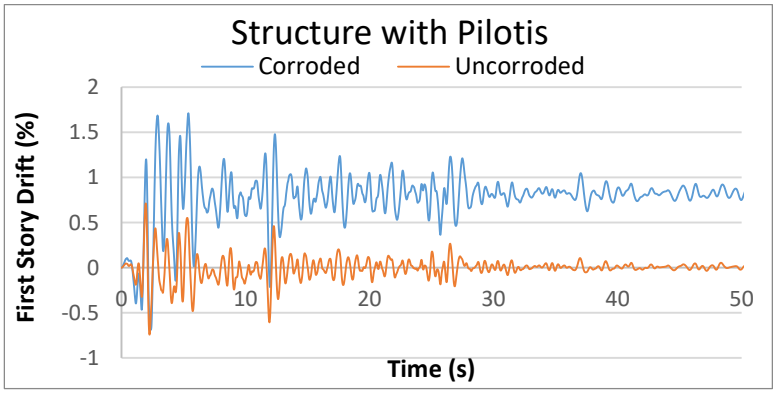

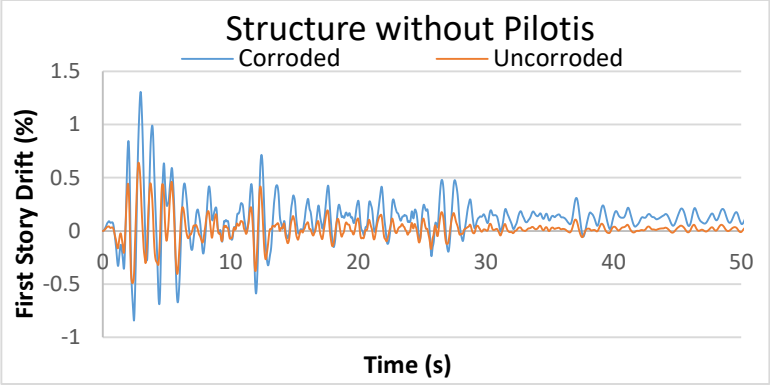

Figure 9-11. First Story drift response to El Centro N-S 1940 earthquake excitation (a) for structure with pilotis (b) for structure without pilotis

Figure 9-11 plots the calculated time history response to the El Centro N-S (1940) component of the excitation, for the first story drift of the corroded and uncorroded structures. It is observed that the reduction in stiffness of the corroded structure leads to an increased demand in first story drift. In the case of the Pilotis structure, the first story drift of the corroded structure reached a drift of 1.7%, leading to a 0.8% residual first story drift at the end of the analysis. For the uncorroded building, the same earthquake demanded a maximum of 0.74% drift (40% of the demand on the corroded structure) and the residual first story drift was 0.016%. In the case of the structure without pilotis, the maximum first story demand of the corroded building was 1.18% whereas it was only 0.62% for the uncorroded structure (50% of the corroded building demand).

Tables 9-2 and 9-3 summarize the maximum drift demands for the corroded and uncorroded cases of the two structures (with and without pilotis). The structures were analysed to 10 ground motions as follows: The El Centro N-S (1940), San Fernando (1971) and Helena Montana (1935) earthquakes as well as their scaled versions, and the CHICHI N-S (1999) ground motion which was not scaled up on account of its very high peak ground acceleration intensity (0.42g). It was observed that drift demand, on average, was doubled in the presence of corrosion.

Corroded models did not yield any tangible values in the case of the CHICHI N-S 1999 earthquake as the structure collapsed immediately.

As expected, the structure with pilotis experienced a greater drift demand compared to the structure without pilotis, owing due to the difference in the distribution of lateral stiffness between the ground and first floor which was effected by the exterior masonry cladding. The corroded structure without pilotis experienced a maximum residual lateral drift of 1.4% whereas this value was

increased to 3% (i.e., collapse) for the structure with pilotis. It was also observed that for ground motions with a pga less than 0.3g, no significant residual drift was calculated. Limit state criteria for corroded columns were calculated based on ASCE 41-17 using Table 10-8 of the reference document (ASCE 41, 2017) and are shown in Table 9-1:

Table 9-1. Limit State Drifts of corroded and uncorroded columns

ID	*IO (Drift)*	*LS (Drift)*	*CP (Drift)*
Un corroded	0.5%	0.9%	1.3%
Corroded	0.45%	0.8%	1.1%

It was observed that corrosion shifted the structural performance of the building either from Life Safety Performance (LS) to Collapse Prevention (CP) or from Immediate Occupancy (IO) to LS as can be seen in Table 9-2.

Table 9-2 Maximum drift demands and residual drift ratios of the structure with pilotis under various ground motion excitations

PILOTIS	PGA		Max Drift (%)	Change (%)	Residual Drift (%)	Limit State
CHICHI	0.42g	Uncorroded	2.6	N/A	0.64	C
		Corroded	//		//	//
El Centro	0.4g	Uncorroded	1.16	191	0.14	CP
		Corroded	2.5		1.9	C
	0.35g	Uncorroded	0.74	130	0.016	LS
		Corroded	1.7		0.81	C
	0.3g	Uncorroded	0.7	83	0.03	LS
		Corroded	1.28		0.34	C
San Fernando	0.275g	Uncorroded	0.53	117	0.08	LS
		Corroded	1.15		0.42	C
	0.225g	Uncorroded	0.42	88	0.014	IO
		Corroded	0.79		0.09	LS
	0.175g	Uncorroded	0.32	91	0	IO
		Corroded	0.61		0	LS
Helena Montana	0.206g	Uncorroded	0.29	162	0	IO

		Corroded	0.76		0.07	LS
	0.156g	Uncorroded	0.22	159	0	IO
		Corroded	0.57		0	LS
	0.106g	Uncorroded	0.15	160	0	IO
		Corroded	0.39		0	IO
			Average	131		

Table 9-3. Maximum drift demand and residual drift of the structure without pilotis under various ground motion excitations

Non-Pilotis	PGA		Max Drift (%)	Change (%)	Residual Drift (%)
CHICHI	0.42g	Uncorroded	2.59	184	0.2
		Corroded	//		//
El Centro	0.4g	Uncorroded	0.72	118	0.064
		Corroded	1.57		0.16
	0.35g	Uncorroded	0.64	103	0.036
		Corroded	1.3		0.12
	0.3g	Uncorroded	0.55	98	0.02
		Corroded	1.09		0.03
San Fernando	0.275g	Uncorroded	0.42	83	0.011
		Corroded	0.77		0.014
	0.225g	Uncorroded	0.34	97	0
		Corroded	0.67		0.013
	0.175g	Uncorroded	0.26	100	0
		Corroded	0.52		0
Helena Montana	0.206g	Uncorroded	0.31	106	0
		Corroded	0.64		0
	0.156g	Uncorroded	0.24	104	0
		Corroded	0.49		0
	0.106g	Uncorroded	0.16	106	0
		Corroded	0.33		0
			Average	102	

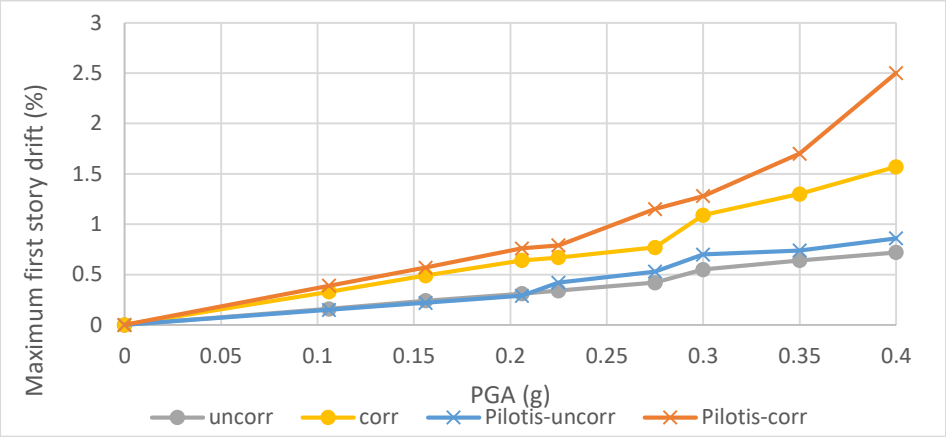

Figure 9-12. Maximum first story drift at different peak ground accelerations.

Figure 9-12 plots the maximum first story drift with respect to increasing peak ground accelerations (PGA). Using the obtained data from the simulations and the calculated limit states, fragility curves for the corroded and uncorroded pilotis structure were generated using a VBA coded spreadsheet by Gandage, S., et *al.* (2019). Figure 9-13 shows the probability of the structure to exceed drift demands of three limit states (IO, LS, CP) with increasing PGAs (horizontal axis) with 0 being the least probable and 1 being the most probable (vertical axis). It is observed that corrosion significantly impacts the probability of failure; for the example case-study, the probability of the uncorroded structure to surpass the IO limit state becomes the probability of the corroded structure to surpass the LS limit state.

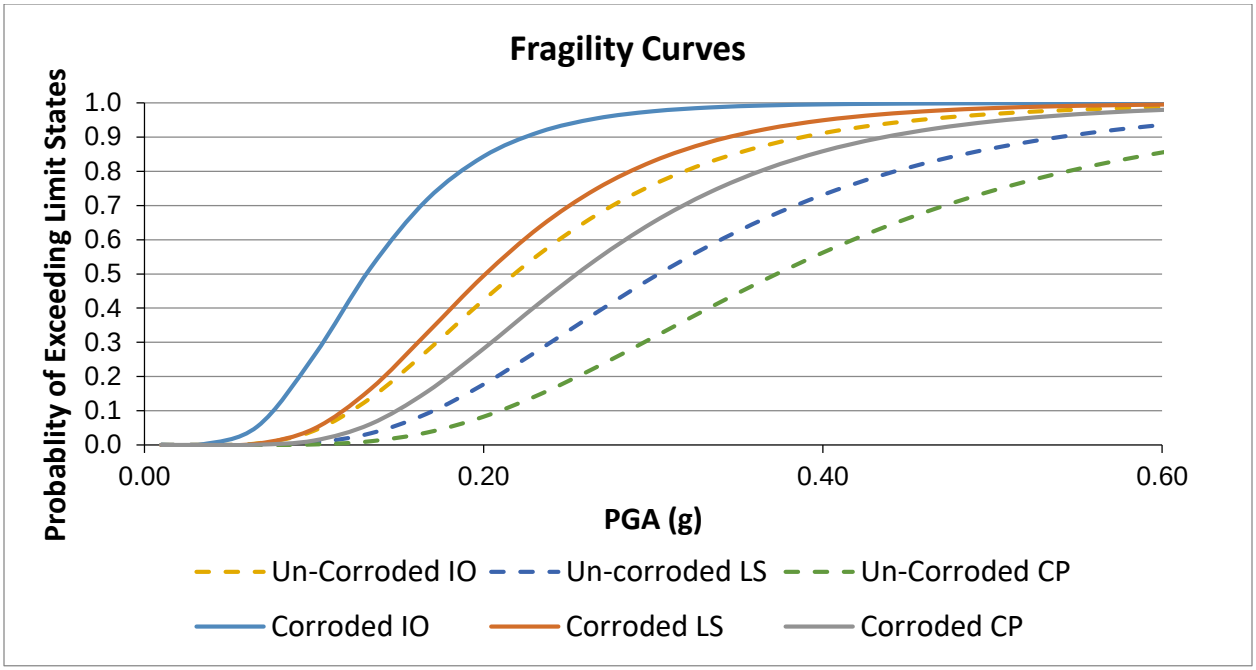

Figure 9-13. Fragility curves for the corroded (straight line) and un-corroded structure (dashed line) at the three limit states.

9.3. Seismic Drift Demands as a Function of the Stiffness index

The reason why stiffness reduction (or increasing compliance) of structures to lateral load is of importance is because lateral stiffness is the determining factor in estimating the magnitude of drift demands and the ensuing damage in the event of an earthquake. Rapid seismic assessment procedures have already been developed based on this concept (Pardalopoulos, Thermou and Pantazopoulou, 2013; Pardalopoulos, Pantazopoulou and Lekidis, 2018), that link lateral drift demand of the critical storey to a pertinent index of lateral stiffness; this comprises a weighted contribution of the area ratio of the columns, walls and masonry infills in the plan of the critical floor (the last two being considered when oriented in the direction of the earthquake action). From this work, vulnerability curves had been derived using the EC8-I design spectrum (Type I) shown in Figure 9-14 where the drift demand is plotted against the stiffness index (note that this Figure was derived for unit peak ground acceleration $a_g=1m/s^2$, and assuming a mass density per floor area equal to 1 tn/m^2 - this corresponds to a distributed total dead load of 10 kN/m^2 which is common for residential reinforced concrete construction; for different values of ground acceleration and mass density the values in the ordinate of the vulnerability plot have to be properly

scaled: for example, if a_g = 0.36g = 3.53m/s^2 and γ = 0.5tn/m^2, then the ordinate should be multiplied by the product 3.53 · 0.5 = 1.765).

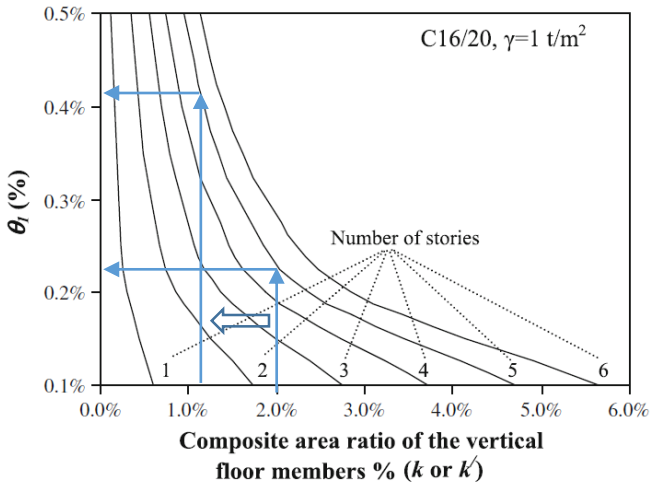

Figure 9-14. Seismic vulnerability curves for multi-storey buildings with uniform plan (Pardalopoulos, Thermou and Pantazopoulou, 2013)

Note that in Figure 9-14, term θ_1 is the drift demand of the first story, k is the combined stiffness index for dual systems shown in Equation (9-8) and k' is the stiffness index of infilled framed structures as shown in Equation (9-10):

$$k = \rho_c + \eta_{wm}\rho^e_{wm} \text{ where } \eta_{wm} = \frac{25E_{wm}}{E_c\cdot\left(\frac{h_{st}^2}{l_{m.ave}^2}+2.5\right)} \tag{9-8}$$

$$\rho^e_{wm,i} = \rho_{wm,i} + \frac{\left(4\frac{h_{st}^2}{l_{m,ave}^2}+2.5\right)E_c}{\left(4\frac{h_{st}^2}{l_{w,ave}^2}+2.5\right)E_{wm}}\rho_{wc,i} \tag{9-9}$$

$$k' = \rho_c + \eta'_{wm}\rho_{wm} \text{ where } \eta'_{wm} = \frac{10\cdot f_{wk}\sqrt{1+\left(\frac{h_{st}^2}{l_{w,ave}^2}\right)}}{E_c\theta_1} \tag{9-10}$$

In the above equations, ρ_c is the effective area ratio of columns in the floor plan, E_c and E_{wm} are the elastic moduli of concrete and masonry respectively, ρ^e_{wm} is an equivalent dimensionless area index representing both masonry and RC walls expressed in terms of masonry properties, h_{st} is the clear storey height, $l_{m,ave}$ and $l_{w,ave}$ are the average lengths of masonry and RC walls in the plane of action, respectively, f_{wk} is the masonry's compressive strength and Θ_1 is the estimated chord rotation demand of the first story. For a building comprising reinforced concrete frames only, without either structural or masonry walls, the stiffness index $k' = \rho_c$. In order to account for the

deprecating effects of corrosion on lateral stiffness, the reduction coefficient r_k is introduced in the calculation of k, as follows: The effective (i.e. reduced from its nominal value) area ratio of the columns, $\rho_{c,i}$, may be related to the aggregate secant-to-yield floor stiffness K_{cor} using Equations (9.10) and (9.11).

$$k_{cor} = r_k \cdot \frac{12 E_c d_c^2 \rho_{c,i} A_f}{3 h_s^3} \tag{9.10}$$

$$\rho_{c,i} = \frac{K \cdot 3 h_{st}^3}{12\, E_c d_c^2 A_f} \tag{9.11}$$

where, E_c is the modulus of elasticity of concrete, d_c is the depth of the section, A_f is the total floor area and h_{st} is the clear column height; cracked sections have been assumed in deriving the above (this corresponds to a stiffness reduction by 66%=2/3 of gross stiffness for columns). By multiplying k or k' by r_k (≤1) then it necessarily follows that the stiffness index will be reduced, leading to higher drift demands. For example, consider a 5-story building comprising of frames only, having $\rho_{c,i}$ = *2%* and a mass per unit area of the floor γ*=1 t/m*^{2}. For an earthquake with a_g*=2.5m/s*^{2}, the drift demand in the first floor according to Figure 9-13 is *0.55%* (0.22% x 2.5). If the same structure has suffered from corrosion damage accounting for 7% mass loss, then r_k = 0.67. The modified $\rho_{c,cor}$ = 1.34% = 0.67×2%, thus the amplified drift demand would be 1% (0.4% x 2.5), which represents an 80% increase in deformation demand. This increase falls within the range estimated earlier in the case study of the five story structure presented in Section 9.2 for earthquakes having a pga of 0.25g.

9.4. Conclusions

This chapter proposed a complete methodology by which to take corrosion damage into consideration in the seismic evaluation frameworks of both Tier-3 (advanced, nonlinear) and Tier-2 (rapid) assessment guidelines. For the advanced nonlinear procedure, in evaluating the backbone resistance response curve of an existing structural member subjected to lateral loads, the benchmark modelling parameters recommended by ASCE/SEI 41 (2017) for uncorroded structures are modified through pertinent attenuating factors that consider the deprecating effects of corrosion. Expressions quantifying the degradation in stiffness, strength and ultimate deformation of corroded columns were developed in order to define these attenuating factors. These expressions provide an analytical tool that allow the rapid definition of nonlinear backbone

resistance envelopes and acceptance criteria of corroded columns without the need of detailed calculation. This enables the modelling of plastic hinges in structural analysis software for versatile modelling of corroded structural members and systems for the needs of detailed seismic evaluation.

A five-story structure with pilotis, representative of old construction (based on older detailing practices) was assessed using the proposed procedures, under a suite of different earthquake excitations. Four different variations of the structure were modelled, namely: with and without cladding in the upper floor (which created conditions of sort story in the first floor) and with and without corrosion damage in the first floor columns. A modelling procedure based on the derived backbone curves for corroded members was proposed in order to take corrosion into consideration. Results show a significant alteration to the response of the structure in terms of maximum and residual drift demands, and exhaustion of the critical members' reduced deformation capacity. The key takeaway is that it is imperative to consider pre-existing corrosion damage in seismic assessment of existing structures as it may significantly alter the result of the seismic evaluation process.

Simpler, Tier-2 level procedures based on demands defined by the design spectra were also shown to be easily incorporated in rapid assessment: here, only the stiffness reduction factor is considered in order to attenuate the estimated lateral stiffness of the structure, which determines the demand through the period elongation. Because relative displacement is proportional to the absolute response acceleration and the second power of the period, it is clear that any stiffness reduction is directly reflected by a proportional increase of the displacement demand. For rapid assessment, by setting criteria for limiting the operational limit (e.g. a drift of 0.75% in the critical floor, or less if the building has brittle details), comparison with the estimated demands is straightforward and produces immediate results.

9.5. References

ACI-374 (2016) *ACI 374 - Guide to Nonlinear Modeling Parameters for Earthquake-Resistant Structures*. Available at: www.concrete.org (Accessed: 27 March 2022).

ACI 222R-19 (2019) 'Guide to Protection of Reinforcing Steel in Concrete Against Corrosion', *American Concrete Institute*, pp. 1–65.

Al-Saidy, A. H. *et al.* (2016) 'Structural behavior of corroded RC beams with/without stirrups repaired with CFRP sheets', *Materials and Structures*. Springer Netherlands, 49(9), pp. 3733–3747. doi: 10.1617/s11527-015-0751-y.

Al-Sulaimani, G. J. *et al.* (1990) 'Influence of corrosion and cracking on bond behavior and strength of reinforced concrete members', *ACI Structural Journal*, 87(2), pp. 220–231. doi: 10.14359/2732.

Alaskar, A. (2013) 'Shear Behaviour of Slender RC Beams with Corroded Web Reinforcement'. University of Waterloo. Available at: https://uwspace.uwaterloo.ca/handle/10012/7472 (Accessed: 15 July 2019).

Allamt, I. M. *et al.* (1994) *Influence of atmospheric corrosion on the mechanical properties of reinforcing steel, Construction and Building Materials*.

Almusallam, A. A. *et al.* (1996) 'Effect of reinforcement corrosion on bond strength', *Construction and Building Materials*. Elsevier, 10(2), pp. 123–129. doi: 10.1016/0950-0618(95)00077-1.

Almusallam, A. A. (2001a) 'Effect of degree of corrosion on the properties of reinforcing steel bars', *Construction and Building Materials*. Elsevier, 15(8), pp. 361–368. doi: 10.1016/S0950-0618(01)00009-5.

Almusallam, A. A. (2001b) 'Effect of degree of corrosion on the properties of reinforcing steel bars', *Construction and Building Materials*. Elsevier, 15(8), pp. 361–368. doi: 10.1016/S0950-0618(01)00009-5.

Alonso, C. *et al.* (1998) 'Factors controlling cracking of concrete affected by reinforcement corrosion', *Materials and Structures*. Kluwer Academic Publishers, 31(7), pp. 435–441. doi:

10.1007/BF02480466.

American Road & Transportation Builders Association (2020) *ARTBA Bridge Report*. Available at: https://artbabridgereport.org/ (Accessed: 6 July 2020).

Amleh, L., Mirza, M. and Ahwazi, B. (2000) 'Bond deterioration of reinforcing steel in concrete due to corrosion'. Available at: https://books.google.com/books?hl=en&lr=&id=F8HosZdH8BUC&oi=fnd&pg=PA247&ots=Iq_HHO_T-s&sig=3ytv3HtTEhxTvU9yTJRyH6PPLrk (Accessed: 5 July 2019).

Andrade, C., Alonso, M. C. and Gonzalez, J. A. (1990) 'Initial effort to use the corrosion rate measurements for estimating rebar durability', *ASTM Special Technical Publication*. ASTM International, (1065), pp. 29–37. doi: 10.1520/stp25013s.

Andrade, C. and González, J. A. (1978) 'Quantitative measurements of corrosion rate of reinforcing steels embedded in concrete using polarization resistance measurements', *Materials and Corrosion*, 29(8), pp. 515–519. doi: 10.1002/maco.19780290804.

Apostolopoulos, C. A. (2007) 'Mechanical behavior of corroded reinforcing steel bars S500s tempcore under low cycle fatigue', *Construction and Building Materials*. Elsevier, 21(7), pp. 1447–1456. doi: 10.1016/J.CONBUILDMAT.2006.07.008.

Apostolopoulos, C. A. and Papadakis, V. G. (2008) 'Consequences of steel corrosion on the ductility properties of reinforcement bar', *Construction and Building Materials*. Elsevier, 22(12), pp. 2316–2324. doi: 10.1016/J.CONBUILDMAT.2007.10.006.

Apostolopoulos, C., Drakakaki, A. and Basdeki, M. (2019) 'Seismic assessment of RC column under seismic loads', *International Journal of Structural Integrity*. Emerald Publishing Limited , 10(1), pp. 41–54. doi: 10.1108/IJSI-02-2018-0013.

ASCE 41 (2017) *Seismic Evaluation and Retrofit of Existing Buildings, Seismic Evaluation and Retrofit of Existing Buildings*. American Society of Civil Engineers. doi: 10.1061/9780784414859.

Azad, A. K., Ahmad, S. and Al-Gohi, B. H. A. (2010) 'Flexural strength of corroded reinforced concrete beams', *Magazine of Concrete Research*. Thomas Telford Ltd , 62(6), pp. 405–414. doi: 10.1680/macr.2010.62.6.405.

Berra, M., Castellani, A. and Coronelli, D. (1997) 'Bond in reinforced concrete and corrosion of bars', in *Structural Faults and Repair*. Edinburgh, UK, pp. 349–357.

Berrocal, C. G. *et al.* (2017) 'Corrosion-induced cracking and bond behaviour of corroded reinforcement bars in SFRC', *Composites Part B: Engineering*. Elsevier, 113, pp. 123–137. doi: 10.1016/J.COMPOSITESB.2017.01.020.

Blaber, J., Adair, & B. and Antoniou, & A. (no date) 'Ncorr: Open-Source 2D Digital Image Correlation Matlab Software'. doi: 10.1007/s11340-015-0009-1.

Cairns, J., Du, Y. and Law, D. (2008) 'Structural performance of corrosion-damaged concrete beams', *Magazine of Concrete Research*. Thomas Telford Ltd , 60(5), pp. 359–370. doi: 10.1680/macr.2007.00102.

Di Carlo, F., Meda, A. and Rinaldi, Z. (2017) 'Numerical cyclic behaviour of un-corroded and corroded RC columns reinforced with HPFRC jacket', *Composite Structures*. Elsevier, 163, pp. 432–443. doi: 10.1016/J.COMPSTRUCT.2016.12.038.

Castel, A., François, R. and Arliguie, G. (2000) 'Mechanical behaviour of corroded reinforced concrete beams—Part 1: Experimental study of corroded beams', *Materials and Structures*. Kluwer Academic Publishers, 33(9), pp. 539–544. doi: 10.1007/BF02480533.

CEN (2005) *EN 1998 - 3 Eurocode 8-Design of structures for earthquake resistance-Part 3: Assessment and retrofitting of buildings*.

Cervenka Consulting (2007) 'ATENA Program Documentation'. Prague, Czech Republic.

Civjan, S. A. *et al.* (2005) 'Effectiveness of corrosion inhibiting admixture combinations in structural concrete', *Cement and Concrete Composites*. Elsevier, 27(6), pp. 688–703. doi: 10.1016/J.CEMCONCOMP.2004.07.007.

Coronelli, D. and Gambarova, P. (2004) 'Structural Assessment of Corroded Reinforced Concrete Beams: Modeling Guidelines', *Journal of Structural Engineering*. American Society of Civil Engineers, 130(8), pp. 1214–1224. doi: 10.1061/(ASCE)0733-9445(2004)130:8(1214).

Coronelli, D., Hanjari, K. Z. and Lundgren, K. (2013) 'Severely Corroded RC with Cover Cracking', *Journal of Structural Engineering*, 139(2), pp. 221–232. doi:

10.1061/(ASCE)ST.1943-541X.0000633.

Dang, V. H. and François, R. (2013) 'Influence of long-term corrosion in chloride environment on mechanical behaviour of RC beam', *Engineering Structures*. Elsevier, 48, pp. 558–568. doi: 10.1016/j.engstruct.2012.09.021.

Darwin, D. and Pecknold, D. (1974) *INELASTIC MODEL FOR CYCLIC BIAXIAL LOADING OF REINFORCED CONCRETE*. Illinois, Urbana. Available at: https://www.semanticscholar.org/paper/INELASTIC-MODEL-FOR-CYCLIC-BIAXIAL-LOADING-OF-Darwin-Pecknold/5d1fb39809798f4c65b2dfa0fad5c06dd82e2a6f (Accessed: 20 July 2022).

Du, Y., Clark, L. A. and Chan, A. H. C. (2007) 'Impact of Reinforcement Corrosion on Ductile Behavior of Reinforced Concrete Beams', *ACI Structural Journal*, 104(3), pp. 285–293. doi: 10.14359/18618.

Du, Y. G., Clark, L. A. and Chan, A. H. C. (2005) 'Residual capacity of corroded reinforcing bars', *Magazine of Concrete Research*. Thomas Telford Ltd , 57(3), pp. 135–147. doi: 10.1680/macr.2005.57.3.135.

El-Joukhadar, N., Tsiotsias, K. and Pantazopoulou, S. (2019) 'Consideration of the state of corrosion in seismic assessment of columns', *International Journal of Structural Integrity*. Emerald Group Publishing Ltd. doi: 10.1108/IJSI-07-2019-0065.

Fakhri, H., Ragalwar, K. A. and Ranade, R. (2019) 'On the use of Strain-Hardening Cementitious Composite covers to mitigate corrosion in reinforced concrete structures', *Construction and Building Materials*. Elsevier Ltd, 224, pp. 850–862. doi: 10.1016/j.conbuildmat.2019.07.052.

Fang, C. *et al.* (2004) 'Corrosion influence on bond in reinforced concrete', *Cement and Concrete Research*. Pergamon, 34(11), pp. 2159–2167. doi: 10.1016/J.CEMCONRES.2004.04.006.

Farhan, N. A., Sheikh, M. N. and Hadi, M. N. S. (2018) 'Experimental Investigation on the Effect of Corrosion on the Bond Between Reinforcing Steel Bars and Fibre Reinforced Geopolymer Concrete', *Structures*. Elsevier, 14, pp. 251–261. doi:

10.1016/J.ISTRUC.2018.03.013.

Fernandez, I. *et al.* (2018) 'Ultimate Capacity of Corroded Statically Indeterminate Reinforced Concrete Members', *International Journal of Concrete Structures and Materials*. Springer Singapore, 12(1), p. 75. doi: 10.1186/s40069-018-0297-9.

Fernandez, I., Bairán, J. M. and Marí, A. R. (2015) 'Corrosion effects on the mechanical properties of reinforcing steel bars. Fatigue and σ–ε behavior', *Construction and Building Materials*. Elsevier, 101, pp. 772–783. doi: 10.1016/J.CONBUILDMAT.2015.10.139.

Fernandez, I. and Berrocal, C. G. (2019) 'Mechanical Properties of 30 Year-Old Naturally Corroded Steel Reinforcing Bars', *International Journal of Concrete Structures and Materials*. Korea Concrete Institute, 13(1), p. 9. doi: 10.1186/s40069-018-0308-x.

Fernandez, I., Lundgren, K. and Zandi, K. (2018) 'Evaluation of corrosion level of naturally corroded bars using different cleaning methods, computed tomography, and 3D optical scanning', *Materials and Structures/Materiaux et Constructions*. Springer Netherlands, 51(3), pp. 1–13. doi: 10.1617/s11527-018-1206-z.

fib-Model Code (2020) 'Model Code 2020, Draft version MC2020', in. fib.

fib bulletin #10 (2000) *Bond of reinforcement in concrete : state-of-art report*. International Federation for Structural Concrete. Available at: https://www.fib-international.org/publications/fib-bulletins/bond-of-reinforcement-in-concrete-pdf-detail.html (Accessed: 3 July 2019).

fib Model Code (2010) *Fib model code for concrete structures 2010*.

Fischer, C., Ozbolt, J. and Gehlen, C. (2010) 'Numerical investigation on bond behavior of corroded reinforcement', in *7th International Conference on Fracture Mechanics of Concrete and Concrete Structures*. Jeju, Korea, pp. 779–785.

François, R. and Arliguie, G. (1998) 'Influence of Service Cracking on Reinforcement Steel Corrosion', *Journal of Materials in Civil Engineering*, 10(1), pp. 14–20. doi: 10.1061/(ASCE)0899-1561(1998)10:1(14).

François, R., Khan, I. and Dang, V. H. (2013) 'Impact of corrosion on mechanical properties of

steel embedded in 27-year-old corroded reinforced concrete beams', *Materials and Structures*. Springer Netherlands, 46(6), pp. 899–910. doi: 10.1617/s11527-012-9941-z.

Fu, C. *et al.* (2017) 'Corrosion characteristics of a 4-year naturally corroded reinforced concrete beam with load-induced transverse cracks', *Corrosion Science*. Pergamon, 117, pp. 11–23. doi: 10.1016/J.CORSCI.2017.01.002.

Ganesh, P. and Ramachandra Murthy, A. (2020) 'Simulation of surface preparations to predict the bond behaviour between normal strength concrete and ultra-high performance concrete', *Construction and Building Materials*. Elsevier, 250, p. 118871. doi: 10.1016/J.CONBUILDMAT.2020.118871.

Gjørv, O. E. (2014) *Durability Design of Concrete Structures in Severe Environments*. CRC Press. doi: 10.1201/b16469.

Goksu, C. and Ilki, A. (2016) 'Seismic Behavior of Reinforced Concrete Columns with Corroded Deformed Reinforcing Bars', *ACI Structural Journal*, 113(5), pp. 1053–1064. doi: 10.14359/51689030.

Haddad, R. H. and Ashteyate, A. M. (2001) 'Role of synthetic fibers in delaying steel corrosion cracks and improving bond with concrete', *Canadian Journal of Civil Engineering*. NRC Research Press Ottawa, Canada , 28(5), pp. 787–793. doi: 10.1139/l01-037.

Hanjari, K. Z., Coronelli, D. and Lundgren, K. (2011) 'Bond capacity of severely corroded bars with corroded stirrups', *Magazine of Concrete Research*. Thomas Telford Ltd , 63(12), pp. 953–968. doi: 10.1680/macr.10.00200.

Harajli, M. H. (2004) 'Comparison of Bond Strength of Steel Bars in Normal- and High-Strength Concrete', *Journal of Materials in Civil Engineering*, 16(4), pp. 365–374. doi: 10.1061/(ASCE)0899-1561(2004)16:4(365).

Higgins, C. and Farrow, W. C. (2006) 'Tests of Reinforced Concrete Beams with Corrosion-Damaged Stirrups', *ACI Structural Journal*, 103(1), pp. 133–141. doi: 10.14359/15094.

Hou, L. *et al.* (2017) 'Effect of corrosion on bond behaviors of rebar embedded in ultra-high toughness cementitious composite', *Construction and Building Materials*. Elsevier, 138, pp. 141–150. doi: 10.1016/J.CONBUILDMAT.2017.02.008.

Hung, C. C., Lee, H. S. and Chan, S. N. (2019) 'Tension-stiffening effect in steel-reinforced UHPC composites: Constitutive model and effects of steel fibers, loading patterns, and rebar sizes', *Composites Part B: Engineering*. Elsevier Ltd, 158, pp. 269–278. doi: 10.1016/j.compositesb.2018.09.091.

Ioannou, A. *et al.* (2022) 'Experimental Testing of ECC Jackets for Repair of Pre-Damaged R . C . Members Experimental Testing of ECC Jackets for Repair of Pre-Damaged R . C . Members under Cyclic Loading', in *12th National Conference on Earthquake Engineering*. Salt Lake City, Utah: Earthquake Engineering Research Institute, pp. 1–5.

Kashani, M. M., Maddocks, J. and Dizaj, E. A. (2019) 'Residual Capacity of Corroded Reinforced Concrete Bridge Components: State-of-the-Art Review', *Journal of Bridge Engineering*, 24(7), p. 03119001. doi: 10.1061/(ASCE)BE.1943-5592.0001429.

Kondratova, I. L., Montes, P. and Bremner, T. W. (2000) 'Accelerated Corrosion Testing Results for Specimens Containing Uncoated Reinforcing Steel and Corrosion Inhibitors', *Special Publication*, 192, pp. 789–806. doi: 10.14359/5785.

Koulouris, K. and Apostolopoulos, C. (2020) 'An Experimental Study on Effects of Corrosion and Stirrups Spacing on Bond Behavior of Reinforced Concrete', *Metals*. MDPI AG, 10(10), p. 1327. doi: 10.3390/met10101327.

Lee, H. S. and Cho, Y. S. (2009) 'Evaluation of the mechanical properties of steel reinforcement embedded in concrete specimen as a function of the degree of reinforcement corrosion', in *International Journal of Fracture*. Springer, pp. 81–88. doi: 10.1007/s10704-009-9334-7.

Li, D. *et al.* (2018) 'Influence of Non-uniform corrosion of steel bars on the seismic behavior of reinforced concrete columns', *Construction and Building Materials*. Elsevier, 167, pp. 20–32. doi: 10.1016/J.CONBUILDMAT.2018.01.149.

Li, J., Gong, J. and Wang, L. (2009) 'Seismic behavior of corrosion-damaged reinforced concrete columns strengthened using combined carbon fiber-reinforced polymer and steel jacket', *Construction and Building Materials*. Elsevier, 23(7), pp. 2653–2663. doi: 10.1016/J.CONBUILDMAT.2009.01.003.

Li, X. *et al.* (2016) 'Effect of loading rate on the bond behaviour of deformed steel bars in

concrete subjected to lateral pressure', *Materials and Structures*. Springer Netherlands, 49(6), pp. 2097–2111. doi: 10.1617/s11527-015-0636-0.

Lijina, T. and Jithin, J. . (2018) 'Effect of Steel and Polypropylene Fibre on the Tension Stiffening of Ultra High Performance Concrete', *International Journal of Engineering and Advanced Technology (IJEAT)*, 8(4C).

Lin, H. *et al.* (2019) 'State-of-the-art review on the bond properties of corroded reinforcing steel bar', *Construction and Building Materials*. Elsevier, 213, pp. 216–233. doi: 10.1016/J.CONBUILDMAT.2019.04.077.

Liu, X. and Li, Y. (2018) 'Experimental study of seismic behavior of partially corrosion-damaged reinforced concrete columns strengthened with FRP composites with large deformability', *Construction and Building Materials*. Elsevier, 191, pp. 1071–1081. doi: 10.1016/J.CONBUILDMAT.2018.10.072.

Lu, C. *et al.* (2016) 'Mechanical properties of corroded steel bars in pre-cracked concrete suffering from chloride attack', *Construction and Building Materials*, 123(123), pp. 649–660. doi: 10.1016/j.conbuildmat.2016.07.032.

Ma, Y., Che, Y. and Gong, J. (2012) 'Behavior of corrosion damaged circular reinforced concrete columns under cyclic loading', *Construction and Building Materials*. Elsevier, 29, pp. 548–556. doi: 10.1016/J.CONBUILDMAT.2011.11.002.

El Maaddawy, T. A. and Soudki, K. A. (2003) 'Effectiveness of Impressed Current Technique to Simulate Corrosion of Steel Reinforcement in Concrete', *Journal of Materials in Civil Engineering*, 15(1), pp. 41–47. doi: 10.1061/(ASCE)0899-1561(2003)15:1(41).

Mangat, P. S. and Elgarf, M. S. (1999) 'Bond characteristics of corrding reinforcement in concrete beams', *Materials and Structures*. Kluwer Academic Publishers, 32(2), pp. 89–97. doi: 10.1007/BF02479434.

Mangat, Pritpal S. and Elgarf, M. S. (1999) 'Flexural Strength of Concrete Beams with Corroding Reinforcement', *ACI Structural Journal*, 96(1), pp. 149–158. doi: 10.14359/606.

Martín Pérez, B. M. (1999) *Service life modelling of R.C. highway structures exposed to chlorides*. University of Toronto. Available at:

https://books.google.ca/books/about/Service_Life_Modelling_of_R_C_Highway_St.html?id=qQiGtgAACAAJ&redir_esc=y (Accessed: 14 February 2019).

Meda, A. *et al.* (2014) 'Experimental evaluation of the corrosion influence on the cyclic behaviour of RC columns', *Engineering Structures*. Elsevier, 76, pp. 112–123. doi: 10.1016/J.ENGSTRUCT.2014.06.043.

Mehta, P. K. (1991) 'Durability of Concrete--Fifty Years of Progress?', *Special Publication*, 126, pp. 1–32. doi: 10.14359/1998.

Menengotto, M. and Pinto, P. E. (1973) 'Method o f Analysis for Cyclically Loaded Reinforced Concrete Plane Frames Including Changes in Geometry and Nonelastic Behavior of Elements under Combined Normal Force and Bending', in *IABSE Symposium on Resistance and Ultimate Deformability of Structures Acted on*. Lisbon.

Molaioni, F., Carlo, F. Di and Rinaldi, Z. (2021) 'Modelling Strategies for the Numerical Simulation of the Behaviour of Corroded RC Columns under Cyclic Loads', *Applied Sciences 2021, Vol. 11, Page 9761*. Multidisciplinary Digital Publishing Institute, 11(20), p. 9761. doi: 10.3390/APP11209761.

Ou, Y.-C. and Chen, H.-H. (2014) 'Cyclic Behavior of Reinforced Concrete Beams with Corroded Transverse Steel Reinforcement', *Journal of Structural Engineering*, 140(9), p. 04014050. doi: 10.1061/(ASCE)ST.1943-541X.0000932.

Palsson, R. and Mirza, M. S. (2002a) 'Mechanical response of corroded steel reinforcement of abandoned concrete bridge', *ACI Structural Journal*, 99(2), pp. 157–162. doi: 10.14359/11538.

Palsson, R. and Mirza, M. S. (2002b) 'Mechanical Response of Corroded Steel Reinforcement of Abandoned Concrete Bridge', *ACI Structural Journal*, 99(2), pp. 157–162. doi: 10.14359/11538.

Pantazopoulou, S. J. *et al.* (2001) *REPAIR OF CORROSION-DAMAGED COLUMNS WITH FRP WRAPS, JOURNAL OF COMPOSITES FOR CONSTRUCTION*. Available at: http://pubs.asce.org/copyright (Accessed: 23 July 2019).

Pantazopoulou, S. J. *et al.* (2019) 'The performance of corroded lap splices in reinforced concrete beams', *Corrosion Reviews*. De Gruyter, 37(1), pp. 31–44. doi: 10.1515/corrrev-2017-0086.

Papakonstantinou, C. G., Balaguru, P. N. and Auyeung, Y. (2011) 'Influence of FRP confinement on bond behavior of corroded steel reinforcement', *Cement and Concrete Composites*. Elsevier, 33(5), pp. 611–621. doi: 10.1016/J.CEMCONCOMP.2011.02.006.

Pardalopoulos, S. I., Pantazopoulou, S. J. and Lekidis, V. A. (2017) 'Simplified method for rapid seismic assessment of older R.C. buildings'. doi: 10.1016/j.engstruct.2017.10.052.

Pardalopoulos, S. I., Pantazopoulou, S. J. and Lekidis, V. A. (2018) 'Simplified method for rapid seismic assessment of older R.C. buildings', *Engineering Structures*. Elsevier Ltd, 154, pp. 10–22. doi: 10.1016/j.engstruct.2017.10.052.

Pardalopoulos, S. J., Thermou, G. E. and Pantazopoulou, S. J. (2013) 'Screening criteria to identify brittle R.C. structural failures in earthquakes', *Bulletin of Earthquake Engineering*, 11(2), pp. 607–636. doi: 10.1007/s10518-012-9390-7.

Parulekar, Y. M. *et al.* (2020) 'Performance Assessment of Corroded Reinforced Concrete Structure Considering Bond Deterioration', *Journal of Performance of Constructed Facilities*. American Society of Civil Engineers, 34(2), p. 04020009. doi: 10.1061/(ASCE)CF.1943-5509.0001411.

Paul, Suvash CZijl, G. Van (2014) 'Cracked and uncracked SHCC specimens under different exposure conditions', in *Strain Hardening Cementitious Composites 3 (SHCC3)*. Dordrecht, pp. 25–32.

Pourbaix, M. (1974) *Atlas of electrochemical equilibria in aqueous solutions*. National Association of Corrosion Engineers. Available at: https://books.google.ca/books?id=iiLRvQEACAAJ&dq=9780915567980&hl=en&sa=X&ved=0ahUKEwivreD28rfgAhVi6IMKHQm4Dn4Q6AEIKjAA (Accessed: 12 February 2019).

Prieto, M., Tanner, P. and Andrade, C. (2011) 'Bond response in structural concrete with corroded steel bars. experimental results', *RILEM Bookseries*. Springer, Dordrecht, 5, pp. 231–241. doi: 10.1007/978-94-007-0677-4_16.

Rajput, A. S. and Sharma, U. K. (2018) 'Corroded reinforced concrete columns under simulated seismic loading', *Engineering Structures*. Elsevier, 171, pp. 453–463. doi: 10.1016/J.ENGSTRUCT.2018.05.097.

Raza, S. *et al.* (2019) ‘Strengthening and Repair of Reinforced Concrete Columns by Jacketing: State-of-the-Art Review’, *Sustainability*. MDPI AG, 11(11), p. 3208. doi: 10.3390/su11113208.

Robuschi, S. *et al.* (2020) ‘Bond of naturally corroded, plain reinforcing bars in concrete’, *Structure and Infrastructure Engineering*. Taylor and Francis Ltd., pp. 1–17. doi: 10.1080/15732479.2020.1768273.

Rodriguez, J. and Ortega, J. C. (1994) ‘Corrosion of reinforcing bars and service life of reinforced concrete structures: corrosion and bond deterioration’, in *International Conference on Concrete across Borders*. Odense, Denmark, pp. 315–326.

Semendary, A. A. and Svecova, D. (2020) ‘Factors affecting bond between precast concrete and cast in place ultra high performance concrete (UHPC)’, *Engineering Structures*. Elsevier, 216, p. 110746. doi: 10.1016/J.ENGSTRUCT.2020.110746.

Sezen, H. and Moehle, J. P. (2004) ‘Shear Strength Model for Lightly Reinforced Concrete Columns’, *Journal of Structural Engineering*. American Society of Civil Engineers, 130(11), pp. 1692–1703. doi: 10.1061/(ASCE)0733-9445(2004)130:11(1692).

Soudki, K. and Sherwood, T. (2003) ‘Bond Behavior of Corroded Steel Reinforcement in Concrete Wrapped with Carbon Fiber Reinforced Polymer Sheets’, *Journal of Materials in Civil Engineering*, 15(4), pp. 358–370. doi: 10.1061/(ASCE)0899-1561(2003)15:4(358).

Stanish, K., Hooton, R. D. and Pantazopoulou, S. J. (1999) ‘Corrosion Effects on Bond Strength in Reinforced Concrete’, *ACI Structural Journal*, 96(6), pp. 915–921. doi: 10.14359/765.

Suffern, C., El-Sayed, A. and Soudki, K. (2010) ‘Shear strength of disturbed regions with corroded stirrups in reinforced concrete beams’, *Canadian Journal of Civil Engineering*, 37(8), pp. 1045–1056. doi: 10.1139/L10-031.

Takuya, K., Ryuta, I. and Masayuki, T. (2020) ‘Prediction of Hydrogen Embrittlement of Reinforcing Steel Bars in Concrete Poles | NTT Technical Review’, *NTT Technical Review*, 18(11). Available at: https://www.ntt-review.jp/archive/ntttechnical.php?contents=ntr202011ra1.html (Accessed: 16 April 2022).

Tastani, S. P. and Pantazopoulou, S. J. (2007) ‘Behavior of Corroded Bar Anchorages’, *ACI Structural Journal*, 104(6), pp. 756–766. doi: 10.14359/18958.

Tastani, S. and Pantazopoulou, S. J. (2005) 'Recovery of seismic resistance in corrosion-damaged reinforced concrete through FRP jacketing', *International Journal of Materials and Product Technology*, 23(3/4), p. 389. doi: 10.1504/IJMPT.2005.007737.

Tayeh, B. A., Abu Bakar, B. H. and Megat Johari, M. A. (2013) 'Characterization of the interfacial bond between old concrete substrate and ultra high performance fiber concrete repair composite', *Materials and Structures/Materiaux et Constructions*. Springer, 46(5), pp. 743–753. doi: 10.1617/S11527-012-9931-1/FIGURES/13.

Tepfers, R. (1979) 'Cracking of concrete cover along anchored deformed reinforcing bars', *Magazine of Concrete Research*. Thomas Telford Ltd , 31(106), pp. 3–12. doi: 10.1680/macr.1979.31.106.3.

Tondolo, F. (2015) 'Bond behaviour with reinforcement corrosion', *Construction and Building Materials*. Elsevier, 93, pp. 926–932. doi: 10.1016/J.CONBUILDMAT.2015.05.067.

Torres-Acosta, A. A., Navarro-Gutierrez, S. and Terán-Guillén, J. (2007) 'Residual flexure capacity of corroded reinforced concrete beams', *Engineering Structures*. Elsevier, 29(6), pp. 1145–1152. doi: 10.1016/J.ENGSTRUCT.2006.07.018.

Tuutti, K. (1982) *Corrosion of steel in concrete*. Swedish Cement and Concrete Research Institute, Stockholm. Available at: https://portal.research.lu.se/portal/en/publications/corrosion-of-steel-in-concrete(e97795b5-7f3a-4994-8beb-9438f5a51571).html (Accessed: 6 July 2020).

Valikhani, A. *et al.* (2020) 'Experimental evaluation of concrete-to-UHPC bond strength with correlation to surface roughness for repair application', *Construction and Building Materials*. Elsevier, 238, p. 117753. doi: 10.1016/J.CONBUILDMAT.2019.117753.

Vecchio, F. J. and Collins, M. P. (1986) 'MODIFIED COMPRESSION-FIELD THEORY FOR REINFORCED CONCRETE ELEMENTS SUBJECTED TO SHEAR.', *Journal of the American Concrete Institute*, 83(2), pp. 219–231. doi: 10.14359/10416.

Vu, N. S. and Li, B. (2018) 'Seismic Performance of Flexural Reinforced Concrete Columns with Corroded Reinforcement', *ACI Structural Journal*, 115(5), pp. 1253–1266. doi: 10.14359/51702372.

Vu, N. S., Yu, B. and Li, B. (2016) 'Prediction of strength and drift capacity of corroded

reinforced concrete columns', *Construction and Building Materials*. Elsevier, 115, pp. 304–318. doi: 10.1016/J.CONBUILDMAT.2016.04.048.

Wang, L. *et al.* (2015) 'Effects of stirrup and inclined bar corrosion on shear behavior of RC beams', *Construction and Building Materials*. Elsevier, 98, pp. 537–546. doi: 10.1016/J.CONBUILDMAT.2015.07.077.

Xia, J., Jin, W. and Li, L. (2011) 'Shear performance of reinforced concrete beams with corroded stirrups in chloride environment', *Corrosion Science*. Pergamon, 53(5), pp. 1794–1805. doi: 10.1016/J.CORSCI.2011.01.058.

Xu, S. L. and Cai, X. H. (2010) *Bond behavior of corroded reinforcing bar and ultra high toughness cementitious composites (UHTCC)*. Available at: https://framcos.org/FraMCoS-7/06-04.pdf (Accessed: 8 July 2019).

Yang, S.-Y. *et al.* (2016) 'Experimental research on hysteretic behaviors of corroded reinforced concrete columns with different maximum amounts of corrosion of rebar', *Construction and Building Materials*. Elsevier, 121, pp. 319–327. doi: 10.1016/J.CONBUILDMAT.2016.06.002.

Yuan, W., Guo, A. and Li, H. (2017) 'Experimental investigation on the cyclic behaviors of corroded coastal bridge piers with transfer of plastic hinge due to non-uniform corrosion', *Soil Dynamics and Earthquake Engineering*. Elsevier, 102, pp. 112–123. doi: 10.1016/J.SOILDYN.2017.08.019.

Zhang, R., Castel, A. and François, R. (2009) 'The corrosion pattern of reinforcement and its influence on serviceability of reinforced concrete members in chloride environment', *Cement and Concrete Research*. Pergamon, 39(11), pp. 1077–1086. doi: 10.1016/J.CEMCONRES.2009.07.025.

Zhang, W. *et al.* (2012) 'Tensile and fatigue behavior of corroded rebars', *Construction and Building Materials*. Elsevier, 34, pp. 409–417. doi: 10.1016/J.CONBUILDMAT.2012.02.071.

Zhao, Y. *et al.* (2013) 'Bond behaviour of normal/recycled concrete and corroded steel bars', *Construction and Building Materials*. Elsevier, 48, pp. 348–359. doi: 10.1016/J.CONBUILDMAT.2013.06.091.

Zhu, W. *et al.* (2013) 'Effect of corrosion of reinforcement on the mechanical behaviour of

highly corroded RC beams', *Engineering Structures*. Elsevier, 56, pp. 544–554. doi: 10.1016/J.ENGSTRUCT.2013.04.017.

Zhu, W. and François, R. (2014) 'Experimental investigation of the relationships between residual cross-section shapes and the ductility of corroded bars', *Construction and Building Materials*, 69(69), pp. 335–345. doi: 10.1016/j.conbuildmat.2014.07.059.

Van Zijl, G. P. A. G. *et al.* (2012) 'Durability of strain-hardening cement-based composites (SHCC)', *Materials and Structures/Materiaux et Constructions*. Springer, 45(10), pp. 1447–1463. doi: 10.1617/s11527-012-9845-y.

10. Summary, Conclusions and Recommendations for Future Research

10.1. Summary of the Thesis

Mitigating the damage and strength loss from corrosion of reinforced concrete structures was the motivating objective of the present work. The approach taken was to explore the application of the new generation of strain-hardening ultra-high strength fiber reinforced concrete in order to devise a durable retrofitting method that may slow down further continuation of reinforcement mass loss, while at the same time recovering the strength and deformation capacity of structural members without excessive geometry alterations of the component.

The study expanded into several aspects regarding the effects of corrosion on reinforced concrete structures. At first the available experimental evidence on the effects of corrosion damage was assembled and evaluated in order to determine attenuating relations that quantify in practical terms the depreciated yield and ultimate strengths and deformation capacity of steel reinforcement with increasing bar mass loss. These findings were further implemented in a modelling methodology for accounting for the reduction of reinforcement mechanical properties, as well as for the corrosion-induced effects of degraded bond on the response of columns under cyclic displacement reversals simulating earthquake effects. The procedure was calibrated against a collection of corroded column tests conducted under lateral displacement cyclic reversals and was subsequently used to study the parametric sensitivity of the effects of corrosion on the seismic response of columns.

Another pursuit of the research was to determine whether, with the availability of ECC (UHPC-ECC) which is heralded for its impressive durability and ductility, retrofitting solutions could be developed in the form of thin jackets that would protect the reinforcement in future exposure. First, a test series was undertaken to study the rate of corrosion of reinforcement embedded in ECC; parameters of study were, the cover thickness and the type of ECC matrix used (two alternatives, i.e., an Ultra High Performance Fiber Reinforced concrete, and an Engineered Cementitious Composite with different types and contents of fiber.) The reinforcement was conditioned to accelerated corrosion while being stressed in tension under sustained stress at 30% of yielding – this was done to determine whether stress-corrosion would have an effect on the rate of the phenomenon. After conditioning, the specimens were tested under mechanical load so as to also

enable quantification of the tension stiffening effect of bars embedded in strain hardening cementitious matrices.

Next a series of columns were constructed, replicating reinforcing details of older practice (such as sparse stirrups, inadequate lap splice lengths, and an unfavorable aspect ratio). These were conditioned to accelerated corrosion for several months before being tested under cyclic displacement reversals that represented earthquake loads. Upon increasing the intensity of the imposed lateral displacement, bond failure occurred along the lap splices, thereby limiting the lateral strength of the columns. Then, the specimens were repaired after removing the damaged cover, using a UHPC-THFRC material for cover replacement over the damaged region. The repaired columns were re-tested under the same load history, where dramatic improvements in the strength, deformation capacity, ductility and energy absorption capacity were observed in all cases.

The modelling approach developed earlier was used in order to reproduce the experimental response through F.E. analysis; calibrated models were then used as a benchmark for better understanding and verifying the strength and deformability degradation of columns which was quantified independently from experimental evidence from column tests assembled from the literature. In this manner, reduction coefficients were formulated and calibrated from the experimental database, by which to attenuate the coordinates of the backbone response curve that was proposed in the ASCE/SEI-41 (2017) for seismic assessment of existing columns, in terms of steel mass loss. The coefficient that is operating on stiffness was also introduced in a tier-II level rapid assessment to illustrate the effects of increased compliance of the structure after corrosion on the seismic demands against which the structure has to be evaluated.

An illustration example was also presented whereby a medium rise reinforced concrete building having typical geometry and corroded columns in the first-storey was analyzed to a suite of earthquake records in order to quantify the effect of corrosion in terms seismic demands and projected damage. Through fragility analysis, the increase in the probability of exceedance of the performance limit states recommended by the code for seismic assessment was quantified for this example structure, as a function of its corrosion damage.

A graphical overview of the dissertation's content is shown in Figure 10-1 below.

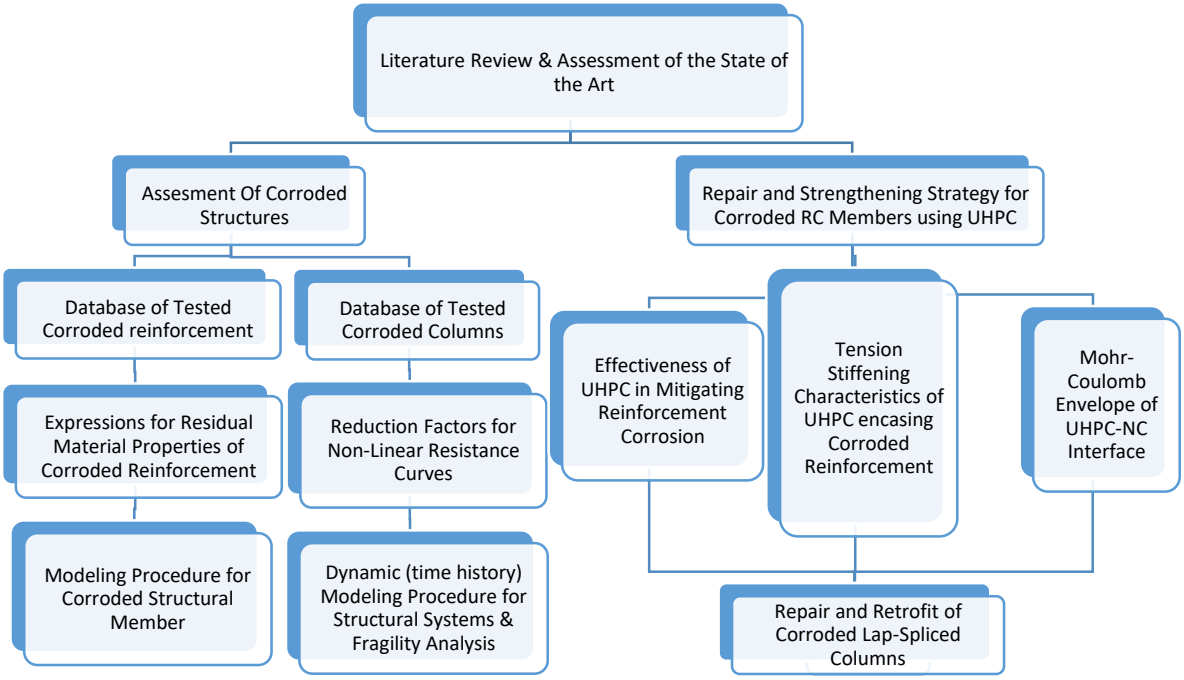

Figure 10-1. Overview of the dissertation's content

10.2. Conclusions

Detailed, pointwise conclusions of each part of this study were drawn at the end of each chapter. In this section the key findings of the study are outlined.

It was found that the most affected reinforcement mechanical property resulting from corrosion was the strain capacity of rebar, which was reduced to just 20% of the original capacity at a mass loss of 80%. The following expressions were derived for the reduced yield stress, ultimate strength and deformation capacity of reinforcement as a function of reinforcement mass loss ratio, through regression of test results assembled for that purpose in a database:

$$f_{y,res} = f_y \cdot e^{-0.013x};\ f_{u,res} = f_u \cdot e^{-0.016x};\ \varepsilon_{u,res} = \varepsilon_u \cdot e^{-0.054x} \qquad (10\text{-}1)$$

Using these results and a corroded bond model, detailed finite element modelling of corroded columns showed that corrosion causes more damage in lap-spliced regions as opposed to regularly anchored columns due to the significant reduction in bond strength capacity. Results were verified through the trends of the experimental database and it was found that corrosion primarily impacted the stiffness and the lateral drift capacity of corroded columns, where recorded degradation reached 45%. Calibration of the models showed that the key parameter for accurately modeling a

corroded member was the incorporated bond model. The following expressions were derived for attenuation multipliers of the reference uncorroded column mechanical properties, so as to reduce the stiffness, strength and deformation capacity of columns from their reference uncorroded values, as a function of the reinforcement mass loss, x, and the axial load ratio, ν:

$$\begin{array}{lll} \underline{Atten.\ Factor.} & \underline{For:\ 0 \le \nu \le 0.2} & \underline{For:\ 0.2 \le \nu \le 0.4} \\ r_k & 1 - 0.013x & 1 - 0.0107x \\ r_v = & 1 - 0.005\theta x & 1 - 0.008\theta x \\ r_d & 1 - 0.022x & 1 - 0.0275x \end{array} \quad (10\text{-}2)$$

These expressions are an important tool for practical seismic assessment of structural components. Using the derived expressions for residual mechanical properties of corroded RC members, the case study focusing on how corrosion may affect the structural response of buildings under dynamic excitations was explored. Two principal parameters were the presence or not of corrosion in the ground story columns (at 10% mass loss of reinforcement) and the simultaneous presence of a soft first storey (a pilotis structure). Results from the analysis showed a significant alteration to the response of the structure in terms of maximum and residual drift demands, and exhaustion of the critical members' reduced deformation capacity. Fragility analysis of the structure showed that the probability of exceedance of the IO, LS and CP limit states at a PGA of 0.2g increased by 50%, 65% and 70% respectively. It was observed that in many cases the limit state of the structure moved from Life Safety (LS) to Collapse (C) once corrosion was introduced. The key takeaway is that it is imperative to consider pre-existing corrosion damage in seismic assessment of existing structures as it may significantly alter the result of the seismic evaluation process.

One of the most important findings of this dissertation was the fact that uncracked UHPC and ECC were both successful in mitigating reinforcement corrosion. For concrete covers of thickness equal to $1D_b$, UHPC showed greater mitigation qualities over ECC, especially in the presence of cracks. For covers equal to $2D_b$, UHPC only showed improved mitigation qualities over ECC in the presence of 2mm cracks whereas for smaller crack widths both sets of specimens had low levels of accumulated mass loss of similar magnitude. Corrosion mitigation characteristics of UHPC and ECC cover from the current study were compared to that of normal concrete and SHCC from a different study. It was found that UHPC/ECC offered orders of magnitude more protection than both normal concrete and SHCC. It is recommended that for commercial practice, a concrete cover

of $2D_b$ of UHPC to be used for corrosion mitigation and for prolonging the service life of structural components. Uncracked UHPC and ECC specimens also showed promising tension-stiffening effects. Specimens developed minimal strains even when loaded up to 100 KN in tension. Strains in UHPC cover reached 0.6% of the bar's strain and 4.8% in ECC. ECC cover however showed a more ductile tension-stiffening behavior than the UHPC cover. The latter instead, showed greater tension-stiffening capacity due to its superior tensile strength. All pre-cracked specimens having a 2mm wide crack, aside from specimens with a thick UHPC cover, lost all tension stiffening capacity. It is recommended to neglect tension stiffening strength in the presence of significant crack widths in structural assessment calculations.

The experimental investigation on the effectiveness of UHPC as a repair material for seismic repair and retrofit of corroded lap-spliced columns was very insightful. It was found that UHPC cover replacement significantly improved the strength and ductility of corroded columns, regardless of presence of previous damage due to cyclic load reversals. Failure modes of repaired columns using UHPC cover replacement changed from either shear or lap splice failure to a ductile, energy dissipating flexural failure. It was also found that, in the strengthened regions of the columns, curvature and shear strains were significantly suppressed. The finite element analysis of these columns showed that corroded columns experienced increased stress demand in their transverse reinforcement, on account of reinforcement slippage. The UHPC-cover replacement mitigated the stress demand from the transverse reinforcement but led to an increase in the stress demand into the footing region where most of the rotation was taking place due to pullout and strain penetration. UHPC was also able to suppress yield penetration into the strengthened region. It was concluded that cover replacement of corroded columns is a very effective repair method that combines several advantages none the least being that it optimizes the use of the UHPC material where it is most effective, while also preserving the external geometry of the component. Practical application in bridge engineering would require an exploration of the size effect (i.e. bigger size elements may require thicker jackets than just replacement of cover); the methodology presented would give maximum benefit if it would be accompanied with measures to mitigate damage in the bar anchorage region in cases where past seismic events may have caused pre-existing damage or yield penetration into the anchorage.

10.3. Recommendations for Future Research

In the course of its development, the research presented in this thesis has opened several inquiries that exceeded the scope of the present study and present significant opportunities for future research:

1) Novel, crystal-forming, waterproofing and porosity-reducing admixtures that have self-healing action present an interesting opportunity for mitigation of reinforcement corrosion that would be ideally combined with ECC to enhance its performance in cover replacement as a competing solution to the more durable UHPC. An experimental study would be necessary to proof-test this concept and ought to include use of the admixture either prior as well as post-casting of the jacket, in order to encompass a range of examples encountered in the built environment. This could be a less expensive alternative to UHPC where moderate strength recovery and protection against further corrosion are the objective.
2) Investigating the effect of steel fiber corrosion on cracked UHPC members. It is very probable that corrosion penetration is rather hard to occur in UHPC materials on account of the great density – and material characterization tests confirm this. UHPC is known to be a very durable material, however its application in the real world is still limited and not enough time has passed to truly understand the limits of its durability in the field. A concern amongst researchers has been expressed regarding the possibility of corrosion of the exposed fibers in a cracked UHPC section – whether that is a justifiable concern remains to be shown through testing.
3) Based on the main experimental program performed in this dissertation on lap-spliced corroded columns, it was determined that a different repair strategy might be profitable. Instead of only repairing the lap-splice zone, the foundation would also be strengthened with UHPC or the previously damaged anchorages into the footing could be injected with repairing epoxy to mitigate the compliance caused by the previous damage of the anchorage and the resulting source of commensurate pullout slip. In this manner the failure would not localize in the footing, but instead it would remain within the lap-splice zone but the strength required to cause failure would be significantly higher.
4) Based on the cumulative knowledge gathered during this dissertation, a rapid non-destructive assessment method should be formulated further to extract fragility curves for

large groups of buildings sharing similar construction characteristics (i.e., built in the same era) and having been exposed to corrosion. An efficient field assessment could combine calibration of the period estimates with the reduction coefficient for structural stiffness, which would then provide a dependable estimate of future seismic demand in terms of drift ratio or lateral displacement. This could be combined with other field assessment technologies (e.g. mapping the structural damage using drones or LIDAR, or other forms of in situ monitoring). The technology should be able to detect hairline cracks and determine their widths and the cause of the crack based on its location and orientation (service crack, corrosion, shrinkage etc.), and when combined with the rapid assessment method presented earlier it ought to enable a quick tool by which the user could assess rapidly the effects of repair or strengthening of any one member on the system response. This is of course an inter-disciplinary project that requires significant funding.

I believe that it is very important for the civil engineering industry to incorporate new technologies into its practices. In the past decade, all engineering disciplines have been revolutionized through technology. However, structural engineering, has lagged behind on account of many theoretical and practical challenges. More, if not all, future research projects into seismic assessment of existing structures could combine technologies from many fields including software development, geomatics, sensor technology, mechanical, electrical and chemical engineering.